Czech Technical University in Prague
Faculty of Nuclear Sciences and Physical Engineering
Department of Materials

DOCTORAL THESIS

Advanced Plasma-Sprayed Ceramic Coatings Prepared from Liquid Feedstocks

Prague, 2021 Ing. Tomas Tesar

Bibliografický záznam

Autor:	Ing. Tomáš Tesař České vysoké učení technické v Praze Fakulta jaderná a fyzikálně inženýrská Katedra materiálů
Název práce:	Pokročilé keramické plazmové nástřiky připravené z kapalin
Studijní program:	Aplikace přírodních věd
Studijní obor:	Fyzikální inženýrství
Školitel:	Ing. Ondřej Kovářík, Ph.D. České vysoké učení technické v Praze Fakulta jaderná a fyzikálně inženýrská Katedra materiálů
Školitel-specialista:	Ing. Radek Mušálek, Ph.D. Ústav fyziky plazmatu AV ČR, v.v.i. Oddělení materiálového inženýrství
Akademický rok:	2020/2021
Počet stran:	108
Klíčová slova:	plazmové stříkání suspenzí, plazmové stříkání roztoků, oxid hlinitý, oxid chromitý, hybridní vodou stabilizovaný plazmový hořák, směsné materiály, hybridní plazmové stříkání

Bibliographic Entry

Author:	Ing. Tomas Tesar Czech Technical University in Prague Faculty of Nuclear Sciences and Physical Engineering Department of Materials
Title of Dissertation:	Advanced Plasma Sprayed Ceramic Coatings Prepared from Liquid Feedstocks
Degree Program:	Application of Natural Sciences
Field of Study:	Physical Engineering
Supervisor:	Ing. Ondrej Kovarik, Ph.D. Czech Technical University in Prague Faculty of Nuclear Sciences and Physical Engineering Department of Materials
Supervisor-Specialist:	Ing. Radek Musalek, Ph.D. Institute of Plasma Physics of Czech Academy of Sciences Department of Materials Engineering
Academic Year:	2020/2021
Number of Pages:	108
Keywords:	suspension plasma spraying, solution precursor plasma spraying, aluminum oxide, chromium oxide, hybrid water-stabilized plasma, intermixed materials, hybrid spraying

Acknowledgements

First and foremost, my boundless appreciation belongs to my super-supervisor and friend Radek Mušálek, who has stood by my first steps in science since the very beginning. Starting with samples preparation, analysis and evaluation, through experiment planning, up to scientific thinking, writing, and presenting, Radek has always been kind, wise, supporting, and cheering in every part of this exciting journey, for which I am endlessly grateful. Thank you, Radek, you have really been a father in science to me.

The next big thank belongs to Honza Medřický, who has been like my older brother, helping me with every thinkable bit, from sprayshop screwing and measurements all the way to writing and presenting. Thank you, Honza.

Many thanks go also to other MIPPsters (fellows from the Department of Materials Engineering at the Institute of Plasma Physics), who have been making IPP a delightful place to work at, namely to Fero Lukáč for having always accepted more alumina samples for XRD evaluation, Štefan Csáki for XRF measurements, Kuba Veverka and Kuba Klečka for always being positive and in for any adventure, and Honza Čížek for always having a piece of advice and the right attitude. Thank you, pals.

This work also heavily relied on the skills and help of all the members of the sprayshop in Laboratory of Plasma Technologies, especially Marek Janata and Zdenda Kutílek, who have my bows and thanks.

Thanks also belong my supervisor Ondra Kovářík from the Department of Materials at the faculty for helping me going through all the necessary duties of a PhD student and for reviewing the thesis.

Also, I have highly appreciated the collaboration with people outside of IPP, which often surpassed the scope of this thesis, naming Mohit Gupta, Stefan Björklund and Shrikant Joshi from University West in Trollhättan, Sweden (lots of spraying and thermal cycling fatigue testing), Richard Trache and Nicholas Curry from Treibacher Industrie in Althofen, Austria (spraying and TCF testing), Václav Římal from Faculty of Mathematics and Physics, Charles University in Prague, Czechia (NMR evaluation), Šárka Houdková from New Technologies Research Centre, University of West Bohemia in Pilsen, Czechia (pin-on-disc tribology testing), Ondrej Panák and Markéta Držková from University of Pardubice, Czechia (thermochromic properties evaluation).

I would not have made it so far in my life without the help, faith, and care I have received from my parents. Thank you, mom and dad.

As much as one episode of life is ending with the PhD study, another one is starting. I could not be more grateful to have Terezka by my side and I am truly looking forward to walk my life path as her husband. Thank you, my dearest, for all the love you are bringing!

Declaration

I hereby declare that this doctoral thesis is my original work and that the sources used within are provided in the list of references in accordance with the Methodological Instructions on Ethical Principles in the Preparation of University Theses.

I also declare that I wrote all of the four original research articles that are presented in the experimental part of the thesis, with the help of co-authors listed therein.

In Prague, July, 2021

"Nanos gigantum humeris insidentes."

Bernardus Carnotensis, 12th century

- Devoted to my beloved grandfather Milan, who taught me the joy of creating. -

Abstract

Suspension and solution precursor plasma spraying techniques represent the latest generation of thermal spraying methods. The liquid feedstocks bring about significantly refined coating microstructures compared to the traditional dry coarse powder feedstocks, enabling the preparation of qualitatively and functionally novel coatings. Inherently, the refined microstructure also yields an opportunity to combine different materials at finer scale, thus offering more extensive control of the coatings composition and microstructure.

Primarily, this thesis presents the implementation of the liquid feedstocks spraying of aluminum oxide-based coatings using the hybrid water-stabilized plasma torch, including formulation of the suspensions and solutions, optimization of deposition conditions, and assessment of the coatings properties. Predominantly, microstructures and phase composition of the coatings, evaluated by SEM and XRD, respectively, were studied and are discussed with respect to the coatings deposition conditions.

Based on the acquired knowledge, unique coatings combining aluminum and chromium oxides were prepared by means of intermixing suspensions of fine powders, intermixing solutions of chemical precursors, and using an innovative concept of hybrid spraying by simultaneous deposition of suspensions and dry coarse powders. All three methods yielded different degree of intermixing of the materials, the description of which is presented in the thesis. An outstanding result of intermixing of materials at atomic level was achieved using the mixture of precursor solutions, producing extremely porous coatings showing thermochromic behavior.

Keywords: suspension plasma spraying, solution precursor plasma spraying, aluminum oxide, chromium oxide, hybrid water-stabilized plasma, intermixing, hybrid spraying

Abstrakt

Plazmové stříkání suspenzí a roztoků patří mezi nejnovějších oblasti žárového stříkání. Depozice materiálů z kapalin přináší zásadní zjemnění mikrostruktury nástřiků oproti konvenčním nástřikům z prášků, což umožňuje přípravu zcela nových vrstev s unikátními vlastnosti. Zmenšení strukturních jednotek nástřiků také nabízí přípravu vrstev ze směsí více materiálů, které jsou jemněji promíchány, což poskytuje nové možnosti řízení složení a mikrostruktury nástřiku.

Tato práce se v první fázi zabývá vývojem techniky depozice plazmových nástřiků oxidu hlinitého (Al_2O_3) z kapalných prekurzorů pomocí hybridního vodou stabilizovaného plazmového hořáku, a to včetně vývoje a charakterizace kapalných prekurzorů (suspenzí a roztoků), studia vlivu vlastností prekurzorů a depozičních parametrů na charakter nástřiku a studia funkčních vlastností nástřiků.

Na základě získaných zkušeností s přípravou nástřiků Al_2O_3 byly ve druhé fázi připraveny a charakterizovány nástřiky ze směsí oxidů hlinitého a chromitého (Cr_2O_3), které byly připraveny metodami depozice směsných suspenzí jemných prášků, směsných roztoků chemických prekurzorů a pomocí inovativní metody hybridní souběžné depozice suchých prášků a kapalin. Nástřiky připravené těmito metodami vykazovaly různý stupeň promísení vstupních složek v závislosti na velikosti částic a druhu promísení vstupních materiálů. Nástřik připravený pomocí směsných roztoků vykázal promísení složek na atomární úrovni, což bylo dokumentováno jak výsledky analýzy krystalové struktury, tak pomocí termochromických vlastností těchto nástřiků.

Klíčová slova: plazmové stříkání suspenzí, plazmové stříkání roztoků, oxid hlinitý, oxid chromitý, hybridní vodou stabilizovaný plazmový hořák, směsné materiály, hybridní plazmové stříkání

Contents

Nomenclature

ANN	Aluminum Nitrate Nonahydrate
APS	Air Plasma Spraying
BSE	Back-Scattered Electron
CNN	Chromium Nitrate Nonahydrate
COF	Coefficient of Friction (-)
DC	Direct Current (A)
DE	Deposition Efficiency (%)
EB-PVD	Electron Beam Physical Vapor Deposition
FA	Feeding Angle (°)
FD	Feeding Distance (mm)
FGM	Functionally-Graded Material
FR	Feeding Rate (g/min)
GSP	Gas-Stabilized Plasma
HAp	Hydroxyapatite
IPP CAS	Institute of Plasma Physics of the Czech Academy of Sciences
POD	Pin-on-Disc
PS	Plasma Spraying
PSD	Particle Size Distribution
SAR	Slurry Abrasion Response
SD	Stand-off Distance (mm)
SEM	Scanning Electron Microscope
SLE	Solid Load Equivalent
SPPS	Solution Precursor Plasma Spraying
SPS	Suspension Plasma Spraying
TBC	Thermal Barrier Coating
TCF	Thermal Cycling Fatigue
TS	Thermal Spraying
WSP	Water-Stabilized Plasma
WSP-H	Hybrid Water-Stabilized Plasma

XRD	X-ray Diffraction
XRF	X-ray Fluorescence
YSZ	Yttria-Stabilized Zirconia

1 Background of plasma spraying

Plasma spraying (PS) is a member of thermal spraying (TS) group of technologies which are employed to deposit coatings onto the surface of solid bodies (components) in order to provide their protection and enhance their functionality [1, 2]. In PS, a stream of plasma (i.e., hot ionized gas(es)) is used for the melting and acceleration of the feedstock material to be spray-deposited. In the following chapters, principles of PS technology will be briefly described to offer broader perspective and motivation for the experimental work presented in this thesis.

1.1 Plasma spraying equipment

The tool used for plasma spray deposition is called a plasma torch or plasma gun. Inside of the so-called arc chamber of a plasma torch, a plasma-forming medium is ionized by e.g., a direct current (DC) electric arc maintained between one or several cathodes and one or several anodes, or by radio frequency (RF) electromagnetic field [3]. This medium is used for the generation of the hot high-speed plasma stream, so-called plasma jet, for the stabilization of the arc, and to prevent the arc from touching the inner walls of the torch chamber. Two basic principles of arc plasma stabilization are schematically depicted in Fig. 1, showing the gas-stabilized plasma (GSP) and water-stabilized plasma (WSP) torches in Fig. 1a and 1b, respectively. Their combination was introduced with so-called hybrid water-stabilized plasma (WSP-H) technology (Fig. 1c) [4].

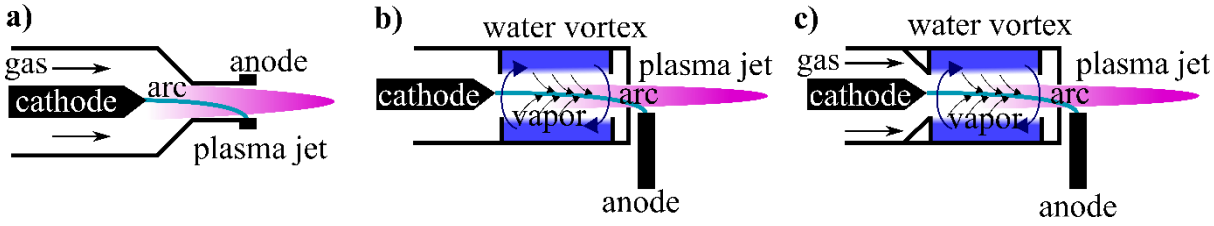

Figure 1. Scheme of a) GSP torch, b) WSP torch, c) hybrid WSP-H torch. Based on [4, 5].

Using the principle of gas stabilization, a mixture of plasma-forming gases (e.g., Ar, H_2, N_2, He) is fed into the arc chamber, dissociated and/or ionized therein by the electric arc, and ejected from the arc chamber through an orifice (called the nozzle), creating the plasma jet [6]. In order to reach high output power (i.e., thermal energy of the plasma), high volume flows (tens to hundreds of slpm) of gases are used for operation of such torches [7, 8]. In the last decade, GSP torches employing multiple electrodes (e.g., three cathodes and a single anode or three anodes arc-connected to a single cathode) have been developed in order to further increase the output power and also to mitigate the inherent fluctuation of the plasma jet of the single cathode-single anode systems. This fluctuation is inevitably present due to the oscillation of the arc attachment point on the anode, which results in variations in the arc voltage and, in turn, in variations in the jet energy [9]. This undesirable effect is to a large extent averaged in the multiple electrode systems by the multiple arcs, thus effectively stabilizing the output energy level of the plasma jet [10].

The water stabilization principle makes use of a water vortex formed inside the cylindrical torch chamber. The arc inside the torch chamber is confined by water flowing tangentially along the chamber walls. When the arc approaches to the chamber surface, water is heated and evaporated, pushing the arc back into the center of the chamber, making in fact a

closed-loop-controlled plasma confinement system. After being vaporized, water molecules are dissociated into hydrogen and oxygen atoms which are then ionized, forming the plasma that emanates from the nozzle [4, 11].

Owing to the different plasma-forming gases used in GSP and WSP torches, gas-stabilized plasma possesses generally greater density due to the heavier atoms, as well as lower velocity, and lower temperature compared to that of WSP [4]. Brief comparison of plasma properties is outlined in Table 1. An important plasma characteristic is the plasma enthalpy, i.e., the thermal energy available for processing of the feedstock per mass unit of plasma. In this regard, WSP torches are superior to GSP ones as they offer an order of magnitude greater enthalpy values, thus generally allowing larger quantities of feedstock material to be processed in the same amount of time [12].

Table 1. Properties of plasma generated by gas- and water-stabilized arcs. [4]

Plasma medium	Arc current (A)	Arc power (kW)	Mass flow rate (g/s)	Enthalpy (MJ/kg)	Temperature (K)
Ar/H_2 (65/3 slpm)	750	44	1.93	13.5	12 100
Ar/H_2 (33/10 slpm)	500	25	0.98	15.3	10 800
N_2/H_2 (235/94 slpm)	500	200	5.00	24	6 200
water	300	54	0.20	157	13 750
water	600	133	0.33	272	16 200

Operation of both types of plasma torches also requires powerful electric supply, gas and fume extraction units with dust separators, cooling systems, torch or samples manipulation system, feeders, injectors, etc., the description of which is beyond the scope of the thesis.

Development of plasma spraying techniques utilizing high-enthalpy torches is of great interest for real-world applications where cost-effective large-scale spraying is often required, e.g., for deposition of thermal barrier coatings (TBC) on high-temperature section components in jet engines or manufacturing of hard coatings for large printing rolls [13, 14]. Taking the aerospace industry as an example, plasma spraying can be considered as a competitor to other coating deposition techniques, e.g., to electron beam physical vapor deposition (EB-PVD), which produces coatings providing longer lifetimes under thermal cycling loading than conventional PS coatings [15]. However, the EB-PVD technique is primarily used for high-added-value components such as single-crystal-grown jet engine turbine blades (see Fig. 2a) owing to its high application costs [16]. Also, the thermal insulation performance of an EB-PVD coating is generally inferior to that of a conventional and more porous PS coating. Therefore, the development of PS coatings combining long lifetimes, low thermal conductivity, and low manufacturing costs presents a great scientific and business opportunity, especially in the case of large-scale applications, where methods like EB-PVD are nonviable. As an example of recent trend towards large scale coating applications, a size comparison is shown in Fig. 2b between the latest GE9X engine used for Boeing 777X aircraft and the fuselage of Boeing 737 aircraft using significantly smaller Leap-1B engines, both employing TBC systems.

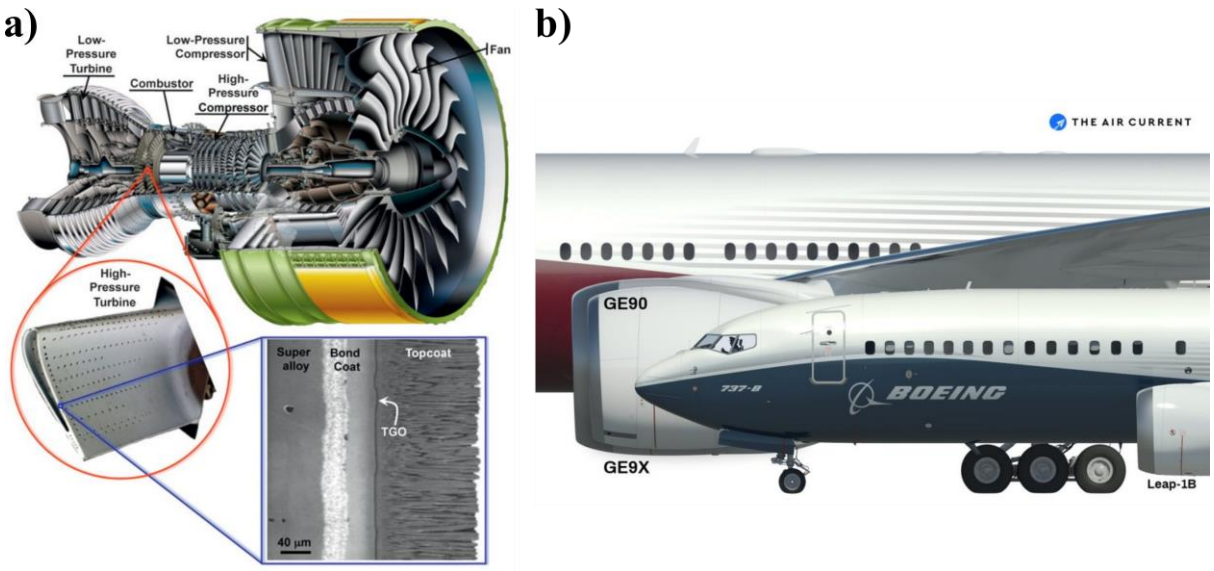

Figure 2. a) cutaway view of Engine Alliance GP7200 aircraft engine with enlarged inlays of a single high-pressure turbine blade and an EB-PVD TBC system applied thereon, b) size comparison between GE9X jet engine and Boeing 737 fuselage. [17]

1.2 Feedstock injection

Thermal spraying is generally able to deposit any material that undergoes melting to the liquid phase before vaporization or decomposition [6]. The material to be deposited onto the coated part (in the TS field so-called "substrate") is delivered into the plasma jet in order to be melted and propelled towards the coated part. Configuration-wise, the feedstock may be introduced into the jet radially or axially, as depicted in Fig. 3. In the former more common case, the material is fed into the plasma jet from the side(s) either outside of the plasma torch, i.e., downstream from the torch nozzle, or even inside of the nozzle. Contrary, in case of axial configuration, the material is delivered directly into the torch along the plasma jet axis and leaves the torch chamber together with the plasma jet through the nozzle. Generally, the radial configuration is applicable to any type of torch with the possibility of simple modification of the injection point distance from the nozzle (i.e., feeding distance - FD), the angle of inclination of the feedstock stream with respect to the plasma jet axis (i.e., feeding angle - FA), and also enables addition of multiple injectors. When using the radial feeding configuration, optimization of feedstock injection velocity is required to assure that the feedstock particles travel in the central hot section of the plasma jet, i.e., to avoid their overshooting or rebounding from the plasma jet. The axial configuration requires specific construction of the torch (so-called axial torch) and may be prone to clogging, but ensures that the feedstock material travels along the plasma jet axis, thus generally offering more consistent heat treatment of the feedstock [18].

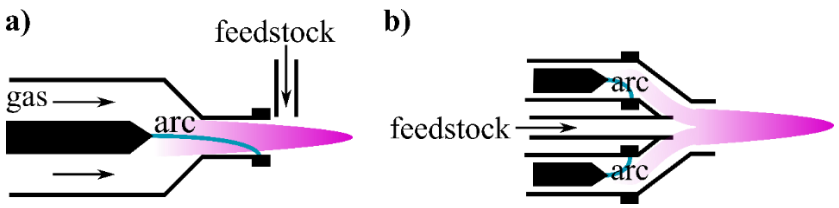

Figure 3. a) radial configuration, b) axial configuration. Based on [1].

1.3 Powder feedstock

Typically, the feedstock materials are introduced into the plasma jet in the form of a dry coarse powder, in the liquid form as a suspension of fine-grained powder, or as a liquid solution of chemical precursors [19]. The coarse powders used for TS deposition have the particle size in order from tens up to several hundreds of micrometers (Fig. 4a, b). The powder particles are carried by so-called carrier gas (e.g., air, Ar, Ar+H_2, etc.) through feeding lines and injected into the plasma jet. Therefore, good flowability of the powder is essential in order to ensure stable flow of the particles into the jet and to prevent clogging of the feeding lines. After being introduced into the plasma jet, the powder particles are heated, melted, and, at the same time, accelerated by the hot plasma gas stream towards the substrate. The melted particles then impact onto the surface of the substrate, flatten out, and solidify thereon, forming so-called splats (Fig. 4c). By stacking of splats, a continuous lamellar layer – coating – is formed (Fig. 4d).

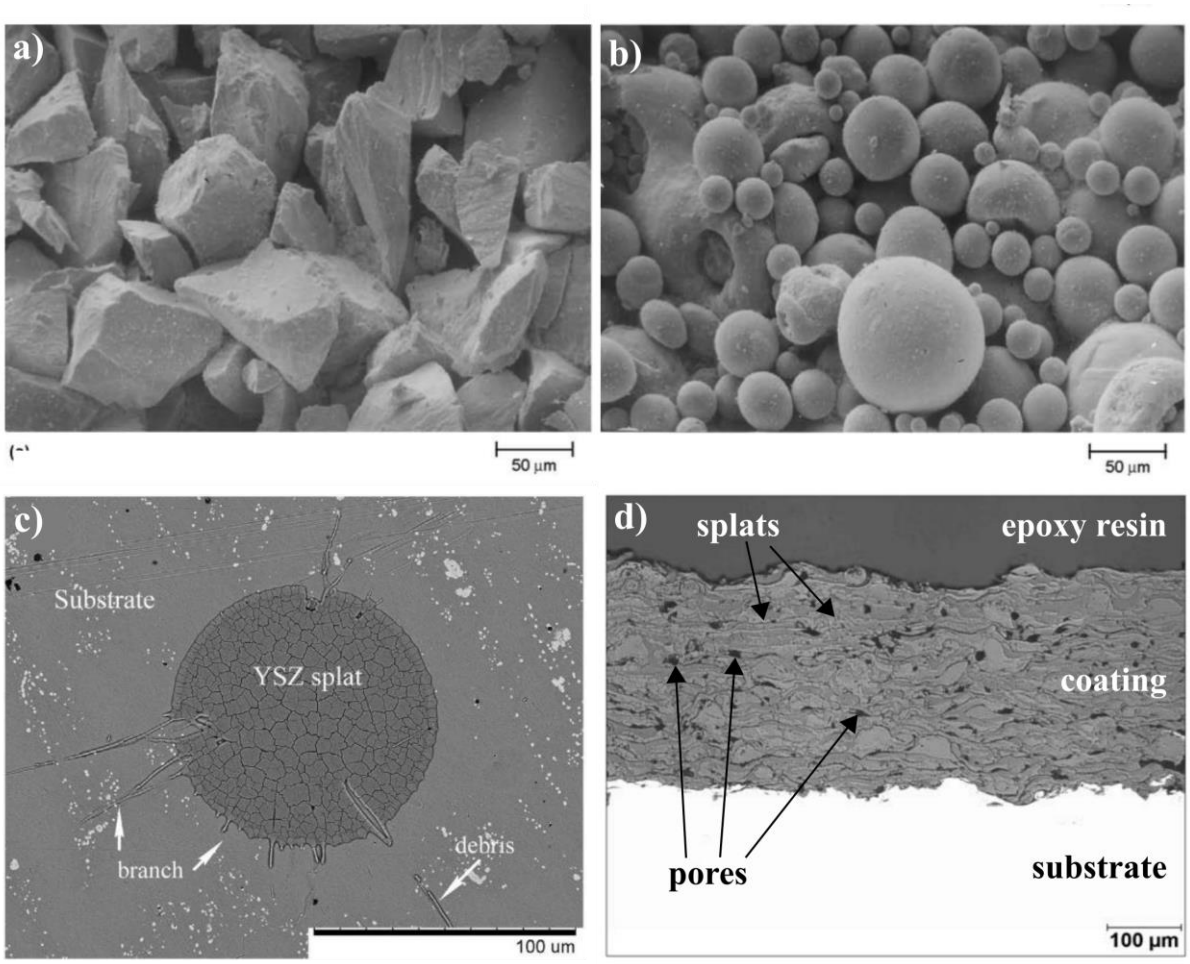

Figure 4. a) fused and crushed powder particles, b) spheroidized powder particles, c) splat on smooth substrate, d) cross-section of powder-sprayed coating. According to [1, 20, 21].

Apart from the splats, coatings may contain also unmelted powder particles, which had not received enough heat for melting, and resolidified particles, which had been fully melted and resolidified during the in-flight stage before reaching the substrate. Among the abovementioned structural units, voids are usually entrained, such as pores and cracks (Fig. 4d).

The pores and cracks are inherent features of the coating microstructure due to the entrainment of surrounding atmosphere underneath the splats, resulting from imperfect splat deformation and compliance on underlying surface, and due to the extremely rapid cooling and solidification of the melted particles upon impact, respectively. The melt cooling rate of up to 10^8 K.s^{-1} results also in the build-up of significant thermal "quenching" stresses due to the shrinkage of the solidified material [22]. This stress may be relieved by formation and opening of the intrasplat cracks, by partial splat sliding, or by plastic flow in case of ductile materials [22]. Partially, the occurrence of such cracks may be mitigated by e.g., more intensive preheating of the coated substrate to reduce the temperature difference between the substrate and the solidified cooling-down splats or by decreasing the size of the deposited particles to decrease their absolute shrinkage with respect to the underlying material during the cooling [23]. After the deposition, cooling of the sprayed component may further introduce "thermal mismatch stresses" resulting from the difference in the coefficient of thermal expansion (CTE) between the coating and the substrate, which may cause the development of through-thickness cracks and, in extreme case, to the delamination of the coating. If desirable, the amount of pores entrained among the splats may be lowered by e.g., achieving greater velocity of the particles to improve their flattening. On the other hand, increased porosity volume may be desired for e.g., lowering of thermal conductivity or increasing of thermal shock resistance of coatings used as thermal barriers [24].

1.4 Liquid feedstocks

Functional properties of the coatings may be significantly adjusted by modification of their microstructure. It has been shown that finer splats and voids may bring about improved functional properties such as hardness, wear resistance, thermal insulation, etc., owing to the decreased size of the structural units and increased number of intersplat interfaces [25]. However, direct deposition of miniature splats by feeding of fine dry powders is problematic or even impossible (e.g., below 5 μm in diameter [26]). Due to their small size and high specific surface area, fine particles tend to agglomerate by means of interlocking and electrostatic forces resulting in poor powder flowability and clogging of the feeding lines [18]. Moreover, owing to their low mass (i.e., low inertia), fine particles are unable to penetrate into the plasma jet (especially in case of radial feeding).

In order to penetrate into the plasma jet, the momentum density of the particle stream has to generally comply with the following equation:

$$\rho_p v_p^2 > \rho_g v_g^2, \tag{1}$$

where ρ and v are densities and velocities of the particle stream (subscript p) and plasma gas (subscript g), respectively [27]. Understandably, increasing the particle injection velocity v_p by means of increased carrier gas flow rate is impractical due to the severe disturbance and cooling of the plasma jet [28]. Therefore, it is viable to exchange the carrier gas for a carrier liquid, leading to an increase in the mean density of the particle stream ρ_p, enabling its penetration into the plasma jet [29]. Formulated suspension is then injected into the plasma jet as a continuous stream or as pre-atomized droplets. In this way, the liquid stream or droplets possess enough momentum to penetrate into the plasma jet, wherein intensive atomization takes place into fine (e.g., micron or submicron) droplets, the solvent is heated and evaporated, and the solid particles receive heat treatment analogously to the case of solid powders.

Formulation of the liquid feedstocks, namely solvent type, solid loading of powder, chemistry and particle size distribution of the powder, solute type, additives, etc., significantly affect the behavior of the feedstocks during the deposition [30]. Generally, viscosity and sedimentation resistance determine the sprayability of the suspensions, while density, surface tension, and viscosity govern the liquid interaction with the plasma jet, thus affecting the subsequent coating buildup [27]. Therefore, all the above mentioned parameters have to be taken into account and controlled, making the development of a sprayable suspension a complex process employing a whole field of research and development, due to the broad spectrum of materials, solvents, additives (stabilizers, surfactants, plasticizers, etc.) and their interactions [31, 32].

Apart from suspensions of solid particles in a carrier solvent, solutions of chemical precursors of the deposited materials may be also used as feedstocks. The material is fully dissolved in the solvent which is thus free of any solid particles, thereby circumventing the stability and sedimentation issues of suspensions. On the other hand, the amount of material delivered within the solution (the solid load equivalent (SLE) to the suspension) is limited by the maximal solubility of the precursors in the selected solvent. After the solution injection into the plasma jet, evaporation of the solvent takes place along with precipitation of the solute, followed by its thermal decomposition or other chemical reactions leading to in-situ formation of the desirable material, and the final products are melted in the plasma. Using this method, fine particles are formed and deposited similarly to the suspension spraying route. However, the additional steps of precursor precipitation and decomposition (as compared to suspensions) may increase the energetic demands on the plasma jet and also bring another complexity to the whole process which may require optimization in order to produce the desired coating microstructures and ultimately properties [33].

1.5 Mixing of feedstock materials

Many applications do not require more than a single-compound feedstock for the coating deposition. Nevertheless, certain applications may require utilization of multiple materials within one coating in order to meet the desired functionality. Typically, phase-stabilizing components are added to the base material (e.g., Y_2O_3 is added to ZrO_2 for stabilization of the zirconia tetragonal phase [34], or Cr_2O_3 is added to Al_2O_3 for the α-phase stabilization [35]) and the mixture is supplied as a prealloyed powder of specified and uniform composition. However, on-site adjustment of the feedstock composition may be required during spraying, e.g., for the deposition of functionally-graded material (FGM) coatings or for delivering of varied functionality of coating components [36]. In this regard, feeding the mechanical mixture with changing content of the selected materials is probably the most straightforward way to deposit a multi-material gradient coating. On the other hand, the drawback of this approach may be the low homogeneity of the deposited coating, i.e., the coating is composed of isolated splats of different chemical composition with limited possibility of material intermixing or even alloying [20].

The use of suspensions offers significantly more efficient intermixing of the selected materials compared to dry coarse powders. Each atomized suspension droplet contains numerous particles of the different materials which are melted and fused together during the in-flight stage (Fig. 5). Thanks to the close material intermixing, chemical reactions may take place during the in-flight stage, as demonstrated in [37] where deposition of calcium titanate ($CaTiO_3$) was achieved from mixture of fine calcium carbonate ($CaCO_3$) and titanium dioxide

(TiO_2) powders in ethanol. On the downside, the formulation of an intermixed suspension of two or more materials may be more challenging than the mixing of dry coarse powders due to the different densities and especially the different surface chemistry of the dispersed materials, their mutual interactions, and interaction with the solvent and the additives. This is further emphasized in case of mixing of single-material ready-to-spray suspensions which are optimized with respect to their solids and solvent chemistry, particle size and density, solid load, etc., [38]. Therefore, mixing of two or more suspensions may cause deterioration of the suspension properties, e.g., leading to undesirable coagulation and/or sedimentation of the fine particles.

Among the abovementioned feedstocks, the most homogeneous mixing of different chemicals may be expected with the deposition of intermixed precursor solutions owing to the fact that the dissolved precursors are intermixed on the atomic scale in the solution. A typical example may be the deposition of YSZ from solution of zirconium acetate and yttrium nitrate presented in [39], which resulted in the formation of chemically homogeneous dense vertically cracked coating having purely tetragonal zirconia phase.

An interesting option of combining powder and liquid feedstocks spraying (so-called hybrid spraying) was recently proposed and demonstrated, e.g., in [40, 41]. The hybrid concept employs simultaneous feeding of powder and liquid feedstocks into the plasma jet (Fig. 5). Both feedstocks are processed and deposited together, bringing a new class of composite coatings combining the relatively large powder-sprayed splats with the miniature liquid-sprayed splats. The feeding of a powder enables high coating deposition rates while the liquid-based splats may serve multiple purposes, such as “bonding agent” between the large powder splats for improved internal cohesion of the coating, nucleation sites for heteronucleation of desired phases from the powder, reservoir of material for self-healing of the coating, solid lubricants, etc. [42–44]. The hybrid spraying concept is currently intensively developed at IPP CAS.

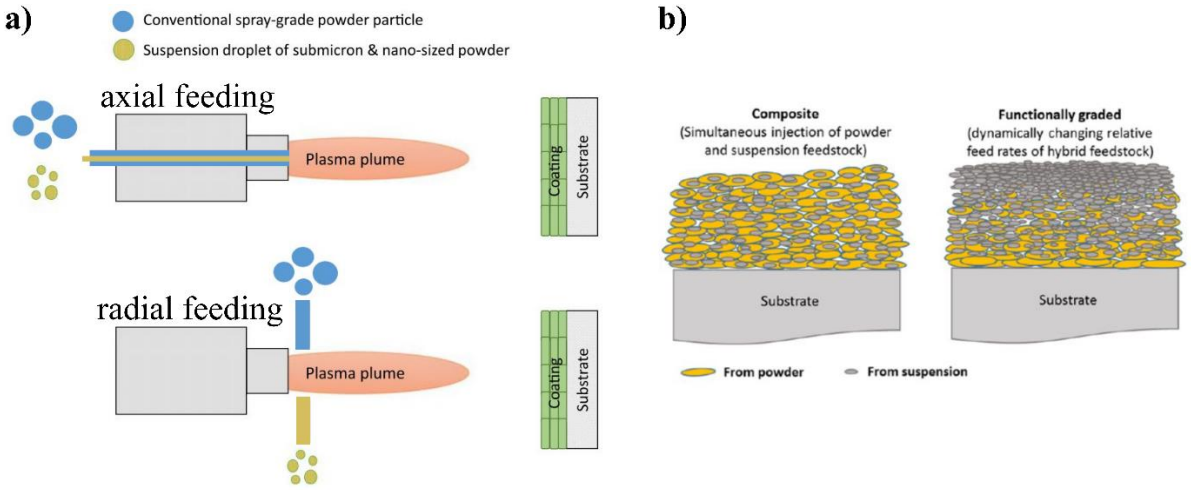

Figure 5. Schematic of a) hybrid spraying using axial and radial feeding configurations, b) examples of hybrid coatings microstructures – homogeneous intermixed composite and functionally graded. According to [41].

2 Deposition process

Since the thesis is primarily focused on suspension and solution precursor plasma spraying, the liquid feedstocks will be prioritized in the following literature review.

2.1 Plasma jet-liquid interaction

After penetration into the plasma jet, the liquid is fragmented into fine droplets, i.e., undergoes so-called atomization, and begins to absorb heat from the jet. According to estimation in [7], the time of fragmentation is approximately 3 orders of magnitude shorter than the time of vaporization. In other words, the injected liquid is first atomized into fine droplets before the solvent is fully evaporated. However, it has to be pointed out that these processes are not independent and that, e.g., smaller droplet size results in significantly shorter vaporization time.

The atomization is finished when equilibrium is reached between plasma shear forces exerted onto the droplet which cause its fragmentation, and the liquid surface tension forces which keep its integrity [7]. The final size of the droplets is governed by multiple factors, namely plasma gas parameters (density ρ_g, velocity v_g) and liquid properties (density ρ_l, velocity v_l, dynamic viscosity η_l, surface tension σ_l), and may be estimated following the Equation 2 as

$$d_{min} = \frac{8\sigma_l}{C_D \rho_g V^2}, \tag{2}$$

where C_D is the plasma drag coefficient according to [45] and V is the velocity difference between plasma gas and liquid.

Experimentally, liquid atomization may be observed using the shadowgraphy technique, the example of which is depicted in Fig. 6. The liquid injection and atomization zone in the jet is illuminated by pulsed laser light which is detected by a camera. The liquid stream and droplets penetrating into the jet hinder the illuminating light and are recorded as dark spots (shadows). Such atomization observation may give a hint on the coating formation as e.g., low degree of atomization (i.e., large droplets) or large liquid stream divergence (compare Fig. 6a and 6c) may lead to the embedding of unprocessed feedstock or overspray material into the coating [46].

The shadowgraphic observation is also particularly useful for regulation of the liquid injection velocity or observation of the liquid breakup under different feeding angles (Fig. 6) in the case of the radial feeding configuration. Optimal injection velocity is essential in order to attain liquid penetration into the plasma jet so that the liquid travels close to the plasma jet axis, i.e., in the hottest zone and is therefore thoroughly heated. Contrarily, injection velocity too low would lead to rebounding of the liquid from the jet, and injection velocity too high would lead to overshooting the liquid through the jet, thereby compromising deposition efficiency. Technically, the control of the liquid injection velocity is done by regulating the feeding pressure in the liquid feeding tank (in case of pressure-based-systems) or by regulating the rotational speed of the peristaltic pump (in case of peristaltic-based-systems) [18]. By regulation of the liquid injection velocity for optimal jet penetration, the feeding rate (FR) of the liquid becomes the dependent variable and is measured after achieving the optimal feeding condition. During the deposition, the continuous online feed rate monitoring may be used to detect possible flaws in the process as an unexpected drop in the FR may indicate instabilities such as partial clogging of the feeding system.

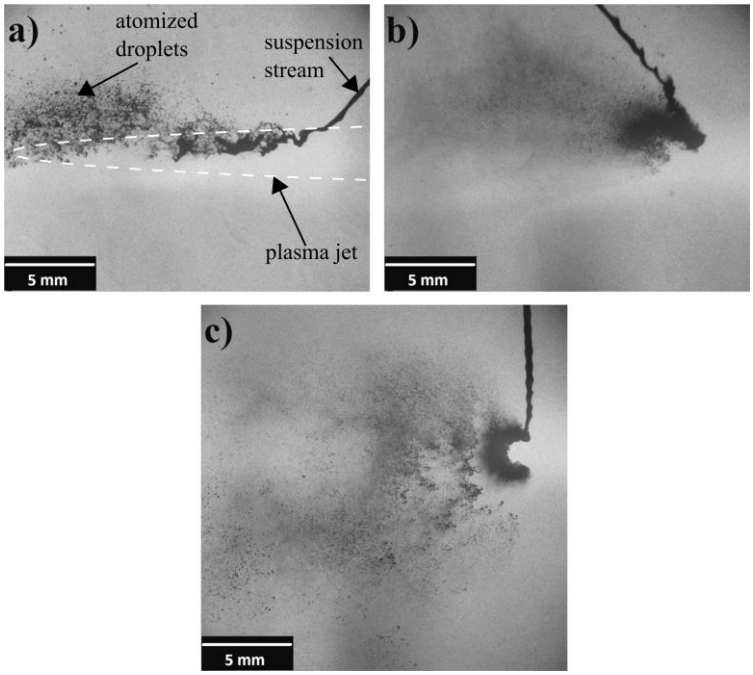

Figure 6. Shadowgraphy images of suspension penetration into the WSP-H plasma jet for different injection angles – a) positive inclination, b) negative inclination, c) perpendicular injection. According to [37].

Along with the atomization phase, liquid heating and vaporization takes place (Fig. 7). In case of the suspensions, the fine powder is exposed to the plasma jet. Each suspension droplet typically contains larger amount of powder particles, which are brought together by the solvent evaporation and melted, forming droplets of melt generally larger than the particle size of the original dispersed powder [47]. Nevertheless, the melt droplets originating from suspensions are several orders of magnitude smaller than those from coarse powders. Therefore, such fine melt particles may suffer from overheating and excessive evaporation of the melt if the heat input from the plasma is too high with respect to the size of the suspension droplet. Such evaporation is usually undesirable as it leads to the loss of the deposited material, thereby lowering the achievable deposition efficiency, or even to unwanted condensation of the vaporized phase elsewhere on the coated component or even on the spraying equipment [48]. Contrarily, in case of an insufficient heat input into the suspension droplet, unmelted powder particles may be retained throughout the in-flight stage and deposited onto the substrate in the form of dried clusters of primary powder [49]. In such case, the deposit may become very loose and may be easily damaged mechanically or even washed away with a stream of water.

In case of spraying of solution of precursor(s), evaporation of the solvent results in saturation of the solution concentration followed by precipitation (crystallization) of the solute. Schematic depiction of the process is in Fig. 7b. The precipitation usually begins at the surface of the liquid droplet where the solvent is vaporized because the solute diffusion within the droplet is not rapid enough to balance out the its concentration gradient [33]. After the precipitation, the precursor usually undergoes thermal decomposition or other chemical reactions. Ultimately, the final products are melted and deposited analogously to the suspension route. In-flight melt vaporization may take place as well as in the suspension case. Contrarily, insufficient heat treatment of the solution results in unfinished precipitation and/or decomposition of the precursors, which may be eventually incorporated into the coating. Subsequently, these

precursors may undergo the remaining transformation steps (e.g., calcination) directly on the substrate surface, which may in turn affect the final coating microstructure and properties [50, 51].

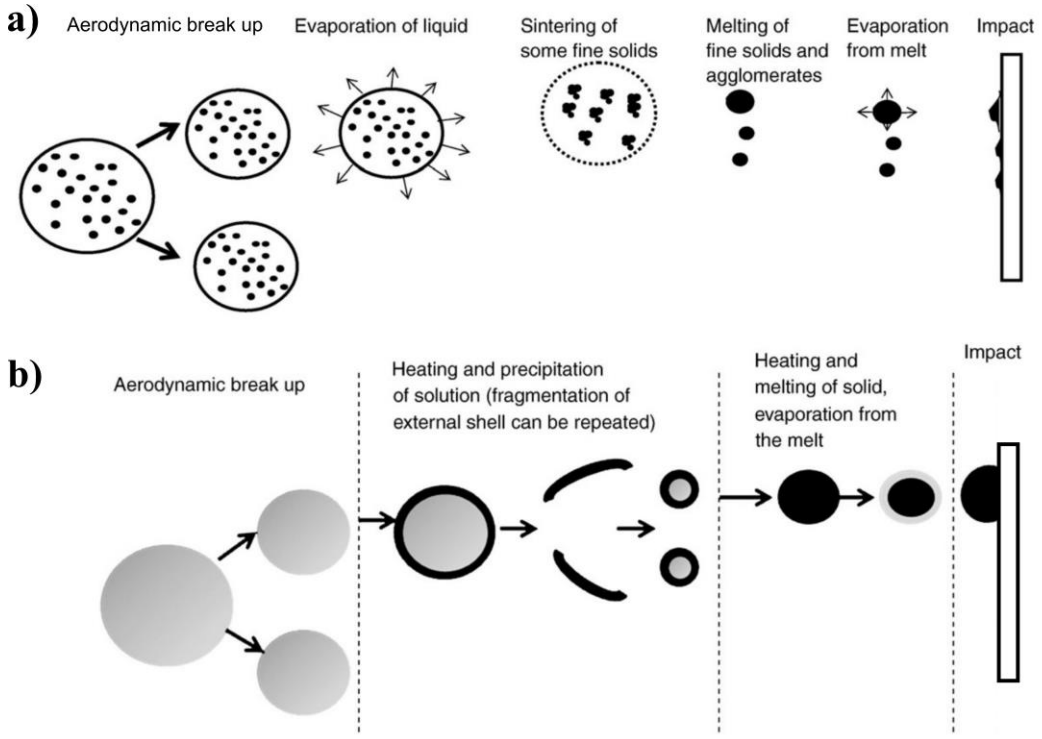

Figure 7. Liquid feedstock droplet atomization and vaporization during the in-flight stage, a) suspension, b) solution. According to [18].

2.2 Impingement onto substrate

The melt droplets arrive at the substrate surface, flatten out, and are cooled down rapidly under the rate of 10^8 K·s^{-1} [52, 53]. Such extreme cooling rates significantly influence the formation of the coatings, e.g., result in the formation of metastable crystallographic phases or in the buildup of high cooling stresses [22, 54].

Regarding the suspension and solution sprayed fine droplets, their low mass and inertia are responsible for the unique coating deposition mechanisms when compared to conventional deposition of powders. Generally, particles large enough retain their trajectory acquired in the plasma jet and impinge perpendicularly onto the surface, forming the rather conventional lamellar coating microstructure (Fig. 8a, 8c) similar to powder-sprayed coatings (cf. Fig. 4d), but with significantly reduced splat size. However, if the particles are very fine (e.g., diameter of few micrometers), they tend to follow the diverging gas streams flowing along the substrate surface (i.e., parallel to the surface) and impinge sideways on the surface asperities (Fig. 8a, 8b) [55]. This so-called shadowing mechanism of deposition became an accepted explanation to the formation of the columnar (or feathery or cauliflower-like) microstructure (Fig. 8d) [56]. Please note that this mechanism was proposed based on coating microstructures deposited using gas-stabilized plasma torches. As mentioned earlier, the plasma parameters of the WSP-H torch used for deposition experiments within this thesis differ considerably from those of GSP torches and thus may affect the above-described buildup mechanism. Therefore, the

elaboration on the coating formation mechanisms will be one of the topics of the experimental work carried out herein.

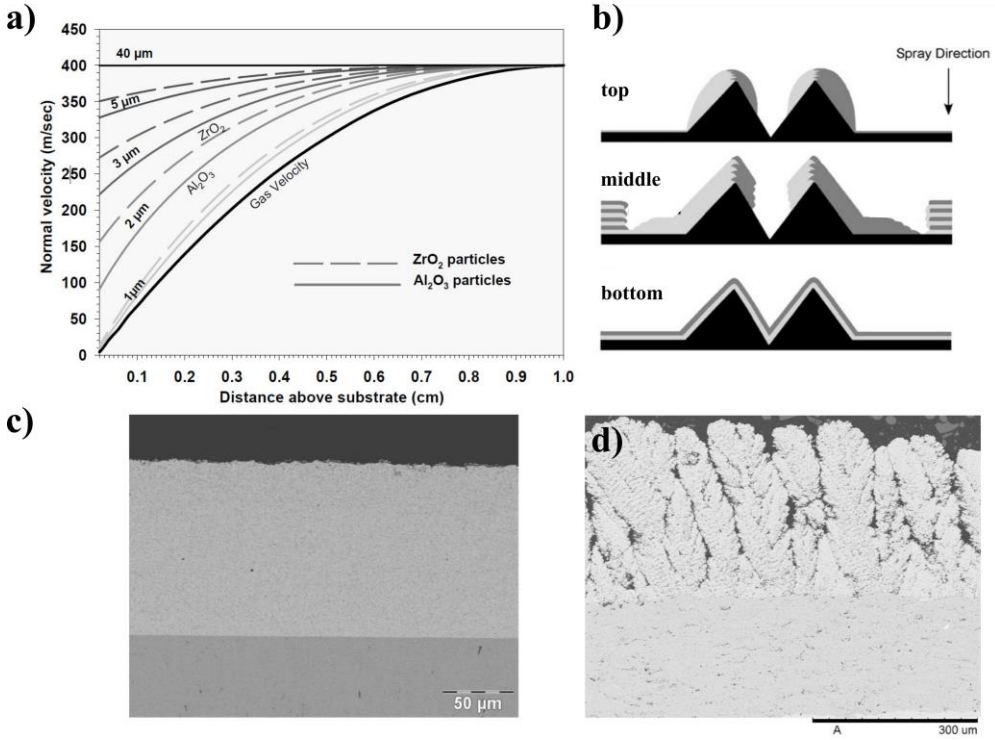

Figure 8. a) numerical computation of particles trajectories according to particle size [55], b) top – deposition of fine particles according to the shadowing mechanism, middle – combined deposition mechanism of mid-sized particles, bottom – conventional layered deposition of large particles [56], c) cross-section of dense microstructure YSZ coating [57], d) cross-section of columnar microstructure YSZ coating [58].

3 Aluminum oxide as a thermal spray material

Aluminum oxide (Al_2O_3, alumina) is generally one of the most important engineering ceramic materials owing to its functional properties (mechanical, chemical, electrical), wide availability, and affordable costs. Typically, aluminum oxide is processed using pressing and sintering methods of powders [59] but is also commonly deposited by thermal spraying from conventional coarse powders. In this thesis, aluminum oxide was used as a baseline material to explore its applicability for plasma spray deposition from liquid feedstocks using the hybrid water-stabilized plasma torch. The following chapter gives a brief overview of alumina features and its characteristics when used as a PS feedstock.

3.1 Properties of Al_2O_3 in Plasma Spraying

Aluminum oxide is a chemically very stable material up to high temperatures close to its melting point (T_m = 2045 °C, [60]). It is practically insoluble in water, organic solvents (e.g., ethanol, methanol), mineral acids, and strong alkali [61]. Also, alumina properties include high hardness, wear resistance, and high breakdown voltage. As a result, Al_2O_3 is typically used as a wear-resistant, corrosion-resistant barrier up to high temperatures, or as a substrate for electronic components [62–64].

Aluminum oxide crystallizes in multiple crystallographic configurations (polymorphs), selection of which is displayed in Table 2. The most employed one is the α-phase (corundum) which possesses the most favorable physical and chemical properties (e.g. hardness and chemical inertness). The α-phase has rhombohedral lattice and is stable up to the melting point. The α-phase crystallizes from the melt at low cooling rates (in the range 1 – 100 $K \cdot s^{-1}$ [65]) or is formed from the other crystallographic phases when they are heated above α-phase recrystallization temperature of approximately 1100 °C [66]. The other (metastable) phases are formed during e.g., chemical processes used for alumina nanopowders production, or under specific thermal conditions during melt solidification such as high cooling rates [65].

Table 2. Alumina polymorphs typically found in PS coatings. [60]

Phase	Crystal lattice	Density ($g.cm^{-3}$)
α-phase	Trigonal*	3.97
γ-phase	Cubic	3.42
δ-phase	Tetragonal	3.40

* often listed also as hexagonal or rhombohedral.

During thermal spraying, high cooling rates of the melt often take place and thus large amounts of metastable phases are found within the coatings. Therefore, majority of the sprayed alumina coatings is typically comprised of γ-phase, δ-phase, and amorphous phase [35, 54].

Numerous studies were devoted to identify the factors that influence the phase composition and namely the formation of the desirable α-phase in thermally sprayed coatings. Possibly, the easiest way to obtain a coating comprising the α-phase is maintaining high substrate temperature during the deposition in order to decrease the cooling rate of the splats which would, in turn, favor the formation of the stable phase. However, this approach may be infeasible due to the substrate material temperature limitations (e.g., increased surface oxidation, loss of mechanical properties due to annealing or even melting). For the same reason, post-spray annealing of the deposit above the transformation temperature from γ- and δ-phases

to α-phase is problematic. Moreover, the phase transformation from γ to α is accompanied by an increase in the density of the solid deposit (see in Table 2), leading to its volumetric shrinkage, increase in porosity, and possible cracking [67, 68].

Alternatively, retention of the unmelted particle core of the original α-phase feedstock was proposed in order to obtain higher amount of the α-phase. By incomplete melting of the powder particles, the unmelted particle cores were expected to serve as the nucleation sites for the melt [54]. However, partial feedstock melting is difficult to control from the technological point of view as a narrow processing window has to be found between full and insufficient feedstock melting. Also, partially melted particles suffer from poor flattening upon impingement onto the surface, thus resulting in inferior coating quality.

Other strategies include e.g., adding of α-phase stabilizing agents to the feedstock, such as Cr_2O_3 (chromia, eskolaite), which has the same rhombohedrical lattice as α-alumina [35]. Using mechanical mixture of powders, the chromia splats may serve as heteronucleation sites for epitaxial growth of α-alumina in the splats deposited thereon. This approach, however, suffers from the insufficient contact between individual splats, thus limiting the number of available α-phase nucleation sites. Alternatively, the prealloyed alumina-chromia powder may be used as chromia and alumina are mutually fully soluble in the melt and crystallize in the form of $(Al,Cr)_2O_3$ mixed oxide having the crystal configuration of corundum. In this case, the high cooling rates of splats during plasma spray deposition are beneficial to mitigate the separation of the two oxides as they exhibit a miscibility gap for specific concentration range during cooling to room temperature (see phase diagram in Fig. 9) [69, 70].

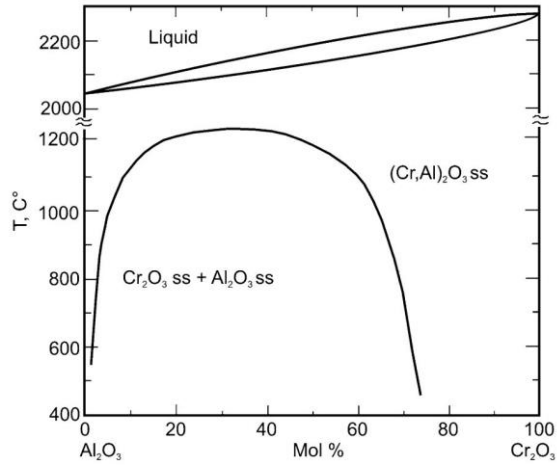

Figure 9. Phase diagram of Al_2O_3 and Cr_2O_3. [20]

3.2 Application of PS alumina

Stemming from its mechanical and chemical properties, alumina is applied in various fields of industry. Most often, it is used for increasing abrasion and erosion wear resistance of metallic components, such as pistons or valves, or as high-temperature corrosion protection for heating elements in furnaces or steam pipes and walls in coal-fired boilers [1, 62]. Furthermore, certain applications make use of intermixing alumina with other oxides, e.g., chromia or titania, for modification of the coating's functional performance [63, 71].

One of the more specific fields employing alumina coatings is paper and pulp industry, where mechanical resistance, chemical inertness, and high dielectric strength are required. An

example application is corona rolls which are used for polyethylene treatment to activate its surface and improve adhesion of the printing ink [2]. Such rolls can have a typical diameter of 250-500 mm, length of up to 5000 mm and, based on the required breakdown voltage, the alumina coatings applied thereon can be 2 mm thick. As mentioned earlier, the plasma-sprayed alumina is predominantly in the γ-phase which is hygroscopic and the absorption of water adversely affects the material's dielectric constant [72]. Therefore, the development of fast and cost-effective method of coatings production with higher α-phase content is of direct application interest.

Another example of large-scale alumina coatings application are the discharge tubes for ozone production which is used for oxidative degradation of hazardous chemicals, in water purification, or for waste water treatment (Fig. 10). In order to increase the ozone yield, high permittivity of the dielectric coating is required [73]. In this case, dense coatings (i.e., low porosity) are required in order to attain high dielectric strength of the separating layer deposited onto the supporting glass tube.

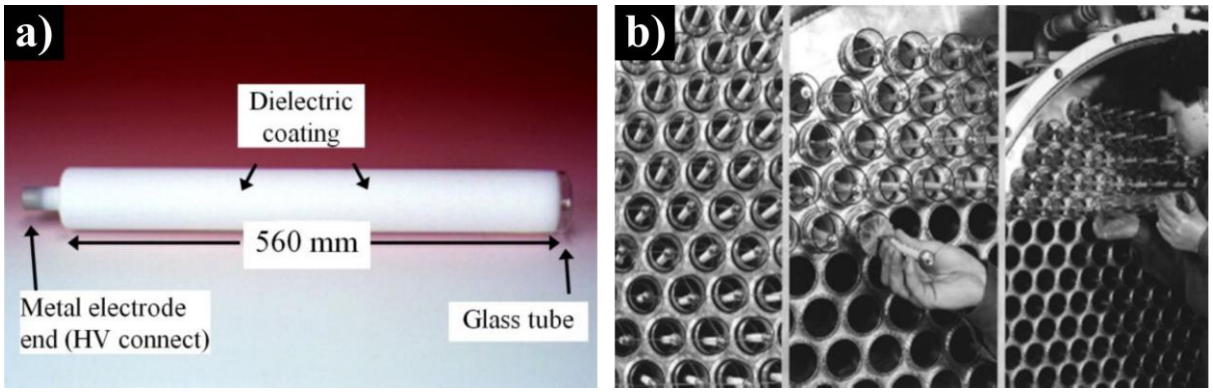

Figure 10. a) single ozonizer tube, b) ozonizer tube array in a reactor. [73]

Objectives of the thesis

Suspension and solution plasma spraying is an innovative method to deposit protective or functional layers utilizing high-temperature plasma stream, building upon the conventional plasma spray deposition of dry coarse powders which is an established and industrially-employed method of coatings fabrication. The introductory part of the thesis presented an overview of the state-of-the-art knowledge regarding liquid feedstock plasma spraying to provide the background to the experimental work carried out within the scope of the thesis. Aluminum oxide was selected as the fundamental material for the liquid feedstock plasma spraying methodology developed within the scope of this doctoral thesis as it has been used within the thermal spraying industry for several decades in the form of dry coarse powders; providing broad scientific and technological knowledge to be compared with the newly developed processes and coatings. The objectives of this thesis are summarized as follows:

1. Development and characterization of suspensions and solutions suitable for thermal spraying and establishment of methodology for the deposition of coatings therefrom, using the hybrid WSP-H plasma torch.
2. Characterization of coating properties with respect to the feedstock formulation and deposition conditions in order to understand the factors affecting the coating character, buildup mechanisms, and resulting properties, eventually allowing further control of the functional performance of the coatings.
3. Preparation of coatings combining aluminum and chromium oxides in order to prepare multimaterial coatings aiming to increase the α-phase content by means of various feedstock modification, namely by intermixing of suspensions of fine powders and solutions of different precursors (intermixed feedstock concept), and by employing simultaneous deposition of suspensions and dry coarse powders (hybrid concept). Study of coatings formation with respect to the different degree of materials intermixing stemming from the feedstock formulation and different particle sizes. Evaluation of how the oxides intermixing affects microstructure, phase composition, and functional properties of the deposits.

4 Samples Preparation and Characterization Methods

The following chapter presents a brief overview of methods employed in preparation and characterization of the plasma sprayed coatings. For details specific to the carried out experiments, the reader is kindly referred to the original research articles included in Section 5.

4.1 Plasma Spray Deposition

Suspension Preparation and Feeding

For the deposition of the coatings, both commercial ready-to-spray and custom in-house-made feedstocks were used. The pre-deposition preparation of the purchased ready-to-spray suspensions comprised mechanical agitation of the slurry in order to re-disperse and homogenize the powder in the solvent. This was done using a cylindrical mill, onto which the suspension container was placed and let roll for several tens of minutes. If necessary, ceramic beads were put into the suspension to help break larger powder agglomerates during milling (Fig. 11a).

The in-house-made feedstocks were both suspensions and solutions. The suspensions were prepared by mixing of the fine powder with the selected solvent (demineralized water, absolute ethanol, or their mixture) and with a dispersing and stabilizing agent. The formulation of the suspensions was optimized prior to the deposition for the highest sedimentation resistance of the suspension by varying the solid load and stabilizer contents. Pre-deposition agitation of the custom suspensions was carried out identically to the commercial ones.

Preparation of the precursor solutions was carried out by dissolving of the crystalline precursors in demineralized water in preselected concentration of the solute.

The feedstocks were delivered into the plasma jet from a custom-built pressure-based liquid feeder initially developed within the scope of [74]. The feeder is equipped with feed rate monitoring and magnetic mechanical agitation to prevent sedimentation of the feedstocks in case of a long spraying run (Fig. 11b). The liquid is delivered into the plasma jet from the feeding tank through feeding hoses and an injection nozzle which is a precise orifice (diameter of 0.35 mm) laser-cut in a small sapphire block, providing a narrow laminar stream of the liquid. Injection velocity, and thus the feeding rate of the liquid stream is controlled by adjustment of the pressure in the feeding tank. The feeder is also equipped with a secondary vessel for storage and feeding of a pure solvent which is fed into the jet during the cooling periods during spraying (see further) to maintain cooling and prevent clogging of the injection nozzle.

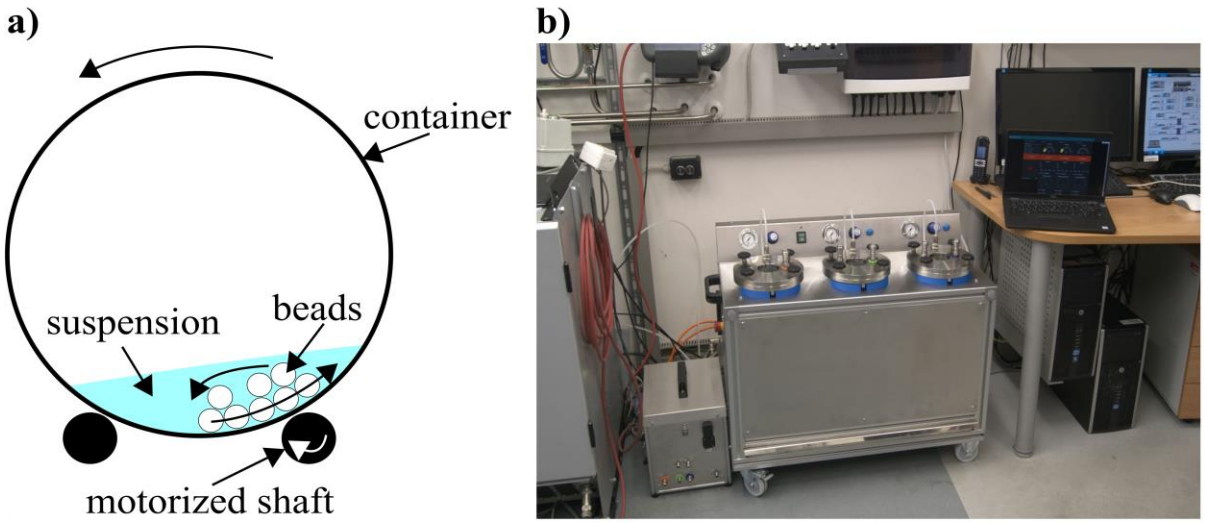

Figure 11. a) scheme of suspension agitation in a cylindrical mill, b) custom-build liquid feedstock feeder in the sprayshop control room.

Spraying

The deposition of the coatings was carried out using the hybrid water-stabilized plasma torch WSP-H 500 (ProjectSoft HK, a.s., Czechia) mounted to a programmable industrial robotic arm, which ensures repeatability of the torch trajectory with respect to the coated substrates and eliminates the possible inaccuracy of manual torch operation. As described in Section 1.1, WSP-H torch produces high enthalpy plasma and, therefore, usage of this torch comes with several specifics usually not encountered when using more common gas-stabilized torches.

Figure 12a shows the configuration of liquid and powder injectors on the body of the WSP-H plasma torch. All three injector tubes offer independent linear movement along the jet axis to allow the adjustment of the feeding distance, as well as axial swiveling to enable precise aiming of the feedstock into the center of the plasma jet. In Fig. 12b, the running torch with engaged powder feeding is depicted.

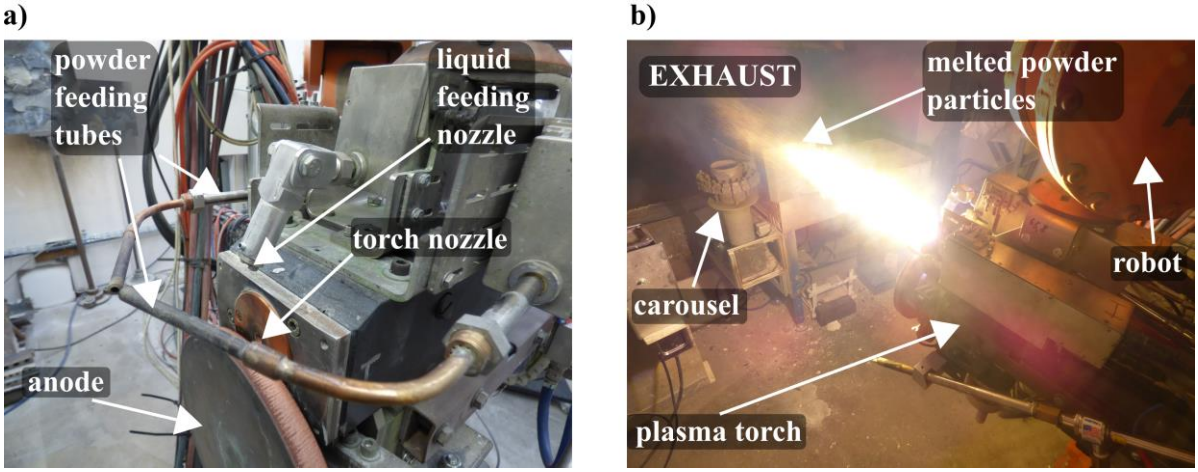

Figure 12. a) photo of torch front end with feedstock feeding lines, b) torch in operation with engaged powder feeding.

Due to the extreme thermal load imposed onto the substrates, the deposition routine consists of several so-called spraying cycles which typically involve three up and down torch strokes in front of the revolving carousel with attached-on substrates (Fig. 13). The spraying cycles are alternated with cooling periods during which the torch is moved away from the substrates. The up and down torch movement in a spraying cycle is harmonized with the revolution speed of the carousel in order to ensure even deposit coverage of the samples. A simplified representation of the torch movement over the covered area – cylindrical surface flattened to a plane figure – is depicted in Fig. 13a; in-scale 3D representation of the covered area is shown in Fig. 13b.

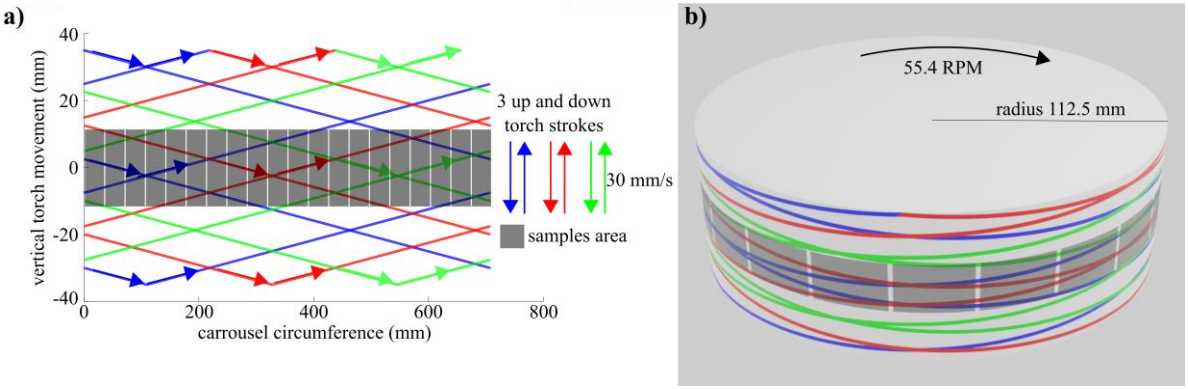

Figure 13. a) plane representation of the torch-covered area of the revolving carousel during three up and down torch moves, b) in-scale 3D representation of the carousel coverage.

The revolving carousel is capable of holding 20 pieces of substrates of various sizes and geometries. Typically, steel rectangles ($20 \times 30 \times 2.5$ mm^3) or discs (diameter of 25 mm, thickness 1 - 6 mm) were used for sample coating deposition. During the spraying, the sample temperature (as measured by a K-type thermocouple on the back side of the samples) rises by several hundred degrees centigrade; typically, from 200 – 300 °C to about 400 – 500 °C. Therefore, the carousel with substrates is intensively cooled using compressed air blown through multiple air knives attached to a fixture located sideways from the carousel (Fig. 14). The air cooling helps to prevent excessive sample temperature increase during one spraying cycle, shortens the time necessary for cooling down to the preselected interpass temperature, and also helps to remove the loose and soft overspray deposit which could be responsible for the development of interpass porosity.

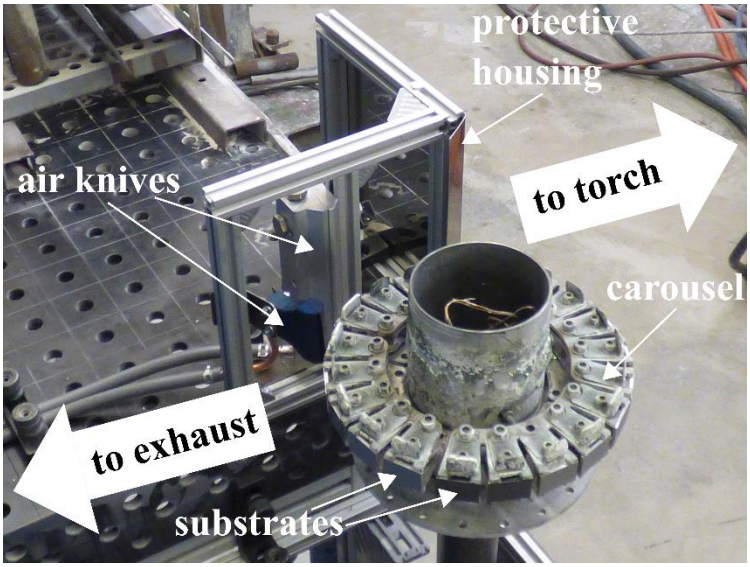

Figure 14. Carousel with substrates and air knives.

4.2 Microstructure analysis

Metallography

In order to observe the microstructure of the coatings, metallographic cross-sections of the samples were prepared. Substrates with coatings were cut using precision metallographic saw, vacuum embedded in low-viscosity epoxy resin, and polished using a semi-automatic polishing machine. For the most fragile samples, epoxy resin pre-embedding was used first prior to cutting to prevent formation of artifacts.

Scanning Electron Microscopy

The polished cross-sections or as-sprayed free-surfaces of the coatings were routinely observed using a scanning electron microscope (SEM) EVO MA 15 (Carl Zeiss, Germany). Predominantly, the back-scattered electrons (BSE) detection regime was used, as it is capable of visualizing the differences in local mean atomic number in the sample via different shades of grey of the acquired image, thus enabling the observation of chemically different phases within the coatings and porosity without imaging artifacts. The topography of the as-sprayed coatings free surfaces was observed also using the topographic secondary electron (SE) detection. In all cases, the low vacuum observation was maintained in order to prevent charge buildup on the non-conductive ceramic coating samples without the necessity of gold-sputtering of the samples prior to the observation.

Thickness and Porosity Evaluation

The SEM micrographs were used to evaluate the coatings thickness and porosity using image analysis (IA). In order to standardize the procedure for all samples, a semi-automated Octave/Matlab script was developed by the author. Using this tool, the micrograph is binarized, the interfaces between epoxy-coating and coating-substrate are found, and the coating thickness is measured at 20 equidistant points. The mean thickness and standard deviation are then calculated. Schematic description of the process is shown in Fig. 15.

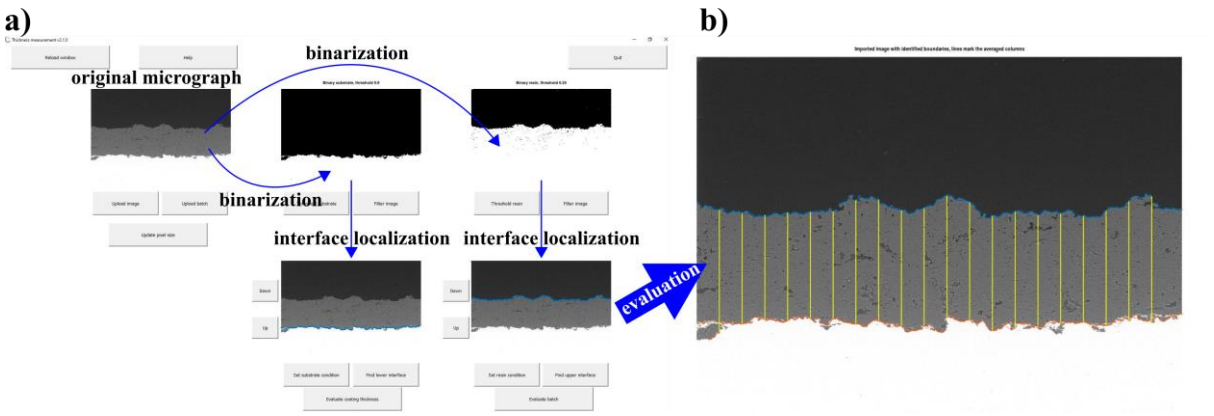

Figure 15. a) screenshot of IA tool for thickness analysis, b) original SEM micrograph with identified interfaces and equidistant points used for mean thickness evaluation.

For the evaluation of coating porosity, IA of cross-section micrographs was used. A procedure inspired by [8] employing two sets of micrographs at two nominal magnifications was established in order to take into account both fine sub-micrometric porosity typical for liquid-sprayed coatings, and also larger pores and cracks typical for coarse-powder-based coatings. Usually, nominal magnification between 3000 x to 5000 x was used for the detection of fine porosity and nominal magnification between 300 x to 500 x was used for evaluation of the coarse porosity. Schematically, the process of porosity evaluation is depicted in Fig. 16. Both high and low magnification cross-section micrographs were binarized. In the high magnification images, large pores exceeding a preset area value were filtered out and vice versa for the low magnification images in order to obtain two disjunctive domains for fine and coarse porosity. The sum of both values represents the total porosity of a coating.

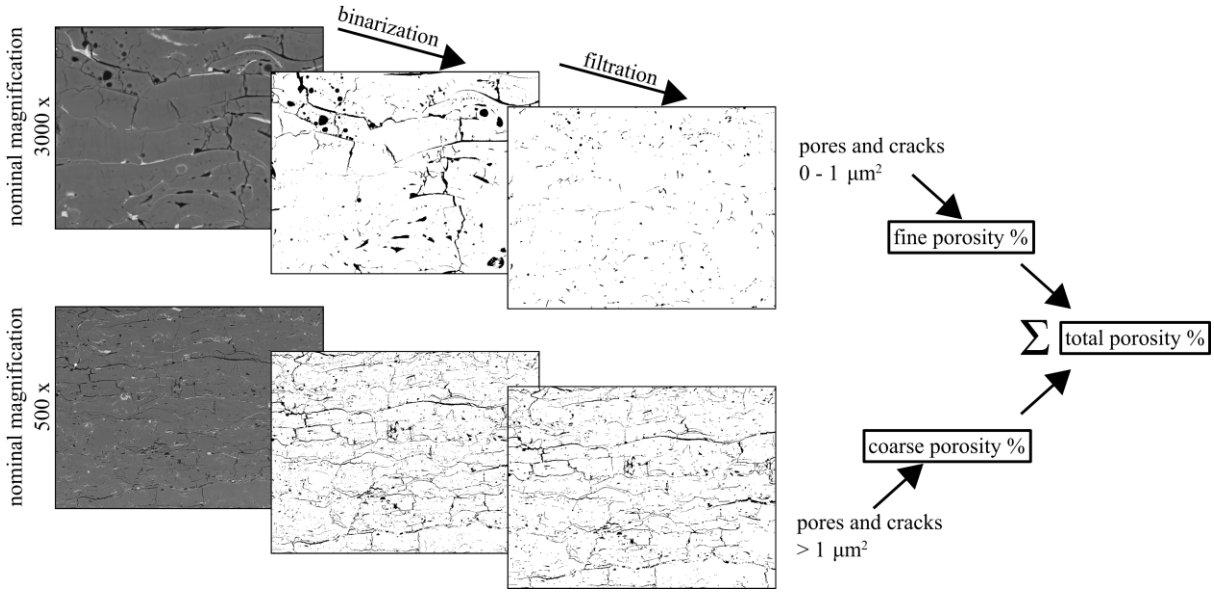

Figure 16. Porosity evaluation of a hybrid coating microstructure using two sets of micrographs.

4.3 Phase and Chemical Composition

X-ray Diffraction

The phase composition of the coatings was studied using primarily the X-ray diffraction (XRD). The diffraction patters were acquired from the free surface of as-sprayed coating samples using a D8 Discover diffractometer (Bruker, Germany) with 1D detector LynxEye, Cu K_α radiation, using Bragg-Brentano configuration. The diffraction patterns were then analyzed via the Rietveld refinement method [75] using Topas V5 software for both qualitative and quantitative evaluation of the sample's phase composition and phases' crystallographic parameters, such as crystalline size (i.e., coherently diffracting domains' (CDD) size) and lattice parameters sizes.

Nuclear Magnetic Resonance

The phase composition of the samples was also analyzed by ^{27}Al nuclear magnetic resonance (NMR) with 14 kHz magic angle spinning (MAS) using Bruker Avance III HD spectrometer. Unlike XRD, the NMR is able to distinguish the coordination of the Al atoms by O atoms, which is in the case of α-Al_2O_3 fully octahedral, while in the case of γ-Al_2O_3, there are octahedral and tetrahedral Al sites in the ratio of 3:1 [76], thereby distinguishing the two polymorphs. This method was used as a complimentary technique for the verification of the XRD results, For the NMR analysis, the coatings were stripped off of the substrates and ground to fine powder.

X-ray Fluorescence

Chemical analysis of the alumina-chromia coatings was analyzed using energy-dispersive X-ray Fluorescence (EDXRF) spectrometer S2 PUMA (Bruker, Germany) equipped with HighSense LE SDD detector.

4.4 Mechanical properties

Hardness

Hardness of the selected coatings was determined from the polished coating cross-sections according to ASTM C1327-08 standard using Vickers indenter. For the finely structured suspension-sprayed coatings, indentation load of 300 g was used. For the hybrid coatings, loads of 300 g and 1000 g were used, with dwell time of 10 s in all cases. Due to the brittle nature of the coatings, high hardness (i.e., small indents), and poor contrast of the indents in the light microscope of the hardness tester, the indents were photographed in SEM for the evaluation of their sizes and calculation of the hardness values.

Wear Resistance

Wear resistance of selected coatings was evaluated using a slurry abrasion resistance (SAR) method according to ASTM G-75 standard, and using a pin-on-disc (POD) method according to ASTM G99-05 standard. For the SAR test, samples were cut to match the footprint size of 10 x 24.5 mm^2 and the coatings' free surface was left in as-sprayed condition. For the POD test, the coating free surface was ground and polished down to 1 μm diamond suspension. After the tests, the wear resistance was evaluated in terms of the wear coefficient k = mm^3/Nm; the POD test provided also the coefficient of friction (COF) value.

Tensile Adhesion Strength

The adhesion-cohesion strength of the developed coatings was evaluated according to a modified ASTM C633-13 standard using a universal mechanical testing machine Instron 1362 (Instron, UK). For the test, coating samples were glued in between two steel cylinders using FM-1000 adhesive film (Cytec Industries Inc., USA, following a procedure [77]) and attached to the testing machine. The coating was then loaded by a constant-speed cross-head travel of 0.5 mm/min until rupture.

5 Collection of Papers

The following section presents the experimental work carried out within the scope of the thesis in the form of four core papers which were published in the impacted journals. Using the scheme in Fig. 17, one can overview the experimental roadmap to acquire the "big picture" before reading the individual papers. Each paper represents an individual step in the development of plasma sprayed alumina-based coatings; in Fig. 17, these are represented by the blue ovals. Within Fig. 17, the key goals of each paper are highlighted in red boxes, experimental content is highlighted in orange, and main outcomes are in green.

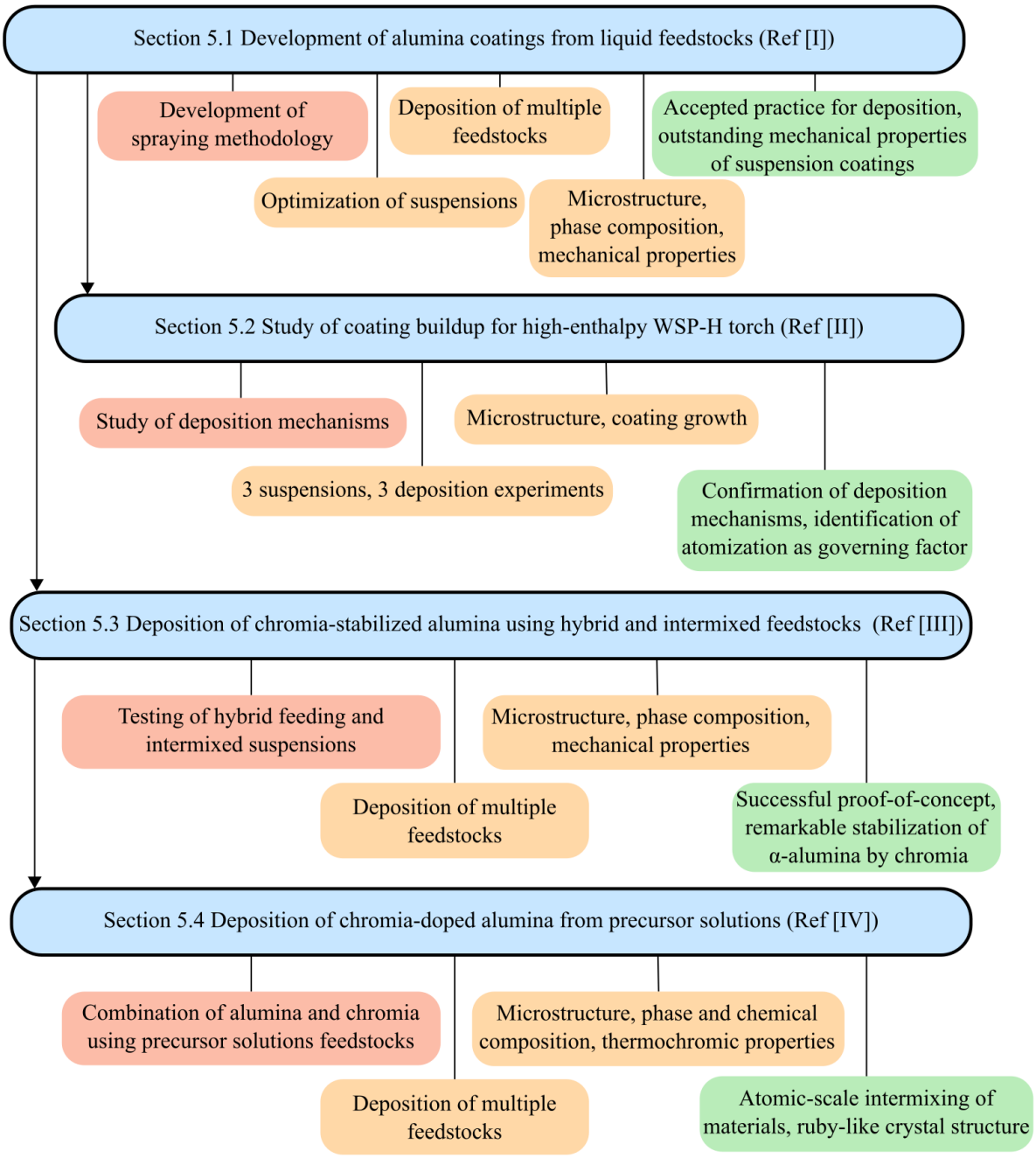

Figure 17. Flowchart of case studies carried out within the thesis.

In the first study [I], the initial experiences with alumina coatings deposition from liquid feedstocks were gathered, including the formulation of suspensions and solutions prior to the deposition and subsequent coating evaluation. The following study [II] elaborated on the deposition mechanisms leading to the formation of different coating microstructure types depending on the starting feedstock suspensions. The third and fourth studies [III, IV] built on the knowledge collected in [I] and focused on the deposition of alumina intermixed with chromia using multitude of feedstock combinations, including intermixed suspensions, precursor solutions and hybrid deposition, in order to study their mutual interactions and the ability to increase the amount of the corundum phase in the as-sprayed coatings.

5.1 Development of alumina coatings from liquid feedstocks

Based on the long-term tradition of alumina deposition from coarse powders at IPP, it was decided to attempt preparation of alumina coatings using liquid feedstocks. For the task, the hybrid water-stabilized plasma torch WSP-H 500 was used as it is capable of high-throughput powder spraying and was expected to deliver the high-enthalpy plasma necessary for successful liquid-feedstock deposition. The first attempts are dated back to the author's Research project [78], where nanometric alumina powder was used for formulation of ethanol-based suspension and sprayed. The resulting deposit was, however, very soft and brittle. The microscopic evaluation revealed that it mostly comprised of feathery-like structures which probably originated as redeposited condensate of feedstock material evaporated due to overheating of the fine particles. Based on this experiment, a more systematic approach was carried out for further development of alumina-based coatings from liquid feedstocks, presented in [I].

The fact that feedstock formulation may decisively influence the resulting coating microstructure has been reported in the literature. Therefore, it was decided to carry out a mapping of multiple feedstocks and deposit coatings therefrom. In order to do that, first feedstocks were developed in-house using multiple powder granulometries, solid load concentrations, solvent types, and stabilizing additive concentrations. Following the feedstock optimization study, suspensions of 300 nm nominal particle size powder dispersed in water and ethanol in 10 and 20 wt.% concentrations were used for deposition. For comparison, a commercial ready-to-spray water-based alumina suspension was used along with the custom-made ones. In order to evaluate the influence of the deposition parameters on the coating microstructure, feeding distance was varied for the ready-to-spray suspension. Also, a water-based aluminum nitrate solution was used to test the possibility of coating deposition from a solution of a precursor using the WSP-H 500 torch.

Using the multitude of feedstocks, coating microstructures ranging from highly dense, over columnar cauliflower-like to extremely porous were fabricated, thereby confirming the influence of feedstock formulation on the coating microstructure. The densest microstructure (porosity < 10 %) was prepared using the in-house-made ethanol-based suspension while the water-based ready-to-spray suspension produced the porous columnar microstructure. The influence of the feeding distance variation on the coating microstructure was found rather insignificant, thus providing the process robustness favorable for potential industrial application.

Regarding phase composition of the coatings, the metastable γ- and δ-phases were prevalent in the suspension sprayed coatings, as confirmed both by XRD and NMR. To the best of author's

knowledge, this was the first time NMR was used for the analysis of thermally sprayed alumina coatings. The solution sprayed coating contained over 80 wt.% of the α-phase.

Two coatings – the columnar one from water-based commercial suspension and the dense one from ethanol-based custom-made suspension – were selected for evaluation of mechanical properties: hardness, tensile adhesion strength, wet abrasive wear (slurry abrasion response test), and dry sliding wear resistance (pin-on-disc test). It was proved that the highly dense coating showed outstanding performance in all tests; especially the application-relevant values of dry sliding wear resistance and adhesion strength were among the best reported in the literature. This coating also significantly outperformed the conventional powder-sprayed counterparts, providing the evidence that liquid-feedstock plasma spraying with high-enthalpy torches may be the future of high-performance coatings for cutting-edge applications.

Surface & Coatings Technology 325 (2017) 277–288

Contents lists available at ScienceDirect

Surface & Coatings Technology

journal homepage: www.elsevier.com/locate/surfcoat

Development of suspension plasma sprayed alumina coatings with high enthalpy plasma torch

Tomas Tesar [a,*], Radek Musalek [a], Jan Medricky [a], Jiri Kotlan [a], Frantisek Lukac [a], Zdenek Pala [a], Pavel Ctibor [a], Tomas Chraska [a], Sarka Houdkova [b], Vaclav Rimal [c], Nicholas Curry [d]

[a] Institute of Plasma Physics CAS, v.v.i., Department of Materials Engineering, Za Slovankou 3, 182 00 Praha 8, Czech Republic
[b] New Technologies Research Centre, University of West Bohemia, Univerzitni 8, 306 14 Plzen, Czech Republic
[c] Charles University, Faculty of Mathematics and Physics, V Holesovickach 2, 180 00 Praha 8, Czech Republic
[d] Treibacher Industrie AG, Auer-von-Welsbach-Straße 1, 9330 Althofen, Austria

ARTICLE INFO

Article history:
Received 15 March 2017
Revised 14 June 2017
Accepted in revised form 15 June 2017
Available online 16 June 2017

Keywords:
Suspension plasma spraying
Aluminium oxide
Mechanical properties
Hardness
Adhesion
Wear resistance

ABSTRACT

Deposition of aluminium oxide (Al_2O_3) coatings from liquid feedstocks using a high enthalpy hybrid water-stabilized plasma torch was investigated. The entire process included the optimization of spraying parameters using a commercial ready-to-spray suspension, optimization and deposition of custom-made suspensions and one solution and evaluation of mechanical properties of the most durable coatings. Acquired coating microstructures varied from porous with typical columnar morphology to well-sintered dense structures with low porosity. The microstructural features were clearly linked to the feedstock formulation. The most durable coating with the highest density microstructure prepared from ethanol-based suspension showed outstanding mechanical properties, e.g. high values of hardness (up to 1211 HV0.3), tensile adhesion strength (up to 51 MPa) and wear resistance (material removal rate as low as $1.94 \cdot 10^{-5}$ $mm^3 \cdot N^{-1} \cdot m^{-1}$ as measured by pin-on-disc test). Moreover, deposition from a water-based solution of aluminium nitrate resulted in deposition of highly porous coating composed predominantly of stable α-alumina phase.

1. Introduction

Aluminium oxide (Al_2O_3) coatings are commonly used in various applications where good chemical and thermal stability, electric insulation or wear resistance are required [1]. These coatings are usually prepared by atmospheric plasma spraying (APS) technique using coarse powders of typical particle size in tens of micrometers. However, suspension plasma spraying (SPS) has lately gained immense attention since it provides the possibility to prepare finely structured (even nanostructured) coatings with better functional properties than with conventional coating techniques. The main benefit stems from the fact that very fine powders, typically with particle size in tens or hundreds of nanometers, are introduced into the plasma jet in the form of a suspension. After the carrier liquid (solvent) is evaporated, the small melted particles form a coating with structural units in the submicron range [2]. Another added value for alumina spraying is the possible retention of the initial α-phase of the powder and preparation of the desirable α-phase rich coatings [3]. This stable phase is favored for its high hardness and corrosion resistance. Conventional plasma spraying of powders generally leads to coatings with high content of metastable γ and δ phases due to the rapid cooling of the deposited material [4].

The resulting coating microstructure is, however, a function of many variables, such as plasma characteristics (enthalpy, density, velocity, etc.), feedstock properties, and process parameters (standoff distance, feeding distance, feed rate, etc.) to name a few [5]. It may be challenging to find the right set of parameters for a specific application but it also provides desirable potential of variability of the deposition process for the fine tuning of the coating microstructure through modification of the input parameters. The relations between the operating parameters and the coating properties need to be understood to be able to tailor the microstructure for a desired application.

One of the key parameters governing the coating build-up are the properties of selected feedstock, i.e. in the case of SPS it is the suspension concentration (solid load), solvent type, additives, etc. which influence fragmentation of the feedstock in the plasma jet. According to results obtained for gas-stabilized plasma torches [6–8], it is generally assumed that water-based suspensions lead to more compact microstructures whereas alcohol-based ones lead to less dense, porous microstructures. This is usually attributed to the fact that water forms bigger droplets due to the higher surface tension and the resulting particles impinge the surface more perpendicularly and with higher momentum than the smaller ones. However, the bigger droplets with lower degree of atomization

* Corresponding author.
E-mail address: tesar@ipp.cas.cz (T. Tesar).

http://dx.doi.org/10.1016/j.surfcoat.2017.06.039
0257-8972/

may result in the presence of unmelted material embedded in the coating due to insufficient melting of the core of particle or agglomerates [6,9]. If presence of this feature (i.e. untreated feedstock) is not desirable, it may be mitigated by modification of the suspension atomization to yield smaller droplets (e.g. by lowering the liquid surface tension or by pre-atomization of the feedstock before injection into the plasma jet [10]), by choice of the injection point position or torch standoff distance from the workpiece to ensure optimal melting of the powder.

An alternative route of plasma spraying with liquid feedstocks is solution precursor plasma spraying (SPPS), where the deposited material is prepared in-situ from the solution injected into the plasma jet [11–13]. A major benefit of this approach is that the feedstock does not contain any solid particles, which for example eliminates the risk of sedimentation and, in case of a solution of multiple chemicals, the homogenization is significantly facilitated. On the other hand, both SPS and SPPS share the same challenges as compared to the conventional spraying of powders in terms of additional energy consumption due to the solvent evaporation or the relatively low deposition rate achievable as compared to conventional spraying.

The use of a liquid carrier in SPS and SPPS raises the need for high enthalpy plasma source, as substantial amount of heat is required for the processing of the feedstock, i.e. heating and evaporating of the liquid followed by heating and melting of the powder. From this point of view, torches based on water stabilization of plasma (WSP technology) provide a high enthalpy plasma jet, which makes them particularly suitable for preparation of coatings from liquid feedstocks [14,15]. The most recent "hybrid" WSP technology (WSP-H) combines the principles of gas (GSP) and water vortex (WSP) arc stabilization producing plasma jet of relatively low density (about 6.8 $g \cdot m^{-3}$) but high enthalpy (up to 300 $MJ \cdot kg^{-1}$) and high velocity (up to 7000 $m \cdot s^{-1}$) [16,17]. Due to these plasma characteristics, WSP-H torch was proven to be convenient for large-scale coating production due to a high achievable feedstock throughput (more than 100 ml of suspension per minute) combined with high deposition efficiency [15,18].

This paper examines the possibility of suspension plasma spraying of aluminium oxide with WSP-H plasma torch at high feed rate. The entire process is described, including the optimization of suspensions, the deposition of coatings, and the evaluation of mechanical properties of the deposits. The aim of the study was to find suspension formulations suitable for WSP-H spraying, to prepare durable dense coating microstructure with low porosity and possibly high α-phase content, and to compare the coating properties with those of conventional powder-sprayed coating deposited also with WSP-H. Possibility of using WSP-H torch for solution plasma spraying of alumina will also be illustrated on the deposition of coating with extreme porosity (up to 70%).

2. Experimental

Firstly, optimization of the deposition parameters was carried out using a commercial ready-to-spray water-based suspension. Three feeding (injection) distances were tested (19, 25, and 31 mm) in order to evaluate how much this parameter influences the resulting coating microstructure for WSP-H technology. Next, optimization of custom-made suspensions (further denoted as IPP suspensions) was carried out in order to attempt deposition from suspensions of different formulation to possibly obtain various microstructures. Attention was paid to the optimization of suspension formulation in terms of sedimentation stability and viscosity. Two commercially available powders with different particle size distributions were used to formulate both water and ethanol-based suspensions. In the next step, the optimized IPP suspensions were also used for the deposition of coatings. At last, water-based solution of aluminium nitrate nonahydrate was sprayed to test the feasibility of solution precursor plasma spraying of alumina with WSP-H technology.

Microstructure and phase composition of all suspension and solution-sprayed deposits were evaluated. In the last step, mechanical properties including hardness, adhesion/cohesion strength and wear resistance in dry and wet conditions were measured for one selected coating from the commercial suspension and one from the custom-made suspension. Coatings were compared with the coating deposited by WSP-H torch using conventional plasma spraying of coarse dry powder.

2.1. Feedstocks

Commercial ready-to-spray water-based suspension of α-alumina powder ($d_{50} = 2.2$ μm) with 40 wt% solid particle content supplied by Treibacher Industrie AG (Austria) was used for the optimization of the spraying parameters. To formulate the custom-made IPP suspensions, commercial α-alumina submicron-sized powders with nominal particle sizes of 300 and 1000 nm (as designated by manufacturer - Allied High Tech Products, INC, USA) were dispersed with 10 and 20 wt% solid concentrations in water or ethanol solvents. Micrographs of both powders are compared in Fig. 1 revealing partial agglomeration and noticeably bigger particles of the 1000 nm powder. For preparation of the solution, aluminium nitrate nonahydrate $Al(NO_3)_3 \cdot 9H_2O$ (Lach-Ner, s.r.o., Czech Republic) was dissolved in water with the concentration of 5 wt% of aluminium in the solution. For the deposition of the conventional coating, SURPREX AW24 powder was used (Fujimi INC., Japan, granulometry $-75 + 38$ μm).

For the stabilization of the IPP suspensions, BYK-LP C 22587 stabilizer (BYK-GARDNER GmbH, Germany) was used in concentration of 0.5 wt%. Sedimentation resistance of the prepared suspensions with 20 wt% of solid phase was compared to that of the non-stabilized ones. Sedimentation process was monitored using an automated time-lapse camera taking photographs of the suspensions in test tubes regularly over a time period of 4 h. The sedimentation progress was evaluated as the position from the distinguishable sediment-solvent interface to the initial liquid column height.

Viscosity of suspensions selected after the sedimentation evaluation was measured using DV2TLV viscometer (Brookfield, USA) with coaxial cylinder-cylinder geometry. An automated regime was used measuring a sequence of speeds from 10 to 100 and back to 10 RPM with 10 RPM increment (decrement) taking 5 measurements averaged over 2 s at each speed.

2.2. Deposition process and design of experiment

The design of deposition experiments (see Table 1) is reflected also in the experiment code in the form of *XXsolventYY* which comprises of the feeding distance in mm (*XX*), solvent used ("W" for water-based IPP suspensions, "E" for ethanol-based IPP suspension, "Tr" for the commercial water-based Treibacher suspension, and "Sol" for the water-based IPP solution) and solid phase concentration in wt% (*YY*). All other parameters of the deposition were constant for all experiments. The custom made suspensions were prepared by adding the 300 nm nominal particle size powder (see Fig. 1a) and stabilizing agent to the solvent while maintaining continuous mechanical stirring. The mixture was then subjected to one hour long mechanical stirring in a cylindrical mill with a set of ceramic balls to further homogenize the feedstock and disintegrate agglomerates. The solution was prepared by mixing the required amount of $Al(NO_3)_3 \cdot 9H_2O$ (5 wt% of Al in the solution) until completely dissolved.

Conventional coating for benchmarking of mechanical properties was prepared from alumina powder according to the deposition process parameters listed in Table 2. The rather long spraying distance of 380 mm was chosen based on the long term experience with spraying of alumina powders using WSP-H torch as the selected conditions provide a reasonable compromise between the coating porosity and deposition efficiency.

Hybrid water-stabilized torch WSP®-H 500 (ProjectSoft HK a.s., Czech Republic) operated at 500 A (~150 kW) was used for deposition with argon flow of 15 slpm [17]. For all deposition experiments, radial

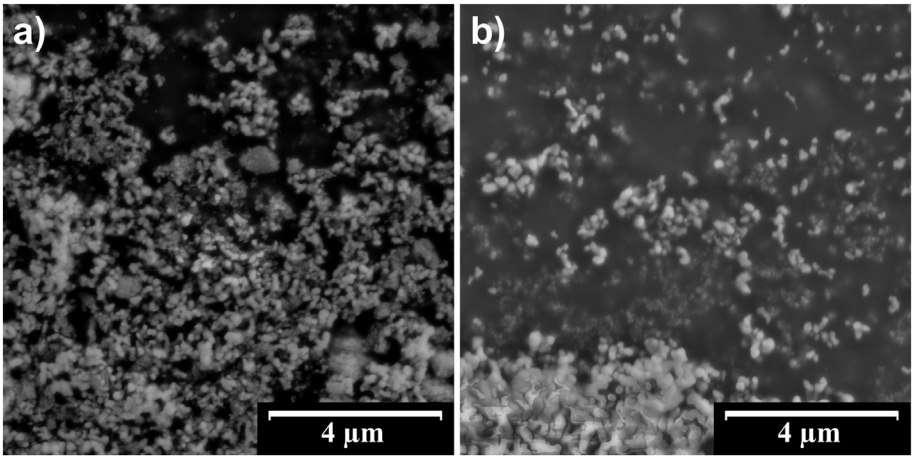

Fig. 1. Micrographs of 300 nm nominal particle size powder (a), and of 1000 nm nominal particle size powder (b).

injection with 100 mm standoff distance (SD) was used. Also, downstream injection was used based on our previous optimization study [18], in this case 65° (see Fig. 2a). In the first optimization stage, feeding distances (FD) of 19, 25, and 31 mm were used with the commercial suspension (see Table 1) in order to explore the sensitivity of the deposition process to this variable. Feeding distance of 25 mm was then selected as a standard value for the spraying of custom-made suspensions and solution.

Substrates for the deposition were manufactured from AISI 304 stainless steel and S235 structural steel in the form of rectangular coupons (dimensions 20 × 30 × 2.5 mm). These were first grit-blasted with alumina grit, then cleaned and degreased in acetone in ultrasound bath and mounted to a rotating carousel (see Fig. 2b) which was cooled by two air knives from the side to reduce the heat build-up on the samples. Prior to the deposition, substrates were preheated with the plasma torch, which moved vertically in front of the carousel. At the preselected substrate temperature of 200 °C, the feedstock injection was started and the coating was deposited directly on the substrates. Each deposition cycle consisted of three "up-and-down" strokes followed by cooling period. The interpass cooling temperature was set to 250 °C. Such deposition cycle was repeated until the preselected number of deposition passes was achieved. For more details on deposition setup please see [15]. The liquids for spraying were fed from a custom-built pneumatic feeder equiped with mechanic stirrer preventing sedimentation of the solid phase. The liquid was injected into the plasma jet as a laminar stream through a calibrated sapphire orifice with internal diameter of 0.35 mm. Feeding pressure adjustment was based on a direct observation of the liquid penetration into the plasma jet using the SprayCam shadowgraphy system (Control Vision, INC, USA) to ensure optimal liquid trajectory along the centerline of the plasma jet.

2.3. Samples characterization

Coated samples were cut by a high-precision metallographic saw (Secotom-50, Struers, Denmark) using diamond blade, mounted in EpoFix epoxy resin (Struers, Denmark) using vacuum impregnation and polished down to 1 μm diamond suspension using automated polishing system (Tegramin-25, Struers, Denmark) following a standardized metallographic procedure. The cross-sections were observed by scanning electron microscope EVO MA 15 (Carl Zeiss SMT, Germany). Micrographs of the cross-sections were used to evaluate the average thickness of the deposits from 9 equidistant points. The average porosity was evaluated by image analysis (IA) from 8 micrographs at 500× magnification and 8 micrographs at 3000× magnification for each sample in order to take into account both micrometric and nanometric-sized voids (pores and cracks) using ImageJ 1.50e software [19]. From the known coating thickness and variable number of deposition passes, growth rate in terms of thickness per deposition cycle was evaluated. This value may be used as a measure of the coating deposition efficiency.

Phase composition of the initial powders and deposits were determined by powder X-ray diffraction technique (XRD) using D8 Discover diffractometer (Bruker AXS, Germany) with Bragg-Bretano geometry and CuKα radiation. Rietveld analysis of the diffraction patterns was used to quantify presence of identified crystalline phases. In addition to XRD, ^{27}Al nuclear magnetic resonance (NMR) with 14 kHz magic angle spinning (MAS) using Bruker Avance III HD spectrometer with ^{27}Al frequency 130 MHz was applied to alternatively evaluate the phase composition and validate XRD results. Spectra were modeled as linear combinations of the spectra of pure α and γ-phases. Corrections for second-order quadrupolar effects [20] were found negligible. For the NMR analysis, the coatings were removed from the substrates and

Table 1
List of deposition experiments denoted by the feedstock code with the most important process parameters and resultant coating properties. TI AG stands for Treibacher Industrie AG, IPP stands for Institute of Plasma Physics.

Feedstock code	19Tr40	25Tr40	31Tr40	25W10	25W20	25E10	25E20	19Sol5	25Sol5
Manufacturer	TI AG	TI AG	TI AG	IPP	IPP	IPP	IPP	IPP	IPP
Feeding distance (mm)	19	25	31	25	25	25	25	19	25
Solvent type	Water	Water	Water	Water	Water	Ethanol	Ethanol	Water	Water
Solid load (wt%)	40	40	40	10	20	10	20	5	5
Nominal* median particle size (nm)	2200	2200	2200	300	300	300	300	–	–
Feeding pressure (bar)	4.0	4.0	3.2	3.5	3.5	4.0	4.0	4.0	4.0
Feed rate (ml/min)	94	94	86	100	87	120	114	98	98
Total number of deposition cycles	5	5	**7**	10	5	25	5	10	10
Microstructure	Column	Column	Column	Dense	Dense	Dense	Dense	Foamy	Foamy
Total thickness (μm)	228 ± 33	227 ± 22	300 ± 36	55 ± 6	101 ± 20	176 ± 12	91 ± 9	163 ± 3	158 ± 11
Growth rate (μm/cycle)	45.5 ± 6.7	45.5 ± 4.4	42.8 ± 5.1	5.5 ± 0.6	20.1 ± 4.0	7.0 ± 0.5	18.3 ± 1.7	16.3 ± 0.3	15.8 ± 1.1
Porosity (IA) (%)	20.9 ± 4.0	18.7 ± 2.9	19.4 ± 3.5	16.3 ± 0.5	22.1 ± 2.9	6.5 ± 1.1	8.6 ± 3.0	69.7 ± 1.5	70.3 ± 1.2

* As provided by manufacturer.

Table 2
Deposition parameters of powder-sprayed coating.

Feedstock	Fujimi AW24
Feeding distance (mm)	55
Spraying distance (mm)	380
Feed rate (kg/h)	8.8
Total number of deposition passes	24
Growth rate (μm/pass)	9.6 ± 0.5

crushed into homogenized powder. Only the coatings of sufficient thickness were evaluated using this method (31Tr40, 25E10, 25Sol5, AW24).

Hardness testing of the coatings was carried out on the polished cross-sections by Nexus 4504 hardness tester (Innovatest, the Netherlands) with Vickers indenter at load of 0.3 kgf. Size of the indents for the hardness evaluation was measured from SEM micrographs.

Tribological properties were measured by CSEM High Temperature Tribometer (CSM Instruments, Switzerland) by dry sliding Pin-on-Disc test according to the ASTM G99-05 standard. The tests were carried out at room temperature, in air atmosphere (31% relative humidity) without lubrication using alumina counterpart ball (6 mm diameter) with 10 N normal load, 0.1 $m \cdot s^{-1}$ speed and measured distance of 1099.27 m in 50,000 cycles (track radius 3.5 mm). Prior to the testing, surface of the samples was polished on metallographic polishing machine down to 1 μm diamond suspension. For wear evaluation of coating performance in the wet conditions, abrasion wear in a slurry of sharp alumina particles was evaluated also by SAR test (Slurry Abrasion Response) according to the ASTM G75 standard. Slurry mixture of 150 g alumina (mesh F240) with 150 g of water were used as the abrasion medium.

Tensile adhesion/cohesion strength measurement was carried out using Instron 1362 (Instron, UK) mechanical testing machine following the ASTM C633-13 standard. For the tests, the substrate coupons with coatings were glued between two grit-blasted cylinders (18 mm in diameter) using FM 1000 adhesive film (Cytec Industries Inc., USA) according to [21]. Cured samples were mounted in the testing machine, preloaded to 50 N and loaded by a constant rate of cross-head travel of 0.5 $mm \cdot min^{-1}$ until rupture.

3. Results

3.1. Deposition optimization

In the first stage, optimization of the deposition process was carried out using the commercial ready-to-spray suspension with three feeding distances of 19, 25, and 31 mm (see Table 1). Resulting coating microstructures are shown in Fig. 3.

In all three cases, the coatings showed similar columnar-like microstructure with comparable porosity of about 19%. Boundaries between flattened splats were barely distinguishable within the coating and the splats were well connected, as visible in the detailed micrographs in Fig. 3. There was found no unmelted material embedded in the coatings, however, some loose spherical particles were locally attached to the inner walls of internal cavities or intercolumnar gaps, which indicates melting and re-solidification of some droplets before impact on the substrate (see Fig. 3b, d, f). The fact that all three deposition experiments led to similar coating microstructures with comparable deposition rates (see Table 1) indicates that the variation of feeding (injection) distance within the selected range has limited influence on the coating microstructure for WSP-H spraying. This also demonstrates a robustness of the deposition process.

3.2. Custom suspensions optimization

Firstly, sedimentation resistance was evaluated for the stabilized and non-stabilized suspensions formulated with 300 nm and 1000 nm powders. Second, based on the sedimentation test results, viscosity evaluation was carried out to assess the difference in rheology of the selected stabilized and non-stabilized suspensions.

The suspension sedimentation test results are illustrated for ethanol-based suspensions in photographs in Fig. 4. Each pair represents a fresh suspension and the same sample after four hours. The arrow marks the position of the distinguishable sediment-solvent interface. Both non-stabilized and stabilized suspensions prepared from 1000 nm powder (Fig. 4a and b, respectively) sedimented rapidly and the position of the sediment-solvent interface was clearly identifiable. On the other hand, the sedimentation of the suspensions from 300 nm powder was practically immeasurable even after four hours (Fig. 4c and d, non-stabilized and stabilized, respectively). The results for the water-based suspensions were analogous.

The time evolution of the sedimentation of the 1000 nm powder suspensions is presented in chart in Fig. 5. From the comparison of the sedimentation rate of both water and ethanol-based suspensions it is evident, that prepared suspensions sedimented rapidly, however, the addition of the stabilizing component substantially increased the stability of the suspensions for both water and ethanol solvents. The sediment-solvent interface in the stabilized water-based suspension descended to 80% of the initial liquid column height after 4 h compared to less than 50% in the case of the non-stabilized suspension. Similar effect of the BYK addition on the sedimentation rate of the ethanol-based suspensions was observed as the interface in the stabilized suspension descended down to approximately 60%, compared to less than 30% of the non-stabilized one within 4 h.

Not only the higher final position of the sediment-solvent interface, but also the sedimentation rate observed within the first hour proved the favorable effect of the stabilizer. Non-stabilized 1000 nm suspensions settled down very quickly right after being poured into the test tubes. These suspensions reached the saturated state (practically no further sedimentation takes place) within the first hour whereas the powder in the stabilized suspensions kept floating up to 90% of the liquid column height after the first hour. Similar results were observed by Rampon et al. in [22] when evaluating the stabilization of an aqueous suspension of YSZ with ammonium salt of polyacrylic acid. Such suspension stabilization may be sufficient when the suspension is prepared on-site immediately before the spraying session and the whole volume of

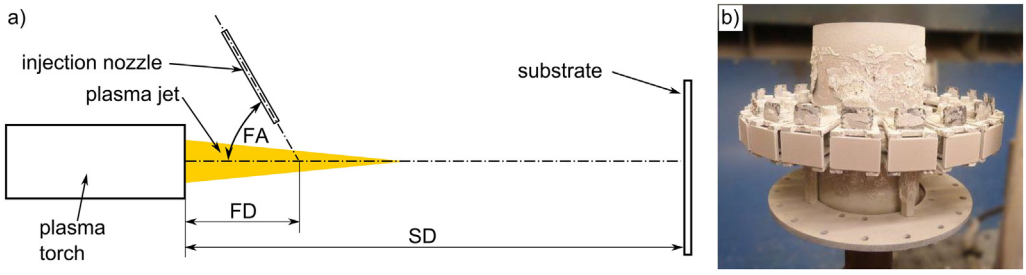

Fig. 2. Scheme of the spraying geometry (a) and photograph of samples on the carousel after the coating deposition (b).

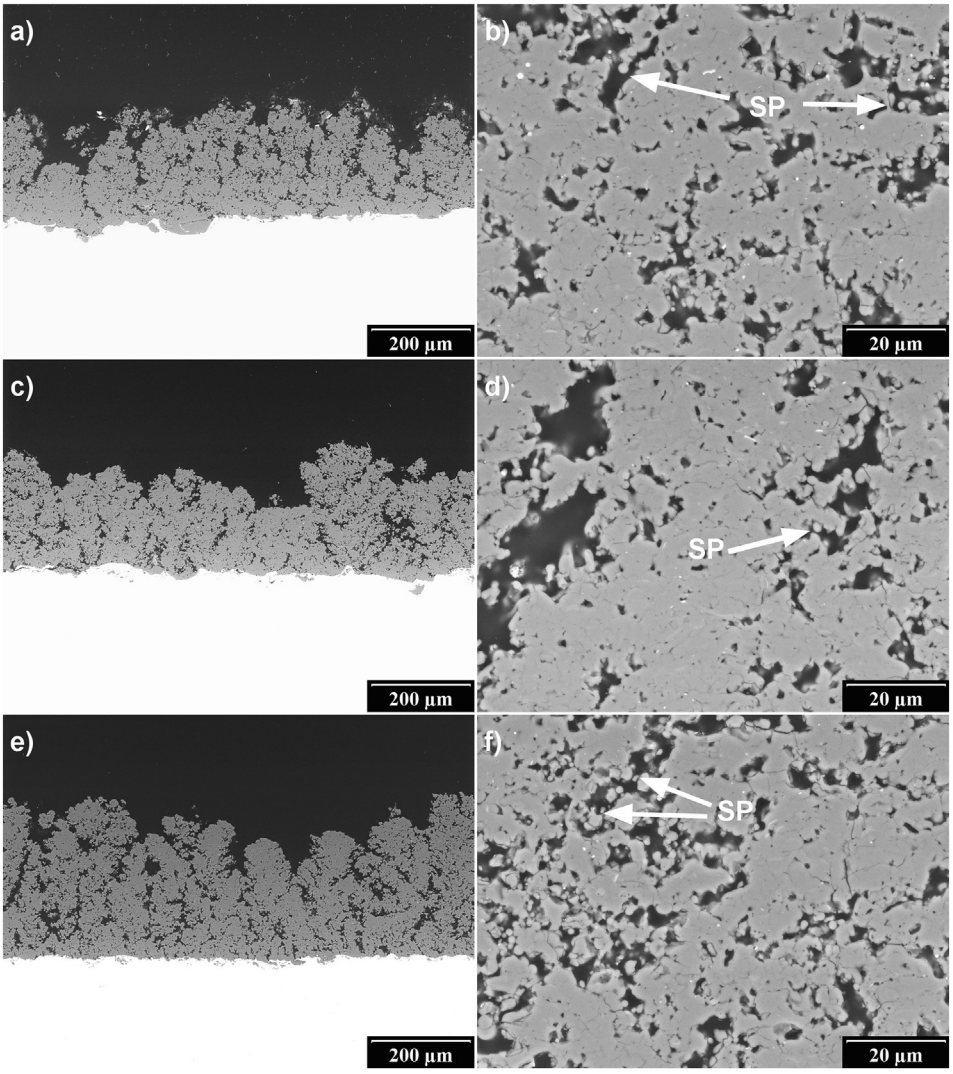

Fig. 3. Cross sections of the coatings prepared from the commercial suspension: a) FD 19 mm, c) FD 25 mm, e) FD 31 mm and details of the microstructures in b), d), f), respectively. Spherical particles (SP) are marked by arrows.

the suspension is depleted without the need for its long-term storage [11].

Moreover, it was observed that mechanical re-dispersion of the stabilized suspensions by shaking and stirring was much easier than in the case of the non-stabilized ones. Based on that, continuous mechanical stirring in the suspension container during the spraying time is expected to prevent the suspension sedimentation completely, ensuring unchanging feedstock concentration during the whole spraying process.

However, due to much higher sedimentation resistance (Fig. 4), the 300 nm powder suspensions were selected for further experiments as the more promising. Viscosity of both water and ethanol-based suspensions with 10 and 20 wt% concentrations was evaluated with and without stabilization in order to observe the possible change in their rheology due to the stabilizer addition.

Plot in Fig. 6 illustrates the relation between the viscosity and the rotation speed of the viscometer probe for the 20 wt% suspensions. All

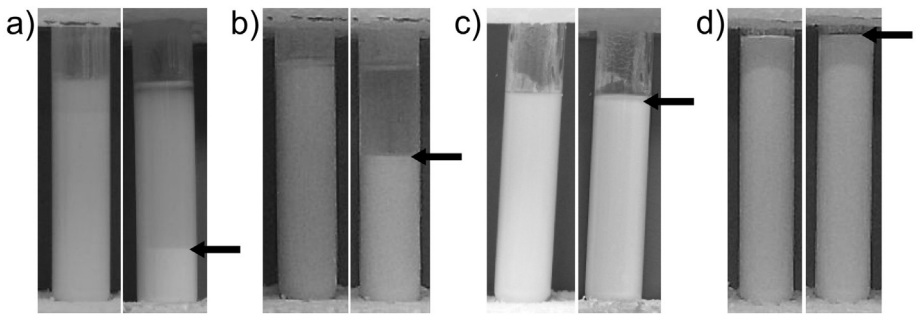

Fig. 4. Comparison of a) non-stabilized 1000 nm ethanol suspension, b) stabilized 1000 nm ethanol suspension, c) non-stabilized 300 nm ethanol suspension, d) stabilized 300 nm ethanol suspension. Fresh suspension (left), after 4 h (right).

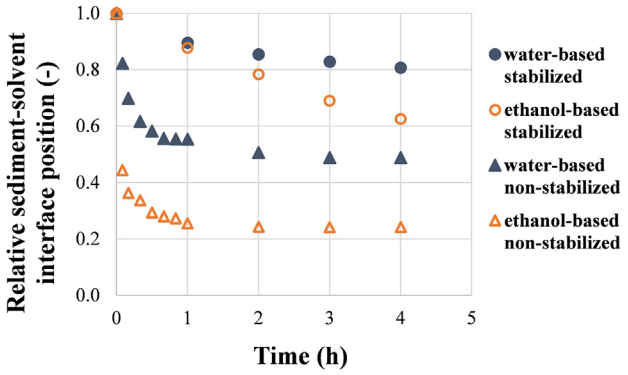

Fig. 5. Sedimentation evolution of the 1000 nm powder 20 wt% suspensions.

suspensions showed negligible hysteresis. It is clear that the stabilizing additive increased the viscosity of both water and ethanol-based suspensions, especially at low RPM. A non-Newtonian shear-thinning behavior was observed for all samples with the exception of the non-stabilized ethanol-based suspension.

Since high shear rates can be expected in the injection nozzle with typical internal diameter of several hundreds of micrometers, the most relevant viscosity value is at the highest testing RPMs where the highest shear rates occur. Viscosity at the highest shear rates was approximately doubled by addition of the stabilizer from around 38 mPa·s to 88 mPa·s for the non-stabilized and stabilized water-based suspensions, respectively, and from 6 mPa·s to 10 mPa·s for the non-stabilized and stabilized ethanol-based suspensions, respectively. Even though these values are one or two orders of magnitude higher than those of the pure solvents ($\eta_{H_2O} = 1.00$ mPa·s and $\eta_{ethanol} = 1.14$ mPa·s at 20 °C [23]), the suspensions were still able to be continuously injected through the used nozzle and were suitable as feedstocks for spraying.

Shear thinning was negligible for 10 wt% suspensions which showed also significantly lower viscosity values, i.e. approximately 4 mPa·s for the stabilized ethanol-based suspension and around 8 mPa·s for the stabilized water-based one. For the non-stabilized suspensions, viscosities were even lower, i.e. 1 mPa·s and 1.7 mPa·s, respectively.

Based on the optimization experiments, stabilized water and ethanol-based suspensions formulated from 300 nm powder with 10 and 20 wt% concentration were selected for further spraying experiments as more promising due to much better sedimentation resistance when compared to 1000 nm powder suspensions.

Viscosity of all suspensions selected for the deposition experiments related to the shear rate (in terms of probe RPM) are presented in Fig. 7. Compared to the IPP suspensions, the viscosity of the commercial water-based suspension supplied by Treibacher Industrie AG was rather low with values from 60 mPa·s at 10 RPM to 20 mPa·s at 100 RPM

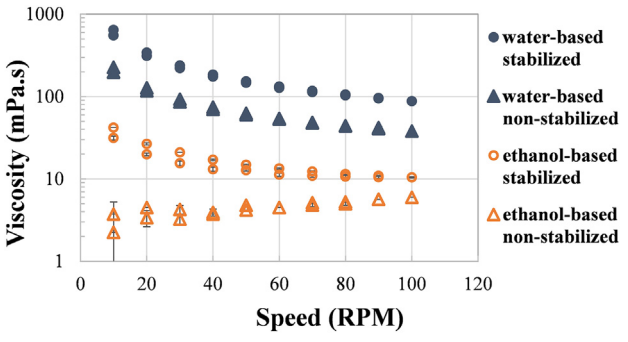

Fig. 6. Relation between shear rate (in terms of probe RPM) and the viscosity of the stabilized and non-stabilized 20 wt% 300 nm suspensions. Scatter bounds are smaller than the data points.

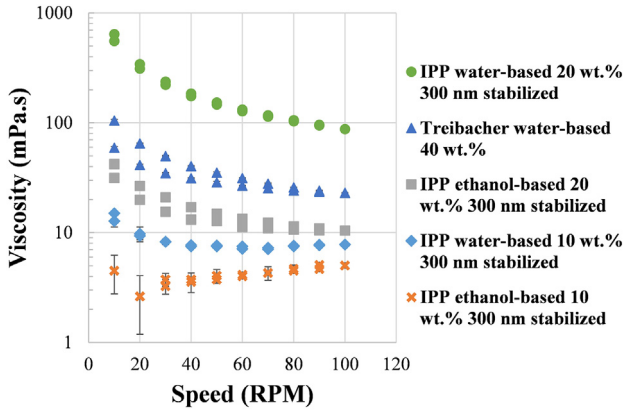

Fig. 7. Relation between shear rate (in terms of probe RPM) and the viscosity of the suspensions used for deposition. Scatter bounds are smaller than the data points.

despite a high solid load of 40 wt%. Such a low value was most probably connected to the higher particle size distribution median ($d_{50} = 2.2$ μm).

3.3. Deposition of custom-made suspensions and solution

Based on the results of the optimization stage of the deposition process with commercial suspension (Section 3.1), it was decided to carry out deposition of coatings from custom-made suspensions with feeding distance of 25 mm. The solution was deposited using feeding distance of 25 mm and also 19 mm to further probe the influence of the feeding distance.

Successful deposition of thick coatings homogeneously covering the substrates (Fig. 2b) was achieved. However, dense character of microstructure of the 25E10 coating combined with its high thickness and a high coefficient of thermal expansion (CTE) mismatch led to its partial delamination from the stainless steel substrate. Results of this coating are therefore presented for S235 steel substrate, where the coating adherence was excellent.

Depending on the feedstock formulation, microstructure of the acquired deposits varied from well-sintered dense for the ethanol-based suspension over moderately porous for the water-based suspension to extremely porous foamy microstructure deposited from the solution. Representative examples of the coating microstructures are depicted in Fig. 8.

Water-based and ethanol-based custom-made IPP suspensions yielded relatively dense coatings when compared to coatings deposited from the commercial suspension. Coatings also showed different nature of porosity (Fig. 8a, c). The lowest porosity was found in the 25E10 coating (6.5 ± 1.1%) with only a negligible amount of unmelted material (Fig. 8b), whereas the highest degree of porosity among the IPP suspension-sprayed coatings was found in the 25W20 coating (22.1 ± 2.9%). A more detailed view in Fig. 8d shows that pores in this coating were filled with unmelted powdery feedstock. Similar pores morphology was found also in the 25W10 and 25E20 coatings and the density of pores was proportionally related to the composition of the suspension, i.e. the higher the solid content, the higher the porosity (see Table 1).

A completely different type of microstructure was observed for the solution-sprayed coatings which showed a highly porous (around 70%) "foamy" microstructure where, in a more detailed view (Fig. 8f), islands of well-melted splats of irregular shape (typical size from 1 to 20 μm) can be found surrounded by thin-walled hollow shells (Fig. 8e, f). The microstructure was very similar for both coatings sprayed with feeding distance of 19 and 25 mm showing again the minimal influence of this parameter in WSP-H spraying of this solution. Both coatings adhered well to the substrate but since the connection between splats was provided by the foamy material, the coatings were prone to mechanical

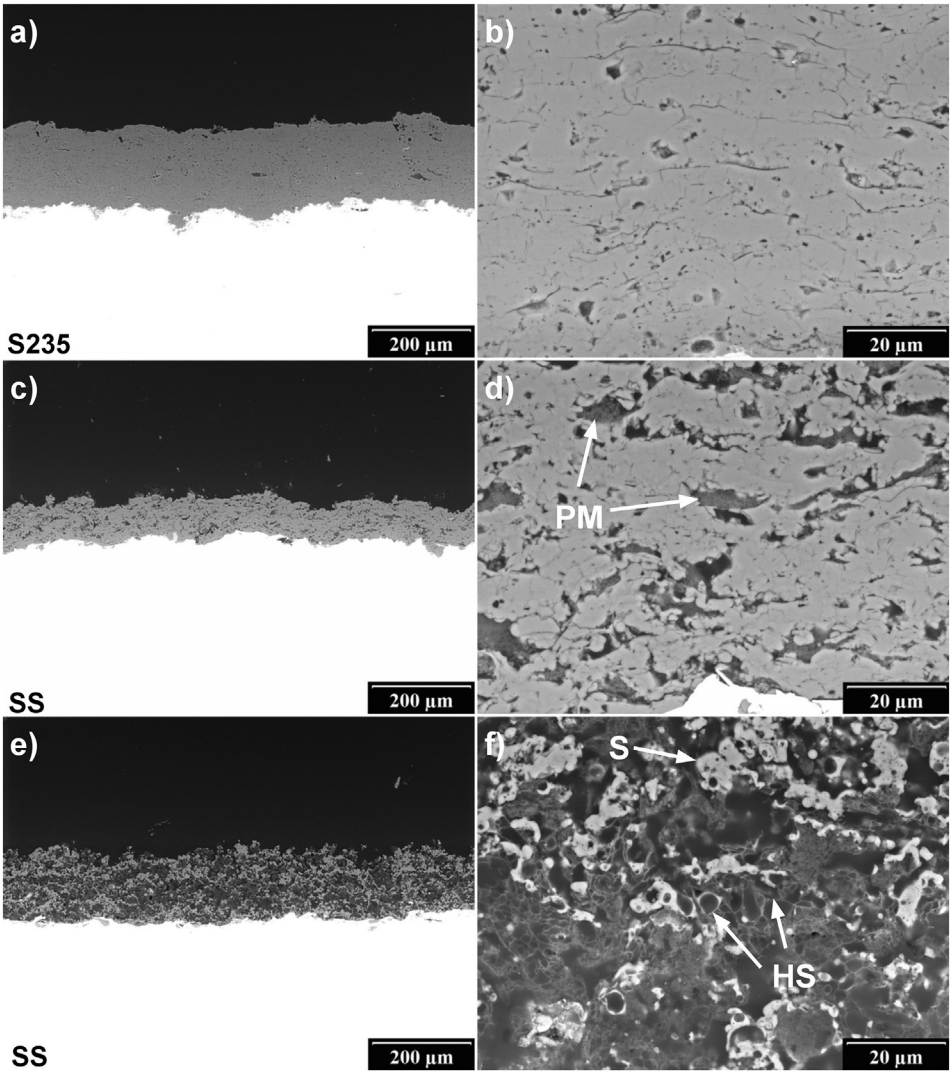

Fig. 8. Examples of deposits microstructures: a) 25E10 coating, c) 25W20 coating, e) 25Sol5 coating. SS – stainless steel, S235 – structural steel. Details of microstructures: b) 25E10 coating, d) 25W20 coating (PM – powdery material), f) 25Sol5 coating (S – splat, HS – hollow shells).

damage and thus did not comply with the aim of the study to prepare durable coatings. Microhardness of the coatings could not be reliably evaluated on the embedded cross-sections due to the penetration of the mounting epoxy into the pores and substantial reinforcement of the microstructure.

Comparison of the growth rates listed in Table 1 shows that the concentration of the solid phase is the key parameter of the coating build-up rate. The coating thickness increase per deposition cycle (DE in µm/cycle) was more than doubled when doubling the concentration of the feedstock powder in the suspension. However, the relatively high growth rate of the solution sprayed coatings which was comparable to the 20 wt% suspensions (around 8 µm/pass) was caused by the extreme porosity of the deposits (~70%), i.e. the thickness increase was achieved with a low volume of solid material.

3.4. Phase composition

XRD analysis revealed substantial differences in the phase composition of the deposited coatings, as well as dependence of phase composition of the deposit on the feedstock formulation. The illustrative diffraction patterns are shown in Fig. 9. All powders used for suspension preparation were pure α-phase alumina, however, after the deposition the volume of this phase decreased significantly. The commercial water-based suspension (31Tr40 experiment) produced a coating with a relatively high α-phase content of about 25 wt% (Table 3). The remaining part of the phase content was represented by amorphous material, γ-phase, and δ-phase. Spraying the more diluted ethanol-based suspension (25E10) led to the coating with higher content of metastable γ- and δ-phases and only a small amount of α-phase of about 10 wt%. A notably different phase composition was found for the solution-sprayed 25Sol5 coating which was mainly composed of the stable α-phase (83 wt%).

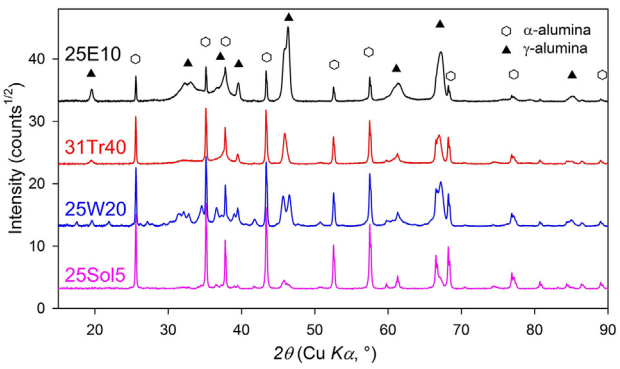

Fig. 9. Diffraction patterns of a) 25E10, b) 31Tr40, c) 25W20, and d) 25Sol5 coatings.

Table 3
Comparison of α-phase content in initial feedstock powders and resulting coatings measured by XRD and NMR.

Experiment	Feedstock α-phase content (wt%)	Coating α-phase content (wt%)
	XRD/NMR	XRD/NMR
25E10	100/97 +	9/10
31Tr40	100/100	25/26
25Sol5	−/−	83/91
AW24	100/100	10/16

However, the XRD method evaluates the phase composition from the sample surface with a limited penetration depth of several tens of μm. To validate the phase composition for the whole volume of coatings, the NMR method was used. The α-phase contents obtained by XRD and by NMR were in a good agreement (Table 3). It may be therefore concluded that NMR may be a useful tool for evaluation of the phase composition of plasma sprayed coatings as the Rietveld refinement of XRD diffraction patterns of nanostructured material is challenging.

3.5. Mechanical properties

From the IPP coatings, sample 25E10 was selected for mechanical testing as it showed the densest microstructure which was most promising for a high mechanical endurance. On the other hand, all coatings prepared from commercial suspension showed comparable columnar microstructure typical for suspension plasma spraying and promising some other potential benefits such as increased strain-tolerance. Coating 31Tr40 was selected from these coatings for mechanical testing due to its highest thickness.

The hardness of the suspension-sprayed coatings reached quite remarkable values of 1211 ± 11 HV0.3 for dense 25E10 and 919 ± 200 HV0.3 for more porous 31Tr40 coatings documenting a good bonding of the deposited material and high internal cohesion of the coatings. The extremely narrow scatter of the hardness values of the 25E10 coating reflected a high structural homogeneity of the coating (see microstructure detail in Fig. 8a). On the contrary, the porous 31Tr40 (Fig. 3e) coating showed a bimodal distribution of hardness values leading to a high scatter as the compact well-sintered columns also reached hardness values of 1100 HV0.3 whereas the porous areas reached values of approximately 700 HV0.3. Quite surprisingly, the α-phase richer 31Tr40 coating exhibited lower hardness even in the dense areas than the compact 25E10 coating which shows that the microstructure and quality of mutual bonding between splats play a more important role for the mechanical durability than the phase composition. Compared to the hardness of 911 ± 69 HV0.3 of the conventional coating AW24, hardness values were encouraging for further mechanical tests as the high hardness is often an indication of for example good wear resistance [24].

Tensile adhesion test results are shown in plot in Fig. 10. The highest value of tensile adhesion strength of 51 ± 6 MPa was measured for the densest 25E10 coating. The almost 100% adhesion failure proved the exceptional internal cohesion of the 25E10 coating (Fig. 10). The columnar 31Tr40 coating also showed a relatively high value of adhesion/cohesion strength of 28 ± 3 MPa (failing due to loss of cohesion, see Fig. 10). The conventional coating AW24 failed in mixed cohesion/adhesion failure and showed a value of 19 ± 2 MPa being more than 60% lower than that of the dense coating and about 30% lower than that of the columnar coating.

After the tensile adhesion tests, cross sections were prepared from the ruptured samples to observe whether any glue penetrated into the coatings, since glue penetration may reinforce the coating and affect the results [25]. The glue was well recognizable in the SEM micrographs as it contained microscopic spherical particles unlike the metallographic embedding resin (Fig. 11). The observation showed that the adhesive film did not penetrate into the coating microstructure and copied the free surface of the coatings. Even in the case of the columnar 31Tr40 coating, the glue ran only into the openings of the widest intercolumnar gaps not penetrating into the fine pores and did not reach the substrate. It may be therefore concluded that the glue did not influence the adhesion/cohesion strength of the coatings and the measured values are representative for the coatings.

The wear resistance of the coatings was found to be strongly dependent on the coating microstructure (see Fig. 12). Please note that even though both methods use the same units, the measured values obtained using pin-on-disc (POD) test are not comparable to those obtained using slurry abrasion response (SAR) test due to significant qualitative differences in the wear damage mechanisms and nature of the tests. The best results were obtained for the dense suspension-sprayed 25E10 coating for both methods with the values of wear coefficients $K_{POD} = (1.94 \pm 0.53)\cdot 10^{-5}$ $mm^3\cdot N^{-1}\cdot m^{-1}$ and $K_{SAR} = (23.6 \pm 5.8)\cdot 10^{-5}$ $mm^3\cdot N^{-1}\cdot m^{-1}$ for pin-on-disc and SAR tests, respectively. The value of the wear coefficient K_{POD} was approximately 10-times lower than the respective values of 31Tr40 and AW24 coatings.

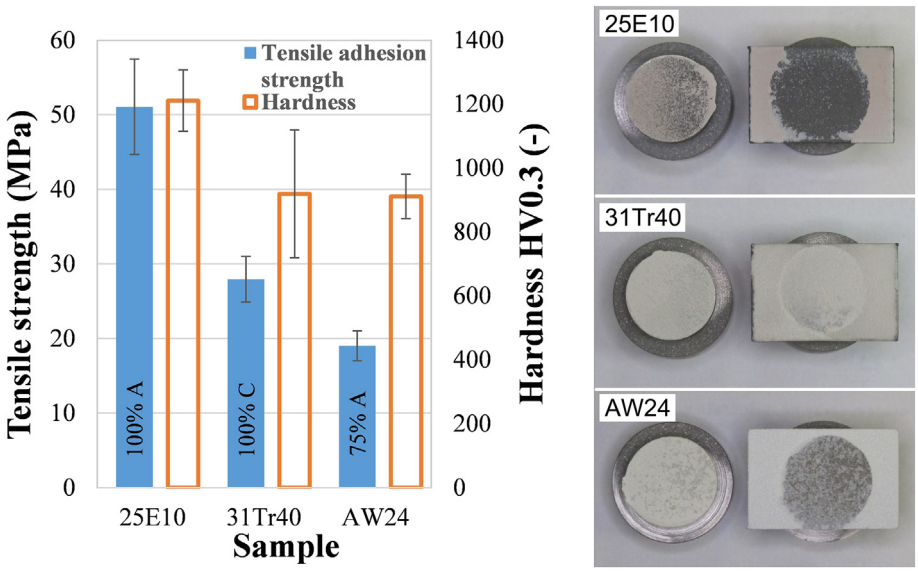

Fig. 10. Comparison of hardness and tensile adhesion/cohesion strength of suspension- and powder-sprayed coatings with percentage of adhesive (A) or cohesive (C) failure. Photographs in the right hand side show the fracture surfaces after test.

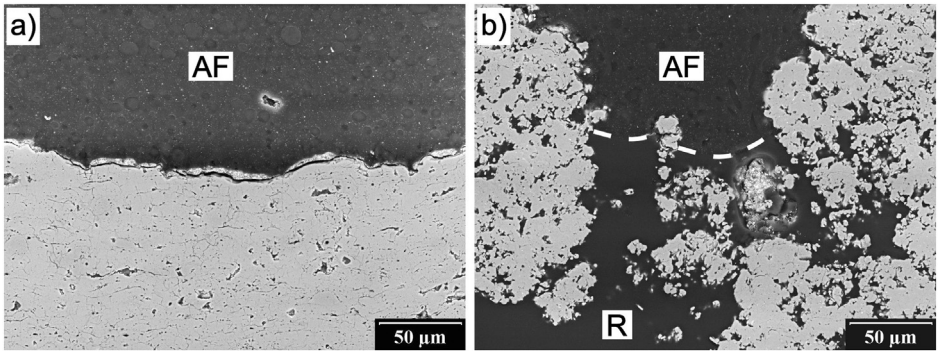

Fig. 11. Coating-glue interface of 25E10 coating (a) and coating-glue-resin interface of 31Tr40 coating (b). The dashed line indicates the interface between the adhesive film (AF) and the metallographic embedding resin (R).

However, the mean value of coefficient of friction (COF) in pin-on-disc test was comparable for all tested coatings in the range from 0.60 to 0.68.

The significantly better performance of the compact suspension-sprayed coating may be attributed to the high density of this coating, absence of large-scale voids and strength of mutual interconnection between splats. Micrographs in Fig. 13 show the overview of the wear tracks (Fig. 13a, c, e) and detailed damage in the center of the grooves (Fig. 13b, d, f) from pin-on-disc test. For instance, in the case of 25E10 coating, the smaller well-sintered splats led to noticeably finer wear debris (Fig. 13b) which provided also a smoother sliding of the counterpart ball, corresponding to lowest measured COF value. On the contrary, the coarser fragments of the more loosely connected splats in the case of the conventional AW24 coating further promoted the damage of the material in the groove leading to a higher material removal rate ($K_{POD} = (20.3 \pm 7.4)\cdot 10^{-5}$ mm$^3\cdot$N$^{-1}\cdot$m^{-1}). In the case of the columnar 31Tr40 coating, the mechanism of the material removal was the breaking and crushing of the column tips which filled the deep intercolumnar gaps leading to the wear coefficient $K_{POD} = (23.8 \pm 10.6)\cdot 10^{-5}$ mm$^3\cdot$N$^{-1}\cdot$m^{-1}.

In the case of slurry abrasion test, the local damage by sharp alumina particles was more severe and therefore the differences between the tested samples were less pronounced than in the Pin-on-Disc test (Fig. 12). However, the 25E10 coating outperformed the other samples again having the lowest K_{SAR} value of $(23.6 \pm 5.8)\cdot 10^{-5}$ mm$^3\cdot$N$^{-1}\cdot$m^{-1}. As for the columnar coating, a still relatively low value of $K_{SAR} = (42.3 \pm 19.0)\cdot 10^{-5}$ mm$^3\cdot$N$^{-1}\cdot$m^{-1} was measured. The highest K_{SAR} of $(68.8 \pm 18.1)\cdot 10^{-5}$ mm$^3\cdot$N$^{-1}\cdot$m^{-1} was measured for the conventional AW24 coating showing that the prevalent mechanical interconnection of splats

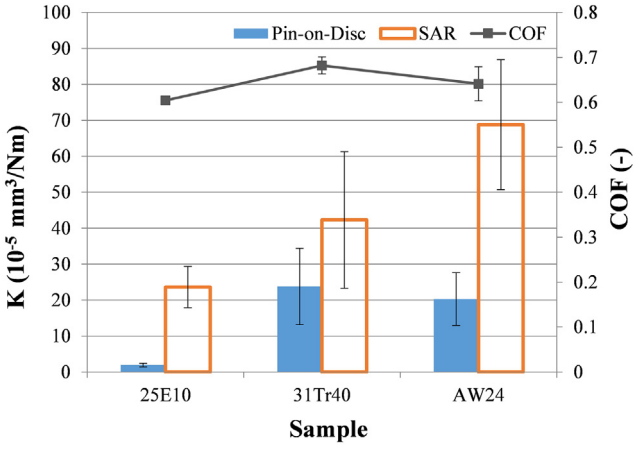

Fig. 12. Comparison of wear resistance of suspension- and powder-sprayed coatings for Pin-on-Disc test and SAR test.

was incapable to resist the abrasion by the hard particles. In this case, the much larger splats were easily broken and removed from the coating surface by the slurry, thus exposing the underlying coating and accelerating the damage.

4. Discussion

The alumina coatings prepared in this study and their properties showed several remarkable aspects of suspension plasma spraying carried out by hybrid water-stabilized plasma torch. The shadowgraphy technique showed that the solvent type has a crucial role in the liquid atomization as illustrated in the shadowgraphy images of the injection area (Fig. 14). The ethanol-based suspensions undergo more intensive droplet fragmentation than water-based ones (compare Fig. 14b to the others). This could be beneficial for the formation of the compact microstructure as the fine droplets gain higher speed and higher temperature and impinge with a high flattening ratio. Moreover, spraying with ethanol-based suspensions led to more intensive heating of the substrate during the deposition due to the combustion of the ethanol in the plasma jet (for details see [15]). This indicates that the enthalpy available for thermal treatment of the droplets was substantially higher.

On the contrary to the ethanol solvent, bigger droplets of the water-based feedstocks were retained further downstream the plasma jet due to the higher surface tension of water [26] potentially allowing retention of unmelted material in the core of bigger particles or agglomerates when the droplets were deflected from the optimum trajectory in the hottest section of the plasma jet.

However, the atomization and solvent evaporation takes place along the whole trajectory of the particles downstream in the plasma jet affecting the thermal history of individual droplets at the spraying distance, i.e. where the particles hit the substrate and form the deposit. Please note that the length of the plasma jet of the WSP-H torch is around 90 mm which is almost over the entire length of the spraying distance (100 mm). Therefore, despite a rather long spraying distance, the particles traveling along the optimum trajectory are accelerated and heated over the entire distance without significant deceleration and cooling before impact. Judging also from the absence of unmelted material embedded in the coatings, the best atomization and feedstock melting took place with the custom-made ethanol-based suspensions (e.g. 25E10 experiment) and the commercial water-based suspension (e.g. 31Tr40 experiment).

Please note that water-based suspensions produced porous and even columnar microstructures whereas ethanol-based suspensions led to more compact dense structures, which is the opposite of the general experience with gas-stabilized torches [6–8]. According to [27], lighter and slower particles tend to produce coatings with cauliflower-like structure due to the fact that they easily follow the divergent gas stream parallel to the surface and deposit on the sides of asperities of roughened surface. However, both the high velocity and the low

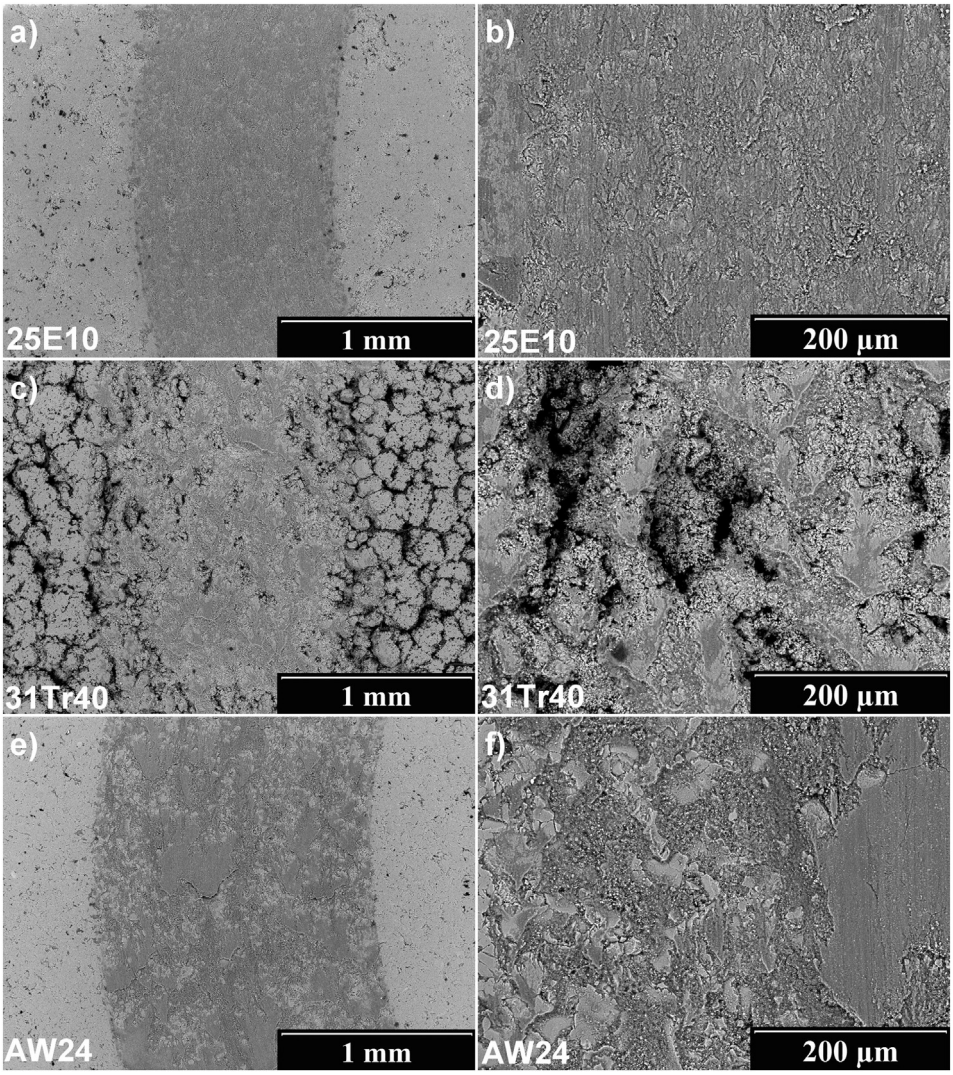

Fig. 13. SEM micrographs of wear tracks (grooves) after pin-on-disc test. Overview – left, detail – right.

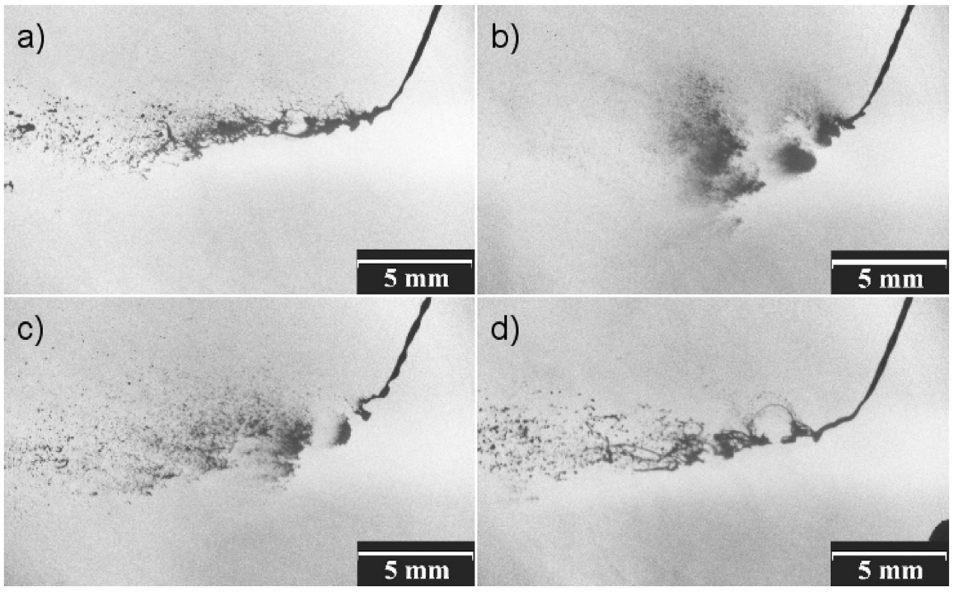

Fig. 14. Shadowgraphy images of feedstock atomization, a) 31Tr40 suspension, b) 25E10 suspension, c) 25W20 suspension, d) 25Sol5 suspension. Bright area is plasma jet.

viscosity of the WSP-H plasma jet possibly provided the particles with high momentum and produced only a thin deflective boundary layer of gasses above the surface [28]. Under such conditions, even the small particles probably gained a high velocity and impacted mostly perpendicularly onto the surface, which promoted formation of the dense microstructure. This result shows that the choice of plasma torch as well as the feedstock formulation has a strong influence on the coating microstructure, as the plasma properties influence its interaction with the liquid feedstock i.e. the atomization, heating and acceleration leading to substantial differences in the build-up mechanisms.

Apart from the liquid atomization and resulting coating microstructure, the phase composition also helps to understand the thermal history of the feedstock and coating build-up. The smaller droplets of ethanol-based suspension absorb more heat but also undergo a more rapid cooling after flattening on the substrate or on the previous coating layer. This leads to the preferential formation of the metastable γ and δ phases at the expense of the α-phase. On the contrary, the coating from the water-based commercial suspension retained a higher content of the initial alpha phase. This should probably be attributed to the lower intensity of atomization (Fig. 14a) and to the coarser powder dispersed in the suspension ($d_{50} = 2.2$ μm for the commercial suspension compared to $d_{50} = 410$ nm for the IPP suspension). Thus, the retention of the original phase is promoted either in the core of the bigger particles or in agglomerates sintered along the travel of the particle in the plasma jet [11]. Another source of the α-phase could be the re-solidified particles which had enough time to crystalize in the stable phase during the in-flight-stage [4].

Concerning the mechanical properties of the suspension-sprayed coatings, the 25E10 and 31Tr40 coatings promised the best performance based on their microstructure consisting dominantly of well-sintered splats. This was proved by the remarkable values of hardness and tensile adhesion strength of the SPS coatings due to effective bonding between splats (as visible in Figs. 3f, 8b) when compared to the conventional powder-sprayed coatings with much higher density of internal voids (both intersplat and intrasplat cracks and pores) which compromise the mutual bonding of the splats by reduction of the mutual contact area and effectivity of mechanical interlocking of the splats [29]. Additionally, based on the results of the wear tests, it was found that improved mutual interconnection of miniature splats and homogeneity of the coating also leads to enhanced wear resistance of the coatings sprayed from suspension. From the microscopic point of view, the wear damage was less pronounced and localized in the compact 25E10 coating whereas in the 31Tr40 and AW24 coatings, the crumbling of the column tips or breaking and delamination of splats were responsible for the higher material removal rate (compare Fig. 13b with d and f). However, the coefficient of friction (COF) in pin-on-disc test was similar for all tested coatings ranging from 0.60 to 0.68. This result may be attributed to the fact that after the running-in period, the COF value is dependent mainly on the materials of friction pairs, in this case the matching Al_2O_3 pairs and finely crushed alumina coating between them. The slight differences between the measured COF values can be assigned to the different wear mechanisms. Similar COF values were measured for instance for CVD Al_2O_3 hard coatings tested against Al_2O_3 counterpart in [30].

The extremely porous (around 70%) coatings deposited from the solution also shows the applicability of WSP-H plasma spraying for the manufacturing of coatings with a high porosity and large specific surface areas. Based on the "foamy" character of the coating microstructure with embedded compact splats and the high fraction of the α-phase, the following deposition mechanism may be suggested. Majority of the droplets did not have enough time to evaporate, crystallize and melt. Instead, the solution droplets impinged the hot surface where calcination of solid phase accompanied with intensive generation of the gasses took place [31] and the hollow shells solidified into the stable α-phase. However, some fraction of droplets calcined already during the in-flight phase resulting in the compact Al_2O_3 splats embedded in the coating (see micrograph in Fig. 8f). Nevertheless, even though the solution-sprayed coatings were not mechanically durable, the highly porous microstructure composed mainly of the stable α-phase may be interesting for example for catalytic applications as a carrier of the catalytic component.

5. Conclusions

A complex study of suspension and solution plasma spraying of aluminium oxide was carried out. The samples were prepared using a high enthalpy hybrid water-stabilized plasma torch WSP®-H 500 with considerable feed rate of more than 100 ml/min demonstrating the convenience of the WSP-H technology for large scale alumina suspension plasma spraying.

Deposition parameters were optimized using a commercial ready-to-spray suspension and coatings of typical columnar microstructure were prepared. The microstructure was found to be not so dependent on the feeding distance.

In order to deposit custom-made suspensions, numerous formulations were evaluated in terms of sedimentation stability and viscosity. The best results were obtained with 0.5 wt% addition of stabilizing agent which resulted in a significantly delayed sedimentation and improved mechanical dispersibility of the powder. Despite the fact the additive measurably increased the viscosity of the suspensions, it represented no major problem in suspension injection and therefore, the stabilized suspensions were selected for the deposition experiments.

In the next step, custom-made stabilized suspensions of powder concentrations of 10 and 20 wt% with water and ethanol solvents were used to produce coating samples. Preparation of homogeneous coatings covering the entire surface of the substrates was accomplished. The densest coating was obtained with the custom-made ethanol-based 10 wt% suspension which produced a compact, well-sintered, and highly durable coating with only a small amount of inhomogeneities such as pores, cracks, etc. Quite surprisingly, this result goes against the widely accepted rule of thumb for conventional gas-stabilized plasma torches that compact coatings are more likely to be produced from water-based feedstocks as indicated in [32,33]. This coating consisted mainly of the metastable γ-phase (about 90 wt% according to XRD and NMR method) which shows intensive quenching of the impinging melted particles. The other suspensions and solution produced coatings with a higher content of stable α-phase but also higher porosity and regions of unmelted material embedded in the microstructure which deteriorated the mechanical properties.

Spraying of the solution feedstock of aluminium nitrate nonahydrate resulted in highly porous soft coatings composed dominantly (~90%) of α-phase. Their microstructure was predominantly formed by thin-walled hollow shells surrounding individual splats which could potentially by interesting for example for catalytic applications as the carrier of the active component.

The variety of microstructures prepared in this study proved the high variability of the WSP-H deposition process. Achievable microstructures include a) durable well-sintered dense coatings, b) columnar coatings with intermediate porosity and still preserving favorable mechanical properties, and c) "foamy" soft coatings with extreme porosity prepared from solutions.

Mechanical testing of the selected suspension sprayed coatings showed a significantly improved performance of these coatings when compared to conventional coating deposited from dry coarse powder. High achievable hardness (up to ~1200 HV0.3), adhesion/cohesion strength (up to ~50 MPa) and wear resistance (up to ~$1.94 \cdot 10^{-5}$ $mm^3 \cdot N^{-1} \cdot m^{-1}$ in Pin-on-Disc test and ~$24 \cdot 10^{-5}$ $mm^3 \cdot N^{-1} \cdot m^{-1}$ in SAR test) show the promising potential of the Al_2O_3 suspension plasma spraying with WSP-H torch. Moreover, the fact that the coating microstructures were quite insensitive of the injection point setting (feeding distance) showed the robustness of the deposition process with the WSP-H technology which may be valuable for industrial spraying.

Acknowledgements

Financial support of the GA15-12145S grant "Physical aspects of plasma spray deposition from liquid feedstock" funded by Czech Science Foundation is gratefully acknowledged. The NMR measurements were enabled through the Project CZ.2.16/3.1.00/21566 funded by the Operational Programme Prague – Competitiveness.

References

[1] L. Pawłowski, The Science and Engineering of Thermal Spray Coatings, 1995http://dx.doi.org/10.1016/0263-8223(96)80006-7.
[2] P. Fauchais, A. Joulia, S. Goutier, C. Chazelas, M. Vardelle, A. Vardelle, S. Rossignol, Suspension and solution plasma spraying, J. Phys. D. Appl. Phys. 46 (2013) 224015, http://dx.doi.org/10.1088/0022-3727/46/22/224015.
[3] F.-L. Toma, L.-M. Berger, C.C. Stahr, T. Naumann, S. Langner, Thermally Sprayed Al2O3 Layers Having a High Content of Corundum Without Any Property-Reducing Additives, and Method for the Production Thereof, 8318261 B2, 2012.
[4] P. Chraska, J. Dubsky, K. Neufuss, J. Pisacka, Alumina-base plasma-sprayed materials part I: phase stability of alumina and alumina-Chromia, JTST 6 (1997) 320–326.
[5] P. Fauchais, R. Etchart-Salas, V. Rat, J.F. Coudert, N. Caron, K. Wittmann-Ténèze, Parameters controlling liquid plasma spraying: solutions, sols, or suspensions, J. Therm. Spray Technol. 17 (2008) 31–59, http://dx.doi.org/10.1007/s11666-007-9152-2.
[6] F.L. Toma, L.M. Berger, C.C. Stahr, T. Naumann, S. Langner, Microstructures and functional properties of suspension-sprayed Al2O3 and TiO2 coatings: an overview, J. Therm. Spray Technol. 19 (2010) 262–274, http://dx.doi.org/10.1007/s11666-009-9417-z.
[7] O. Tingaud, P. Bertrand, G. Bertrand, Microstructure and tribological behavior of suspension plasma sprayed Al2O3 and Al2O3–YSZ composite coatings, Surf. Coat. Technol. 205 (2010) 1004–1008, http://dx.doi.org/10.1016/j.surfcoat.2010.06.003.
[8] P. Müller, A. Killinger, R. Gadow, Comparison between high-velocity suspension flame spraying and suspension plasma spraying of alumina, J. Therm. Spray Technol. 21 (2012) 1120–1127, http://dx.doi.org/10.1007/s11666-012-9783-9.
[9] O. Tingaud, A. Grimaud, A. Denoirjean, G. Montavon, V. Rat, J.F. Coudert, P. Fauchais, T. Chartier, Suspension plasma-sprayed alumina coating structures: operating parameters versus coating architecture, J. Therm. Spray Technol. 17 (2008) 662–670, http://dx.doi.org/10.1007/s11666-008-9218-9.
[10] R. Rampon, O. Marchand, C. Filiatre, G. Bertrand, Influence of suspension characteristics on coatings microstructure obtained by suspension plasma spraying, Surf. Coat. Technol. 202 (2008) 4337–4342, http://dx.doi.org/10.1016/j.surfcoat.2008.04.006.
[11] L. Pawłowski, Suspension and solution thermal spray coatings, Surf. Coat. Technol. 203 (2009) 2807–2829, http://dx.doi.org/10.1016/j.surfcoat.2009.03.005.
[12] E.H. Jordan, C. Jiang, M. Gell, The solution precursor plasma spray (SPPS) process: a review with energy considerations, J. Therm. Spray Technol. 24 (2015) 1153–1165, http://dx.doi.org/10.1007/s11666-015-0272-9.
[13] P. Fauchais, G. Montavon, Latest developments in suspension and liquid precursor thermal spraying, J. Therm. Spray Technol. 19 (2010) 226–239, http://dx.doi.org/10.1007/s11666-009-9446-7.
[14] R. Musalek, G. Bertolissi, J. Medricky, J. Kotlan, Z. Pala, N. Curry, Feasibility of suspension spraying of yttria-stabilized zirconia with water-stabilized plasma torch, Surf. Coat. Technol. 268 (2015) 58–62, http://dx.doi.org/10.1016/j.surfcoat.2014.07.069.
[15] R. Musalek, J. Medricky, T. Tesar, J. Kotlan, Z. Pala, F. Lukac, T. Chraska, N. Curry, Suspensions plasma spraying of ceramics with hybrid water-stabilized plasma technology, J. Therm. Spray Technol. (2016) 1–10, http://dx.doi.org/10.1007/s11666-016-0493-6.
[16] M. Hrabovsky, Thermal plasma generators with water stabilized arc, Open Plasma Phys. J. 2 (2009) 99–104, http://dx.doi.org/10.2174/1876534300902020099.
[17] M. Hrabovsky, V. Kopecky, V. Sember, T. Kavka, O. Chumak, M. Konrad, Properties of hybrid water/gas DC arc plasma torch, IEEE Trans. Plasma Sci. 34 (2006) 1566–1575, http://dx.doi.org/10.1109/TPS.2006.878365.
[18] J. Kotlan, Z. Pala, R. Musalek, P. Ctibor, On reactive suspension plasma spraying of calcium titanate, Ceram. Int. 42 (2016) 4607–4615, http://dx.doi.org/10.1016/j.ceramint.2015.11.159.
[19] W. Rasband, ImageJ, https://imagej.nih.gov/ij/ 1997 (accessed February 12, 2016).
[20] D. Massiot, C. Bessada, J.P. Coutures, F.A. Taulelle, Quantitative study of 27Al MAS NMR in crystalline YAG, J. Magn. Reson. 90 (1990) 231–242, http://dx.doi.org/10.1016/0022-2364(90)90130-2.
[21] Accepted Practice to Test Bond Strength of Thermal Spray Coatings, 2013, http://www.asminternational.org/documents/17679604/17683439/AcceptedPracticeBondStrengthApprovedformatted_Intro.pdf/4bcf5903-414d-413f-ab69-7cf0cc9123bd.
[22] R. Rampon, C. Filiatre, G. Bertrand, Suspension plasma spraying of YPSZ coatings: suspension atomization and injection, J. Therm. Spray Technol. 17 (2008) 105–114, http://dx.doi.org/10.1007/s11666-007-9143-3.
[23] Cheric.org, http://www.cheric.org/research/kdb/hcprop/showcoef.php?cmpid=8818&prop=VSL8 2016 (accessed January 5, 2015).
[24] J. Oberste Berghaus, J.-G. Legoux, C. Moreau, F. Tarasi, T. Chraska, Mechanical and thermal transport properties of suspension thermal-sprayed alumina-zirconia composite coatings, J. Therm. Spray Technol. 17 (2008) 91–104, http://dx.doi.org/10.1007/s11666-007-9146-0.
[25] R. Musalek, V. Pejchal, M. Vilemova, J. Matejicek, Multiple-approach evaluation of WSP coatings adhesion/cohesion strength, J. Therm. Spray Technol. 22 (2013) 221–232, http://dx.doi.org/10.1007/s11666-012-9850-2.
[26] D. Chen, E.H. Jordan, M. Gell, The solution precursor plasma spray coatings: influence of solvent type, Plasma Chem. Plasma Process. 30 (2010) 111–119, http://dx.doi.org/10.1007/s11090-009-9200-4.
[27] K. VanEvery, M.J.M. Krane, R.W. Trice, Parametric study of suspension plasma spray processing parameters on coating microstructures manufactured from nanoscale yttria-stabilized zirconia, Surf. Coat. Technol. 206 (2012) 2464–2473, http://dx.doi.org/10.1016/j.surfcoat.2011.10.051.
[28] P. Fauchais, M. Vardelle, S. Goutier, A. Vardelle, Key challenges and opportunities in suspension and solution plasma spraying, Plasma Chem. Plasma Process. 35 (2014) 511–525, http://dx.doi.org/10.1007/s11090-014-9594-5.
[29] G.J. Yang, C.J. Li, C.X. Li, K. Kondoh, A. Ohmori, Improvement of adhesion and cohesion in plasma-sprayed ceramic coatings by heterogeneous modification of non-bonded lamellar interface using high strength adhesive infiltration, J. Therm. Spray Technol. 22 (2013) 36–47, http://dx.doi.org/10.1007/s11666-012-9831-5.
[30] A. Riedl, N. Schalk, C. Czettl, B. Sartory, C. Mitterer, Tribological properties of Al2O3 hard coatings modified by mechanical blasting and polishing post-treatment, Wear 289 (2012) 9–16, http://dx.doi.org/10.1016/j.wear.2012.04.022.
[31] I.F. Myronyuk, V.I. Mandzyuk, V.M. Sachko, V.M. Gun'ko, Structural and morphological features of disperse alumina synthesized using aluminum nitrate nonahydrate, Nanoscale Res. Lett. 11 (2016) 153, http://dx.doi.org/10.1186/s11671-016-1366-0.
[32] E. Aubignat, M.P. Planche, A. Allimant, D. Billieres, Effect of Suspension Characteristics on In-flight Particle Properties and Coating Microstructures Achieved by Suspension Plasma Spray, Htpp, 12019, 2014http://dx.doi.org/10.1088/1742-6596/550/1/012019.
[33] E. Aubignat, M.P. Planche, D. Billieres, A. Allimant, L. Girardot, Y. Bailly, G. Montavon, Optimization of the injection with a twin-fluid atomizer for suspension plasma spray process using three non-intrusive diagnostic tools, J. Vis. (2015) 21–36, http://dx.doi.org/10.1007/s12650-015-0281-2.

5.2 Study of coating buildup for high-enthalpy WSP-H torch

The previous study provided rather unexpected result that the dense microstructure was prepared using an ethanol-based suspension while columnar coating was sprayed using water-based one. This finding was contradictory to the commonly accepted rule-of-thumb of suspension plasma spraying using GSP torches where the practice is usually the other way round. Therefore, in order to elaborate on the coating buildup mechanisms using the WSP-H torch, three suspensions already known to produce distinctive microstructure types (dense, semi-developed columnar, and fully-developed columnar) were used in deposition experiments designed to visualize the formation of the first splats on the substrate, the growth of the columnar microstructure, and the shape of the spray trace.

It was demonstrated that the suspension producing large splats on the substrate (originating from large atomized droplets) provides the dense lamellar microstructure similar to conventional coatings. On contrary, the suspension producing a mixture of fine and coarse splats results in the columnar microstructure, the development of which depends on the ratio of large to fine spats. Therefore, it was shown that there is a smooth transition between these microstructure types depending on the atomization of the feedstock which, in turn, depends on the its overall characteristics and not solely on the solvent type or the size of primary powder particles.

The study of columnar microstructure growth showed that the onset of column formation can be identified as early as after the first 3 deposition cycles which correspond to approximately 20 – 30 μm of deposit thickness. Afterwards, a competitive growth between neighboring columns was recognized which results in the formation of the structure of alternating widening and receding columns. This competitive lateral growth was shown to reach a saturated state, i.e., that the in-plane width of the columns reaches a maximum when certain coating thickness is reached.

The study of the spray trace profile as a function of the stand-off distance revealed that with increasing SD, the spray trace becomes wider and flatter, apparently due to the wider spread of material and decreasing deposition efficiency along the centerline. It was also shown that a soft and loose overspray material is deposited on the fringes of the spray trace under the specific deposition configuration used for this experiment regardless of the feedstock type. However, this overspray and resulting interpass porosity was not observed in coating samples sprayed using the standard carousel configuration (Fig. 14 in section 4.1). Therefore, the overspray material is expected to be entirely removed by the intensive plasma gas flow during successive torch passes and by the air knives used for deposit cooling.

In conclusion, the coating formation mechanisms when spraying with the WSP-H torch were shown comparable to those observed when using the more conventional GSP torches. The key factor is the atomization of the liquid which is a result of its properties and a complex interaction with the plasma jet.

The following paper [II] was based on a poster presentation given at international conference Rencontres Internationales sur la Projection Thermique 2017, which was held in Limoges, France. The poster was awarded the Best poster award.

Surface & Coatings Technology 371 (2019) 333–343

Contents lists available at ScienceDirect

Surface & Coatings Technology

journal homepage: www.elsevier.com/locate/surfcoat

On growth of suspension plasma-sprayed coatings deposited by high-enthalpy plasma torch

Tomas Tesar[a,b,*], Radek Musalek[a], Jan Medricky[a], Jan Cizek[a]

[a] Institute of Plasma Physics CAS, v.v.i., Department of Materials Engineering, Za Slovankou 3, 182 00 Praha 8, Czech Republic
[b] Czech Technical University in Prague, Faculty of Nuclear Sciences and Physical Engineering, Department of Materials, Trojanova 13, 120 00 Praha 2, Czech Republic

ARTICLE INFO

Keywords:
Suspension plasma spraying
Buildup
Dense microstructure
Columnar-like microstructure
Spray bead
Hybrid water-stabilized plasma torch (WSP-H)

ABSTRACT

Introduction of suspension plasma spraying (SPS) brought novel coating microstructures unachievable by other thermal spraying techniques. Both columnar and dense layers are of particular interest for various applications. Deeper understanding of the coating buildup mechanisms is essential for tailoring of the coatings microstructure and properties. This paper contributes to elucidation of the buildup mechanisms with focus on high enthalpy plasma torches, in particular the hybrid water/argon-stabilized plasma torch WSP-H 500. The main differences between the formation of finely structured dense coatings and columnar coatings were studied for alumina and yttria-stabilized zirconia (YSZ) by comprehensive evaluation of individual splat formation, gradual coating growth, and geometrical characteristics of the deposits.

It was clearly demonstrated that the coating microstructure is generally controlled by morphology of individual deposited splats which is influenced namely by formulation of the suspension and mean trajectory of the fragmented suspension droplets in the plasma jet, both influencing size, flattening ratio and thermal history of deposited splats.

Larger droplets having proper thermal treatment provided miniature lamellae similar to conventional plasma spraying, eventually leading to the development of low porosity (dense) structures. With decreasing splat size and increasing distance from the plasma jet axis, coatings tended to develop more porous columnar structures. After characteristic number of deposition cycles, lateral growth of the columnar structures became saturated, i.e. the equivalent diameter of the columnar structures became stabilized at about 75 μm, when observed from the free-surface. Material deposited from the plasma fringes was only loosely bonded and could be easily blown away from the surface which explains absence of interpass porosity in the deposited coatings.

1. Introduction

The use of liquid feedstocks (suspensions and solutions) gained a lot of interest in the world of plasma spraying and finally became an industrially recognized technique. The main reason of interest in the emerging technology of suspension plasma spraying (SPS) and solution precursor plasma spraying (SPPS) is the ability to produce a broad range of coatings of unique characteristics [1,2]. Aside from forming the relatively dense lamellar structure resembling that of the conventional coarse powders, only with splats size lower by two orders of magnitude [3], the liquid-sprayed coatings can also produce extremely porous structures [4] or even columnar branched structures that mimic the morphology of the electron beam physical vapor-deposited (EB-PVD) coatings [5]. All the above mentioned microstructures originate from the small size of the impinging particles and hence the formed structural units (splats) as well as from the small size of the voids encapsulated within the coating. SPS/SPPS coatings are able to outperform the conventional ones in terms of mechanical properties [6], thermal properties [7,8], electronic properties [9,10], biocompatibility [11], and others.

In the field of aerospace industry or power generation, the segmented columnar morphology is one of the most intensively studied types due to its promising properties potentially enabling further increase in efficiency of the engines through the use of advanced thermal barrier coatings (TBC) [12]. The driving force for the development of SPS/SPPS TBCs is their ability to combine high service lifetime comparable to that of the competitive EB-PVD deposits, with a low thermal conductivity, as well as cost-efficient deposition achievable by plasma spraying [13,14].

The superior properties of SPS/SPPS TBCs stem from the so-called

* Corresponding author at: Institute of Plasma Physics CAS, v.v.i., Department of Materials Engineering, Za Slovankou 3, 182 00 Praha 8, Czech Republic.
E-mail address: tesar@ipp.cas.cz (T. Tesar).

https://doi.org/10.1016/j.surfcoat.2019.01.084
Received 31 August 2018; Received in revised form 21 December 2018; Accepted 23 January 2019
Available online 25 January 2019
0257-8972/

columnar "cauliflower-like" structure, which received its name for the visual resemblance of the coating free-surface with the rather unpopular *Brassica oleracea* var. *botrytis* vegetable species [15]. One of the main advantages of the cauliflower-like structure is presence of the vertical intercolumnar gaps which enable increased strain tolerance compared to conventional powder-sprayed coatings. Such coating is potentially able to more effectively accommodate to the deformation of the substrate without detrimental cracking and spallation. Furthermore, the fine micron and submicron porosity improves phonon-scattering, thus effectively reducing the coating thermal conductivity [16].

A phenomenological description of the development of the columnar structure was proposed in [17], where the authors suggested that the coating grows both in vertical and lateral directions, i.e. that the particles build up on the surface not only perpendicularly as in conventional spraying, but also side-ways. The perpendicular component of particle velocity is acquired from its acceleration in the plasma jet, whereas the lateral velocity component parallel with the coated surface is received from the flow of plasma gases that are deflected by the coated part which exhibits an obstacle to the gas flow. This flow is strong enough to deflect only the light particles as the larger and heavier ones possess enough momentum to retain their original vector of velocity perpendicular to the substrate [18]. Consequently, the particles with the lateral velocity component may impact onto the sides of surface asperities formed e.g. by substrate grit-blasting or previously deposited large particles. The stochastic nature of emergence of the column-nucleation centers on the surface asperities and competitive growth of the branching columns leads to the formation of the characteristic cauliflower-like structure.

The formation of the columnar structure is influenced by many factors such as plasma properties or feedstock formulation which are responsible for the atomization, acceleration, and heat treatment of the liquid droplets [19,20], torch transverse velocity over the surface which affects the growth rate, surface preparation which controls the initial stage of microstructure development [21], etc. These factors have to be considered when real industrial components with complex shape such as turbine blades or vanes have to be coated.

Conversely, the dense microstructure is formed when the particles are large enough (i.e. have higher momentum) to retain their trajectory acquired in the plasma jet and impact perpendicularly on the coated surface. These particles form disc-shaped splats similar to those originating from coarse powders and by splat stacking, a lamellar microstructure is formed.

This study focused on the comparison of the coating buildup of both columnar and dense microstructures using the hybrid water/argon-stabilized plasma torch (WSP-H 500) which were presented elsewhere [6,22]. This torch has unique plasma parameters unparalleled by the standard gas-stabilized torches (GSP), namely the high plasma velocity and enthalpy, long jet, and lower plasma density [23]. In order to understand the coating buildup for high-enthalpy torches, three different suspension feedstocks optimized to yield distinct microstructures were used to study the phenomena leading to the different coating formation independently on the material being deposited (see Table 1). To identify the difference between the dense and columnar coating buildup, the first splats formed on the substrate were prepared in the frame of a "single pass" experiment for two alumina suspensions yielding dense and columnar porous microstructures. Subsequently, the incremental growth of the cauliflower-like microstructure was studied in a "columnar growth" experiment using YSZ suspension as it is the primary material of choice for thermal barrier coatings and, therefore, the coating buildup mechanism is essential for tailoring of the coating properties. Lastly, the "spray beads" experiment was carried out using the dense-coating-forming alumina suspension and the columnar-coating-forming YSZ suspension in order to evaluate deposition mechanisms for both the plasma jet centerline and jet fringes.

Table 1
Overview of the experiments carried out in the study.

Experiment	Material	Microstructure	Goal
Single pass	Alumina Alumina	Dense Columnar	Observe individual splats for microstructure formation.
Columnar growth	YSZ	Columnar	Observe the evolution of cauliflower-like structure.
Spray bead	Alumina YSZ	Dense Columnar	Observe deposit formation on large-scale substrate for the whole spray trace.

2. Experimental

All deposits were prepared using the hybrid argon/water-stabilized plasma torch WSP-H 500 (ProjectSoft HK, a.s., Czech Republic). The torch was operated at 500 A generating a total jet power of ~150 kW with consumption of plasma forming gasses of only 15 slpm of Ar and approximately 3 l/h of water. Details on the torch parameters as well as the plasma conditions can be found elsewhere [24,25]. The torch was mounted on a programmable robotic arm.

For the deposition experiments, 3 suspensions were used (Table 2): (1) a custom-made ethanol-based suspension of Al_2O_3 powder with 10 wt% solid load (Dv_{50} = 0.3 μm, Allied High Tech Products, Inc., USA) and 0.5 wt% stabilizer content (BYK-LP C 22587, BYK-GARDNER, GmbH, Germany), (2) a commercial ready-to-spray water-based Al_2O_3 suspension with 40 wt% solid load (Dv_{50} = 2.2 μm, Treibacher Industrie AG, Austria), and (3) a commercial ready-to-spray ethanol-based suspension of YSZ with 25 wt% solid load (Dv_{50} = 0.58 μm, Treibacher Industrie AG, Austria).

2.1. Single pass (SP) experiment

The single pass experiment was carried out to study the size and morphology of the initial splats deposited onto the substrate. This was done in order to identify the conditions leading to the onset of formation of dense and columnar coatings. In order to deposit the individual splats, a single quick stroke of the torch in front of stationary substrates was made. The torch transverse velocity was set to 600 mm·s^{-1} to match the mutual transverse velocity of the substrate surfaces and the torch during standard SPS/SPPS spraying performed with WSP-H torch [6,7]. Mirror polished AISI 304 stainless steel coupons of dimensions of 30 × 20 × 2.5 mm were used as substrates in order to allow formation of splats unaffected by the substrate surface morphology. For single pass experiment, suspensions A and B were used.

2.2. Columnar growth (CG) experiment

The experiment visualizing the growth of the cauliflower-like microstructure was based on the previous experience gained with spraying of YSZ coatings using WSP-H torch [7,22]. Samples with different numbers of deposition cycles (i.e., having different thicknesses) were prepared in order to study both the initial and final stadia of the coating growth. Substrates from grit-blasted AISI 304 stainless steel of dimensions of 30 × 20 × 2.5 mm and surface roughness R_a ~ 7 μm were used. A total of 20 coupons were mounted on a revolving carousel. Each time, four samples were taken away after a preselected number of deposition cycles, and the deposition was resumed. The samples were collected after exposition to 1, 3, 6, 12, and 24 deposition cycles, each including 3 up and down torch strokes over the rotating carousel. Due to the high enthalpy provided by the torch, each deposition cycle was followed by a cooling period. At the same time, the samples were continually cooled by a flow of compressed air and water mist to avoid overheating during the spraying. The temperature was measured at the back side of the samples by a remote K-type thermocouple. Formation of the columnar microstructure was examined for suspension C.

Table 2
Parameters of the suspensions.

Suspension	Microstructure	Solvent	Material	Solid load (wt%)	Viscosity at 122 s^{-1} (mPa·s)	Density ($g \cdot cm^{-3}$)	Feed rate ($g \cdot min^{-1}$)
A	Dense	Ethanol	Al_2O_3	10	5.0 ± 0.2	0.86	103
B	Columnar	Water	Al_2O_3	40	23.0 ± 0.2	1.43	134
C	Columnar	Ethanol	YSZ	25	1.7 ± 0.3	1.01	100

2.3. Spray bead (SB) experiment

For the spray bead experiments, S235 low carbon steel substrates having dimensions of 125 × 20 × 2.5 mm were mounted vertically on a revolving carousel and the plasma jet axis was positioned to the center of the samples in order to acquire deposit both from the plasma center line and from the top and bottom plasma jet fringes (commonly referred as "overspray"). This configuration enabled formation of the spray bead along the vertical cross-section of the spray trace, i.e. along its axis of symmetry (the suspension injector was positioned above the plasma jet).

In order to deposit representative spray beads, 9 deposition cycles were made during which the torch was stationary for 5 s in front of the revolving carousel with samples. Schematic drawing of the deposition setup is displayed in Fig. 1.

For suspension A, the deposition of spray beads was carried out at the standard stand-off distance (SD) of 100 mm (Fig. 1a). Additionally, the influence of stand-off distance on the spray bead formation was evaluated for suspension C using a modified sample holder (Fig. 1b) which allowed setting 4 different stand-off distances (100, 110, 120, and 130 mm) during one deposition experiment. To prevent overheating of the substrates, the deposition cycles were alternated with cooling periods where the torch was moved horizontally away from the samples. The air cooling from outside of the samples was used during the deposition.

2.4. Deposits evaluation

Metallographic samples from the cauliflower growth and from the spray bead experiments were prepared following a standard metallographic procedure consisting of precision cutting (Secotom-50, Struers, Denmark), vacuum EpoFix epoxy mounting (Struers, Denmark), and semiautomatic polishing (Tegramin 25, Struers, Denmark). Prior to cutting, the samples from the spray bead experiment were mounted in EpoFix epoxy resin in order to support the fragile overspray deposits on the edges of the samples and to prevent their damage during the metallographic preparation. All the observations of the SB samples were done along the long side of the samples in order to follow the symmetry of the deposition setup The free surfaces of SP, CG and SB experiments deposits and cross-sections of CG and SB deposits were observed by a scanning electron microscope (SEM) EVO MA-15 (Carl Zeiss, Germany) using back-scattered electrons mode (BSE).

The SEM micrographs were used to evaluate thickness and porosity of the deposits prepared in the spray bead and cauliflower growth experiments by image analysis (IA); 20 readings for thickness and 5 readings for porosity (at 1000× nominal magnification) were used to calculate the mean values. In the columnar growth experiment, the distribution of cauliflowers diameters was evaluated from the free-surface SEM micrographs using ImageJ v1.52h software. Manual thresholding of the cauliflowers and the intercolumnar grooves with subsequent watershed procedure were applied in order to measure the area and, in turn, equivalent diameters of the columns. In the spray bead experiment, the thickness profiles measured from 11 equidistant points were fitted by a Gaussian function using the least-square method in order to provide descriptive characteristics of the spray trace along the vertical axis. Deposit center and spray trace diameter were described from the fits in terms of position of maximum of the fit and FWHM (full width half maximum), respectively.

The inclination angles of the columns in the spray beads from suspension C were measured manually from the micrographs using AxioVision software (Carl Zeiss, Germany) in order to estimate the position of the virtual point where the deposited particles seemingly originate from, i.e. the point on the intersection of the straight lines following the inclination of the columns (Fig. 2). This point will further be referred as the dispersion point (DP). The inclination was evaluated at 2 spots spaced 20 mm (distance $w/2$) from the coating center from 10 measurements. The dispersion cone projection was then defined as the triangle defined by the dispersion point and the full width at half maximum (FWHM) of deposit thickness. The vertex angle α of the dispersion cone is the dispersion angle (see Fig. 2). The resulting height h of the dispersion cone is the position of the dispersion point (DP) above the surface.

3. Results

3.1. Single pass experiment

Splats deposited from the alumina suspensions A and B in the single pass experiments are depicted in Fig. 3. The ethanol-based suspension A yielding dense microstructure provided distinguishable individual circular splats of up to 20 μm in diameter scattered on the polished metallic substrate (Fig. 3a). Several submicron circular pores were observed within the large splats showing the release of gasses entrained inside the agglomerated and melted primary particles of the feedstock. Cracking observed in the largest splats (Fig. 3a) documented the rapid quenching of the melt. On the contrary, the deposit from the water-based suspension B yielding columnar coating consisted of a mixture of very fine spherical particles and evenly distributed larger splats (several

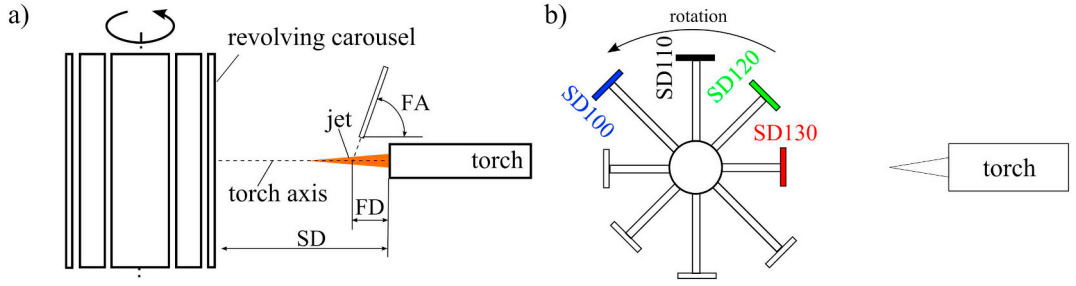

Fig. 1. Scheme of the deposition setup of the spray bead experiment. a) Side view, b) top view on the carousel allowing spraying with variable SD. Feeding angle (FA), Feeding distance (FD), stand-off distance (SD).

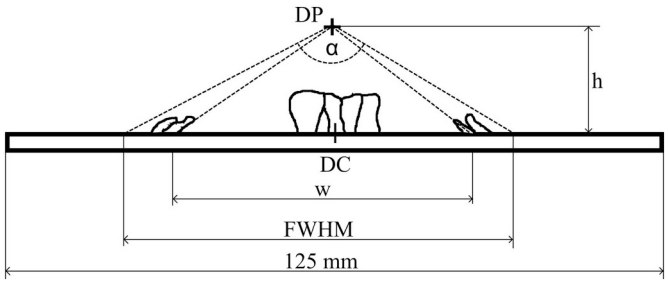

Fig. 2. Schematic evaluation of the dispersion point (DP) position *h* above the substrate. The span *w* of the measurement spots was 40 mm. Dispersion cone with dispersion angle α is delineated by FWHM of thickness and *h*.

μm in diameter). However, the deposit practically entirely covered the sample even after single quick scan of the torch over the substrate (Fig. 3b). The lower coverage of the substrate by the deposit from suspension A is to be attributed to its low concentration of 10 wt%, whereas the highly concentrated suspension B (40 wt%) resulted in almost entire overlay of the surface by continuous thin layer of deposit.

In both cases, the size of the majority of splats and resolidified spherical particles was much higher than the size of the primary particles introduced into the suspensions. This can be explained by the fact that each droplet of fragmented suspension contains numerous primary powder particles which readily fuse and melt together resulting in the observed splat sizes up to several tens of micrometers.

3.2. Columnar growth experiment

The overview of the free surfaces exposed to multiple depositions of suspension C is shown in Fig. 4. The substrate was thoroughly covered by the coating even after one deposition cycle (Fig. 4a) copying original substrate roughness introduced by grit blasting (original substrate roughness $R_a = 6.5 \pm 0.7$ μm, deposit $R_a = 6.6 \pm 1.3$ μm). After 3 deposition cycles (Fig. 4b), the first miniature cauliflowers started to form on the roughness asperities, but some of the grit-blasting traces were still observable on the surface (deposit $R_a = 8.7 \pm 0.7$ μm). After 6 deposition cycles, fine cauliflowers can be seen on the free surface intermingled with few larger columns (LC) overgrowing the surrounding surface (deposit $R_a = 8.3 \pm 0.4$ μm). Free surfaces after 12 and 24 deposition cycles showed fully developed cauliflower-like structure (deposits $R_a = 11 \pm 1$ μm and 17 ± 3 μm, respectively). The increasing roughness of the deposits indicates increasing occurrence of individual taller columns protruding from the deposit surface.

The distributions of the column diameters after the varying number of deposition cycles as measured by IA are shown in Fig. 5. Example of the original, thresholded, and watersheded image is shown in Fig. 5b. High number of fine cauliflowers was observed after 3 deposition cycles as the first columns emerged. With increasing number of deposition cycles, the distribution broadened towards smaller quantity of larger columns. However, the distributions of cauliflowers after 12 and 24 cycles were practically identical showing a saturated state where new cauliflowers emerge on top of previously developed columns, hindering their further lateral growth, which is obvious also from cross-sections in Fig. 7.

The observation of the free surfaces at higher magnification (Fig. 6) revealed that the surfaces were visually practically undistinguishable even after different number of deposition cycles. All deposits showed a combination of larger flattened splats (FS) surrounded by fine spherical particles (SP) having diameters typically below 1 μm.

Cross-sections of the evolving columnar microstructure are displayed in Fig. 7. After 1 deposition cycle, a very thin deposit was formed closely following the original roughness of the substrate. Nevertheless, the mixture of large flattened splats and fine spherical particles was observed, in accordance with the free surface observations. After 3 deposition cycles, the coating covered the substrate homogeneously and its surface was already sectioned by shallow grooves indicating the onset of the column formation (Fig. 7b). Apparently, the emerging columns preferentially grew from the asperities on the grit-blasted substrate surface. After 6 deposition cycles, the columns were already well distinguishable and also the combination of growing (shadowing) and receding (shadowed) columns was detected (Fig. 7c). In the deposit formed after 12 cycles, the neighboring diverging columns merged which led to the full development of the columnar cauliflower-like features. After a total of 24 cycles, columns further grew mostly parallel to each other, leaving vertical intercolumnar gaps between them. Furthermore, narrow vertical segmentation cracks were also found between columns showing their mutual interconnection.

3.3. Spray bead experiment

The samples deposited in one spray session with different stand-off distances using suspension C yielding columnar structure are shown in Fig. 8. It is evident that central parts of the samples were coated uniformly by the deposit, the thickness of which was diminishing towards the top and bottom edges of the substrates. This is not surprising as it may be anticipated that the deposition rate should be the highest along the plasma jet axis, where the thermal treatment and acceleration of the fragmented droplets is most efficient. Fig. 8b shows an in-scale scheme

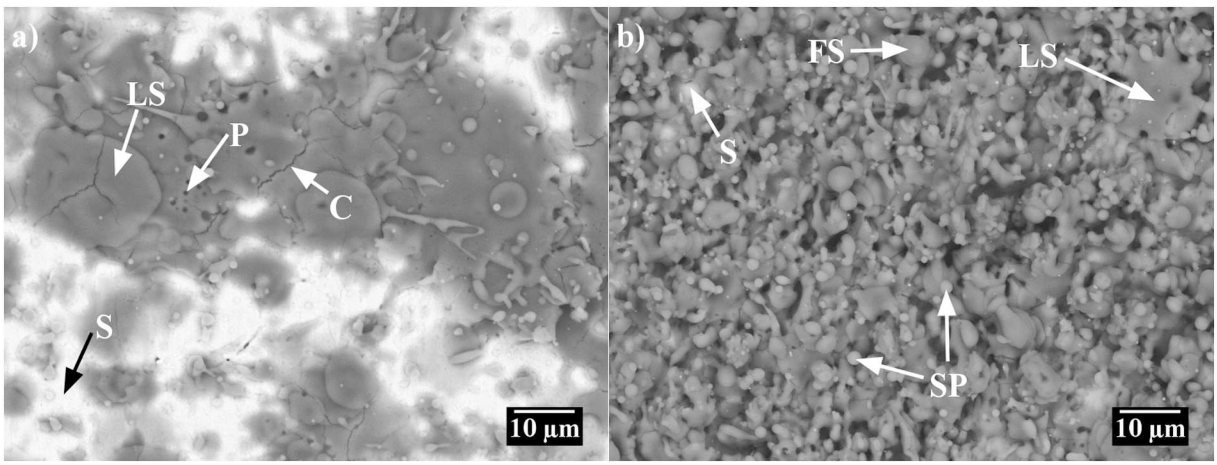

Fig. 3. Deposit from the single pass experiment: a) suspension A yielding dense microstructure, b) suspension B yielding columnar microstructure. Large splats (LS), cracks (C), pores (P), underlying steel substrate (S), fine splats (FS), spherical particles (SP).

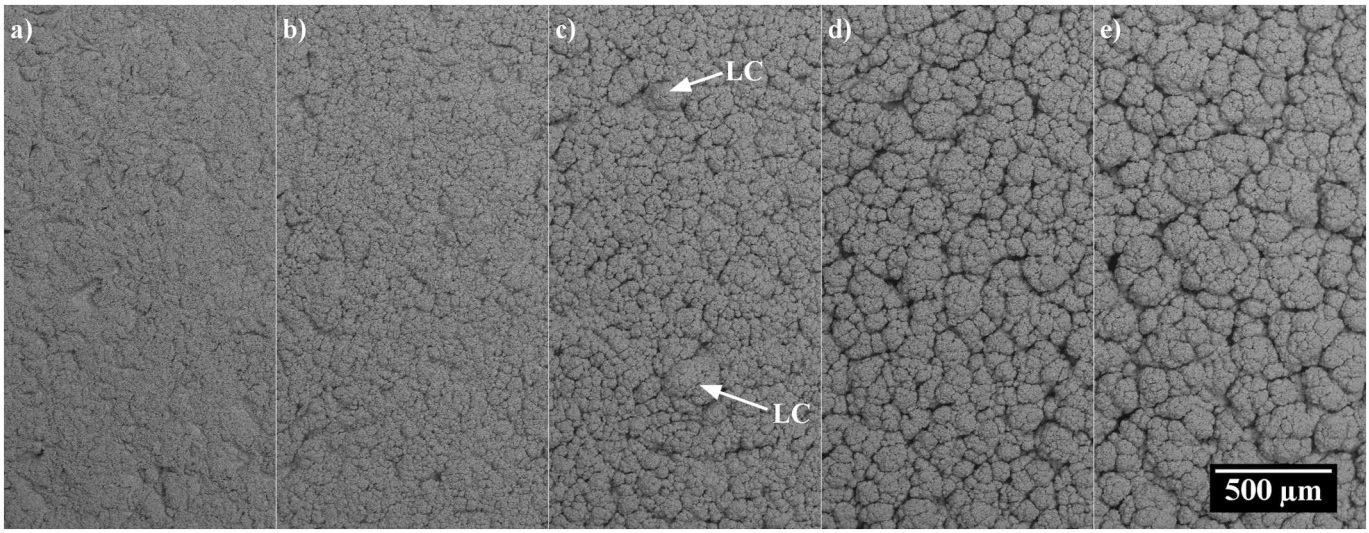

Fig. 4. Free surfaces of deposits after a) 1 cycle, b) 3 cycles, c) 6 cycles, d) 12 cycles, and e) 24 cycles. Large columns (LC).

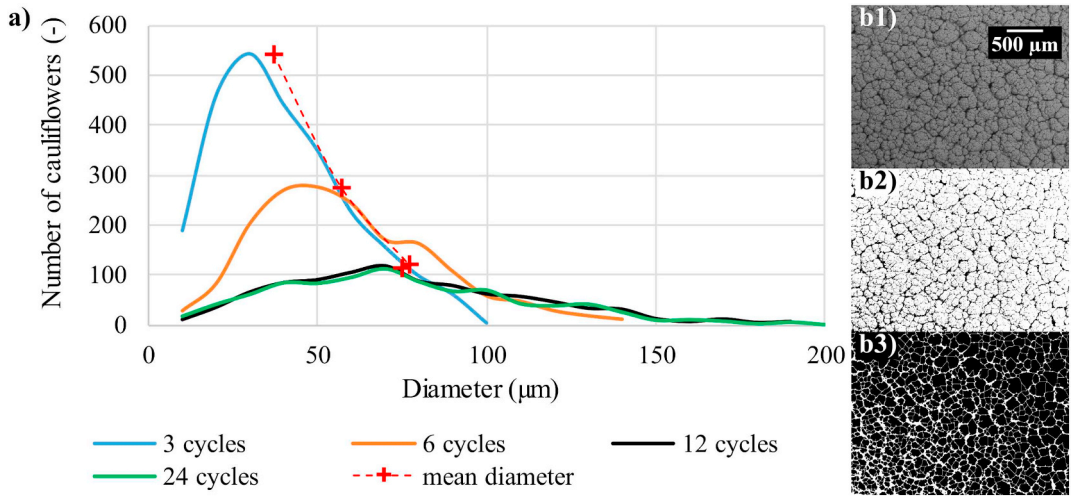

Fig. 5. a) Distribution of the diameters of the cauliflower-like features measured from the free surface by IA, b) example of the evaluation procedure for sample after 24 deposition cycles: b1) original SEM micrograph, b2) thresholded image, b3) inverted and watersheded image.

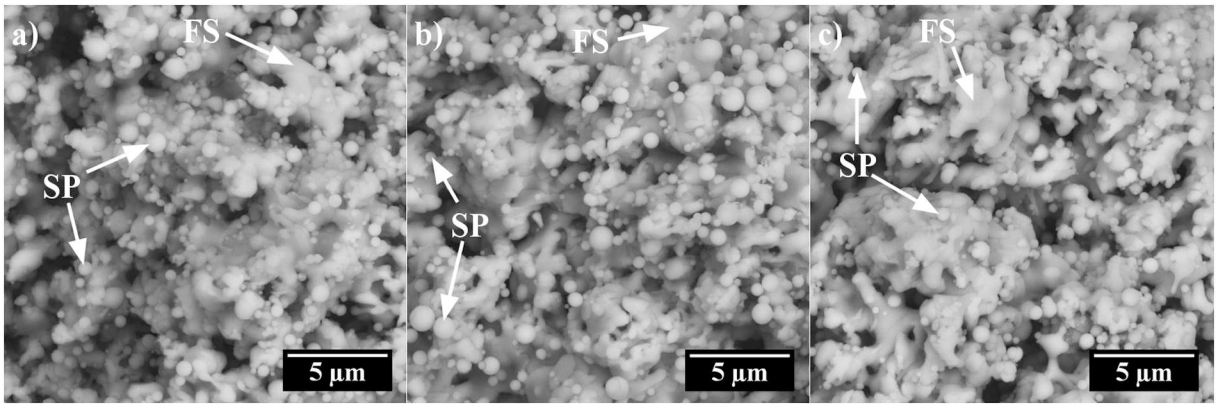

Fig. 6. Detailed views of the free surfaces of the deposits after a) 1, b) 6, and c) 24 deposition cycles. Large flattened splats (FS) and spherical particles (SP).

of the deposition setup.

Thickness profiles of the deposits, respective Gaussian fits, and an example of entire spray bead cross-section (at SD of 100 mm) are displayed in Fig. 9. The spray beads centers were positioned from 3 mm to 6 mm above the plasma jet centerline, indicating a slight upwards deflection of the injected liquid within the plasma jet. The width of the spray trace slightly increased with increasing SD due to the droplets dispersion broadening which was documented by the increase in the full width at half maximum of the Gaussian (Table 3).

Micrographs of representative areas of the deposits cross-sections

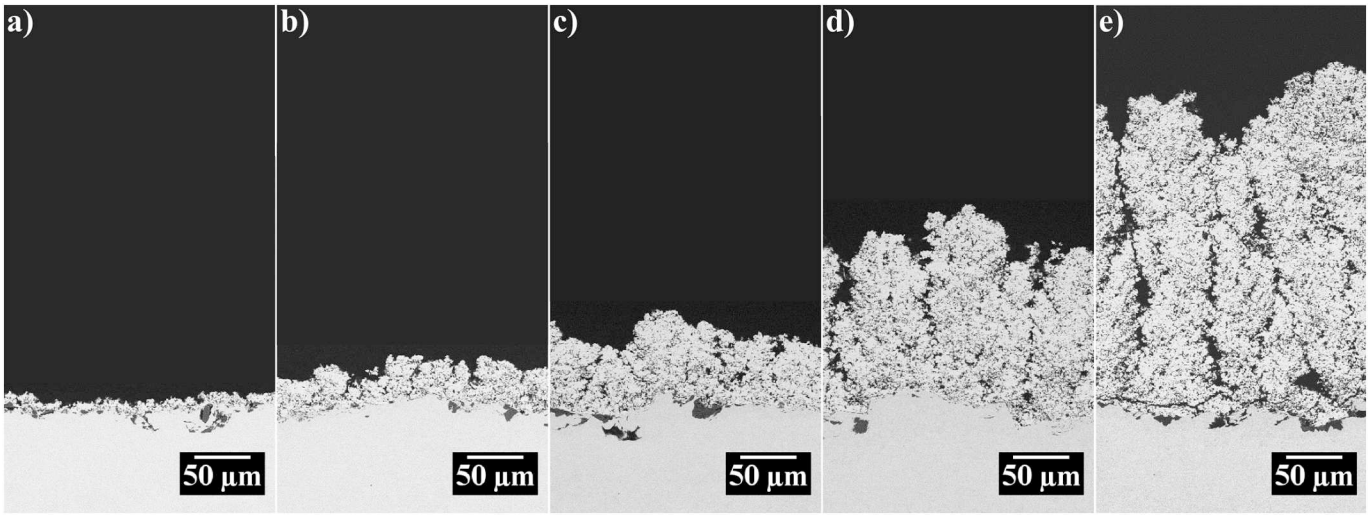

Fig. 7. Cross-sections of columnar deposits after a) 1 cycle, b) 3 cycles, c) 6 cycles, d) 12 cycles, e) 24 cycles. Suspension C.

sprayed at different stand-off distances are displayed in Fig. 10. The micrographs in the middle column show coating microstructure in the central part of the deposit. It is clearly visible that the columnar features in the central part of the deposit prepared at SD of 100 mm were rather dense and were separated by narrow intercolumnar gaps or segmentation cracks. With increasing stand-off distance, the coating porosity increased gradually from ~17% at SD = 100 mm to ~36% at SD = 130 mm. Rather interestingly, the total thickness did not vary significantly with the stand-off distance (Fig. 9) as the deposits formed at longer stand-off distances grew at the expense of their density. Taking into account both the porosity and the thickness of the deposits in the central part of the substrates, relative deposition efficiency in terms of "mass per pass" (DEr) could be estimated with respect to the SD100 coating. The result is displayed in chart in Fig. 11. DEr decreased monotonically with the increasing stand-off distance. Apparently, fewer particles impinged the substrate or more poorly adhering particles were blown away from its surface. Moreover, lower particle impingement velocity led to a lower degree of flattening and thus a more porous deposit.

The left and right columns in Fig. 10 show the off-axis deposits distanced 20 mm above and below the center of the sample, respectively. Evidently, porosity substantially increased with vertical distance from the plasma jet axis and the deposition rate decreased. Also, formed columns inclined towards the center of the deposits and the angle between the columns and substrate plane slightly decreased with the increasing SD. This can be attributed to the increasing influence of the lateral component of impingement velocity resulting in a shallower incident angle. Therefore, dispersion point position above the substrate decreased from ~34 mm to ~30 mm over the range of different SD (Fig. 11). Dispersion point position and the full width at half maximum were used to estimate the dispersion angle which increased from ~63° to ~83° with increasing SD.

Only one stand-off distance of 100 mm was used for the deposition of spray bead using the in-house-made alumina suspension (A) since no column formation was observed for this suspension. The representative cross-sections micrographs are displayed in Fig. 12. In the central part of the deposit, relatively dense microstructure (porosity 9.5 ± 0.9%) was formed, while rather uneven deposit with increased porosity was formed towards the edges. Contrary to the YSZ spray beads, the Al_2O_3 deposit was centered 10 ± 1 mm below the sample center which was

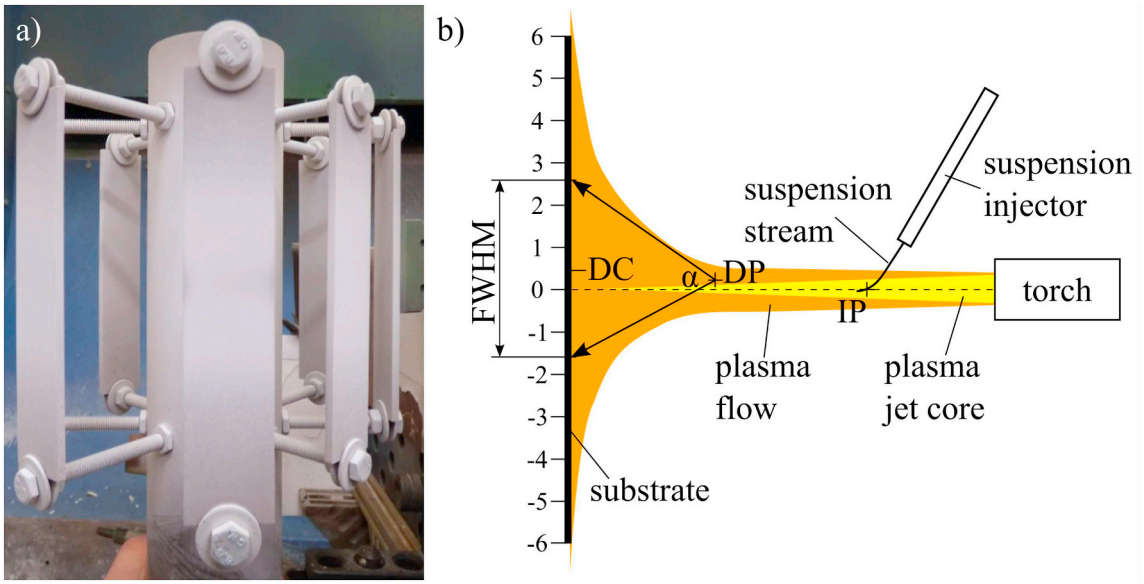

Fig. 8. The spray bead experiment: a) overall photograph of the spray bead samples after deposition, b) in-scale scheme of the deposition on the sample at SD of 100 mm: injection point (IP), dispersion point (DP), dispersion angle (α), deposit center (DC), full width at half maximum (FWHM) of coating thickness.

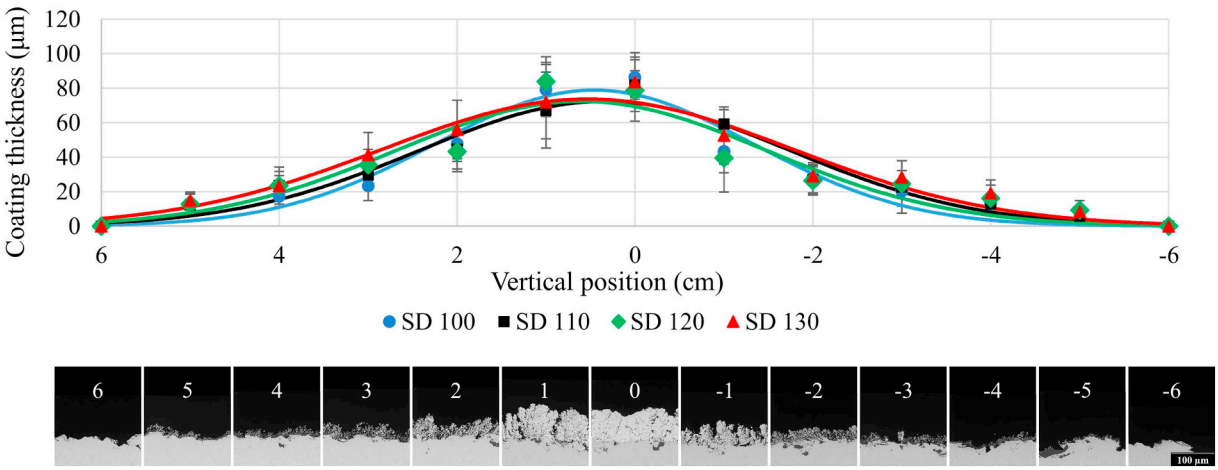

Fig. 9. Gaussian fit of the thickness profiles and cross-section SEM micrographs of the spray bead deposited at SD of 100 mm (numbers denote the vertical position on the substrate in centimeters, width of each SEM micrograph segment is 200 μm).

Table 3
Geometrical parameters of Gaussian fits of the thickness profiles.

Stand-off distance (mm)	Center offset (mm)	FWHM (mm)
100	5 ± 2	42 ± 4
110	3 ± 1	49 ± 3
120	6 ± 2	49 ± 5
130	5 ± 2	54 ± 4

probably caused by the higher injection pressure (4 bar compared to 3 bar) and partial overshooting of the suspension through the plasma jet. The mismatch between the deposit center position and the substrate center can also explain the difference in the microstructure above and below the deposit center (compare Fig. 12a and c). Fig. 12a displays the deposit formed 10 mm above the torch centerline where the melt particles impinged more perpendicularly with a greater velocity thus forming rather dense microstructure. Contrary, the particles that formed the deposit 30 mm below the torch centerline (Fig. 12c) impinged at a shallower angle possibly having a lower velocity resulting in a more porous deposit. The FWHM of the dense spray bead of 40 ± 1 mm was comparable to that of the YSZ one deposited at SD of 100 mm.

The micrographs of free surfaces of both columnar and dense spray beads obtained with SD of 100 mm are compared in Fig. 13. In the central part of the spray bead, the columnar structure formed from suspension C (Fig. 13a) consisted of mixture of fine spherical particles and coarse flattened splats. On the contrary, the central part of the dense coating deposited from suspension A (Fig. 13c) consisted predominantly of significantly larger well-flattened splats and only a limited number of finer spherical particles. However, in the outer parts of the spray beads, both deposits (Fig. 13b, d) consisted mostly of re-solidified, poorly adhering spherical particles rendering the deposits very soft and easy to remove mechanically. The resolidified particles were again significantly smaller for YSZ deposit.

4. Discussion

Multiple deposition approaches were used in order to visualize the growth of suspension plasma-sprayed deposits and to provide deeper understanding of the buildup mechanisms triggering either a columnar-like microstructure or a dense microstructure. The cauliflower growth and the single pass experiments confirmed that the columnar microstructure is developed when the feedstock yields a mixture of fine particles which are easily deflected by the stream of gasses parallel to the substrate surface and impact on the sides of surface asperities, and coarse particles that impact perpendicularly in a molten or semimolten state, forming the nuclei of the columns. This observation is in accordance with [26], suggesting that the deposition mechanism is comparable both for the conventional GSP torches and for the high enthalpy WSP-H torch.

Comparison of the first layer of splats and corresponding fully-developed coatings deposited under identical deposition parameters is provided in Fig. 14. The comparison between the two columnar-forming feedstocks (Fig. 14e and f for suspension B and C, respectively) showed that the finer impinging melt particles from suspension C yielded more pronounced columnar structure with narrower inter-columnar gaps reaching through the whole thickness down to the coating-substrate interface. On the contrary, the coarser melt droplets of suspension B created rather improperly developed interconnected columns showing the greater influence of the coarser particles governing the vertical growth over the lateral development of the columns.

Conversely, the dense microstructure (Fig. 14d) is formed when the feedstock suspension yields rather large melt particles with high perpendicular velocity that form highly flattened splats with diameters of up to several tens of micrometers (Fig. 14a). Momentum of these particles is large enough to retain their trajectory perpendicular to the coated surface, thus avoiding the lateral deposit growth.

Considering the microstructure obtained using suspension B, it appears that there is no specific threshold value of impinging melt particle size dividing the coating buildup between either purely columnar-like or purely dense microstructures. Instead, the transition is rather gradual depending on the prevalence of either fine droplets for columnar-like coatings or coarse droplets for dense coatings.

Regarding the obtained results, it has to be pointed out that the splat size and, in turn, final coating microstructure, was not directly correlated neither with the size of the primary particles dispersed in the suspensions nor with the solid loading (see Table 2). The governing factor was the degree of atomization of each suspension which determined the final size of the impinging melt particles. In other words, regardless to the solid load chemistry, suspension of fine powder may result in large melt droplets when undergoing poor atomization in the plasma jet and vice versa. However, suspension atomization in the plasma jet depends also on many other variables, e.g. suspension viscosity, solid loading, surface tension, solvent specific and latent heats, etc., the study of which was not the aim of this work.

The study of the columnar structure development with increasing number of deposition cycles showed that the first columns formation can be identified as early as after 3 deposition cycles. As the coating is formed, faster growing columns overlap the slower ones which forms the pattern of alternating widening and receding columns. The

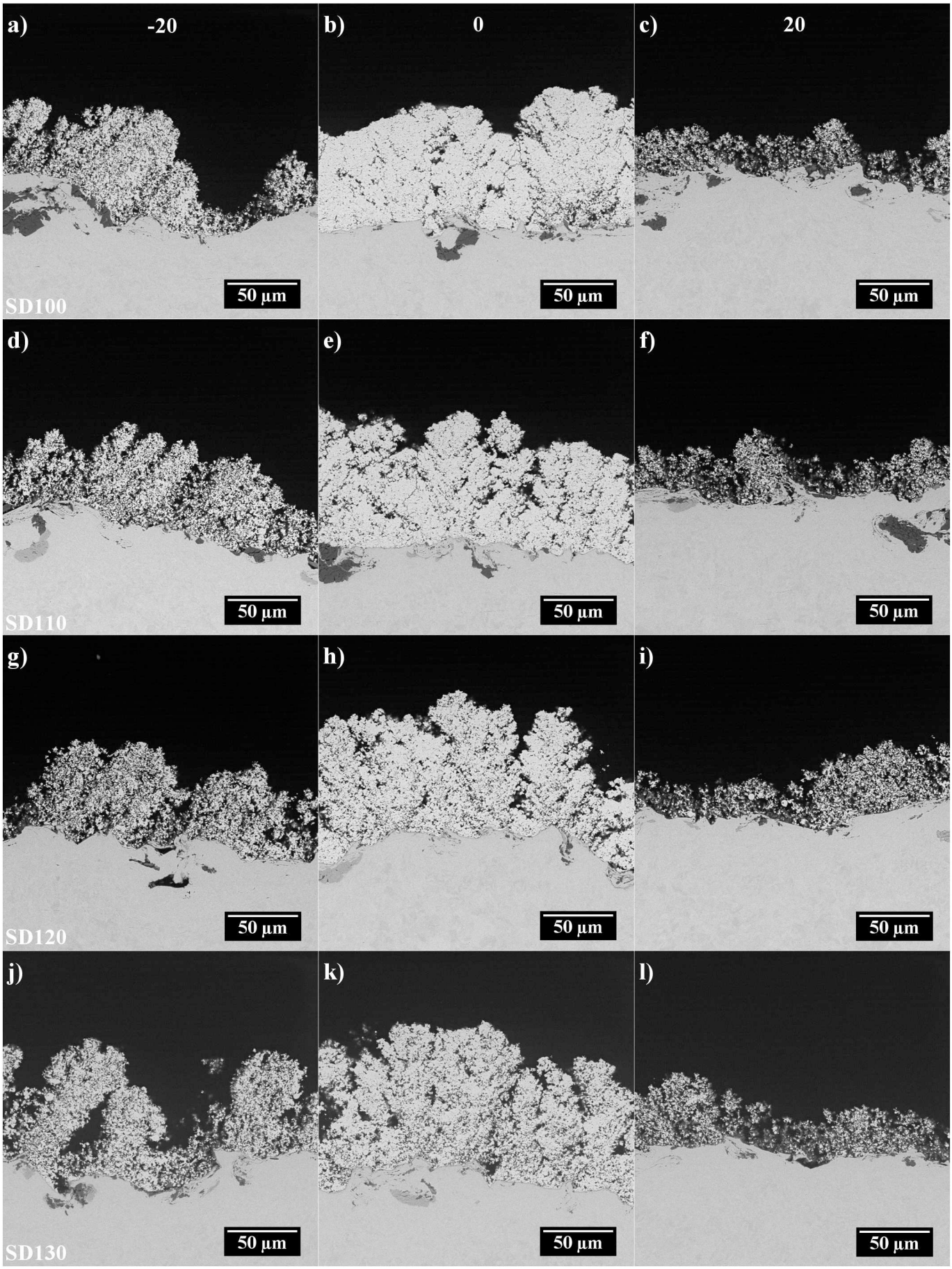

(caption on next page)

Fig. 10. Cross-sections of the deposits. Rows represent stand-off distances of 100, 110, 120, and 130 mm, respectively. Columns represent spots above (20 mm), at the middle (0 mm), and below (−20 mm) the sample center.

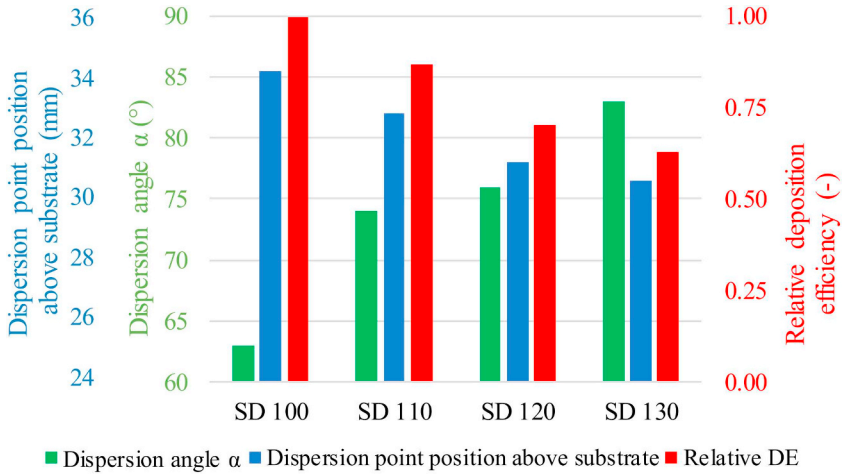

Fig. 11. Comparison of dispersion angle, dispersion point position above the substrate, and relative deposition efficiency for the spray beads deposited at different stand-off distances.

roughness of the free surface was increasing with increasing coating thickness, however, as measured from the cauliflowers diameters, the lateral growth of the diverging columns fully stabilized after 12 cycles as the peaks of the largest columns become new nucleation sites for further column vertical growth.

The spray beads of the columnar YSZ deposit showed the importance of the stand-off distance. Presumably, the particles arriving at the substrate from a greater distance impact at lower velocities having lower temperature [18]. Both facts contribute to the inferior flattening of such particles, leading to an increased deposit porosity which is in agreement with [27]. Moreover, the increased stand-off distance allows broadening of the area covered by the deposited material resulting in a wider spray trace, as documented by the increased FWHM of the deposits. The overspray formed at the substrates' peripheries is usually considered to be responsible for the interpass porosity found in SPS coatings [28]. The interpass porosity may be regarded undesirable since it deteriorates the internal coating cohesion [29], but it may be also useful in e.g. hindering the heat transfer through the coating [30] or tailoring the coating stiffness for abradable coatings. However, the deposit peripheries were very soft and could be easily damaged mechanically and even blown away from the surface. This explains the fact that this faulty deposit observed for spray bead experiment did not cause development of interpass porosity in the coatings deposited with WSP-H torch using standard deposition procedure as described e.g. in [22]. Under such conditions and unlike in the spray bead experiment with static torch, the sample surface is repeatedly exposed to successive torch passes and cooling air knives imposing intensive plasma/gas flow which blows away the loose deposit, thereby actively hindering the formation of interpass porosity.

5. Conclusions

The deposition experiments carried out in this study showed that the deposit formation mechanisms for the high enthalpy torch with radial suspension injection correspond to those reported for conventional GSP torches. It was observed that the suspension C (YSZ) yielded well-developed columnar structure as it produced fine melt droplets which were highly susceptible to be deflected by the lateral flow of plasma following the substrate surface. In the case of suspension B (Al_2O_3), the feedstock formed coarser droplets resulting in a columnar structure with mediocrely defined columnar “cauliflower-like” features separated by shallower intercolumnar gaps. In both cases, the columnar microstructure grew as a mixture of large flattening particles that ensure the vertical coating growth, and fine spherical particles that enable the lateral development of cauliflowers and porosity desirable for low thermal conductivity. Finally, when the feedstock produced rather large melt particles of several micrometers in diameter (suspension A), dense (i.e. low porosity) coating was formed by a mechanism similar to the those taking place during the conventional deposition from dry coarse powders. It therefore appears that there is a gradual transition from the well-developed columnar structure to the uniform dense coating depending on the size distribution of the impinging particles rather than a threshold value of impacting particle size that divides the coating buildup into purely columnar or purely dense. Moreover, the

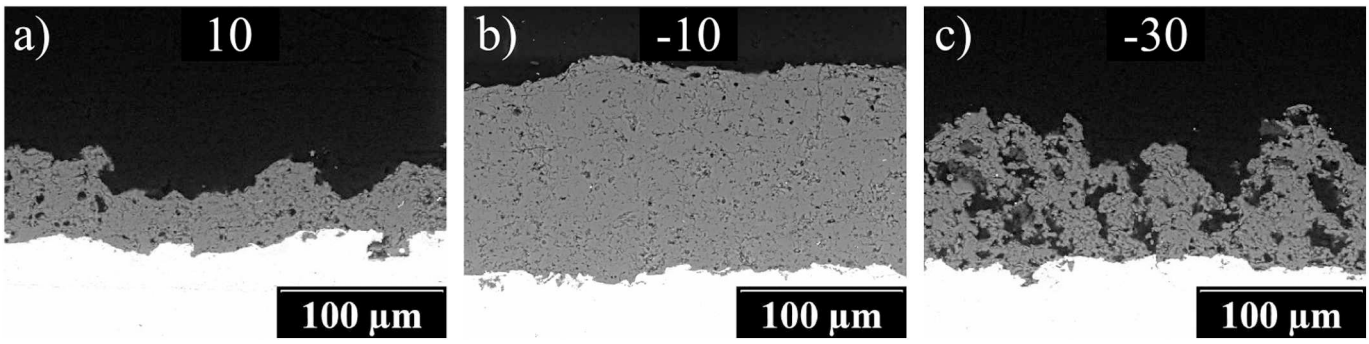

Fig. 12. Cross-section detail of the Al_2O_3 spray bead at SD 100 mm. Numbers denote the distance from the substrate center in mm.

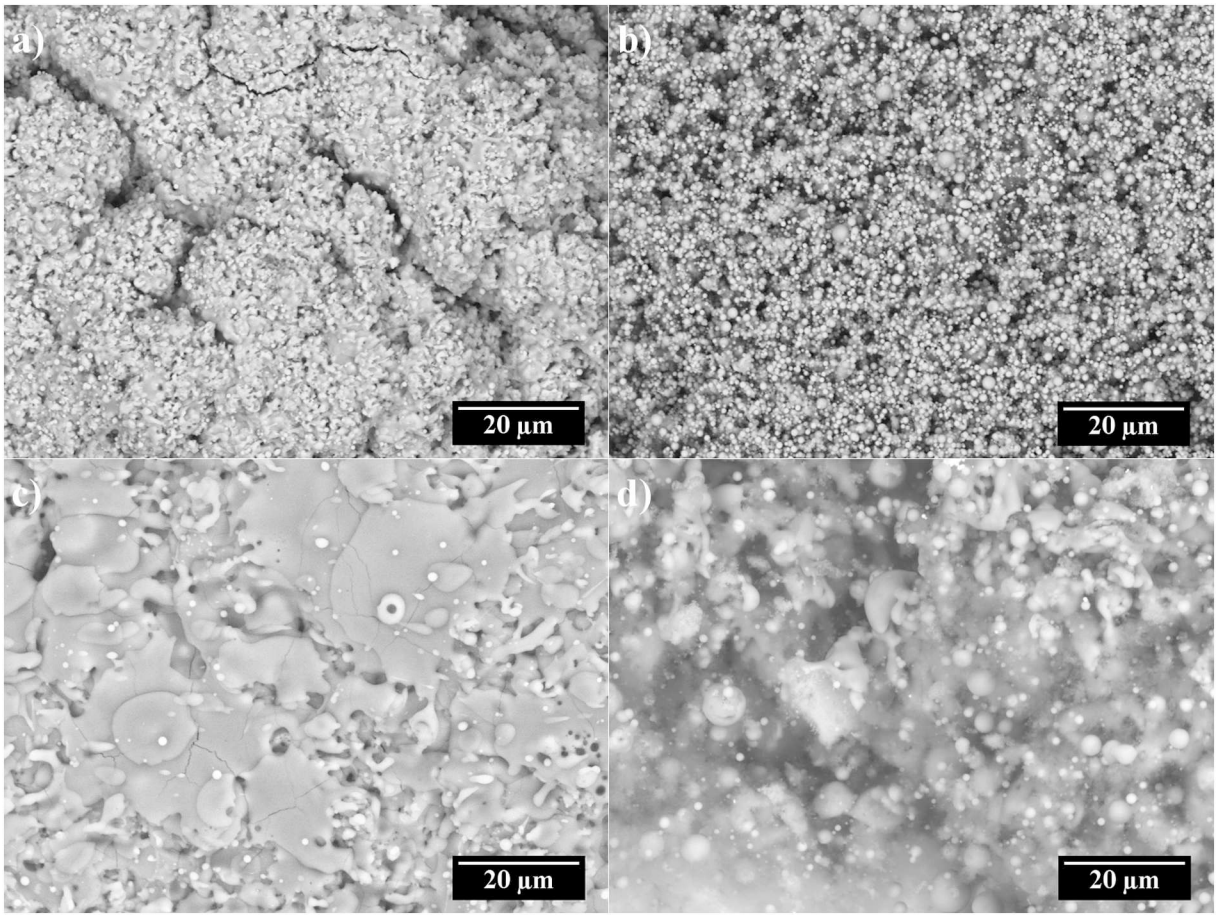

Fig. 13. Free surface of a) central part, b) periphery of YSZ deposit, and c) central part, d) periphery of dense Al_2O_3 deposit, both sprayed at SD = 100 mm.

suspension atomization seems to be more important than the primary suspension particle size or solid load alone, as when properly molten, larger atomized droplets result in larger melt particles and vice versa, regardless to the size of primary powder.

The development of the cauliflowers showed that the distinguishable columns were developed after the deposition of about 25 µm thick

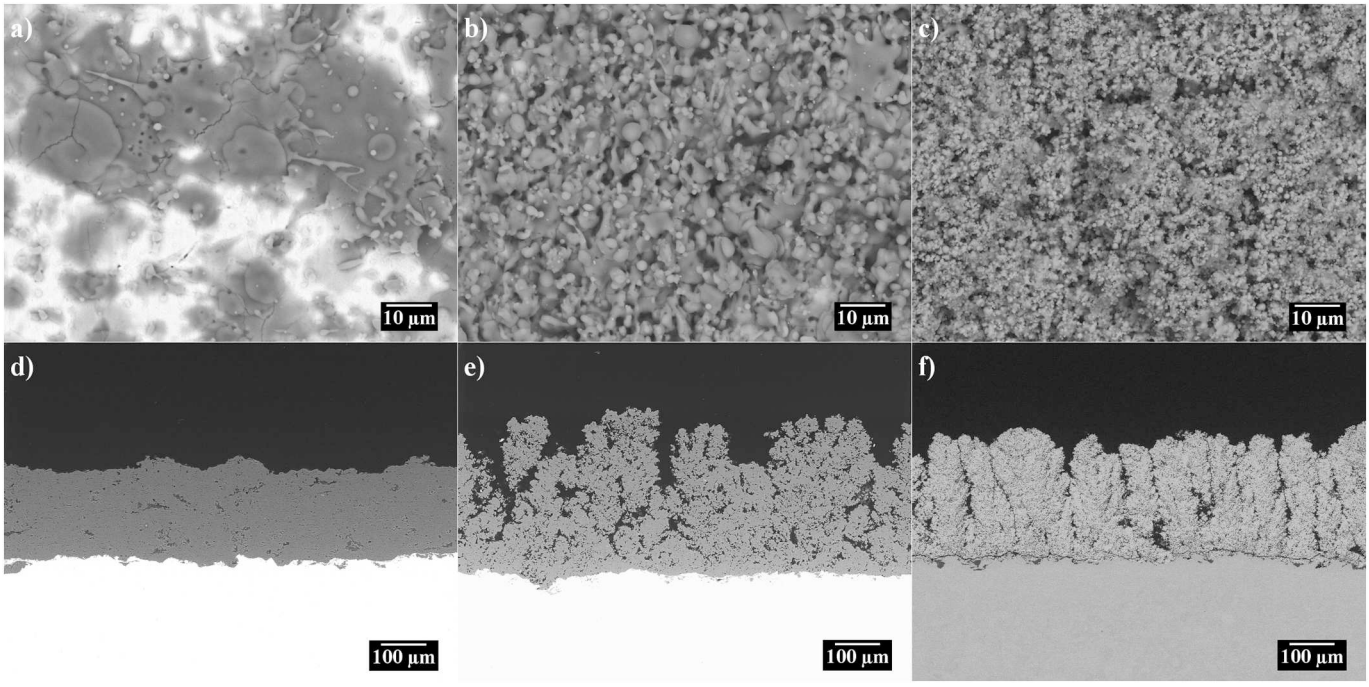

Fig. 14. First splats a), b), c) and the respective coatings d), e), f) from suspension A, suspension B, suspension C, respectively.

coating. However, the lateral growth of the columns practically stopped after 12 deposition cycles. Then, the columns generally grew either parallel to each other.

The spray beads experiments showed that the spray trace of the WSP-H torch when spraying liquid feedstocks has an effective diameter of about 40 mm or greater (from FWHM evaluation) making it suitable for spraying of large-area components. For both columnar and dense coatings, formation of the porous and loose overspray deposited on the edges of large substrates was observed. This overspray deposit is, however, blown away from the surface during the standard spraying procedure due to the successive passes of plasma torch and cooling air knives imposing intensive flow of plasma/gas on the coated surface, which effectively removes this poorly adhering deposit and thereby reduces risk of formation of interpass porosity.

Acknowledgements

Financial support of the GB14-36566G grant “Multidisciplinary research center for advanced materials” funded by the Czech Science Foundation is gratefully acknowledged.

References

[1] L. Pawlowski, Suspension and solution thermal spray coatings, Surf. Coat. Technol. 203 (2009) 2807–2829, https://doi.org/10.1016/j.surfcoat.2009.03.005.
[2] P. Fauchais, A. Joulia, S. Goutier, C. Chazelas, M. Vardelle, A. Vardelle, S. Rossignol, Suspension and solution plasma spraying, J. Phys. D. Appl. Phys. 46 (2013), https://doi.org/10.1088/0022-3727/46/22/224015.
[3] D. Chen, E.H. Jordan, M. Gell, X. Ma, Dense TiO2 coating using the solution precursor plasma spray process, J. Am. Ceram. Soc. 91 (2008) 865–872, https://doi.org/10.1111/j.1551-2916.2007.02225.x.
[4] R. Rampon, O. Marchand, C. Filiatre, G. Bertrand, Influence of suspension characteristics on coatings microstructure obtained by suspension plasma spraying, Surf. Coat. Technol. 202 (2008) 4337–4342, https://doi.org/10.1016/j.surfcoat.2008.04.006.
[5] A. Ganvir, N. Curry, S. Björklund, N. Markocsan, P. Nylén, Characterization of microstructure and thermal properties of YSZ coatings obtained by axial suspension plasma spraying (ASPS), J. Therm. Spray Technol. 24 (2015) 1195–1204, https://doi.org/10.1007/s11666-015-0263-x.
[6] T. Tesar, R. Musalek, J. Medricky, J. Kotlan, F. Lukac, Z. Pala, P. Ctibor, T. Chraska, S. Houdkova, V. Rimal, N. Curry, Development of suspension plasma sprayed alumina coatings with high enthalpy plasma torch, Surf. Coat. Technol. 325 (2017) 277–288, https://doi.org/10.1016/j.surfcoat.2017.06.039.
[7] R. Musalek, J. Medricky, T. Tesar, J. Kotlan, Z. Pala, F. Lukac, K. Illkova, M. Hlina, T. Chraska, P. Sokolowski, N. Curry, Controlling microstructure of yttria-stabilized zirconia prepared from suspensions and solutions by plasma spraying with high feed rates, J. Therm. Spray Technol. 26 (2017) 1787–1803, https://doi.org/10.1007/s11666-017-0622-x.
[8] N. Curry, K. VanEvery, T. Snyder, J. Susnjar, S. Bjorklund, Performance testing of suspension plasma sprayed thermal barrier coatings produced with varied suspension parameters, Coatings 5 (2015) 338–356, https://doi.org/10.3390/coatings5030338.
[9] F.-L. Toma, L.-M. Berger, S. Scheitz, S. Langner, C. Rödel, A. Potthoff, V. Sauchuk, M. Kusnezoff, Comparison of the microstructural characteristics and electrical properties of thermally sprayed Al2O3 coatings from aqueous suspensions and feedstock powders, J. Therm. Spray Technol. 21 (2012) 480–488, https://doi.org/10.1007/s11666-012-9761-2.
[10] M. Marr, O. Kesler, Permeability and microstructure of suspension plasma-sprayed YSZ electrolytes for SOFCs on various substrates, J. Therm. Spray Technol. 21 (2012) 1334–1346, https://doi.org/10.1007/s11666-012-9829-z.
[11] Y. Xiao, L. Song, X. Liu, Y. Huang, T. Huang, J. Chen, Y. Wu, F. Wu, Bioactive glass-ceramic coatings synthesized by the liquid precursor plasma spraying process, J. Therm. Spray Technol. 20 (2011) 560–568, https://doi.org/10.1007/s11666-010-9594-9.
[12] S. Mahade, N. Curry, S. Björklund, N. Markocsan, P. Nylén, Failure analysis of Gd2Zr2O7/YSZ multi-layered thermal barrier coatings subjected to thermal cyclic fatigue, J. Alloys Compd. 689 (2016) 1011–1019, https://doi.org/10.1016/j.jallcom.2016.07.333.
[13] N. Curry, K. VanEvery, T. Snyder, N. Markocsan, Thermal conductivity analysis and lifetime testing of suspension plasma-sprayed thermal barrier coatings, Coatings 4 (2014) 630–650, https://doi.org/10.3390/coatings4030630.
[14] D.E. Wolfe, J. Singh, R.A. Miller, J.I. Eldridge, D.M. Zhu, Tailored microstructure of EB-PVD 8YSZ thermal barrier coatings with low thermal conductivity and high thermal reflectivity for turbine applications, Surf. Coat. Technol. 190 (2005) 132–149, https://doi.org/10.1016/j.surfcoat.2004.04.071.
[15] L. Raggio, A. Gambaro, Study of the reasons for the consumption of each type of vegetable within a population of school-aged children, BMC Public Health 18 (2018) 1–11, https://doi.org/10.1186/s12889-018-6067-4.
[16] U. Schulz, C. Leyens, K. Fritscher, M. Peters, B. Saruhan-Brings, O. Lavigne, J.M. Dorvaux, M. Poulain, R. Mévrel, M. Caliez, Some recent trends in research and technology of advanced thermal barrier coatings, Aerosp. Sci. Technol. 7 (2003) 73–80, https://doi.org/10.1016/S1270-9638(02)00003-2.
[17] K. Vanevery, M.J.M. Krane, R.W. Trice, H. Wang, W. Porter, M. Besser, D. Sordelet, J. Ilavsky, J. Almer, Column formation in suspension plasma-sprayed coatings and resultant thermal properties, J. Therm. Spray Technol. 20 (2011) 817–828, https://doi.org/10.1007/s11666-011-9632-2.
[18] J. Oberste Berghaus, S. Bouaricha, J.-G. Legoux, C. Moreau, Injection conditions and in-flight particle states in suspension plasma spraying of alumina and zirconia nano-ceramics, in: C. Berndt, E. Lugscheider (Eds.), Therm. Spray Connects: Explore Its Surfacing Potential!, DVS-ASM, Basel, 2005, https://www.asminternational.org/home/-/journal_content/56/10192/CP2005ITSC0512/CONFERENCE-PAPER.
[19] P. Fauchais, R. Etchart-Salas, V. Rat, J.F. Coudert, N. Caron, K. Wittmann-Ténèze, Parameters controlling liquid plasma spraying: solutions, sols, or suspensions, J. Therm. Spray Technol. 17 (2008) 31–59, https://doi.org/10.1007/s11666-007-9152-2.
[20] J. Fazilleau, C. Delbos, V. Rat, J.F. Coudert, P. Fauchais, B. Pateyron, Phenomena involved in suspension plasma apraying part 1: suspension injection and behavior, Plasma Chem. Plasma Process. 26 (2006) 371–391, https://doi.org/10.1007/s11090-006-9019-1.
[21] B. Bernard, L. Bianchi, A. Malié, A. Joulia, B. Rémy, Columnar suspension plasma sprayed coating microstructural control for thermal barrier coating application, J. Eur. Ceram. Soc. 36 (2016) 1081–1089, https://doi.org/10.1016/j.jeurceramsoc.2015.11.018.
[22] R. Musalek, J. Medricky, T. Tesar, J. Kotlan, Z. Pala, F. Lukac, T. Chraska, N. Curry, Suspensions plasma spraying of ceramics with hybrid water-stabilized plasma technology, J. Therm. Spray Technol. 26 (2017) 37–46, https://doi.org/10.1007/s11666-016-0493-6.
[23] M. Hrabovsky, V. Kopecky, V. Sember, T. Kavka, O. Chumak, M. Konrad, Properties of hybrid water/gas DC arc plasma torch, IEEE Trans. Plasma Sci. 34 (2006) 1566–1575, https://doi.org/10.1109/TPS.2006.878365.
[24] M. Hlina, A. Maslani, J. Medricky, J. Kotlan, R. Musalek, M. Hrabovsky, Diagnostics of hybrid water/argon thermal plasma jet with water, ethanol and their mixture injection to plasma, Plasma Phys. Technol. 3 (2016) 62–65.
[25] M. Hlina, M. Hrabovský, Enthalpy probe diagnostics of steam/argon plasma jet, Plasma Phys. Technol. 2 (2015) 142–145.
[26] B. Bernard, A. Quet, L. Bianchi, V. Schick, A. Joulia, A. Malié, B. Rémy, Effect of suspension plasma-sprayed YSZ columnar microstructure and bond coat surface preparation on thermal barrier coating properties, J. Therm. Spray Technol. 26 (2017) 1025–1037, https://doi.org/10.1007/s11666-017-0584-z.
[27] C. Delbos, J. Fazilleau, V. Rat, J.F. Coudert, P. Fauchais, L. Bianchi, Finely structured ceramic coatings elaborated by liquid suspension injection in a DC plasma jet, Int. Therm. Spray Conf. 2004 Conf. Proc. DVS-GmbH, Osaka, 2004.
[28] O. Aranke, M. Gupta, N. Markocsan, B. Kjellman, X.H. Li, Effect of spray parameters on porosity and lifetime of suspension plasma sprayed thermal barrier coatings, in: F. Azarmi (Ed.), ITSC 2018—Proceedings Int. Therm. Spray Conf. ASM International, Orlando, 2018, pp. 84–91.
[29] A. Ganvir, N. Curry, N. Markocsan, P. Nylén, F.L. Toma, Comparative study of suspension plasma sprayed and suspension high velocity oxy-fuel sprayed YSZ thermal barrier coatings, Surf. Coat. Technol. 268 (2015) 70–76, https://doi.org/10.1016/j.surfcoat.2014.11.054.
[30] E.H. Jordan, C. Jiang, J. Roth, M. Gell, Low thermal conductivity yttria-stabilized zirconia thermal barrier coatings using the solution precursor plasma spray process, J. Therm. Spray Technol. 23 (2014) 849–859, https://doi.org/10.1007/s11666-014-0082-5.

5.3 Deposition of chromia-stabilized alumina using hybrid and intermixed feedstocks

The results in study [I] showed that the metastable alumina phases are prevalent in the coatings sprayed from liquid feedstocks similarly as in the conventional powder-sprayed coatings. Therefore, the third study [III] aimed at maximization of the α-phase content in the alumina coatings by virtue of alloying the aluminum oxide with the α-phase stabilizing chromium oxide using the spraying of intermixed suspensions and solutions and by the hybrid plasma spraying concept. Contrary to the case of a mechanical mixture of alumina and chromia powders, the finer microstructure of the liquid-sprayed coatings could provide more intensive intermixing of the materials and thus more effective phase stabilization. Hybrid deposition attempts carried out within this study were one of the first ones carried out at IPP, providing thus the proof-of-concept for hybrid deposition route using the hybrid water-stabilized plasma torch WSP-H 500.

As for the liquid feedstocks, an intermixed suspension of fine Al_2O_3 and Cr_2O_3 powders and an alumina suspension doped with dissolved chromium nitrate nonahydrate (CNN) as the chromia precursor were used. The ratio of alumina to chromia (or chromia equivalent) was identical in both liquids. The microstructures of liquid-sprayed coatings exhibited highly homogeneous dispersions of the two oxides, evidencing the thorough intermixing of both materials during the in-flight stage. The α-phase contents in the intermixed coatings were approximately two times greater compared to that of a reference alumina coating sprayed from a suspension using the same deposition conditions (~20 wt.% in intermixed coatings vs ~10 wt.% in pure coating).

The hybrid coatings were sprayed using a conventional dry coarse alumina powder and two chromia suspensions of different solid phase concentrations (25 wt.% and 40 wt.%) in order to assess the influence of chromia content on the α-phase amount formed in the coatings. The hybrid coatings were successfully deposited, exhibiting the anticipated microstructure of large alumina splats intermingled with fine chromia splats. As expected, the denser suspension resulted in higher chromia content in the coating in the form of larger splats while the more diluted suspension produced a finer dispersion of smaller chromia splats in the alumina matrix. The α-phase content was greater in the latter coating containing lower amount of more finely dispersed chromia, probably as a result of the greater amount of α-phase nucleation sites (α-phase contents of 87 wt.% and 81 wt.% were measured for the hybrid coatings sprayed using the diluted and dense chromia suspensions, respectively). Most importantly, the α-phase content in the hybrids was approximately two-fold greater than that in a pure Al_2O_3 coating sprayed under identical deposition conditions, thus proving the α-phase stabilizing function of liquid-deposited chromia on the powder-deposited alumina.

In this study, the deposition of hybrid and intermixed multimaterial coatings was demonstrated. Furthermore, the stabilizing effect of chromia on the alumina α-phase was successfully achieved for both hybrid and intermixed-liquid-feedstock coatings with respect to their pure alumina counterparts. Furthermore, the comparison between the α-phase contents in the hybrid (i.e., predominantly coarse-powder-based) coatings and intermixed liquid-based coatings showed that the coarser splats more willingly form the α-phase despite the inferior degree of intermixing with the stabilizing chromia; supposedly due to the overall lower cooling rates. Partial formation of an intermixed $(Al,Cr)_2O_3$ oxide was confirmed in the Cr-containing coatings by both XRD via the elongation of the corundum phase lattice parameters, and by

NMR via substantial shortening of ^{27}Al longitudinal relaxation times as compared to pure alumina.

The following paper was published in a special issue of Surface and Coatings Technology journal based on an invited talk given by author's supervisor Dr. Musalek at the conference Rencontres Internationales sur la Projection Thermique 2017, which was held in Limoges, France.

Surface & Coatings Technology 371 (2019) 298–311

Contents lists available at ScienceDirect

Surface & Coatings Technology

journal homepage: www.elsevier.com/locate/surfcoat

Increasing α-phase content of alumina-chromia coatings deposited by suspension plasma spraying using hybrid and intermixed concepts

Tomas Tesar[a,b,*], Radek Musalek[a], Frantisek Lukac[a], Jan Medricky[a,b], Jan Cizek[a], Vaclav Rimal[c], Shrikant Joshi[d], Tomas Chraska[a]

[a] Institute of Plasma Physics CAS, v.v.i., Department of Materials Engineering, Za Slovankou 3, 182 00 Praha 8, Czech Republic
[b] Czech Technical University in Prague, Faculty of Nuclear Science and Physical Engineering, Department of Materials, Trojanova 13, 120 00 Praha 2, Czech Republic
[c] Charles University, Faculty of Mathematics and Physics, V Holesovickach 2, 180 00 Praha 8, Czech Republic
[d] University West, Gustava Melins gata 2, 461 32, Trollhättan, Sweden

ARTICLE INFO

Keywords:
Hybrid suspension plasma spraying
Phase composition
Aluminum oxide
Chromium oxide
α-Phase
WSP-H

ABSTRACT

The novel method of hybrid suspension plasma spraying of dry coarse aluminum oxide powder with chromium oxide suspension using hybrid water/argon-stabilized (WSP-H 500) plasma torch was utilized for the deposition of coatings with very high α-phase content reaching up to 90%. The deposition mechanism and phase composition were compared with those of coatings deposited from i) intermixed alumina-chromia suspension and ii) alumina suspension doped with chromium nitrate nonahydrate solution. All deposition routes showed alternative ways of preparation of novel multimaterial coatings. It was demonstrated that the chromia addition and the deposition route play the crucial role in the pronounced formation of the thermodynamically stable α-phase.

1. Introduction

Surface engineering has an irreplaceable role in enhancing the service properties of functional and structural industrial parts. The modification of material's surface enables the utilization of parts in harsher conditions while prolonging their service lifetime. One of the modification techniques usable for large scale applications is thermal spraying which applies coatings through melting and propelling particles of added material towards a surface to which they adhere [1]. By layering the flattened impinged particles (splats), a coating is formed. Plasma spraying is a particular member of the thermal spraying techniques family which utilizes plasma stream as the heating and accelerating medium. Despite being an industrially established method, rapid development of this technique takes place both in the industrial and academic community [2,3].

Due to the number of process variables, plasma spraying is a versatile tool capable of processing numerous materials and their combinations for countless applications such as biomedical [4,5], wear-resistant [6,7], thermal and corrosion protection [8–10], and many others. One of the most recent advancements in plasma spraying is the introduction of so-called hybrid spraying concept [11–14], which combines the traditional spraying of coarse cut powders (typical particle size in tens of micrometers) with the more recent spraying of liquids, i.e. suspension plasma spraying (SPS; typical particle size from submicron to several micrometers) or solution precursor plasma spraying (SPPS; chemical precursor dissolved in the liquid). As a result, both liquid feedstock methods provide up to two orders of magnitude smaller splats when compared to the spraying of coarse dry powders. Combining powder and liquid feedstock spraying is motivated by bringing together the high material throughput achievable with powder spraying and the benefits of fine microstructural features achievable through the use of liquid feedstocks. The combination of coarse and fine splats has a potential in enhancing the functional properties of the coatings, such as e.g. improved coating cohesion by improved splat bonding or interconnecting the coarse splats by filling the intersplat voids with fine SPS/SPPS splats, thus aiming for higher hardness, wear resistance, or low porosity required e.g. for gas-tight coatings [11]. Another benefit of more effective intermixing of the fine SPS splats with the powder sprayed matrix is a potential of improved phase control of the final coating via stabilization of desirable crystallographic-phases by alloying the coating material with an additional stabilizer (typically second material with lattice similar to the desirable phase [15]). Hybrid processing potentially opens a more efficient, one-step route to prepare a desirable fine mixture of dissimilar compounds (i.e. matrix and stabilizing agent) which interact during the in-flight, splat formation, and cooling stages of the deposition. In other words, the hybrid coatings are

* Corresponding author.
E-mail address: tesar@ipp.cas.cz (T. Tesar).

https://doi.org/10.1016/j.surfcoat.2019.04.091
Received 31 August 2018; Received in revised form 16 April 2019; Accepted 29 April 2019
Available online 30 April 2019

expected to bring the properties matching or exceeding those of the suspension/solution-sprayed coatings while being cheaper in terms of lowering the consumption of costly liquid feedstocks and significantly increasing the deposition rate leading to shorter spraying time, thereby greatly improving the cost-efficiency of the whole coating preparation process. Also, in this process, not only the ratio of the feedstocks composition may be easily adjusted, but several technological steps needed for preparation of conventional pre-alloyed or intermixed coarse powders may be simply omitted. However, as liquid feedstocks generally require shorter stand-off distances than dry coarse powders, deposition parameters have to be optimized in order to ensure proper thermal treatment of both feedstocks to provide their desired interaction.

Phase composition control of the deposits is one of the key challenges in plasma-spraying, mainly due to the rapid solidification of the deposited material (cooling rates about $10^6\,K.s^{-1}$) accompanied by non-equilibrium transformations, frequently leading to complex phase structure of the deposits [16,17]. For example, tetragonal crystallographic configuration of zirconia (t-ZrO_2) is often stabilized by the addition of yttria (Y_2O_3) in order to prevent the detrimental transformation to monoclinic phase during in-service conditions [18].

Regarding alumina (Al_2O_3), an extensive research has also been conducted in the field of phase control [15,16,19–21], in particular the stabilization of the of α-phase (α-alumina, corundum), a desirable phase with better thermal, chemical, and electric properties. Unfortunately, the plasma-sprayed Al_2O_3 coatings constitute a limited content of the α-phase due to the preferred formation of metastable γ- and δ-phases during the rapid solidification of the melt upon its impact on the substrate [16,22]. In fact, the α-phase in the coatings is often attributed to the unmelted particles of the feedstock or their cores which retained the original phase structure [22]. These particles are further believed to serve as potential nucleation sites for the α-phase upon the impact of the melt onto the surface [23]. However, due to the natural stochastic character of the deposition and scatter in the particle size distribution of the feedstock, a controlled amount of unmelts is difficult to be guaranteed. Also, high amount of unmelts in the coating deteriorates its mechanical properties due to poorer intersplat connection and increased heterogeneity of the microstructure. The amount of the α-phase in the coating can also be enhanced by increasing the temperature of the substrate in the spray process or post-deposition annealing of the deposit. However, both ways require temperatures exceeding 1150 °C (the transformation temperature of corundum), which may be unfeasible if not impossible due to either the substrate material limitations or the size of the coated components. Moreover, the transformation of γ- to α-phase is accompanied by a density change from 3.65 $g{\cdot}cm^{-3}$ to 3.97 $g{\cdot}cm^{-3}$ which leads to material shrinkage and consecutively to the increase in porosity or even cracking of the deposit [19,24]. Long-term exposure to high temperatures may also lead to undesirable deformation of the whole coated component or even sintering of the coating microstructure compromising original benefits of the lamellar microstructure.

For the stabilization of corundum during spraying, addition of Cr_2O_3 (eskolaite) is often used, taking advantage of its higher thermal stability and lattice compatibility with α-alumina (both crystalize in rhombohedral lattice), thus serving as the nucleation sites for the α-alumina phase [16,20]. Also, Cr_2O_3 is able to form a $(Al,Cr)_2O_3$ solid solution with Al_2O_3, which also crystalizes in the rhombohedral configuration [25]. Mechanical mixture of coarse alumina and chromia powders as well as pre-alloyed powders were used for stabilization of α-alumina by chromia addition previously [15,16,21]. The former approach brings potentially greater variability in terms of easy composition tailoring while the latter generally provides higher homogeneity of the resulting coating due to spraying of relatively homogenized feedstock. In this regard, hybrid suspension/solution plasma spraying is a promising route combining the benefits of both concepts thanks to the easily adjustable composition and the fine dispersion of the additive within the matrix.

Considering the hybrid SPS method as an economical variant for preparation of advanced intermixed coatings, the characteristics of plasma source in terms of operating cost and power has to be taken into account. Concurrent feeding of both liquid and powder feedstocks at high feed rates requires enthalpy higher than SPS or high-throughput powder spraying alone. Due to its unique properties, the hybrid water-stabilized plasma torch WSP-H 500 appears particularly suitable for this task: its high-enthalpy jet [26] provides enough thermal energy available for the heat treatment of both feedstocks, while its high plasma velocity and jet length of ~10 cm ensure efficient fragmentation of the injected liquid and acceleration of the particles along the majority of the stand-off distance. As opposed to conventional gas-stabilized plasma (GSP) torches, its lower plasma density further allows easier penetration of the feedstocks into the plasma jet core [27]. Also, the relatively big diameter of the WSP-H plasma jet (given by the diameter of the plasma torch nozzle) eases targeting of the feedstocks into the plasma core which is essential for proper heat treatment of the injected particles. Lastly, the torch can be operated using very low amounts of plasma forming gases, in particular argon consumption as low as 12 slpm and water consumption as low as 20 ml/min (cf. hundreds of slpm of plasma-forming gases needed for high-enthalpy gas-stabilized plasma torches). Therefore, significantly lower operating cost can be achieved along with short production times.

In this study, two spray routes for stabilization of the α-Al_2O_3 by Cr_2O_3 were attempted:

- Hybrid – co-spraying of coarse alumina powder together with chromia suspension. Both materials were injected into plasma via separate feeding lines.
- Intermixed – spraying of mixture of alumina suspension with i) chromia suspension, or ii) solution of chromium nitrate nonahydrate ($Cr(NO_3)_3{\cdot}9H_2O$, further abbreviated as CNN) precursor. Mixtures were injected into plasma by one injector

The main difference between the two approaches is the way in which the constituents interact. In the hybrid route, both constituents travel in the plasma jet independently and their mutual interaction generally takes place after the deposition. On the contrary, the intermixed suspension or solution brings the deposited compounds together already in the in-flight stage inside the liquid droplets injected into the plasma jet. Therefore, they may be readily melted together (Fig. 1). In both concepts, interaction between the compounds can be expected thanks to the elevated temperature. In the hybrid coatings, the larger splats undergo significantly slower solidification which enables longer time available for mutual diffusion of the components. On the other hand, the intermixed coatings may be favored compared to the hybrid ones due to the small size of all splats, yielding a higher density of dissimilar splat boundaries in the coatings, which promises more intimate intermixing of fine Cr_2O_3 with the Al_2O_3 matrix. As a result, a higher contact area between the phases is available for the desired interaction, potentially resulting in the superior homogeneity of the coating.

Comparison of microstructures and phase composition of the alumina-chromia coatings deposited using both hybrid and intermixed spraying concepts was carried out in order to explore the possibility of stabilization of the α-phase by the introduction of finely dispersed chromia in the alumina matrix. As benchmark materials, pure alumina powder and alumina suspension were also deposited under identical spray conditions in order to evaluate the stabilization effect of the added chromia.

2. Materials and methods

Two powder-based hybrid coatings denoted as H-AC-1 and H-AC-2 (both coarse alumina powder + chromia suspension) as well as two

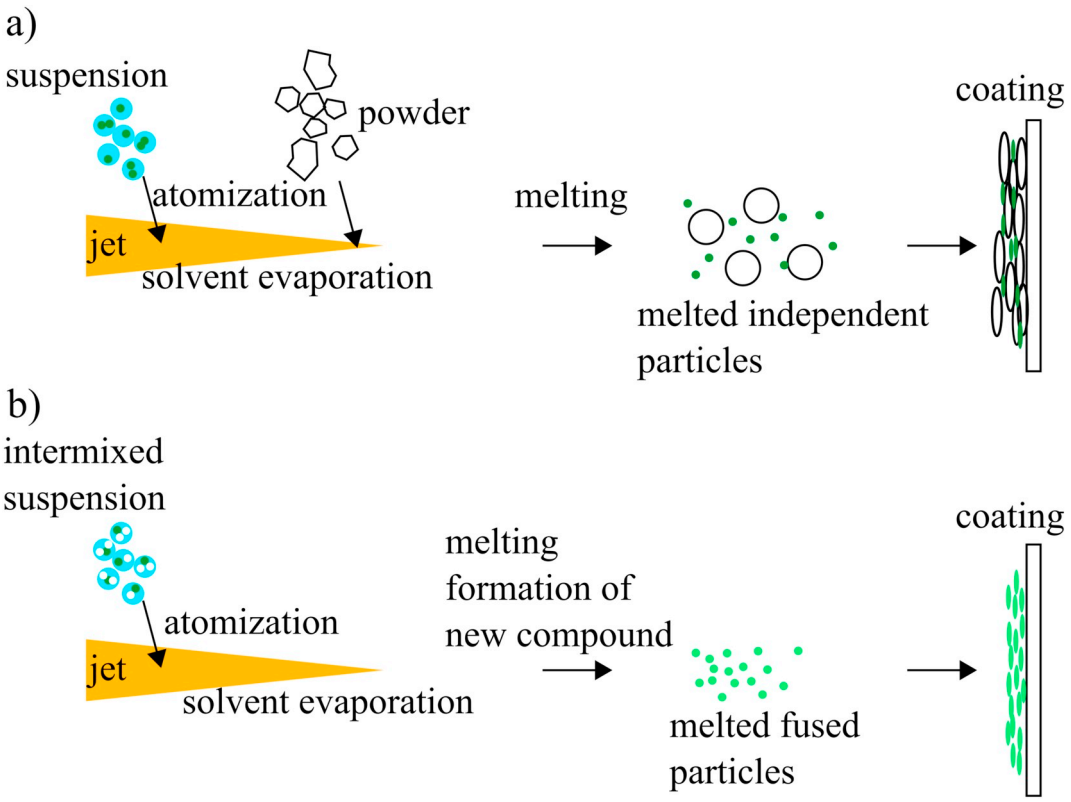

Fig. 1. Schematics of a) hybrid powder + suspension spraying, and b) intermixed suspension spraying.

Table 1
Feedstock compositions and deposition parameters. Stand-off distance (SD), feeding distances (FD) and feed rates (FR) are specified for powder and suspension (subscripts p and s), respectively. *dissolved precursor.

	Coating	Coarse powder material	Suspension			SD (mm)	FD_p/FD_s (mm)	FR_p/FR_s (g/min)	Deposition cycles
			Material	Solid load (wt.%)	Solvent				
Powder-based	P-A	Al_2O_3	–	–	–	130	35/–	116/–	5
	H-AC-1	Al_2O_3	Cr_2O_3	25	H_2O:C_2H_5OH 1:1	130	35/20	117/105	5
	H-AC-2	Al_2O_3	Cr_2O_3	40	H_2O:C_2H_5OH 1:1	130	35/20	116/107	5
Suspension-based	S-A	–	Al_2O_3	30	H_2O	100	–/25	–/126	7
	S-AC	–	Al_2O_3, Cr_2O_3	20	H_2O:C_2H_5OH 1:1	100	–/25	–/98	20
	SS-AC	–	Al_2O_3, $Cr(NO_3)_3$*	30	H_2O	100	–/25	–/120	7

suspension-based intermixed coatings denoted as S-AC (alumina suspension + chromia suspension) and SS-AC (alumina suspension + chromia solution) were prepared. For comparison, sample P-A was deposited by conventional spraying of coarse alumina powder and sample S-A was deposited from alumina suspension without any alpha-stabilizing compound. See Table 1 for details.

2.1. Feedstock materials

The powder-based coatings were deposited using a spray-grade commercial fused and crushed Al_2O_3 powder SURPREX AW 24 (Fujimi INC, Japan) with d_{50} = 73 µm. The P-A coating was deposited using this coarse powder only, while, in the case of H-AC-1 and H-AC-2 coatings, simultaneous injection of the powder and ready-to-spray Cr_2O_3 suspension in 1:1 water-ethanol solvent (d_{50} = 0.4 µm, Millidyne C101A, Millidyne Oy, Finland) was used. The concentrations of solid chromia in the suspensions were 25 wt% for H-AC-1 coating and 40 wt% for H-AC-2 coating. The lower solid load of the suspension used in H-AC-1 experiment aimed at easier fragmentation of the suspension by the plasma jet and thus for finer dispersion of chromia within the surrounding alumina. The injection pressure (and, in turn, feed rates) of both the powder and the suspensions were adjusted in order to ensure the optimal feedstock trajectory inside the core of the plasma jet (Fig. 2c) as monitored via direct observation of the feedstock penetration by a shadowgraphy technique (SprayCam, Control Vision INC, USA). Due to the different solid load content in the suspensions, the resulting alumina-to-chromia (A:C) solid-content weight ratio from the respective feed rates yielded lower amount of chromia for H-AC-1 experiment (~9:2) and higher amount of chromia for H-AC-2 experiment (~8:3) (Table 1).

The suspension-based coatings were sprayed using a water-based spray-grade SURPREX SA37 W30 Al_2O_3 suspension (Fujimi INC, Japan) with median particle size of d_{50} = 6 µm. Coating S-A was prepared using the suspension only, for the S-AC coating, the alumina suspension was mixed with a chromia suspension (same as used in H-AC-1 experiment) and pure ethanol (to maintain 1:1 water-ethanol ratio) with

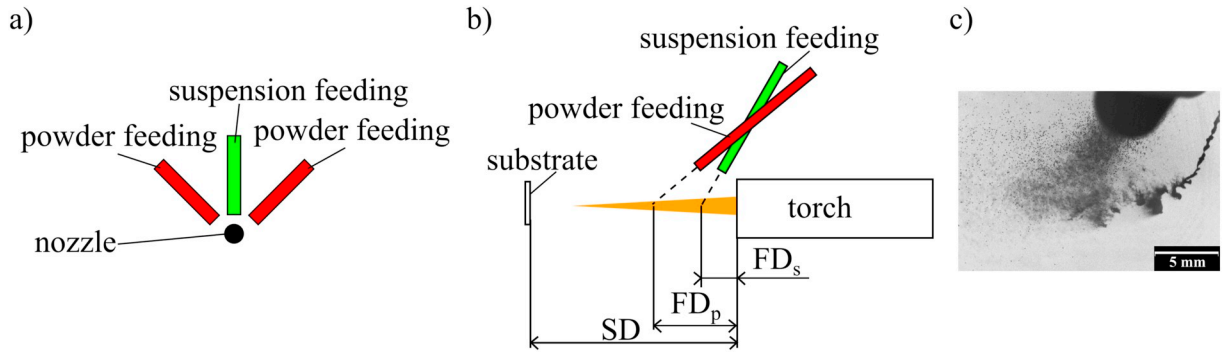

Fig. 2. a) front view of the feeding lines configuration, b) side view of the feeding lines configuration. SD, FD_p, and FD_s denote the stand-off distance, feeding distance of powder, and feeding distance of suspension, respectively, c) shadowgraphy image of concurrent powder and suspension injection (experiment H-AC-1).

the A:C ratio of 9:2 (comparable to H-AC-1 coating). For the SS-AC coating, chromium nitrate nonahydrate ($Cr(NO_3)_3{\cdot}9H_2O$) was dissolved in the alumina suspension with such concentration that the theoretical amount of in-situ created Cr_2O_3 upon thermal decomposition of CNN in the plasma jet resulted to the ratio of A:C = 9:2, too.

Viscosity of all sprayed liquids was measured by a rotational viscometer DV2TLV (Brookfield, USA) with coaxial cylindrical geometry in the shear rate range from 12.2 to 122.3 s^{-1} following an increasing-decreasing ramp of rotational speeds of the viscometer spindle.

2.2. Coatings deposition

The coatings were deposited using the hybrid argon/water-stabilized plasma torch WSP-H 500 (Projectsoft HK, a.s., Czech Republic) with arc current of 500 A (~150 kW net power), 3 l/h of water and 15 slpm of Ar consumption. The torch was mounted on a programmable robotic arm and the spraying procedure consisted of several spraying cycles, each followed by a cooling cycle. The spraying cycles comprised of 3 up & down vertical torch strokes over the substrates attached to a revolving carousel cooled by a set of air blades. Please note, that only about 1/3 of the samples is exposed to the torch during a single deposition pass (up&down stroke) due to the combination of relatively high torch transverse velocity and the rotation of the carousel. Therefore, the deposition process and consequently the deposition rate are described by the number of deposition cycles (see Tables 1 and 2) instead of the number of deposition passes. The deposition rate in terms thickness per pass (as usually presented) would be misleading as the "true" deposition rate would be 3 times higher (due to the duty factor of 1/3). Please see [8] for details. The torch stand-off distance (SD) was 130 mm for the powder-based coatings and 100 mm for the suspension-based coatings. The standard stand-off distance for spraying of alumina powders with water-stabilized torches generally ranges from 250 to 450 mm [16] and therefore, a compromise between the long SD for powder and short SD for suspensions was selected. For the cooling cycle, the torch was moved away from the samples while the samples were continually cooled by an air-blades flow of compressed air. After the temperature of the samples decreased to a preselected value of 250 °C, another deposition cycle was started.

Substrates for the coating deposition were AISI 304 stainless steel and S235 low carbon construction steel coupons sized 20 × 30 × 2.5 mm^3. They were sand blasted with alumina grit (GB series) to increase the surface roughness ($Ra \sim 8$ µm). For each run, 2 additional coupons from both materials were used with smooth, as-received surface (noGB series, $Ra \sim 1$ µm). Both GB and noGB substrates were cleaned in acetone in an ultrasound bath prior to the deposition to remove grease or contamination of the surface. The temperature of the substrates was monitored in-situ by a thermocouple connected to the rear side of one of the coupons and by an IR camera surveying the samples from the frontal side.

The dry powder feedstock was injected into the plasma jet through two independent injectors at the feeding distance (FD_p) of 35 mm from the torch nozzle exit (See Fig. 2) under a calibrated feed rate. The suspensions were fed radially into the plasma jet from a pneumatic liquid feeder equipped with mechanical agitation and online feed rate measurement through a single injector with calibrated orifice diameter of 0.35 mm at the feeding distance (FD_s) as specified in Table 1.

2.3. Coatings characterization

In order to investigate the cross-sections of the prepared coatings, standard metallographic procedure was carried out including precision cutting using Secotom-50 saw with diamond blade (Struers, Denmark), vacuum low-viscosity resin mounting (EpoFix, Struers, Denmark), and semiautomatic polishing using Tegramin-25 polishing system (Struers, Denmark). Scanning electron microscope (SEM) EVO MA15 (Carl Zeiss SMT, Germany) equipped with energy-dispersive spectroscopy (EDS) unit (Quantax XFlash® 5010, Bruker, Germany) was used in back-scattered electrons (BSE) mode to observe the coatings cross-sections and free surfaces (i.e. coatings surface). SEM micrographs of cross-sections were used for image analysis evaluation of thickness (20 readings for mean value) and porosity (5 images for mean value) of the coatings. Also, image analysis of the cross-sections was used to evaluate the amount of residual chromia recognizable in BSE SEM micrographs due to their higher mean atomic number as brightest splats, which was also confirmed by EDS.

Phase composition of the feedstocks (coarse powder and dried suspensions) was analyzed by X-ray diffraction (XRD) using Discover D8 diffractometer (Bruker, Germany) with Cu K_α radiation in Θ-Θ configuration. The XRD patterns were evaluated by Rietveld refinement method, the preferred orientation correction was calculated via March-Dollase approach [28]. Phase identification was done using X'Pert HighScore software (Malvern Panalytical, Ltd., UK), which accessed PDF-2 database of crystalline phases (pattern codes 01-080-0786, 00-056-0457, 00-046-1215, and 01-072-3533 for α-Al_2O_3, γ-Al_2O_3, δ*-Al_2O_3, and Cr_2O_3, respectively). Elemental composition of the feedstocks was analyzed by energy-dispersive X-ray fluorescence (EDXRF) using S2 PUMA spectrometer (Bruker, Germany). XRD measurements were carried out also for the deposits in order to evaluate the change in the phase composition after the deposition. A high thickness of the powder-based coatings enabled supplemental XRD measurement below the original free surface (~250 µm of the coating thickness was removed by grinding). The aim of this experiment was to confirm whether the coating phase composition is the same at the free-surface and deeper in the coating, where the material was exposed to additional thermal input due to the subsequent deposition cycles.

Since a reliable identification of the metastable phases by XRD was challenging due to a partial overlap of their diffraction patterns and a rather irregular nature of metastable phases originating in the ordered

defects in the spinel structure, the phase composition was further independently evaluated by ^{27}Al nuclear magnetic resonance (NMR) which does not require any assumptions on the crystallographic structure. The measurements were carried out under 20 kHz magic-angle spinning (MAS) on a Bruker Avance III HD spectrometer (11.7 T with the ^{27}Al frequency 130.4 MHz) using 200 scans with a single 0.27 μs long π/15 pulse and a relaxation delay 30 s that led to a quantitative excitation with negligible effects of the satellite transitions on the results [29]. Longitudinal relaxations of ^{27}Al were measured by saturation recovery. Evaluation by a linear combination of reference spectra of alpha and gamma phases as carried out in [30] was not possible due to significant presence of other phases, precise spectra of which remain unknown. Instead, in order to determine the fraction of aluminum atoms in octahedral positions, the peak belonging to octahedral sites (centered at 14 ppm) was fitted by a Lorentzian/Gaussian curve and its area was related to the integral of the whole central part of the spectrum. The content of α-alumina was then calculated assuming only α and γ phases are present considering the fact that γ-Al_2O_3 has 75% of all Al atoms in octahedrons [31]; this approach gave the molar fraction of α-Al_2O_3 relative to the total Al_2O_3 content with an absolute error of about 0.1.

Hardness of the deposits was measured on the polished cross-sections using automated hardness tester Qness Q10A+ (Qness, Austria) with Vickers indenter using HV0.3 and HV1 loads from 10 indents at each load.

3. Results

3.1. Feedstocks properties

Viscosity measurements of all sprayed suspensions were carried out in order to examine how the modification of the ready-to-spray suspensions (dilution of chromia suspension and addition of chromia suspension or $Cr(NO_3)_3$ into the alumina suspension) changed their rheology. It is evident from Fig. 3a that dilution of the original chromia suspension from 40 to 25 wt% decreased viscosity dramatically from about 4200 mPa.s to less than 1000 mPa.s at 12 s^{-1} shear rate and from about 700 mPa.s to less than 140 mPa.s at 122 s^{-1}. Lower suspension viscosity is generally desirable as it facilitates its transport through the feeding lines and through the injection nozzle.

The viscosity of alumina-based suspensions (Fig. 3b) was remarkably lower than that of chromia suspensions. The original suspension from experiment S-A showed the lowest mean viscosity of 1.3 ± 0.2 mPa.s at 122 s^{-1} shear rate which is close to that of water. Addition of the chromia suspension for the S-AC experiment increased the viscosity, triggering a characteristic shear thinning shape of the viscosity-shear rate curve. The viscosity increase is to be attributed to the change in solvent from water to 1:1 water:ethanol mixture which exhibits viscosity higher than each of the constituents alone. With the addition of CNN for the SS-AC experiment, only a negligible increase in the viscosity was measured. Nevertheless, the viscosity of all the alumina-based suspensions used for suspension-based coatings deposition was in the range from about 1 to 5 mPa.s at the highest shear rate of 122 s^{-1}.

Table 2
Coatings characteristics. *informative values, see Section 3.2.3.

Coating	Thickness (μm)	Deposition rate (μm/cycle)	HV0.3 (−)	HV1 (−)
P-A	626 ± 21	125	1574 ± 311	1141 ± 188
H-AC-1	721 ± 19	144	1482 ± 194	942 ± 224
H-AC-2	661 ± 20	132	1200 ± 291	1148 ± 296
S-A	142 ± 14	20	1289 ± 184	736 ± 83*
S-AC	227 ± 8	11	1244 ± 153	1068 ± 140*
SS-AC	146 ± 11	20	1386 ± 160	750 ± 102*

3.2. Coatings

All spraying experiments resulted in a successful deposition of coatings. Samples with grit-blasted S235 steel substrate showed no delamination. A partial delamination on the sample edges was observed for the samples with AISI 304 stainless steel grit-blasted substrates, probably due to higher coefficient of thermal expansion (CTE) mismatch between the substrate and the coating (CTE of AISI 304 of $17{\cdot}10^{-6}\,K^{-1}$ compared to $12{\cdot}10^{-6}\,K^{-1}$ of S235 [32,33]) and high stiffness of the coatings. The non-blasted samples (noGB series) exhibited excessive coating peel-off, pronounced mainly for the hybrid coatings. Therefore, the samples without delamination were selected for further metallographic preparation.

3.2.1. Microstructures

The microstructure cross-sections of the coatings are displayed in Fig. 4. All deposits formed relatively dense, uniform coatings with lamellar splat structure as observable in the overview micrographs. A more detailed view in Fig. 4 (right-hand-side column) reveals that the size of the splats was at least an order of magnitude smaller for the suspension-based coatings compared to the powder-based coatings. No unmelted Al_2O_3 feedstock was found in the cross-sections showing proper heat treatment of the injected particles. It is also evident that the powder-based coatings reached significantly higher thickness of more than 500 μm whereas the thickness of the suspension-based ones was in the range of 150–250 μm. Considering the number of torch passes (see Table 1), the deposition rate of the powder-based coatings was significantly higher, reaching about 130 μm per cycle, while the suspension-based coatings were deposited with the deposition rate from 11 to 20 μm per deposition cycle. This may be attributed to the feed rate of the solid feedstock material injected into the plasma jet which was about 5 times higher for the powder-based coatings compared to the suspension-based ones. Nevertheless, these values suggest a slightly lower deposition efficiency of spraying from the suspensions (the efficiency optimization was not aim of this study and will be targeted in the next experiments). The measured thicknesses and deposition rate values are listed in Table 2. Please note that the thin bright layer distinguishable in Fig. 4i is only an artifact from the metallographic preparation, i.e. debris of ground-off substrate accumulated in the gap which formed between the epoxy and the sample due to the epoxy shrinkage.

Porosity in the coatings as evaluated by image analysis was divided into two disjunctive domains: a) submicron-sized porosity (area less than 1 μm^2), predominantly resulting from the imperfect sintering of primary particles, and b) super-micron-sized porosity (voids larger than 1 μm^2), typically intersplat pores and cracks. The sum of the submicron and super-micron porosity was taken as the total porosity and it was in the range of ~4.3–8.3% for all deposited coatings. In all prepared coatings, the coarser super-micron-sized porosity was dominant over the finer submicron porosity. This was most evident in the H-AC-1 coating with the highest super-micron-sized to submicron-sized porosity ratio of 7:1 (Fig. 5). As observable from Fig. 4c and e for the hybrid coatings, most of the voids was represented by large intersplat pores and intrasplat cracks between the coarse Al_2O_3 splats. The residual chromia splats apparently established strong interconnection with the alumina splats, documented by suppressed cracking on the alumina-chromia interface. However, among the powder-based coatings, the lowest overall porosity was measured for the P-A coating, despite the lack of the additive phase.

In the case of the suspension-based coatings, the main source of super-micron-sized porosity were out-of-plane (vertical) segmentation cracks and in-plane (horizontal) cracks. The horizontal cracks seem to follow boundaries between sublayers deposited during individual deposition cycles. The vertical cracks were formed probably due to thermal stress relief during cooling accompanied by uneven shrinkage of the coating. Higher density of vertical cracks was observed in the

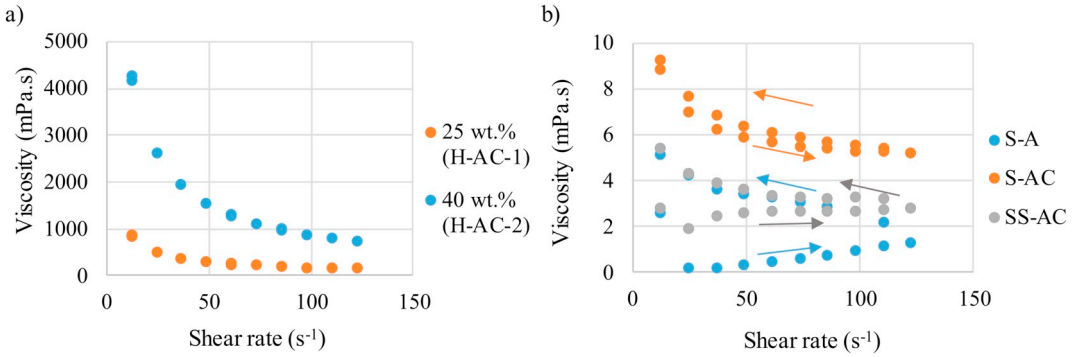

Fig. 3. a) viscosity of Cr_2O_3 suspensions for 25 and 40 wt% concentrations, b) viscosity of alumina and alumina-chromia suspensions used in S-A, S-AC, and SS-AC experiments. Arrows indicating increasing/decreasing spindle rotational velocity.

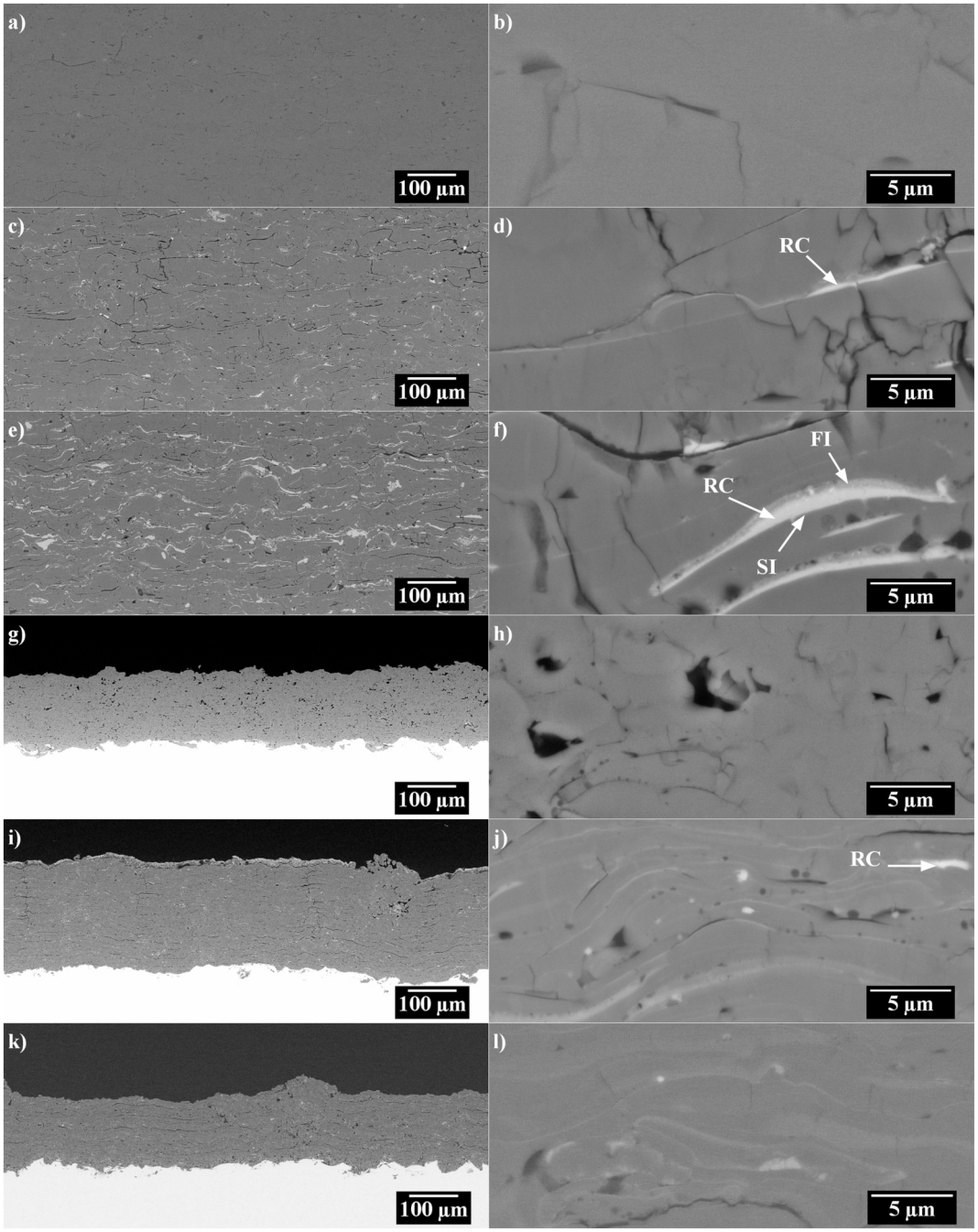

Fig. 4. Overviews (left) and details (right) of the coatings: P-A (a), (b), H-AC-1 (c), (d), H-AC-2 (e), (f), S-A (g), (h), S-AC (i), (j), SS-AC (k), (l). Residual chromia (RC), fuzzy interface (FI), sharp interface (SI). SEM BSE mode.

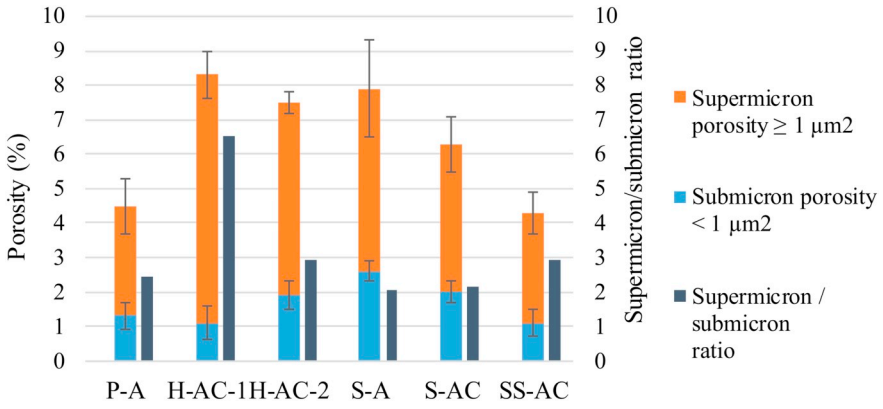

Fig. 5. Comparison of submicron-sized and super-micron-sized porosity of the coatings.

dense suspension-based coatings due to the less effective dissipation of shrinkage stresses (e.g. by splat sliding [34]) due to much smaller splats and their stronger bonding than in their powder-sprayed counterparts with a generally looser microstructure. Among the suspension-based coatings, the highest porosity was measured for the S-A coating reaching a total value of 7.9% where 5.3% was represented by the super-micron-sized porosity and 2.6% by the submicron porosity. These values were comparable to those of S-AC coating and greater than those of SS-AC coating, showing that the addition of CNN promoted densification of the coating. The lower porosity of the SS-AC coating compared to S-AC coating could be explained by overall higher suspension solid load further enriched by the solution of CNN resulting in formation of larger molten droplets receiving higher velocity from the jet.

Detailed micrographs in Fig. 4d, f, j, and l clearly show the distinguishable chromia splats in the chromia-doped coatings, appearing as brighter material among the darker alumina splats. However, varying shading of the splats as observed in BSE-COMPO mode (Fig. 4) sensitive to the local mean atomic number showed also successful intermixing of both constituents forming a transition interface. Intensity of the alloying process varied significantly between the coatings due to the different size and intermixing route of the arriving particles.

In the case of hybrid coatings displayed in Fig. 4c and e, the chromia splats were generally more separated from the alumina matrix, whereas in the suspension-based coatings, most of chromia was well dissolved into the surrounding alumina. For H-AC-1 coating, the amount of undissolved chromia splats as measured by image analysis from the cross-sections represented approximately 3% of the coating whereas in the H-AC-2 coating the fraction of undissolved chromia splats reached approximately 8%. Also, the chromia splats in the H-AC-2 coating were larger in size (compare Fig. 4d and f). In the suspension-based intermixed coatings, the amount of residual chromia was about 1.4% for S-AC coating and only 0.5% for the SS-AC coating.

The different character of alumina-chromia mixing can be also observed in the free-surface SEM micrographs presented in Fig. 6. In the hybrid coatings, the most notable difference is the size and abundance of chromia-rich splats (CRS). Contrary, the intermixed coatings showed almost no bright splats in the free surface declaring high chemical homogeneity of the deposited material.

Mutual comparison of H-AC-1 and H-AC-2 free-surface micrographs demonstrates the finer atomization of the more diluted suspension (H-AC-1). This is beneficial for the heteronucleation of the α-phase from the coarse alumina particles as the large alumina splats cover areas with higher amount of smaller chromia splats which serve as the nucleation sites. Moreover, in the hybrid coatings, isolated regions of unmelted, yet deposited, suspension feedstock were scarcely found as very fine chromia particles clusters (CPC). These agglomerates could be also found in small amount in the hybrid coatings cross-sections. On the contrary, no such particles were found in the intermixed coatings. It can be therefore assumed that, in the case of the hybrid coatings, the plasma jet was partially disturbed by the concurrent injection of both suspension and powder. In such case, the lightest suspension droplets were driven out from the plasma jet by the turbulences further downstream in the jet, i.e. in the area, where the powder was injected. Insufficient thermal treatment of the small portion of droplets traveling through the periphery of the plasma stream then resulted in the presence of dried, unmelted suspension feedstock in the deposited coating (Fig. 7), whereas the heavier powder particles retained their trajectory along the plasma centerline where they received enough heat for melting.

Another difference between the hybrid and intermixed coatings is the presence of dome-shaped structures (DSS) at the surface of the intermixed coatings (see Fig. 6e), indicating partial occurrence of the shadowing effect, which is typical for plasma sprayed coatings from liquid feedstocks [35]. In the shadowing effect, surface asperities (e.g. original substrate asperities or larger previously deposited droplets) serve as the nucleation sites for more rapid vertical and lateral growth of the coating, resulting in a dome-shaped structure.

3.2.2. *Phase composition*

Phase composition was evaluated for both (dried) feedstocks and for the coatings in order to evaluate the phase changes of the original feedstock or a formation of new phases. The Al_2O_3 feedstocks consisted practically of α-alumina phase only (either as a coarse spray-grade powder or as a fine submicron powder dispersed in the suspensions) confirmed by both XRD and ^{27}Al NMR. All deposits were mostly crystalline with the content of the amorphous phase below 10%. Based on the observation of the coatings microstructure (Fig. 4), no unmelted Al_2O_3 feedstock (either coarse powder particles or agglomerates of the fine particles from the suspensions) was found in the coatings, i.e. all crystallographic phases present in the coatings were newly formed from the melted impinging particles. In the hybrid coatings, a small amount (below 1% as measured by image analysis) of the unmelted chromia particles from the suspensions was observed (Fig. 7).

The results of the powder-based coatings phase composition analysis are summarized in Table 3 and the corresponding XRD diffraction patterns are displayed in Fig. 8. From the comparison of the α-phase content in the deposits, it is evident that the addition of Cr_2O_3 significantly promoted the formation of the stable alumina phase. The rest of the structure comprised of metastable alumina phases (γ,δ) exhibiting the structures of a defected spinel [36] and residual eskolaite (Cr_2O_3). In the non-stabilized P-A coating, the amount of α-phase was 40%, while 87% and 81% of stable α-alumina was obtained in H-AC-1 and H-AC-2 coatings, respectively. Increased alpha-phase content was confirmed also by independent NMR measurements based on the distinction between tetra- and octahedral coordination of aluminum atoms.

In the suspension-based coatings, the amount of α-phase was generally lower than in the powder-based ones, both in the pure and chromia-doped coatings. However, the addition of chromia resulted

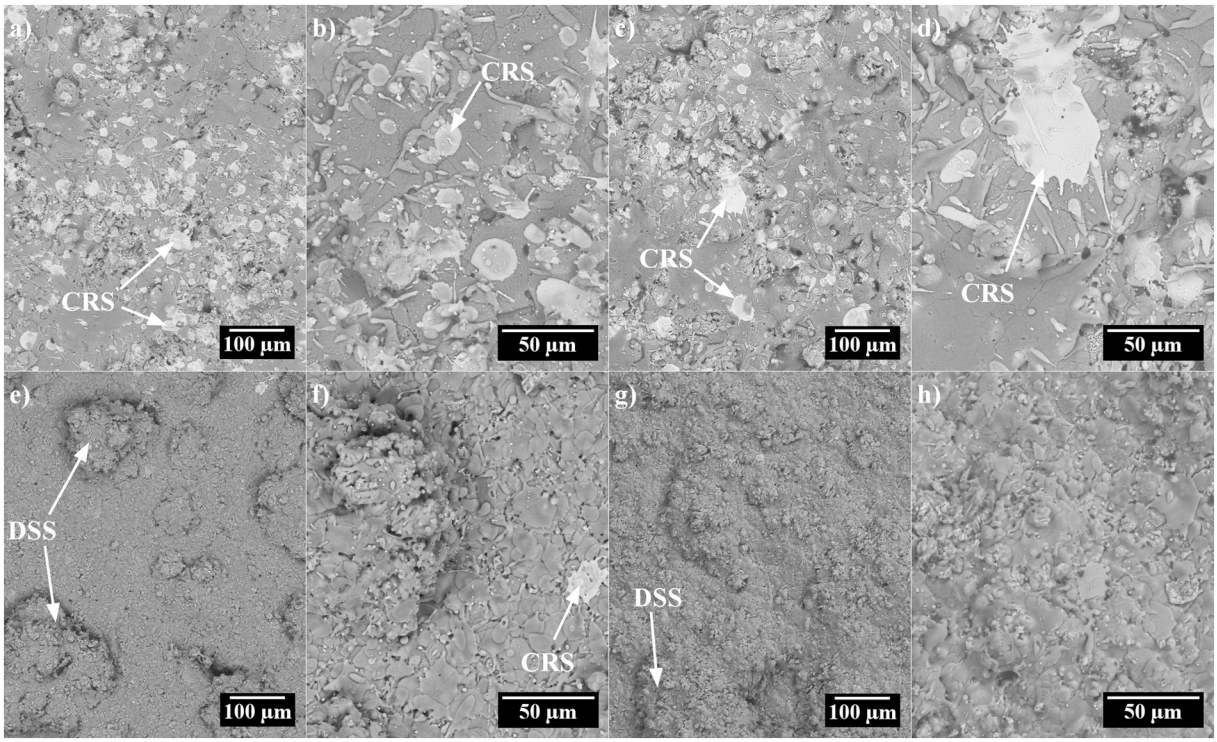

Fig. 6. a) H-AC-1 overview, b) H-AC-1 detail, c) H-AC-2 overview, d) H-AC-2 detail, e) S-AC overview, f) S-AC detail, g) SS-AC overview, h) SS-AC detail. Arrows show chromia-rich splats (CRS), and dome-shaped structures (DSS). SEM BSE mode.

also in this case in a distinguishable increase in the amount of α-alumina from 12% in the S-A coating to 21–22%, in S-AC and SS-AC coatings, confirming the positive effect of chromia presence on the formation of α-phase (see diffraction pattern in Fig. 9 and Table 4).

As for the NMR measurement of the suspension-based coatings, a reliable evaluation of the α-phase content was possible only for the S-A coating, the spectra of which could be well explained as a superposition of α and γ (other transition phases of alumina could be excluded). The α-content was estimated as (24 ± 10) % in the coating S-A. On the other hand, the low fraction of Al atoms on octahedral positions (77% and 74% in the coatings S-AC and SS-AC, respectively) and modified spectral shapes (Fig. 10) proved that there was a significant fraction of other metastable aluminas, namely δ [36,37] or θ [38,39] that have fewer Al atoms in octahedral positions than γ, or amorphous phase. This disallowed the evaluation of the α-phase content due to an unknown composition of these additional phases.

To investigate the possibility of the deposits undergoing in-situ annealing during the successive torch passes, approximately 250 µm thick layers of the powder-based coatings were ground off. It was found that the amount of α-phase deeper inside the hybrid coatings was greater by approximately only 4% than that at the free surface (see Table 5). Correspondingly, the amount of residual eskolaite and metastable phases slightly decreased from the free surface towards the depth of the coating. Therefore, considering the achievable XRD precision, no significant changes were detected. Moreover, no trend in residual chromia content was confirmed by SEM cross-sections observations, indicating very limited additional dissolution of the chromia-rich splats into the alumina matrix. The amount of the α-phase in the P-A coating was fully comparable on the free surface and in the central part showing that the heat from additional torch passes was insufficient to induce the phase transformation by annealing.

Mean interpass (cooling phase) temperatures and mean peak (spraying) temperatures during the deposition were in the range from ~240 to ~450 °C as measured by the thermocouple (Fig. 11). For the powder-based coatings, the higher peak temperatures of both hybrid depositions (compared to P-A experiment) can be attributed to the heat provided by the water:ethanol solvent in the suspension [26]. Contrary, the lowest peak temperature of the SS-AC experiment in the intermixed

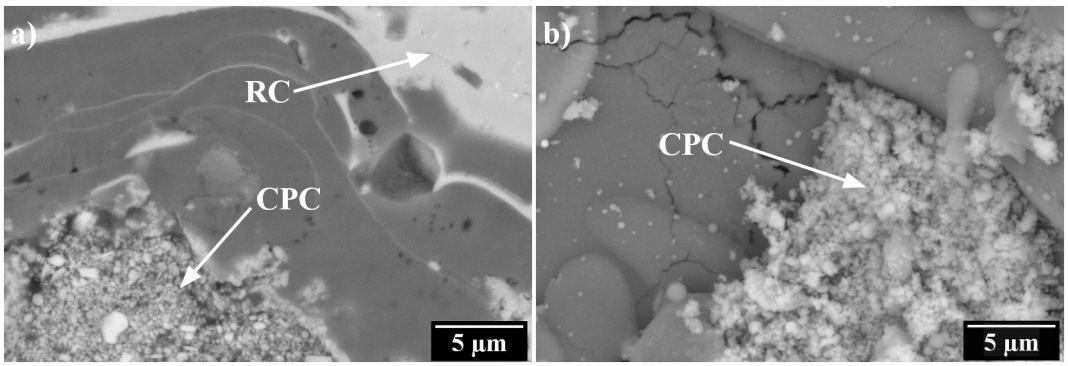

Fig. 7. Unmelted suspension feedstock in the cross-section and on the free surface of H-AC-2 coating. Residual chromia (RC), chromia particles clusters (CPC). SEM BSE mode.

Table 3
Phase composition of powder-based feedstocks and coatings as measured by XRD and ^{27}Al NMR. All values are shown in wt%. NMR data is with respect to total Al_2O_3 content.

Sample	Feedstock			Coating				
	α-Alumina		Eskolaite	α-Alumina		γ−/δ-Alumina		Eskolaite
	XRD	NMR	XRD	XRD	NMR	XRD	NMR	XRD
P-A	100	100	–	40	55	60	45	–
H-AC-1	80	100	20	87	81	9	19	4
H-AC-2	69	100	31	81	80	13	20	6

series (compared to S-A and S-AC) can be attributed to the consumption of available heat by the evaporation of the water solvent and the endothermic CNN thermal decomposition. Nevertheless, all the peak temperatures were far below the crystallization temperature of α-alumina and therefore no significant phase changes can be expected due to this short exposure to the elevated temperatures. Presumably, based on the cross-section observation (Fig. 4d and Fig. 4f), local diffusion of chromia into alumina took place when the chromia splats were covered by the melt having temperature of more than 2500 °C (as indicated by in-flight particle diagnostics DPV-2000 in [40]), potentially leading to the formation of the desirable α-phase in the hybrid coatings [16].

The successful partial incorporation of Cr atoms directly into the alumina structure was detected both by XRD and ^{27}Al NMR. The XRD measurement showed a small (but measurable) increase in the lattice parameters a and c of the α-alumina phase as evaluated by Rietveld analysis (Fig. 12) with respect to the a and c values of pure α-alumina (a = 4.754 Å, c = 12.99 Å [41]). Such change was measurable for all Cr-doped coatings. The most pronounced increase of the lattice parameters was measured for the SS-AC coating suggesting the most intensive formation of the $(Al,Cr)_2O_3$ solid solution. The NMR measurement showed that the ^{27}Al longitudinal relaxation times were significantly reduced in the Cr-containing coatings (e.g. ~1 s observed for H-AC-1 compared to 30 s for P-A coating). Such strong relaxation enhancement together with a non-exponential recovery in H-AC-1 coating indicates the presence of paramagnetic centers [42] which also favors the hypothesis that Cr ions were partially incorporated into the alumina lattice.

3.2.3. Hardness

Hardness testing of the coatings revealed some differences between the samples (Fig. 13). In case of HV1, lower hardness values were obtained due to the higher number of microstructure defects such as porosity or loosely connected splats in the bigger interaction volume which also allowed crack propagation, whereas values of HV0.3 represented rather local characteristics of the closest splats, e.g. their bonding. The highest values of about 1500 HV0.3 were measured for the powder-based P-A and H-AC-1 coatings. However, the scatters of these coatings were relatively high showing the inhomogeneity between the dense well-sintered areas and loosely bound splats. These effects were averaged in the HV1 measurement as the hardness values were comparable to other samples with lower standard deviation. Apparently, the lowest HV1 hardness value of 942 ± 224 HV1 of the H-AC-1 coating is to be attributed to its highest coarse porosity (compare Fig. 5 and Table 2) allowing more pronounced crack propagation or void collapsing. As for the suspension-based samples, the HV1 values could not be reliably evaluated due to the low thickness of the coatings with respect to the diagonal length of the indents (Fig. 14d–f). The hardness values are therefore only informative. The HV0.3 hardness values of about 1250 HV0.3 for the suspension-based coatings could be nevertheless evaluated reliably and were comparable mutually and with the hybrid coatings within the standard deviation.

The failure mechanisms were observed under the HV1 indents (Fig. 14) as the HV0.3 indents did not induce significant damage of the indented area. Under higher load, splats crushing and development of radial cracks from the indents corners were observed (e.g. Fig. 14a and b). Remarkably, in the H-AC-1 and H-AC-2 coatings, the cracks

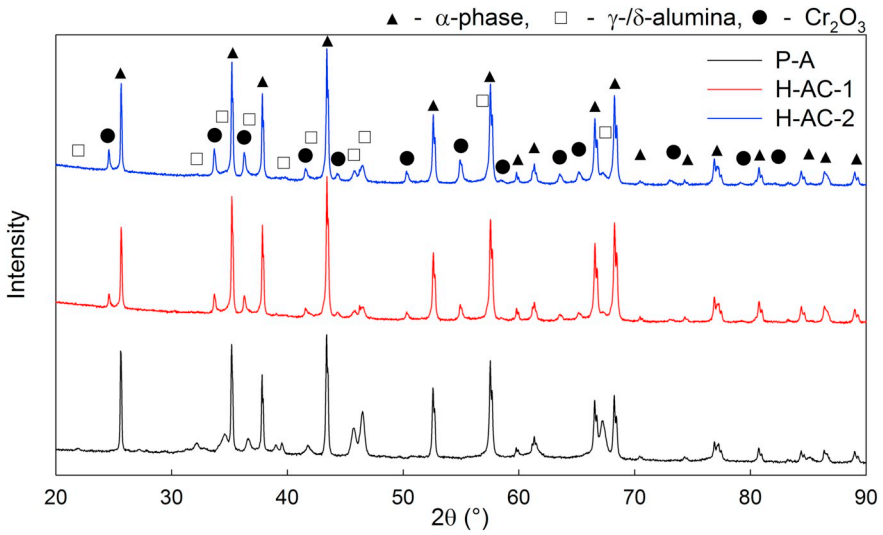

Fig. 8. Diffraction patterns of powder-based coatings.

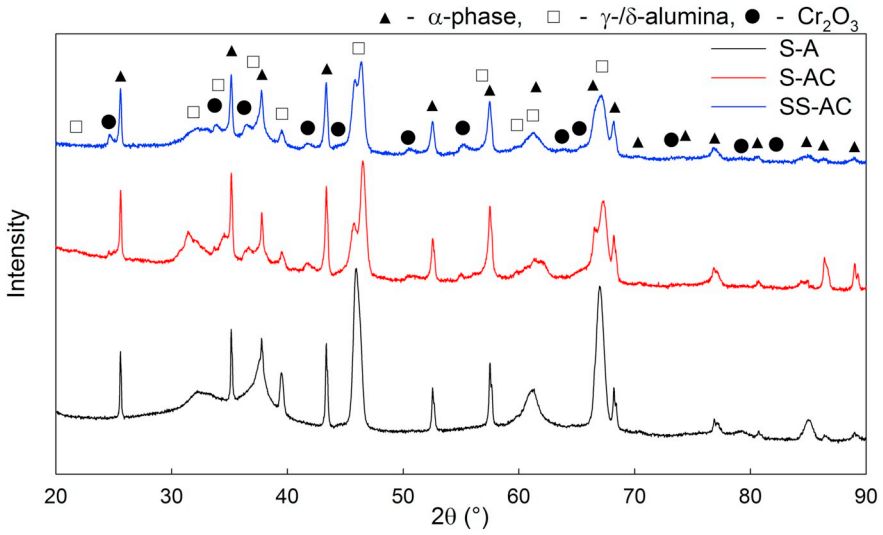

Fig. 9. Diffraction patterns of the suspension-based coatings.

Table 4
Phase composition of suspension-based feedstocks and coatings as measured by XRD. All values are shown in wt%.

Sample	Feedstock		Coating		
	α-Alumina	Eskolaite	α-Alumina	γ−/δ-Alumina	Eskolaite
S-A	100	–	12	88	–
S-AC	82	18	21	77	2
SS-AC	100	–	22	73	5

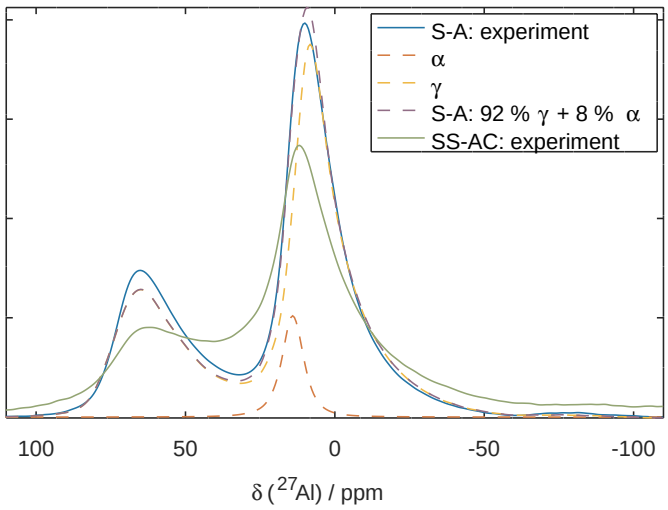

Fig. 10. Central parts of ^{27}Al MAS NMR spectra of S-A and SS-AC coatings, normalized to the same areas, with decomposition of the former into optimal linear combination of spectra of α and γ alumina.

Table 5
Comparison of α-phase content as measured by XRD on the free surface (FS) and in the central section (CS) of the deposits.

Sample	Coating α-alumina (wt%) FS/CS	Coating γ−/δ-alumina (wt%) FS/CS	Coating eskolaite (wt%) FS/CS
P-A	40/40	60/60	−/−
H-AC-1	87/91	9/7	4/2
H-AC-2	81/83	13/11	6/6

propagated preferentially within the coarse Al_2O_3 splats rather than along the heterogeneous alumina/chromia interfaces (Fig. 14b and c), indicating good bonding between both materials.

4. Discussion

It was observed that the dispersion of chromia within the alumina matrix was strongly influenced by the feedstocks characteristics and the deposition route. Comparison of the cross-sections between the powder-based hybrid coatings showed that the more diluted suspension used for H-AC-1 coating resulted in finer dispersion of smaller chromia splats than the higher concentrated suspension used in H-AC-2 experiment. This can be attributed to the finer atomization of the suspension in case of former aided by its lower viscosity, which can be also observed in the shadowgraphy photographs in Fig. 15. The larger droplets of the denser suspension were also richer in solid content for the H-AC-2 coating, resulting in larger chromia splats.

As for the suspension-based intermixed coatings, the distribution of chromia was similar in both S-AC and SS-AC coatings and much more homogeneous than in the hybrid counterparts, resulting in barely distinguishable contrast within smaller thin lamellae (compare e.g. Fig. 4d, f and Fig. 4j, l). This result indicates that the impacting particles were mutually comparable in size and composition (i.e. they contained comparable amount of chromia) regardless whether they originated from the two intermixed suspensions or from the suspension/solution mixture. In terms of coating formation, the SS-AC experiment was unique among the depositions since a chemical reaction took place during the thermal treatment of the feedstock in order to produce the desirable compound in-situ. The thermal decomposition of $Cr(NO_3)_3$ is accompanied by the release of NO_2 and O_2 gases, which could potentially contribute to the final coating porosity by entrainment of the formed gases similarly to [30]. However, the SS-AC coating showed the lowest porosity from all the coatings both in micro and macro scale. This result implies that CNN precursor was thoroughly decomposed and transformed into Cr_2O_3 during the in-flight stage, prior to the impact of the feedstock droplet onto the substrate.

Observing the circular well-defined chromia splats at the free surfaces of hybrid coatings (Fig. 6), it may be assumed that the majority of alumina and chromia particles arrived mostly independently onto the surface. With such coating buildup mechanism, intermixing of alumina and chromia was not very effective, probably due to the short time interval between the melted particles impact and their complete solidification. Two distinctive deposition scenarios may be therefore considered. In the first, a molten droplet impacts onto a previously

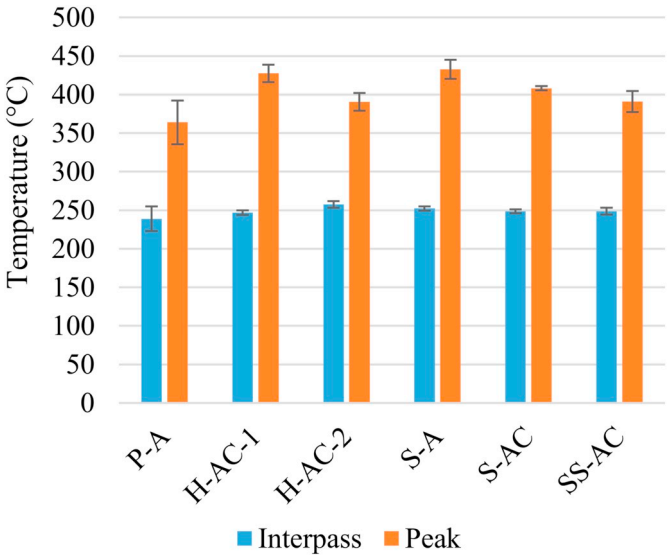

Fig. 11. Interpass and peak temperatures of the samples during the plasma spray deposition.

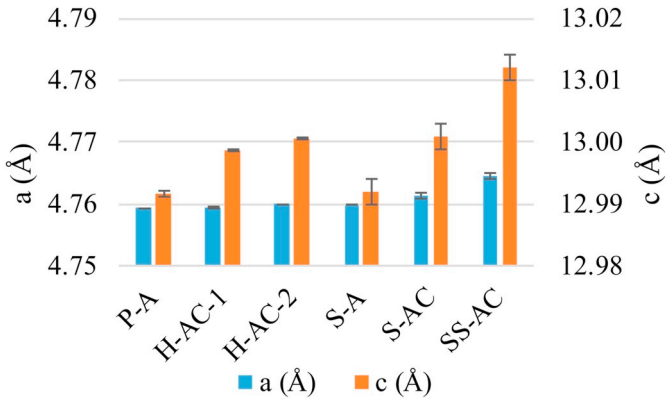

Fig. 12. α-phase lattice parameters *a* and *c* of the coatings.

deposited solidified splat, forming a sharp interface visible in the cross-section (Fig. 4f). In the second, a molten droplet impacts onto a molten or semi-molten (i.e. hot) splat, the two compounds mix by convection and a fuzzy interface visible in the cross-section is formed (Fig. 4f). If both splats remain molten for long enough time, desirable dissolution of chromia in alumina may be successfully completed. On the contrary, mixing of alumina and chromia in the intermixed suspension feedstocks may occur already in-flight on a large scale. Mixing of the two compounds in injected liquid ensures presence of both alumina and chromia in the liquid droplets already upon atomization, followed by evaporation of the solvent and simultaneous melting of the compounds. Due to the high number of particles of both original compounds in the individual droplets, only slight deviations in the alumina-chromia ratio may be expected leading to superior homogeneity of the deposited material. Also, the close intermixing of the constituents allows to form $(Al,Cr)_2O_3$ solid solution of oxides where some of the Al^{III} atoms are replaced by Cr^{III} ones in the crystal lattice [24].

As for the phase composition, it has to be pointed out that the powder-based coatings P-A, H-AC-1, and H-AC-2 were deposited using rather extreme spraying conditions for WSP-H technology, in particular using the short stand-off distance of 130 mm and a rather low feeding distance of 35 mm (standard SD is around 350 mm and FD 45 mm [40]). The short SD could be used thanks to the intensive cooling of the samples but might not be suitable for standard applications due to possible overheating of the coated part. Nevertheless, such a short stand-off distance significantly contributed to the final properties of the coatings.

Firstly, the reason for the low porosity of P-A coating can be attributed to the low SD and to the configuration of the feedstocks injection (see Fig. 2). Since no suspension was injected into the plasma jet in P-A experiment, the jet was not disturbed by its stream. Therefore, the powder particles in the P-A experiment received greater acceleration which together with the high thermal input led to high impingement velocity and good flattening of the splats, eventually resulting in low porosity of the deposit.

Secondly, the short SD promoted the formation of the stable α-phase, which is in agreement with previous findings [16], where a decrease in the stand-off distance from 450 to 250 mm increased the amount of corundum from about 10 wt% to about 20 wt%. In this study with even shorter stand-off distance (i.e. 130 mm), the amount of α-phase was further increased to 40 wt% for the pure alumina powder feedstock. Similar results were obtained in e.g. [43] where intensive heat input provided by the slow torch transverse velocity and reduced cooling was used to produce coatings with almost pure α-phase. The α-phase formation was explained by the substrate and coating temperatures exceeding 1300 °C, which may be inapplicable for many industrial substrate materials. On the contrary, the substrate peak temperatures reported in this work were kept at much lower temperature below 450 °C (Fig. 11).

Coatings containing high amount of the desired α-phase can be prepared also by other ways than by adding phase-stabilizing components to the feedstock (such as chromia used in this study) or by increasing the process temperature discussed above. In [44], the authors managed to prepare suspension-plasma-sprayed and suspension-HVOF-

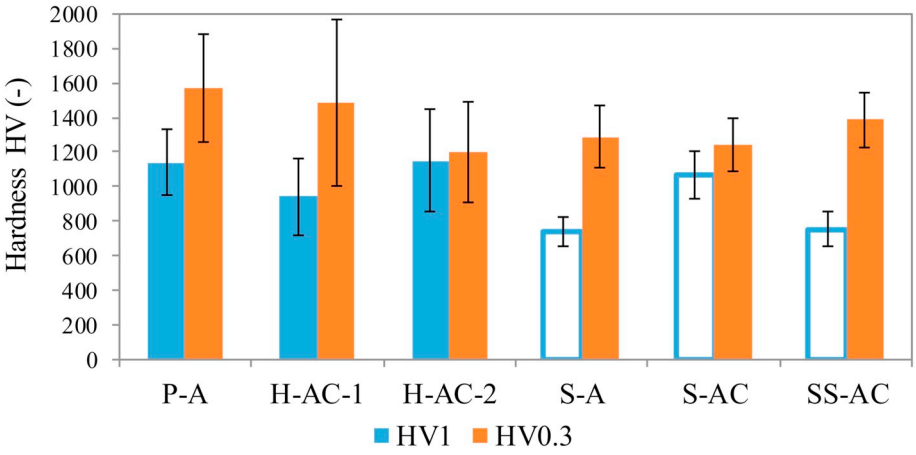

Fig. 13. Hardness of the coatings. HV1 values of the suspension-based coatings are only informative.

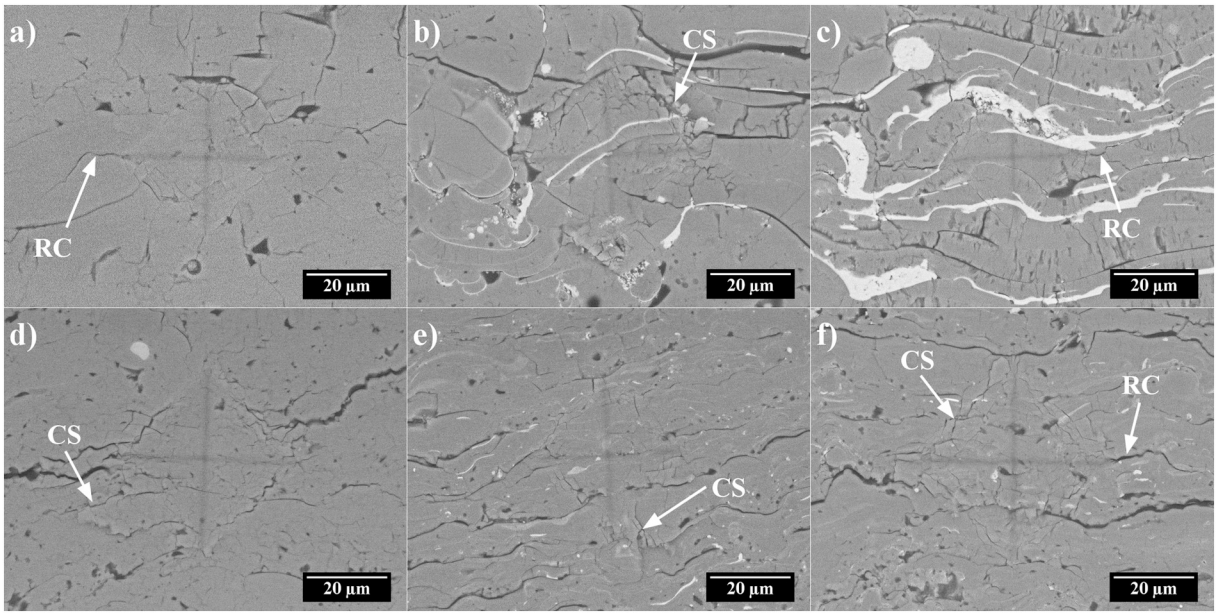

Fig. 14. Micrographs of HV1 indents in the cross-sections of a) P-A, b) H-AC-1, c) H-AC-2, d) S-A, e) S-AC, and f) SS-AC coatings. Radial cracks (RC), crushed splats (CS). SEM BSE mode.

sprayed coatings having α-phase content of up to 77 vol% and 73 vol%, respectively. According to the authors, the coatings with the highest content of the α-phase contained considerable amount of the unmelted or partially melted powder from the suspensions, thus retaining the feedstock phase composition. As also shown in [44], the amount of unmelted material in the HVOF-sprayed deposits could be reduced by increasing the total gas flow rates in the deposition process promoting melting of the feedstock which resulted in higher hardness of the coatings (increase from 300 HV0.3 to around 880 HV0.3, respectively), but also in the more intensive formation of the metastable alumina phases. In the case of the hybrid coatings presented in this study, not only the α-phase content exceeded 80 wt% but, at the same time, the deposited layers exhibited compact microstructure consisting of well-flattened splats and a negligible content of unmelted feedstock material. Such coating showed hardness values of more than 1000 HV0.3 promising good performance in e.g. sliding wear applications.

The comparison of α-alumina content between hybrid and intermixed coatings brings two major deductions:

- Firstly, stabilization of α-phase is possible for WSP-H technology using both the hybrid and the intermixed spraying routes. For the hybrid coatings, highly effective α-phase stabilization close to 90% was achieved with feedstock content of chromia significantly lower than the one reported in [20] where 33 wt% of chromia in mixed alumina-chromia powder resulted in ~60 wt% of α-phase (cf. 18 wt % of chromia resulted in 87 wt% of α-phase in this study). Moreover, the comparison between the hybrid coatings in this study further showed that the finer dispersion of the added chromia in H-AC-1 coating yielded higher amount of α-phase than in the H-AC-2, despite smaller chromia content (18 wt% compared to 27 wt%). These findings show that the finer dispersion of the stabilizer within the alumina matrix has a stronger effect than its absolute content.
- Secondly, the final amount of α-phase not only depends on the presence of chromia, but also strongly on the deposition route, i.e. significant difference was found between powder-based and suspension-based coatings where the original alumina was in a form of powder or a suspension, respectively. Despite both types of the feedstocks contained pure α-alumina and comparable amounts of chromia, the coatings deposited from coarse powders contained approximately 4 times higher content of α-phase than those deposited from the liquid feedstocks. This result indicates that the cooling rate of the splats plays a crucial role in the formation of α-phase which is in agreement with the conclusions drawn in [20,22,45]. In case of the powder-based coatings, the impinging

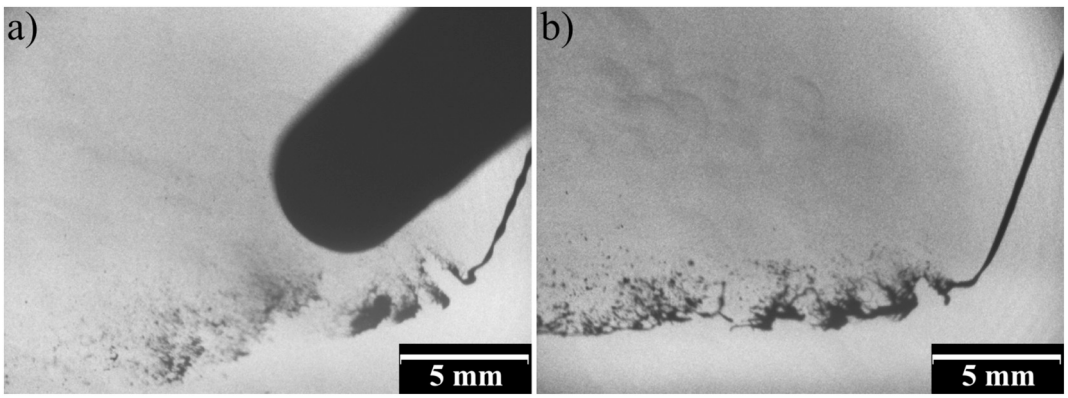

Fig. 15. Illustrative shadowgraphy photographs of a) injection of 25 wt% suspension in H-AC-1 experiment, and b) injection of 40 wt% suspension in H-AC-2 experiment prior to engagement of dry powder injectors.

alumina particles were at least an order of magnitude larger than those formed from liquids. This means that their volume was at least three orders of magnitude larger and the molten droplets thus carry significantly higher thermal energy resulting in a slower solidification allowing more time for the nucleation of α-phase.

5. Conclusions

This study focused on the plasma spraying of alumina with the addition of chromia in order to explore its effect on the α-alumina phase formation. WSP-H plasma torch was used as a source of high-enthalpy plasma for spraying. Hybrid coatings deposited from coarse spray-grade alumina powder co-sprayed with chromia suspension as well as alumina suspension intermixed with chromia suspension or chromia precursor were compared to coatings prepared from the pure alumina feedstocks only. The depositions were carried out under identical conditions in order to eliminate any other deposition effects (apart from the chromia addition).

Viscosity measurement of the chromia suspensions used for the preparation of hybrid coatings revealed that the dilution of the suspension from 40 wt% to 25 wt% of solid load lowered the viscosity of the suspension fourfold resulting in its finer fragmentation and thus finer dispersion of chromia within the coating. Viscosity measurements of suspensions used for the suspension-based coatings showed that neither the addition of chromia suspension nor the addition of chromium nitrate nonahydrate had strong unfavorable effect on the viscosity.

Successful deposition of coatings was achieved with increased content of the desirable α-phase depending both on the added chromia amount and the deposition route. In all cases, the addition of chromia promoted the formation of desirable corundum. In the case of the powder-based coatings, an increase from ~40 wt% to ~80–90 wt% was recorded. Moreover, it was found that the finer dispersion of chromia is more important than the absolute amount of the additive in the feedstock (and the deposit) as the less-doped H-AC-1 coating showed higher amount of α-phase than the chromia-richer H-AC-2 coating.

In the case of suspension-based coatings, the corundum amount increased from ~12% in the non-doped to ~21% in the doped form. The content of corundum was practically the same in the coatings prepared from the mixture of alumina/chromia suspensions (sample S-AC) and from the combination of alumina suspension and chromia precursor CNN (sample SS-AC). Moreover, the microstructure of the above mentioned coatings was comparable, as well, showing superior homogeneity. This result indicates that for both S-AC and SS-AC coatings, the molten droplets were comparable in terms of composition and size, thus forming similar splats on the substrate, and, also, that the CNN precursor successfully transformed into Cr_2O_3. Moreover, formation of small amount of $(Al,Cr)_2O_3$ was detected in the chromia-doped coatings; elongation of the α-phase lattice parameters from the values of pure alumina towards the values of pure chromia was observed. The increase measured in the α-phase lattice parameters of the powder-based hybrid coatings was smaller than that of the intermixed coatings (indicating smaller amount of $(Al,Cr)_2O_3$) showing the inferior mixing of the two compounds in the hybrid coatings. The incorporation of Cr atoms in the Al_2O_3 lattice was also confirmed using NMR by longitudinal relaxation enhancement of ^{27}Al nuclei.

Relatively high hardness of the coatings with mean values of around 1400 HV0.3 was recorded. Effective bonding of alumina-rich and chromia-rich splats was documented as negligible cracking or decohesion was observed on the heterogeneous interfaces during indentation. The hardness values were inversely proportional to the porosity of the coatings and also lower indentation load yielded higher hardness value due to the indentation size effect.

The coatings deposited from intermixed liquids showed higher chemical homogeneity than the coatings deposited using the hybrid route. However, the results obtained in this study show that in order to maximize the content of desirable α-phase, hybrid powder-suspension spraying may be a preferable deposition route. The results further show the importance of the local thermal history of the deposit, in particular of the cooling rate of the splats, on the phase composition of the coatings. Deposition of larger splats originating from the coarse powder presumably led to lower cooling rates of the deposited material, allowing longer time for the nucleation of the stable α-phase.

Finally, it was proven that both hybrid suspension plasma spraying and spraying of intermixed suspensions are viable routes for the preparation of coatings containing high contents of corundum.

Acknowledgements

Financial support of the TE02000011 grant “Research center of surface treatment” funded by the Technology Agency of the Czech Republic is gratefully acknowledged. The NMR measurements were supported through the Project CZ.2.16/3.1.00/21566 funded by the Operational Programme Prague – Competitiveness.

References

[1] H. Herman, Plasma-sprayed coatings, Sci. Am. (1988) 112–117, https://doi.org/10.2307/24989234.
[2] B. Lv, R. Mücke, X. Fan, T.J. Wang, O. Guillon, R. Vaßen, Sintering resistance of advanced plasma-sprayed thermal barrier coatings with strain-tolerant microstructures, J. Eur. Ceram. Soc. 38 (2018) 5092–5100, https://doi.org/10.1016/j.jeurceramsoc.2018.07.013.
[3] V. Carnicer, C. Alcazar, E. Sánchez, R. Moreno, Aqueous suspension processing of multicomponent submicronic Y-TZP/Al2O3/SiC particles for suspension plasma spraying, J. Eur. Ceram. Soc. 38 (2018) 2430–2439, https://doi.org/10.1016/J.JEURCERAMSOC.2018.01.006.
[4] J. Cizek, K.A. Khor, Z. Prochazka, Influence of spraying conditions on thermal and velocity properties of plasma sprayed hydroxyapatite, Mater. Sci. Eng. C 27 (2007) 340–344, https://doi.org/10.1016/j.msec.2006.05.002.
[5] S. Saber-Samandari, C.C. Berndt, K.A. Gross, Selection of the implant and coating materials for optimized performance by means of nanoindentation, Acta Biomater. 7 (2011) 874–881, https://doi.org/10.1016/j.actbio.2010.09.023.
[6] V. Matikainen, K. Niemi, H. Koivuluoto, P. Vuoristo, Abrasion, erosion and cavitation erosion wear properties of thermally sprayed alumina based coatings, Coatings 4 (2014) 18–36, https://doi.org/10.3390/coatings4010018.
[7] H. Ageorges, P. Ctibor, Comparison of the structure and wear resistance of Al2O3–13 wt.%TiO2 coatings made by GSP and WSP plasma process with two different powders, Surf. Coat. Technol. 202 (2008) 4362–4368, https://doi.org/10.1016/J.SURFCOAT.2008.04.010.
[8] R. Musalek, J. Medricky, T. Tesar, J. Kotlan, Z. Pala, F. Lukac, K. Illkova, M. Hlina, T. Chraska, P. Sokolowski, N. Curry, Controlling microstructure of yttria-stabilized zirconia prepared from suspensions and solutions by plasma spraying with high feed rates, J. Therm. Spray Technol. 26 (2017) 1787–1803, https://doi.org/10.1007/s11666-017-0622-x.
[9] A. Ganvir, S. Joshi, N. Markocsan, R. Vassen, Tailoring columnar microstructure of axial suspension plasma sprayed TBCs for superior thermal shock performance, Mater. Des. 144 (2018) 192–208, https://doi.org/10.1016/j.matdes.2018.02.011.
[10] J. Matejicek, T. Kavka, G. Bertolissi, P. Ctibor, M. Vilemova, R. Musalek, B. Nevrla, The role of spraying parameters and inert gas shrouding in hybrid water-argon plasma spraying of tungsten and copper for nuclear fusion applications, J. Therm. Spray Technol. 22 (2013) 744–755, https://doi.org/10.1007/s11666-013-9895-x.
[11] S.V. Joshi, G. Sivakumar, Hybrid processing with powders and solutions: a novel approach to deposit composite coatings, J. Therm. Spray Technol. 24 (2015) 1166–1186, https://doi.org/10.1007/s11666-015-0262-y.
[12] S. Björklund, S. Goel, S. Joshi, Function-dependent coating architectures by hybrid powder-suspension plasma spraying: injector design, processing and concept validation, Mater. Des. 142 (2018) 56–65, https://doi.org/10.1016/j.matdes.2018.01.002.
[13] G. Bolelli, A. Candeli, L. Lusvarghi, T. Manfredini, A. Denoirjean, S. Valette, A. Ravaux, E. Meillot, “Hybrid” plasma spraying of NiCrAlY + Al2O3 + h-BN composite coatings for sliding wear applications, Wear. 378–379 (2017) 68–81, https://doi.org/10.1016/j.wear.2017.02.027.
[14] J.W. Murray, A. Leva, S. Joshi, T. Hussain, Microstructure and wear behaviour of powder and suspension hybrid Al2O3–YSZ coatings, Ceram. Int. 44 (2018) 8498–8504, https://doi.org/10.1016/j.ceramint.2018.02.048.
[15] J. Dubsky, P. Chraska, B. Kolman, C.C. Stahr, L.-M. Berger, Phase formation control in plasma sprayed alumina-chromia coatings, Ceramics-Silikáty 55 (2011) 294–300.
[16] P. Chraska, J. Dubsky, K. Neufuss, J. Pisacka, Alumina-base plasma-sprayed materials part I: phase stability of alumina and alumina-chromia, J. Therm. Spray Technol. 6 (1997) 320–326, https://doi.org/10.1007/s11666-997-0066-9.
[17] P. Fauchais, M. Fukumoto, A. Vardelle, M. Vardelle, Knowledge concerning splat formation: an invited review, J. Therm. Spray Technol. 13 (2004) 337–360, https://doi.org/10.1361/10599630419670.
[18] X. Ren, M. Zhao, J. Feng, W. Pan, Phase transformation behavior in air plasma

sprayed yttria stabilized zirconia coating, J. Alloys Compd. 750 (2018) 189–196, https://doi.org/10.1016/J.JALLCOM.2018.03.011.
[19] N.N. Ault, Characteristics of refractory oxide coatings produced by flame-spraying, J. Am. Ceram. Soc. 40 (1957) 69–74, https://doi.org/10.1111/j.1151-2916.1957.tb12578.x.
[20] C.C. Stahr, S. Saaro, L.M. Berger, J. Dubsky, K. Neufuss, M. Herrmann, Dependence of the stabilization of α-alumina on the spray process, J. Therm. Spray Technol. (2007) 822–830, https://doi.org/10.1007/s11666-007-9107-7.
[21] B. Dhakar, S. Chatterjee, K. Sabiruddin, Phase stabilization of plasma-sprayed alumina coatings by spraying mechanically blended alumina–chromia powders, Mater. Manuf. Process. 32 (2017) 355–364, https://doi.org/10.1080/10426914.2016.1198028.
[22] R. McPherson, On the formation of thermally sprayed alumina coatings, J. Mater. Sci. 15 (1980) 3141–3149, https://doi.org/10.1007/BF00550387.
[23] K. Yang, X. Zhou, H. Zhao, S. Tao, Microstructure and mechanical properties of Al2O3–Cr2O3 composite coatings produced by atmospheric plasma spraying, Surf. Coatings Technol. 206 (2011) 1362–1371, https://doi.org/10.1016/j.surfcoat.2011.08.061.
[24] W. Gitzen, Alumina as a ceramic material, American Ceramic Society, Columbus, 1970.
[25] V. Dalbauer, J. Ramm, S. Kolozsvári, C.M. Koller, P.H. Mayrhofer, On the phase evolution of arc evaporated Al-Cr-based intermetallics and oxides, Thin Solid Films 644 (2017) 120–128, https://doi.org/10.1016/j.tsf.2017.10.055.
[26] M. Hlina, A. Maslani, J. Medricky, J. Kotlan, R. Musalek, M. Hrabovsky, Diagnostics of hybrid water/argon thermal plasma jet with water, ethanol and their mixture injection to plasma, Plasma Phys. Technol. 3 (2016) 62–65.
[27] M. Hrabovsky, Generation of thermal plasmas in liquid-stabilized and hybrid dc-arc torches, Pure Appl. Chem. 74 (2002) 429–433, https://doi.org/10.1351/pac200274030429.
[28] W.A. Dollase, Correction of intensities for preferred orientation in powder diffractometry: application of the March model, J. Appl. Crystallogr. 19 (1986) 267–272, https://doi.org/10.1107/S0021889886089458.
[29] D. Massiot, C. Bessada, J.P. Coutures, F. Taulelle, A quantitative study of27Al MAS NMR in crystalline YAG, J. Magn. Reson. 90 (1990) 231–242, https://doi.org/10.1016/0022-2364(90)90130-2.
[30] T. Tesar, R. Musalek, J. Medricky, J. Kotlan, F. Lukac, Z. Pala, P. Ctibor, T. Chraska, S. Houdkova, V. Rimal, N. Curry, Development of suspension plasma sprayed alumina coatings with high enthalpy plasma torch, Surf. Coatings Technol. 325 (2017) 277–288, https://doi.org/10.1016/j.surfcoat.2017.06.039.
[31] M.R. Hill, T.J. Bastow, S. Celotto, A.J. Hill, Integrated study of the calcination cycle from gibbsite to corundum, Chem. Mater. 19 (2007) 2877–2883, https://doi.org/10.1021/cm070078f.
[32] F. Cverna, ASM Ready Reference: Thermal Properties of Metals, ASM International, 2002.
[33] A. Reichel, P. Ackermann, A. Hentschel, A. Hochberg, Building with Steel: Details, Principles, Examples, Birkhauser, 2007.
[34] R. Musalek, J. Matejicek, M. Vilemova, O. Kovarik, Non-linear mechanical behavior of plasma sprayed alumina under mechanical and thermal loading, J. Therm. Spray Technol. 19 (2010) 422–428, https://doi.org/10.1007/s11666-009-9362-x.
[35] K. VanEvery, M.J.M. Krane, R.W. Trice, H. Wang, W. Porter, M. Besser, D. Sordelet, J. Ilavsky, J. Almer, Column formation in suspension plasma-sprayed coatings and resultant thermal properties, J. Therm. Spray Technol. 20 (2011) 817–828, https://doi.org/10.1007/s11666-011-9632-2.
[36] L. Kovarik, M. Bowden, A. Genc, J. Szanyi, C.H.F. Peden, J.H. Kwak, Structure of δ-alumina: toward the atomic level understanding of transition alumina phases, J. Phys. Chem. C 118 (2014) 18051–18058, https://doi.org/10.1021/jp500051j.
[37] Y. Repelin, E. Husson, Etudes structurales d'alumines de transition. I-alumines gamma et delta, Mater. Res. Bull. 25 (1990) 611–621, https://doi.org/10.1016/0025-5408(90)90027-Y.
[38] L. Kovarik, M. Bowden, D. Shi, N.M. Washton, A. Andersen, J.Z. Hu, J. Lee, J. Szanyi, J.-H. Kwak, C.H.F. Peden, Unraveling the origin of structural disorder in high temperature transition Al2O3: structure of θ-Al2O3, Chem. Mater. 27 (2015) 7042–7049, https://doi.org/10.1021/acs.chemmater.5b02523.
[39] R.S. Zhou, R.L. Snyder, Structures and transformation mechanisms of the η, γ and θ transition aluminas, Acta Crystallogr. Sect. B Struct. Sci. 47 (1991) 617–630, https://doi.org/10.1107/S0108768191002719.
[40] J. Medricky, R. Musalek, M. Janata, T. Chraska, F. Lukac, Cost-effective plasma spraying for large-scale applications, in: F. Azarmi (Ed.), ITSC 2018—Proceedings Int. Therm. Spray Conf, ASM International, Orlando, 2018, pp. 683–689.
[41] N. Ishizawa, T. Miyata, I. Minato, F. Marumo, S. Iwai, A structural investigation of α-Al_2O_3 at 2170 K, Acta Crystallogr., Sect. B: Struct. Crystallogr. Cryst. Chem. 36 (1980) 228–230, https://doi.org/10.1107/S0567740880002981.
[42] G.B. Furman, E.M. Kunoff, S.D. Goren, V. Pasquier, D. Tinet, Nuclear spin-lattice relaxation via paramagnetic impurities in solids with arbitrary space dimension, Phys. Rev. B 52 (1995) 10182–10187, https://doi.org/10.1103/PhysRevB.52.10182.
[43] G.N. Heintze, S. Uematsu, Preparation and structures of plasma-sprayed γ- and α-Al2O3coatings, Surf. Coat. Technol. 50 (1992) 213–222, https://doi.org/10.1016/0257-8972(92)90004-T.
[44] F.L. Toma, L.M. Berger, C.C. Stahr, T. Naumann, S. Langner, Microstructures and functional properties of suspension-sprayed Al2O3 and TiO2 coatings: an overview, J. Therm. Spray Technol. 19 (2010) 262–274, https://doi.org/10.1007/s11666-009-9417-z.
[45] J. Ilavsky, C.C. Berndt, H. Herman, P. Chraska, J. Dubsky, Alumina-base plasma-sprayed materials—part II: phase transformations in aluminas, J. Therm. Spray Technol. 6 (1997) 439–444, https://doi.org/10.1007/s11666-997-0028-2.

5.4 Deposition of chromia-doped alumina from precursor solutions

The last study focused at broadening the experience with the alumina deposition using precursor solutions. Contrary to the first study [I], higher solution concentration was used in order to attain greater solid load equivalent and thus greater solid phase yield. Moreover, based on the successful corundum phase stabilization by chromia in study [III], intermixed solutions of alumina and chromia precursors (water-based solutions of nitrates) were prepared in several composition ratios to attempt to deposit the $(Al,Cr)_2O_3$ mixed oxide, taking advantage of the atomic-scale precursor intermixing in the solution.

In total, four solution compositions were used for deposition, producing highly porous coatings (over 60 % porosity) displaying different colors from white (pure alumina), over pink-purple, to green, depending on the increasing chromium oxide precursor content in the solutions. The observed colors were in accordance to those of Cr-doped alumina prepared by a solid-state method reported in the literature. Moreover, the colored coatings exhibited a reversible thermochromic behavior (color change with the change of temperature) which was evaluated using quantitative colorimetry. Both the coloring of the coatings and their thermochromic behavior demonstrated that chromia was incorporated into the alumina crystal structure like it is in ruby crystals. The XRD analysis confirmed homogeneous distribution of Cr ions located substitutionally in the Al_2O_3 crystal lattice by virtue of the linear elongation of corundum lattice parameters with increasing Cr content in the deposit. In other words, certain aluminum atomic sites were occupied by chromium atoms leading to the expansion of the crystal lattice. This was achieved by the concurrent formation of both oxides during the in-flight deposition stage as a result of the intermixing of their precursors on the atomic scale in the liquid.

Using XRF, it was shown that the ratio of Al to Cr ions in the coatings was practically identical to that in the feedstock mixtures of precursor solutions, providing evidence of the balanced deposition of both materials without preferential (and undesirable) evaporation of either component.

The following article [IV] was written as an invited one for a special issue of Journal of Thermal Spray Technology based on a conference proceeding [vii] presented at International Thermal Spray Conference 2019 held in Yokohama, Japan.

J Therm Spray Tech (2020) 29:199–211
https://doi.org/10.1007/s11666-019-00945-2

PEER REVIEWED

Solution Precursor Plasma Spraying of Cr-Doped Al_2O_3 Thermochromic Coatings

Tomas Tesar[1,2] · Radek Musalek[1] · Frantisek Lukac[1] · Jan Medricky[1,2] · Jan Cizek[1] · Stefan Csaki[1] · Ondrej Panak[3] · Marketa Drzkova[3]

Submitted: 28 June 2019 / in revised form: 18 October 2019 / Published online: 11 November 2019

Abstract Solution precursor plasma spraying (SPPS) presents a modern route to deposit coatings directly from liquid feedstock. In this study, unique ability of SPPS to intermix different precursors on the atomic scale was employed to deposit pure and Cr-doped Al_2O_3 (technically, synthetic ruby) from several mixtures of aluminum and chromium nitrates. Highly porous coatings (> 60% porosity) were deposited by high-enthalpy WSP-H torch. Homogeneous distribution of Cr atoms in Al_2O_3 resulted in coatings color ranging from pink to grayish-green correlated with increasing Cr content and change of lattice parameters as observed by x-ray diffraction. High content of over 80 wt.% of α-alumina phase was reached for all coatings. For the Cr-doped Al_2O_3 coatings, distinct and fully reversible thermochromic behavior was observed by temperature-resolved colorimetry. Further increase in α-phase content (up to 95 wt.%) and coating densification were achieved by additional surface remelting by plasma torch.

This article is an invited paper selected from presentations at the 2019 International Thermal Spray Conference, held May 26-29, 2019 in Yokohama, Japan and has been expanded from the original presentation.

✉ Tomas Tesar
tesar@ipp.cas.cz

[1] Department of Materials Engineering, Institute of Plasma Physics CAS, v.v.i, Za Slovankou 3, 182 00 Prague, Czech Republic

[2] Department of Materials, Faculty of Nuclear Sciences and Physical Engineering, Czech Technical University in Prague, Trojanova 13, 120 00 Prague, Czech Republic

[3] Department of Graphic Arts and Photophysics, Faculty of Chemical Technology, University of Pardubice, Studentska 95, 532 10 Pardubice, Czech Republic

Keywords Alumina · hybrid plasma torch · mixtures · oxides · phase composition · solution precursor spraying

Introduction

Plasma spraying is a steadily growing family of technologies used for fabrication of functional coatings on the surfaces of broad range of industrial components. The coatings are used for protection against demanding operational conditions such as high temperatures (gas turbines, jet and rocket engines), oxidizing atmosphere (boilers, engines), friction or contact wear (paper rolls, engines), or for improvement in surface biocompatibility with living tissues (bone implants) (Ref 1-5).

The vast application scope of plasma spray technologies stems from the versatility of the deposition process enabling processing of various materials, such as metals, ceramics, cermets, and their combinations (Ref 6). For the deposition, feedstock materials can be supplied in the form of a dry coarse powder (typical particle size in tens of micrometers), suspension of fine powder in a carrier liquid—solvent (typical particle size from tens of nanometers to several micrometers), or a solution of chemical precursors (no solid particles in the liquid). After the introduction into the plasma jet, the feedstock yields a mixture of molten, semi-molten, or already resolidified particles which impact onto the workpiece surface, thereby creating a continuous coating. The motivation for spraying suspensions and solutions is driven by the objective of preparation of coatings with the characteristic size of microstructural features (splats, pores, cracks, etc.) one or two orders of magnitude lower than those obtained by spraying of the dry powders. The refined coating microstructure not only brings improved functional

performance of the coatings when compared to the conventional counterparts sprayed from coarse dry powder (Ref 7-9), but also the fine splats enable formation of qualitatively new microstructures such as columnar cauliflower-like structures (Ref 10). Last but not the least, finer and more intimate intermixing of different materials can be achieved (Ref 11).

One of the most industrially relevant materials in thermal spraying is Al_2O_3. It exists in multiple crystallographic modifications (polymorphs) (Ref 12). Due to the extreme cooling rates of the splats (up to 10^6 $K{\cdot}s^{-1}$), plasma-sprayed Al_2O_3 readily forms metastable crystallographic phases γ and δ (Ref 13), which are unfavorable for many applications. One of the routes to promote formation of the desired thermodynamically stable α-Al_2O_3 phase (corundum, α-alumina) is the addition of chromium oxide (Cr_2O_3, chromia) (Ref 14, 15). Since chromia crystallizes in the same rhombohedral lattice as α-Al_2O_3, chromia splats may serve as the nucleation centers for heteronucleation of the α-phase in aluminum oxide (Ref 16). Moreover, Cr atoms are able to substitute Al atoms in the crystal lattice. This is equivalent to forming a solid solution of Al_2O_3 and Cr_2O_3, thus suppressing the tendency of alumina to form the metastable crystallographic phases and actively promoting the crystallization of the corundum-like structure (Ref 13, 16).

A typical strategy to intermix alumina and chromia in the plasma-sprayed coating is the use of either fused and crushed alumina-chromia powder or a mechanical mixture of alumina and chromia powders (Ref 13, 16). By means of the former, a more homogeneous mixture of the oxides may be generally achieved, while the latter enables on-site tailoring of the ratio between the pure powders and thus the composition of the coating, or even the preparation of a functionally graded material (FGM) coating (Ref 17). As shown in (Ref 18), an alternative route of intermixing of materials in the coating can be also achieved by the co-deposition of dry coarse powder and a suspension or solution [so-called hybrid plasma spraying (Ref 19, 20)], or by the deposition of an intermixed suspension, both providing fine dispersion of chromia splats within the alumina matrix. Hybrid spraying offers composition control analogously to the deposition of mechanical mixture of dry powders, but, at the same time, yielding significantly finer distribution of the additional material (chromia) in the matrix (alumina). Deposition of intermixed suspensions may potentially bring the superior homogeneity of the coating due to even more intimate contact between the fine constituents; however, the preparation of a sprayable suspension from commercially available single-material suspensions may be challenging due to the usually unknown precise formulation of the optimized suspensions and possible interaction between the additives used, e.g., for stabilization or rheology control (Ref 21). However, even in such cases, certain amount of pure Cr_2O_3 or even unmelted residues of the added phase-stabilizing component can be retained in the coatings microstructure (Ref 18). Therefore, in order to prepare finely structured coatings with thorough intermixing of the constituents, the solution precursor spraying route is envisaged to provide the desirable degree of homogeneity of the deposited coatings as intermixing of the constituents takes place immediately after the formulation of the liquid feedstock on the atomic scale. Moreover, solution precursor plasma spraying was reported to be a viable route for deposition of single α-phase Al_2O_3 coatings even without any additive (Ref 22, 23). Also in our previous study with high-enthalpy WSP-H plasma torch, high content of α-phase in the Al_2O_3 deposited from aluminum nitrate nonahydrate was observed (Ref 24). It may be expected that addition of homogenously distributed chromium should further increase the α-phase content.

Apart from affecting the crystallographic phase composition, homogeneously distributed chromia is also known to modify the color of alumina, as studied in (Ref 25). For instance, Al_2O_3 with up to 2% of Al atoms replaced by Cr atoms is red and the mineral is known as ruby (Ref 26, 27). Therefore, the successful incorporation of chromia into the alumina coating may be easily evidenced by the color of the deposit, as pure Al_2O_3 is semi-transparent white and pure Cr_2O_3 is green, while the color of Cr-doped alumina varies, depending on chromia concentration, from light pink to greenish-gray (Ref 28). Moreover, Cr-doped alumina may exhibit thermochromic behavior, i.e., color change accompanying the temperature change of the material which may be used, e.g., in thermochromic dyes for temperature-sensing paints (Ref 29). The thermochromic nature of the Cr-doped alumina results from the O^{2-} anions constraining Cr^{3+} valence orbitals which, depending on the value of the lattice parameter, absorb different parts of the visible (VIS) light spectra (Ref 30). Another interesting property of Cr-doped alumina is its luminescence (Ref 31, 32).

Therefore, making use of the benefits of SPPS, spraying of intermixed solutions of alumina and chromia precursors with various Cr content was attempted in order to demonstrate feasibility of Cr atoms incorporation into the α-Al_2O_3 lattice of the sprayed coating. Successful uniform distribution of Cr in Al_2O_3 should be detected by increased α-phase content, change of lattice parameters, coloration of the deposit and ability to perform thermochromic behavior.

Materials and Methods

Liquid Feedstock Formulation

For the preparation of the liquid feedstocks, precursors of Al_2O_3 and Cr_2O_3 were used in the form of 1 M (mol/dm^3)

aqueous solutions of aluminum nitrate nonahydrate $Al(NO_3)_3{\cdot}9H_2O$ (ANN) and chromium nitrate nonahydrate $Cr(NO_3)_3{\cdot}9H_2O$ (CNN) in demineralized water. ANN and CNN were supplied by Lach-ner, s.r.o. (Czech Republic) and Alfa Aesar (Thermo Fisher (Kandel) GmbH, Germany), respectively, both in 98.5% purity. In total, four solutions with molar ratio of ANN:CNN of 10:0, 9:1, 8:2, and 7:3 were used to deposit coatings A, B, C, and D, respectively. Nitrate-based precursors were selected based on previous experience (Ref 24) and for their easy handling and mixing, stemming from the similar chemical composition.

Coatings Deposition

The prepared feedstocks were fed radially into the plasma jet generated by hybrid water/argon-stabilized plasma torch WSP-H 500 (ProjectSoft HK, a.s., Czech Republic). The net power of the torch was set to 150 kW with arc current of 500 A consuming only 15 slpm of Ar gas and approximately 3 L of water per hour of operation. Details on the torch operation can be found elsewhere (Ref 33). The torch was mounted on programmable robotic arm, and the spray procedure consisted of individual deposition cycles (three up and down torch strokes, so that each sample was sprayed just once, see (Ref 34) for details) followed by cooling periods during which the torch was diverted from the samples. The substrates (coupons of dimensions 20 mm × 30 mm × 2.5 mm made from AISI 304 stainless steel or S235 construction steel) both in grit blasted (GB) and non-grit blasted (noGB) condition were mounted onto a revolving carrousel surrounded by air knives for intensive cooling in order to prevent overheating of the substrates during the deposition cycles. Despite the intensive cooling, the temperature of the samples rapidly rose to approx. 400°C during each deposition cycle, as measured by a K-type thermocouple attached to the back side of one substrate. After samples cooled down to the preselected value of interpass deposition temperature of 250°C (Fig. 1), new deposition cycle was started. The torch standoff distance (SD, distance from torch nozzle exit to substrates) and liquid feeding distance (FD, distance from torch nozzle exit to the liquid injection point) of 100 mm and 25 mm, respectively, were selected based on previous experiments (Ref 24). Custom-built pressure feeder with online feed rate monitoring was used for the feedstock injection. Feeding pressure was adjusted in order to ensure optimal penetration of the liquid into the plasma jet, as observed by shadowgraphy imaging (SprayCam, Control Vision Inc., USA), resulting in feeding rate of 112 g/min.

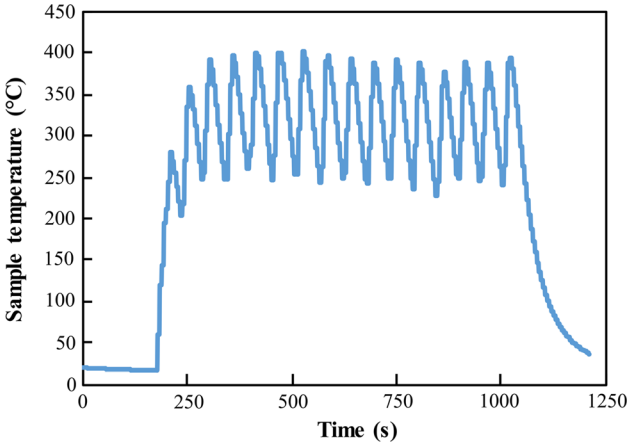

Fig. 1 Temperature profile of coating C deposition

Coating Analysis

All coating cross sections were prepared following a standardized metallographic procedure including precision cutting (Secotom 50, Struers, Denmark), vacuum epoxy impregnation and mounting (EpoFix, Struers, Denmark), and grinding and polishing (Tegramin 25, Struers, Denmark). Cross sections and free surfaces of the coatings were observed with scanning electron microscope (SEM) EVO MA 15 (Carl Zeiss SMT, Germany) using back-scattered electrons (BSE) detection mode sensitive to local elemental composition. Elemental mapping on cross sections was carried out using energy-dispersive x-ray spectroscopy (EDX) SDD detector XFlash® 5010 (Bruker, Germany).

Thickness and porosity of the coatings were evaluated by image analysis (IA) using ImageJ open-source software (v1.52 h, NIH, USA). For the thickness, 20 equidistant spots from SEM micrographs were used. For porosity, six images at nominal magnification of 1000 × were used.

To study a possible thermochromic behavior of the deposited coatings, samples were heated to 400°C and then let to cool down while change of their color was recorded. The heating–cooling cycle was repeated three times for coatings B and C to verify repeatability of the measurements. During measurement, each sample was inserted in the aluminum holder equipped with the temperature sensor (attached in the bottom part) and circular opening in the upper part (opening diameter of 2 cm, Fig. 2). Gray color of the sample holder surface was during thermal cycling used for correction of small drift in the camera color calibration. The holder was placed onto a hotplate with controlled heating rate; in this study, 450°C per hour heating rate was used which was low enough to ensure sufficient time for throughout heating of the sample before the sample imaging. In order to guarantee constant measurement conditions, the whole measurement was taking place

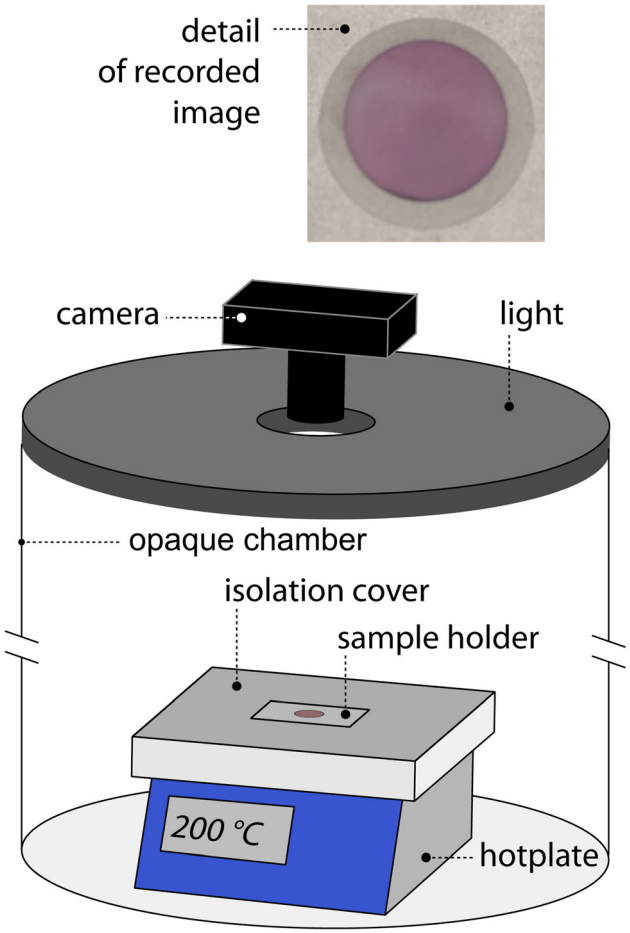

Fig. 2 The experimental setup for the study of thermochromic behavior

in the lightproof chamber with internal illumination (see Fig. 2). Time and sample temperature were recorded along with the imaging of the sample color.

Sample color was monitored by Olympus E PL3 (Olympus Corporation, Japan) digital camera with the 60-mm macro lens. The camera was calibrated using X-Rite ColorChecker calibration target and X-Rite ColorChecker software (X-Rite Pantone, MI, US) prior to each heating cycle. Circular Falcon Eyes DVR-630DVC (Falcon Eyes, Ltd., Hong Kong) LED light source with a diffusive cover was used for repeatable sample illumination. All captured images were saved in the raw image format, and the image data were processed using procedure described in (Ref 35) to represent the sample color by L^*, a^*, and b^* coordinates in the CIELab color space. Besides the path in CIELab space, the dynamic color change during thermal cycling was evaluated using the cumulative color difference ΔE_c, employing L^*, a^*, and b^* components altogether as defined in (Ref 35, 36).

Phase composition of all coatings was evaluated by Rietveld refinement by TOPAS V5 software (Bruker AXS, Germany) of x-ray diffraction (XRD) spectra measured by D8 Discover diffractometer (Bruker AXS, Germany) using Cu $K\alpha$ radiation and Bragg–Brentano Θ–Θ configuration. Elemental composition of the deposits was evaluated by energy-dispersive x-ray fluorescence (XRF) using S2 PUMA spectrometer (Bruker, Germany). Based on the results of thermochromic behavior observation of the coatings, XRD patterns were also measured at elevated temperatures of 100, 200, 300, and 400°C for coatings B and C exhibiting most distinctive thermochromic properties using in situ high-temperature stage (MRI, Germany) in order to evaluate lattice parameters of the deposits at elevated temperatures and to compare the results with the thermochromic measurements.

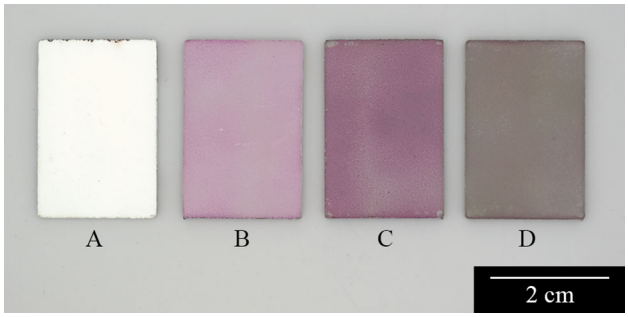

Fig. 3 Photograph of the as-sprayed coatings (Color figure online)

Results

Microstructure

Coatings were successfully deposited using all four feedstocks having different concentrations of chromia precursor. Photograph of the samples is displayed in Fig. 3, showing that the coatings differed in colors depending on the feedstock formulation. Coating A was white as it was prepared from the pure ANN solution and thus contained only Al_2O_3. With the increasing content of CNN in the solutions, the color of the coatings changed from pinkish (Coating B), suggesting the successful incorporation of Cr atoms within the Al_2O_3 lattice (Ref 25), to pink-green (coating C), to a greenish-gray deposit (coating D). It should be noted that color of alumina is white whereas Cr_2O_3 color is "rich racing green." Coloration of Cr-doped samples thus indicates that rather than simple mixing of Al_2O_3 with Cr_2O_3, which should provide different shades of green, Cr atoms were successfully incorporated into alumina lattice as change of the deposit color with increasing Cr content from red, through gray to green corresponds to (Ref 37).

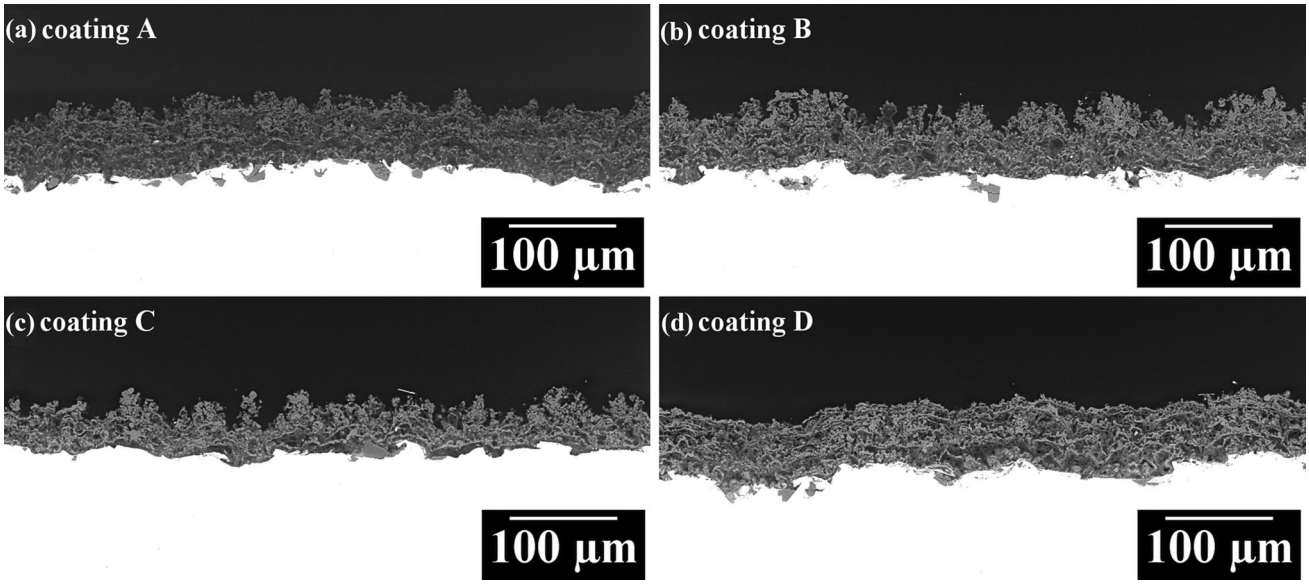

Fig. 4 Overview cross-sectional micrographs of the coatings

Table 1 Concentration of precursors in feedstock, number of deposition cycles, deposition rate (DR), thickness, and porosity of the coatings

Coating	ANN, mol/dm^3	CNN, mol/dm^3	Deposition cycles	DR, µm/cycle	Thickness, µm	Porosity, %
A	1.0	0.0	20	3.5	69 ± 9	67 ± 5
B	0.9	0.1	20	3.2	63 ± 11	62 ± 2
C	0.8	0.2	15*	2.9	44 ± 11*	62 ± 7
D	0.7	0.3	20	3.1	63 ± 9	61 ± 4

*Injection nozzle clogged

SEM micrographs in Fig. 4 show the overview of the coatings cross sections. All feedstock solutions yielded comparable deposition rates of about 3-3.5 µm per deposition cycle, as summarized in Table 1, resulting in final thickness in the range from 60 to 70 µm in 20 deposition cycles. Only in the case of coating C, deposition had to be aborted after 15 deposition cycles due to feeding malfunction, resulting in the final coating thickness of about 40 µm.

Apparently, all coatings were highly porous with a foamy microstructure containing scattered dense areas (splats). This is evident from the detailed micrographs in Fig. 5 showing the isolated splats interconnected by thin-walled bubble-like structures. The dense areas can be attributed to the liquid feedstock droplets which were due to the combination of their size and trajectory in plasma jet thoroughly heated so that the precursors decomposed and converted into alumina-chromia melt. Nevertheless, porosity of all coatings reached values of about 60%, see Table 1. This observation was similar to that in (Ref 24) and indicates that the extensive gas release took place either during the in-flight stage, and/or after the impact of unpyrolyzed solution droplets onto the hot surface. The latter case apparently resulted from the atomization of the feedstock solutions in the plasma jet which yielded large streaks of liquids (Fig. 6) rather than fine droplets as commonly observed in WSP-H spraying of suspensions/solutions. As a consequence, the transformation of the largest solution droplets was not completed when these impacted the hot surface, thereby undergoing thermal decomposition of the precursors accompanied by vigorous gas release and, in turn, forming the hollow shells (bubbles) (Ref 38, 39).

The dense areas (DA) within the coating cross sections were fairly homogeneous in terms of shades of gray color when observed using element-sensitive BSE mode, as shown in Fig. 5, illustrating the successful intermixing of the constituents. Also, elemental mapping of the Cr-doped coatings showed uniform distribution of the dopant with no preferential aggregation within the coatings microstructure (Fig. 7).

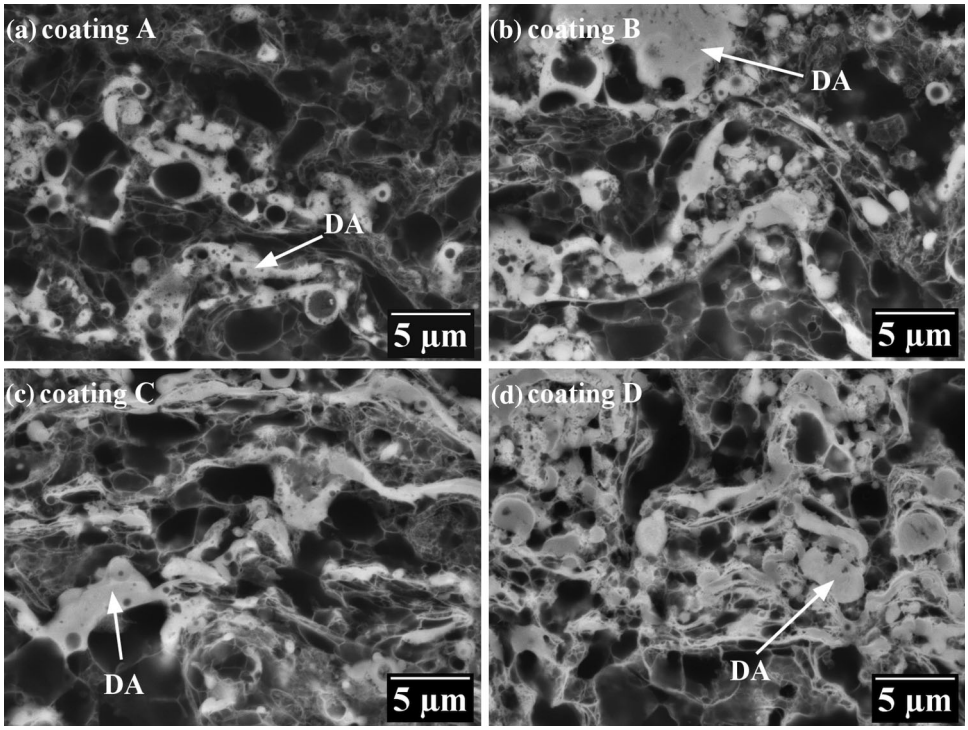

Fig. 5 Detailed cross-sectional micrographs of the coatings; dense areas (DA) are indicated by arrows

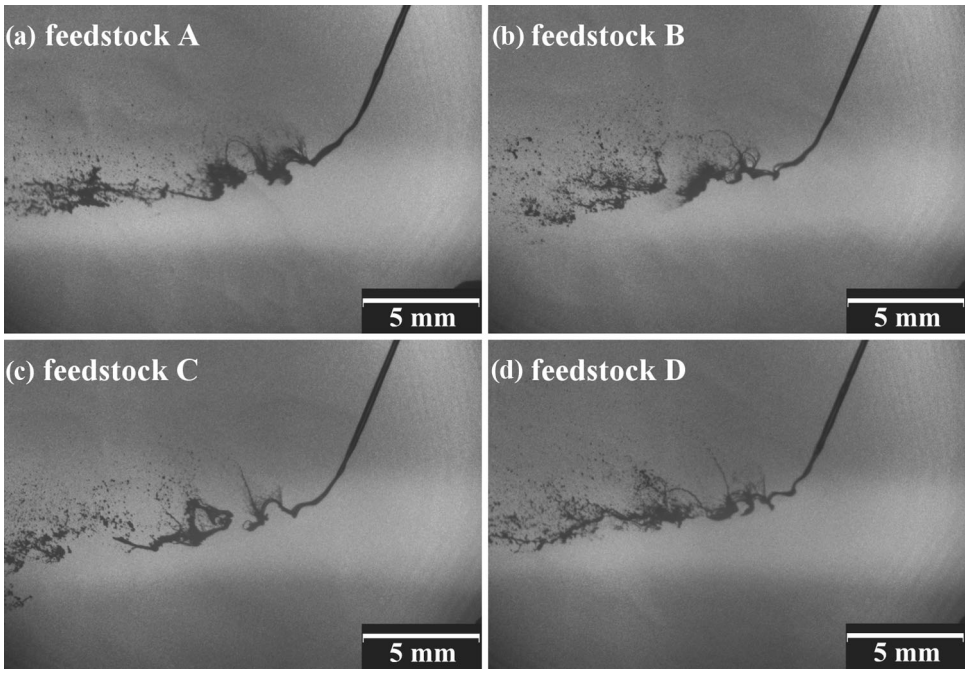

Fig. 6 Shadowgraphy images of feedstocks atomization in plasma jet

Owing to the fact that all coatings largely consisted of thin-walled hollow structures, the deposits were rather soft and susceptible to mechanical damage, i.e., could be scratched by fingernail. Nevertheless, if desirable, densification of the coating microstructure may be achieved by additional remelting of the coatings, e.g., by an additional pass of plasma torch with deactivated feedstock injection over the coatings, as demonstrated for one sample of coating A (Fig. 8). From both cross section (Fig. 8a, c) and free surface (Fig. 8b, d) images, it is evident that the coating surface was completely remelted as the underlying porous microstructure prevented fast heat removal to the substrate. Molten surface then solidified, forming smooth continuous layer which contained spherical pores and vertical cracks which were formed due to escape of entrained gas and thermal stresses development during

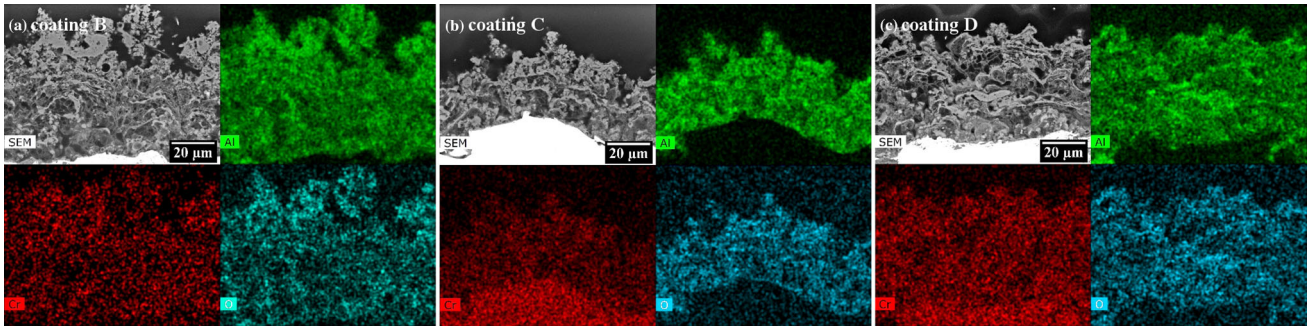

Fig. 7 Elemental maps of Al, Cr, and O of the Cr-doped coatings

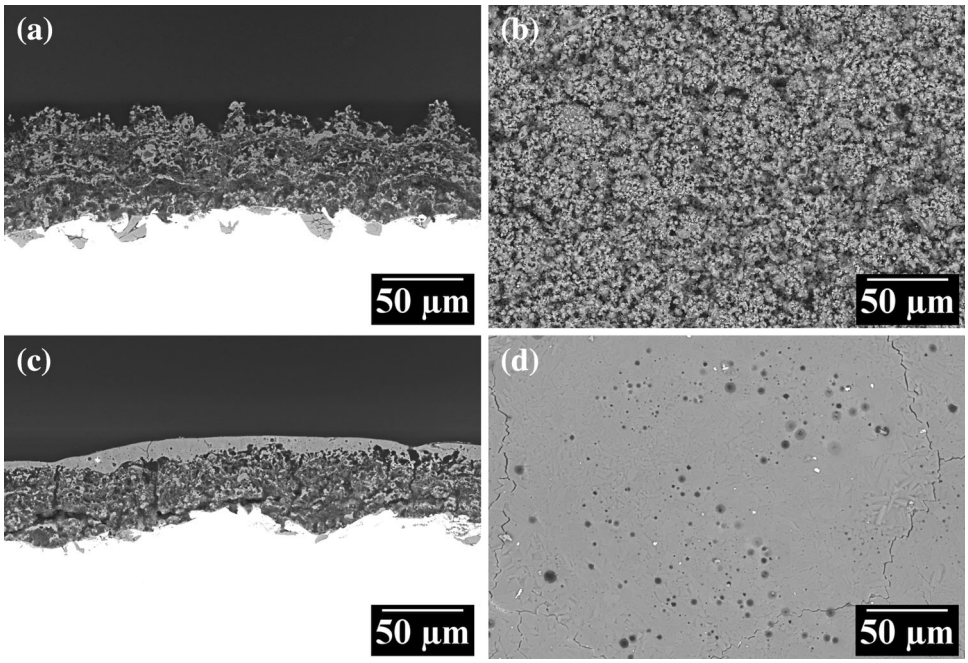

Fig. 8 Coating A, (a) cross section as-sprayed, (b) free surface as-sprayed, (c) cross section remelted, and (d) free surface remelted

Table 2 Concentration of elements in the prepared coatings

Coating	XRF, wt.%			Concentration, mol.%	
	Al	Cr	Fe	Al	Cr
A	69	0	31	100	0
B	57	11	32	90	10
C	50	18	32	82	18
D	45	36	19	68	32

melt pool solidification, respectively. Similar surface modification may be expected to be achieved also by other techniques commonly used for surface remelting (e.g., laser remelting (Ref 40)). Nevertheless, relatively simple process using just additional pass(es) of the plasma torch provides a cost- and time-effective alternative for easy-to-perform surface densification.

Chemical and Phase Composition

Chemical composition of the coatings as evaluated by XRF is summarized in Table 2. Iron from the substrate was detected due to the low thickness and high porosity of the coatings, and also, oxygen was not directly measured due to its low atomic mass. The measured weight fractions of Al and Cr in the coatings were translated into molar percent values which were in a good agreement with the feedstock formulation (compared with Table 1), showing even thermal decomposition of both precursors without any undesired preferential evaporation of either of the constituents.

Results of the phase composition analysis of the coatings as evaluated by Rietveld refinement method of XRD diffraction patterns are summarized in Table 3, and corresponding diffraction patterns are displayed in Fig. 9. Apparently, all four deposits were highly crystalline and contained very high amounts of the stable α-phase, i.e., more than 80%. The α-phase was detected to be present in

Table 3 Phase composition of the coatings according to XRD. Balance to 100 wt.% was the substrate detected below the deposits. α-phase lattice parameters as calculated from the Vegard's law of mixtures (a_T, c_T) and as measured from XRD (a_M, c_M)

Coating	α-phase, wt.%	γ/δ-phase, wt.%	a_T, Å	a_M, Å	c_T, Å	c_M, Å
A	84	13	4.76	4.75897 ± 0.00006	12.994	12.9927 ± 0.0003
B	84	14	4.78	4.77320 ± 0.00020	13.052	13.0337 ± 0.0008
C	89	9	4.80	4.79630 ± 0.00030	13.101	13.0929 ± 0.0010
D	91*	9	4.82	4.82430 ± 0.00030	13.188	13.1720 ± 0.0014

*Including 11 wt.% of pure α-Al_2O_3 phase having lattice parameters values close to those of coating A

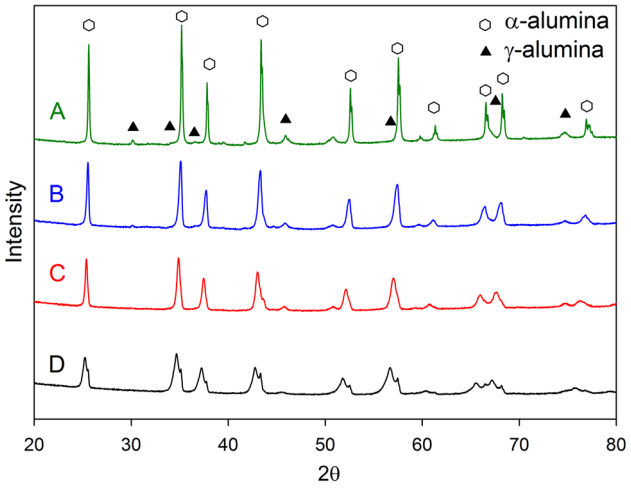

Fig. 9 XRD diffraction patterns of coatings A, B, C, and D at room temperature

two modifications distinguishable by different lattice parameters: (i) pure α-Al_2O_3 [lattice parameters values in agreement with those in the literature (Ref 41)] and (ii) α-Cr:Al_2O_3 (lattice parameters elongated due to Cr addition, see further). The pure α-Al_2O_3 phase was identified in coating A (with no Cr doping) and rather interestingly in coating D (which had the highest Cr addition of the samples) in amount of about 11 wt.%. Coatings B and C comprised solely of the α-Cr:Al_2O_3 phase with increased lattice parameters values according to the Cr content (Table 3). Minor content of metastable γ- and δ-Al_2O_3 phases was also present in the deposits (Table 3); however, due to the peaks overlapping and broadening of the γ/δ-phase peaks, it was challenging to precisely quantify their content in the deposits. Nevertheless, the expected error of the γ/δ-phase content evaluation is < 5 wt.%. Quite interestingly, the XRD evaluation of the deposits did not reveal any presence of pure Cr_2O_3 (eskolaite), not even in the coatings C and D having greenish hue. This also indicates a successful incorporation of Cr atoms directly in the Al_2O_3 lattice even for the coatings with the highest Cr addition.

High α-phase content could be attributed (i) to the fact that certain amount of unpyrolyzed solution droplets impacted the hot surface of the substrate or previously deposited material, eventually forming the stable α-phase by calcination of the precursors (Ref 42), and (ii) to the stabilizing effect of Cr incorporated in the α-phase lattice. Moreover, increasing amount of α-phase with increasing content of Cr in the coatings indicated an actively promoted stabilization of the α-phase. Presence of γ- and δ-phases detected in the coatings in the amounts ranging from 9 to 14% indicates that despite the high amount of stabilizing chromia (e.g., 30 mol.% in coating D), formation of metastable phases took place due to rapid solidification of the fine molten droplets.

XRD evaluation of the coatings also showed that, with increasing content of Cr in the deposits, the lattice parameters a and c of the rhombohedral α-phase were prolonged. As shown in Fig. 10a, the length of both lattice parameters linearly increased from the values typical for pure Al_2O_3 (coating A) toward the values of pure Cr_2O_3 (Ref 41, 43), closely following the empirical Vegard's law for lattice parameters of solid solutions. Comparison of theoretical values of the lattice parameters according to the Vegard's law and values as evaluated from XRD is shown in Table 3. Also, as evaluated from the XRD patterns measured for samples B and C at elevated temperatures, the lattice parameters a and c elongated linearly with increasing temperature (Fig. 10b), showing the correlation of the deposit color with the atoms spacing in the lattice.

Thermochromic Properties

The Cr-doped coatings exhibited notable reversible thermochromic color change. Averaged sample colors of the thermochromic coatings at different temperatures are displayed in Fig. 11. Even though the color changes were apparent for the naked eye, quantitative evaluation of the color variation was carried out in CIELab color space to assess the magnitude of the color change of the coatings.

Evolution of averaged coating color during repeated thermal cycling (three complete heating–cooling cycles) as measured for sample C confirmed that no significant differences occurred between the cycles in either the path

(Fig. 12a) or the magnitude (Fig. 12b) of the color change, showing the absence of hysteresis and/or drift in the color change and confirming repeatability of the measurements.

Evolution of averaged coating colors during thermal cycling of all coatings is presented in Fig. 13a, showing colors in a^*b^* plane projection of CIELab color space, which objectively quantifies the color change of the coatings. Pure Al_2O_3 coating A was almost clear white and underwent practically no change in color during heating and cooling, as the whole path of coating A color represented in the a^* and b^* coordinates (Fig. 13a) remained close to the origin [0,0], i.e., in the colorless region, and lightness value L^* was around 95 (Fig. 13b). Contrarily, reversible thermochromic behavior was observed for all Cr-doped Al_2O_3 samples (B, C, and D). In the case of coatings B and C, the color changed from pinkish tones to neutral shades (Fig. 13a) which were darker in the case of sample C with the lightness (L^*) values lower by almost 20 (Fig. 13b). In the case of sample D prepared from the precursor solution with the highest CNN concentration, the color change was less pronounced and took place in a different region of a^*b^* plane. In other words, the coating D color changed within the region of shades of green. In general, the colors of the coatings B, C, and D moved with temperature along straight path in the a*b* plane of CIELab color space, which is desirable for potential temperature-sensing applications. Contrarily, as expected, the white color of sample A remained stable throughout the whole tested temperatures. The magnitude of the dynamic color change of thermochromic samples B, C, and D during the thermal treatment can be observed in Fig. 13c showing that the pinkish coatings B and C underwent the most notable color change. Therefore, coatings with intermediate concentration of the doping Cr (10 and 20 mol.%) may be preferred for temperature-sensing applications as the temperature change induced the most intensive color change within the examined temperature interval.

Discussion

The aimed substitutional incorporation of Cr atoms in the Al_2O_3 crystal lattice of solution precursor plasma-sprayed coatings was evidenced both by the color of the deposits and by evaluation of the lattice parameters values. Remarkably, all prepared coatings were highly porous (over 60%) and contained high amount of the corundum phase exceeding 80 wt.% including the non-Cr-doped coating A. This corundum content is in accordance with previously reported deposition of Al_2O_3 from ANN precursor (Ref 23) and significantly higher than α-phase contents typically reported for coatings sprayed from powder by atmospheric plasma spray, detonation gun spraying, or high-velocity oxy-fuel deposition where metastable phases are dominant (Ref 44-46). Moreover, as tested by complementary XRD experiment, additional surface remelting by plasma torch provided further increase in α-phase content up to 95 wt.% along with densification of the coatings surface.

The color of Cr-doped Al_2O_3 deposits ranged from pink to green along with increased Cr content, as confirmed by colorimetry and XRF. This observation was fully in accordance with (Ref 29) where Cr-doped alumina was prepared by a solid-state method. Moreover, it was also observed that the color of Cr-doped coatings can be

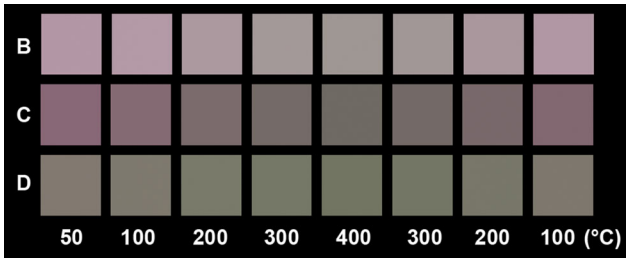

Fig. 11 The color of samples with thermochromic behavior at selected temperatures during heating and cooling (please note that the color rendering may be influenced by reproduction settings) (Color figure online)

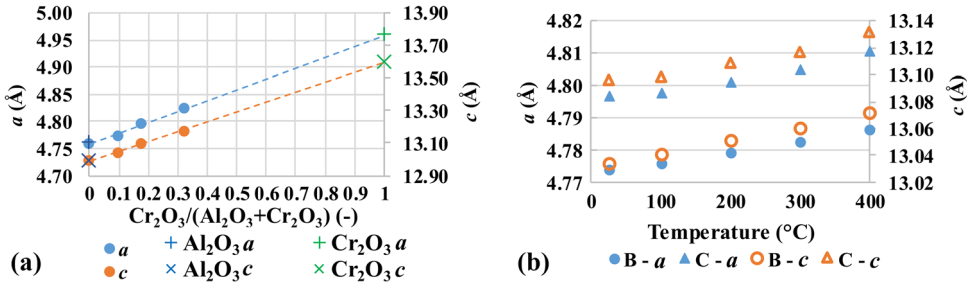

Fig. 10 (a) α-phase lattice parameters dependency on Cr content; dots show the lattice parameters of the deposits, "+" and "×" symbols represent a and c lattice parameters of pure Al_2O_3 (blue) and Cr_2O_3 (green) obtained from the literature (Ref 41, 43), dashed lines represent Vegard's law, (b) α-phase lattice parameters dependency on temperature (Color figure online)

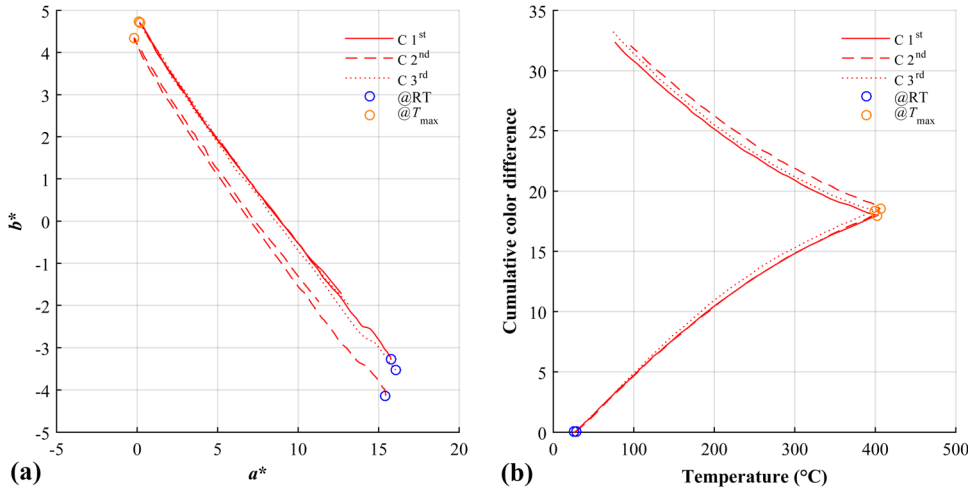

Fig. 12 Dynamic color change of sample C during three heating–cooling cycles, visualized as (a) a path in a^*b^* plane of CIELab space, (b) cumulative color difference ΔE_c; blue circles mark the start of the measurement at the room temperature and orange circles the maximum temperature (Color figure online)

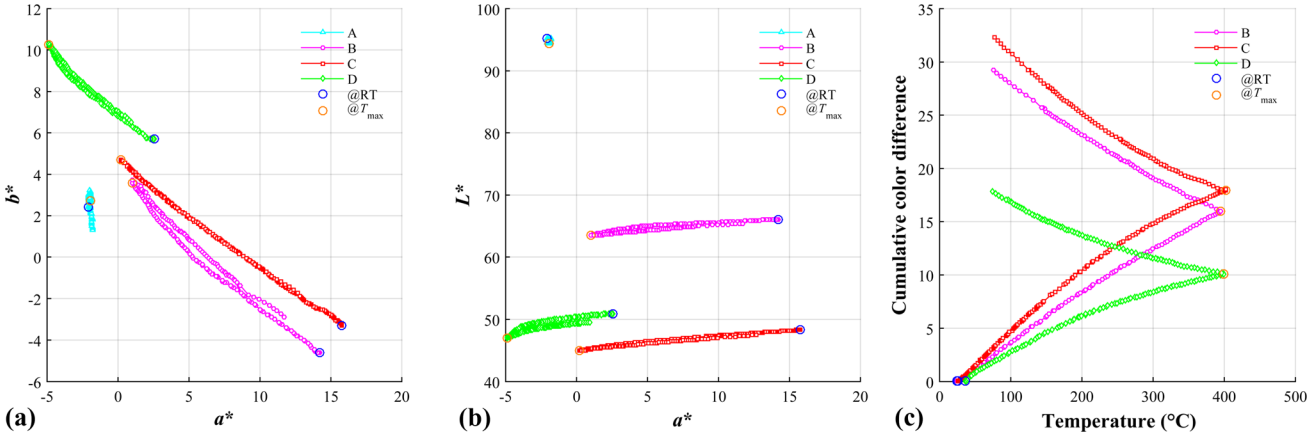

Fig. 13 Dynamic color change of samples during one heating–cooling cycle, visualized as (a) a path in a^*b^* plane of CIELab space, (b) a path in a^*L^* plane of CIELab space, (c) cumulative color difference ΔE_c for samples with a thermochromic behavior; blue circles mark the start of the measurement at the room temperature and orange circles the maximum temperature (Color figure online)

changed from pinkish to grayish-green by increasing the temperature of the coatings from room temperature to 400°C, thus evidencing the thermochromic properties typical for Al_2O_3 with substitutional Cr atoms (Ref 30). Complementary experiment also showed that surface remelting did not compromise thermochromic properties of the coatings.

The XRD measurements showed that the values of the lattice parameters were in a good agreement with the theoretical values according to the composition of the mixture using the Vegard's law (see Table 3). Moreover, linear elongation of the coatings lattice parameters was detected when the temperature of the samples was increased from room temperature to 400°C. The elongation of the lattice parameters is in accordance with the explanation of the thermochromic behavior of the coatings by means of the crystal field theory (Ref 47). As the lattice parameters of the Cr-doped Al_2O_3 are close to those of pure α-alumina, the valence d-orbitals of Cr^{3+} ions containing unpaired electrons are constrained by the octahedrally coordinated O^{2-} anions, leading to the energy splitting of the d-orbitals. As a result, electron transitions between the orbitals result in the absorbance of the yellow-green part of the VIS spectra, rendering the coating red. As the lattice parameters elongate (either due to the thermal expansion of the lattice or due to the increased amount of Cr atoms present in the lattice), the electrostatic field imposed by O^{2-} anions onto Cr^{3+} ions becomes weaker, resulting in decrease in the energy difference between d-orbitals. Therefore, lower energetic red part of the VIS spectra is absorbed and the coating turns greenish. Values of coating D lattice parameters a and c (4.8243 ± 0.0003) Å and (13.172 ± 0.0014) Å, respectively, were greater at room temperature than those of coatings B and C at 400°C, resulting in the green color of the deposit at the room temperature and only a minor color change within the green region of the VIS spectra upon heating (see Sect. 3.3). Coating A exhibited no significant color change

with the changing temperature since no thermochromic species were present in the coating.

As the prepared Cr-doped alumina coatings exhibited reversible thermochromic properties, they could be potentially employed, e.g., as an alternative to temperature-sensing paints (Ref 29). However, contrary to pigments prepared by solid-state method, the presented coatings having thermochromic properties were synthesized and deposited in one step, thereby omitting the need for time- and cost-demanding high-temperature annealing of the pigments (up to 1600°C) for several hours and subsequent formulation and application of paints. Owing to the high throughput and low operational cost of the WSP-H 500 torch (Ref 48), the presented method of solution precursor plasma spraying could be relatively easily adopted for spraying of large-scale components, such as pipes, for temperature monitoring of the media transported inside, or for complex-shaped parts for thermal mapping (Ref 49).

Conclusions

Aqueous solutions of aluminum nitrate nonahydrate and chromium nitrate nonahydrate with precursor ratios of 10:0, 9:1, 8:2, and 7:3 were used for the plasma spray deposition of coatings of pure Al_2O_3 and Cr-doped Al_2O_3, aiming at mixing of the materials at atomic scale in the deposits. The coatings were successfully deposited using the hybrid water/argon-stabilized plasma torch WSP-H 500, and the successful mixing of the constituents in the deposits was independently verified by:

- Observation of the coatings cross sections using BSE-SEM and EDX showing high chemical homogeneity of the deposited material.
- Elongation of the lattice parameters proving substitutional incorporation of Cr atoms into the α-phase lattice as evaluated from the XRD diffraction patterns.
- Absence of pure Cr_2O_3 as evaluated by XRD.
- Colors of the coatings ranging from pink (sprayed from 9:1 and 8:2 solutions) to green (sprayed from 7:3 solution).

Moreover, coatings having pink hue underwent distinct and fully reversible thermochromic color change without hysteresis, shifting their color from pink tones at room temperature to grayish-green tones at temperature of 400°C and back, making the coatings suitable for easy temperature monitoring.

All coatings were highly porous having a foamy-like microstructure with isolated splats, possibly result of extensive gas formation during the thermal decomposition of the precursors. Densification of the microstructure was achieved by surface remelting of the coatings by additional passing of the plasma jet over the deposited coatings, thereby forming continuous dense layer on the coating surface.

All prepared coatings in the as-sprayed state consisted predominantly (over 80 wt.%) of stable α-alumina phase, the amount of which was further increased up to 95 wt.% by remelting of the surface, while retaining the thermochromic properties of the coatings.

Acknowledgment Financial support of the 19-10246S grant "Deposition mechanisms and properties of multiphase plasma-sprayed coatings prepared with liquid feedstocks" funded by Czech Science Foundation is gratefully acknowledged.

References

1. X. Ma and P. Ruggiero, Practical Aspects of Suspension Plasma Spray for Thermal Barrier Coatings on Potential Gas Turbine Components, *J. Therm. Spray Technol.*, 2018, **27**(4), p 1-12
2. J. Smith, N. Shores, J. Scheibel, D. Classen, S. Paschke, S. Elbel, K. Fick, and D. Carlson, Thermal Barrier Coating Validation Testing for Industrial Gas Turbine Combustion Hardware, *J. Eng. Gas Turbine Power*, 2016, **138**(March), p 1-7
3. G. Darut, F. Ben-Ettouil, A. Denoirjean, G. Montavon, H. Ageorges, and P. Fauchais, Dry Sliding Behavior of Sub-Micrometer-Sized Suspension Plasma Sprayed Ceramic Oxide Coatings, *J. Therm. Spray Technol.*, 2010, **19**(1-2), p 275-285
4. T.P.S. Sarao, H. Singh, and H. Singh, Enhancing Biocompatibility and Corrosion Resistance of Ti-6Al-4V Alloy by Surface Modification Route, *J. Therm. Spray Technol.*, 2018, **27**(8), p 1388-1400. https://doi.org/10.1007/s11666-018-0746-7
5. J. Cizek, V. Brozek, T. Chraska, F. Lukac, J. Medricky, R. Musalek, T. Tesar, F. Siska, Z. Antos, J. Cupera, M. Matejkova, Z. Spotz, S. Houdkova, and M. Kverka, Silver-Doped Hydroxyapatite Coatings Deposited by Suspension Plasma Spraying, *J. Therm. Spray Technol.*, 2018, **27**(8), p 1333-1343. https://doi.org/10.1007/s11666-018-0767-2
6. P.L. Fauchais, J.V.R. Heberlein, and M.I. Boulos, *Thermal Spray Fundamentals*, Springer, Berlin, 2014, https://doi.org/10.1007/978-0-387-68991-3
7. N. Curry, K. VanEvery, T. Snyder, and N. Markocsan, Thermal Conductivity Analysis and Lifetime Testing of Suspension Plasma-Sprayed Thermal Barrier Coatings, *Coatings*, 2014, **4**(3), p 630-650. https://doi.org/10.3390/coatings4030630
8. M. Gell, L. Xie, E.H. Jordan, and N.P. Padture, Mechanisms of Spallation of Solution Precursor Plasma Spray Thermal Barrier Coatings, *Surf. Coat. Technol.*, 2004, **188-189**(1-3 SPEC.ISS.), p 101-106
9. V.E. Oliker, A.E. Terent'Ev, L.K. Shvedova, and I.S. Martsenyuk, Use of Aqueous Suspensions in Plasma Spraying of Alumina Coatings, *Powder Metall. Met. Ceram.*, 2009, **48**(1-2), p 115-120
10. K. VanEvery, M.J.M. Krane, R.W. Trice, H. Wang, W. Porter, M. Besser, D. Sordelet, J. Ilavsky, and J. Almer, Column Formation in Suspension Plasma-Sprayed Coatings and Resultant Thermal Properties, *J. Therm. Spray Technol.*, 2011, **20**, p 817-828
11. E.H. Jordan, C. Jiang, and M. Gell, The Solution Precursor Plasma Spray (SPPS) Process: A Review with Energy Considerations, *J. Therm. Spray Technol.*, 2015, **24**(7), p 1153-1165. https://doi.org/10.1007/s11666-015-0272-9
12. W.H. Gitzen, Ed., *Alumina as a Ceramic Material*, American Ceramic Society, Columbus, 1970

13. P. Chraska, J. Dubsky, K. Neufuss, and J. Pisacka, Alumina-Base Plasma-Sprayed Materials Part I: Phase Stability of Alumina and Alumina-Chromia, *J. Therm. Spray Technol.*, 1997, **6**, p 320-326
14. J. Dubsky, P. Chraska, B. Kolman, C.C. Stahr, and L.-M. Berger, Phase Formation Control in Plasma Sprayed Alumina-Chromia Coatings, *Ceram. Silikáty*, 2011, **55**(3), p 294-300
15. C.C. Stahr, S. Saaro, L.M. Berger, J. Dubský, K. Neufuss, and M. Herrmann, Dependence of the Stabilization of α-Alumina on the Spray Process, *J. Therm. Spray Technol.*, 2007, **16**, p 822-830
16. K. Yang, X. Zhou, H. Zhao, and S. Tao, Microstructure and Mechanical Properties of Al2O3–Cr2O3 Composite Coatings Produced by Atmospheric Plasma Spraying, *Surf. Coat. Technol.*, 2011, **206**(6), p 1362-1371. https://doi.org/10.1016/j.surfcoat.2011.08.061
17. J.R. Davis, Ed., *Handbook of Thermal Spray Technology*, ASM International, Materials Park, 2004
18. T. Tesar, R. Musalek, F. Lukac, J. Medricky, J. Cizek, V. Rimal, S. Joshi, and T. Chraska, Increasing α-Phase Content of Alumina-Chromia Coatings Deposited by Suspension Plasma Spraying Using Hybrid and Intermixed Concepts, *Surf. Coat. Technol.*, 2019, **2018**, p 1-14. https://doi.org/10.1016/j.surfcoat.2019.04.091
19. S. Björklund, S. Goel, and S. Joshi, Function-Dependent Coating Architectures by Hybrid Powder-Suspension Plasma Spraying: Injector Design, Processing and Concept Validation, *Mater. Des.*, 2018, **142**(1), p 56-65. https://doi.org/10.1016/j.matdes.2018.01.002
20. S.V. Joshi, G. Sivakumar, T. Raghuveer, and R.O. Dusane, Hybrid Plasma-Sprayed Thermal Barrier Coatings Using Powder and Solution Precursor Feedstock, *J. Therm. Spray Technol.*, 2014, **23**(4), p 616-624
21. A. Potthoff, R. Kratzsch, M. Barbosa, and N. Kulissa, Development and Application of Binary Suspensions in the Ternary System Cr2O3-TiO2-Al2O3 for S-HVOF Spraying, *J. Therm. Spray Technol.*, 2018, **27**(4), p 710-717. https://doi.org/10.1007/s11666-018-0709-z
22. G. Sivakumar, R.O. Dusane, and S.V. Joshi, A Novel Approach to Process Phase Pure α-Al2O3 Coatings by Solution Precursor Plasma Spraying, *J. Eur. Ceram. Soc.*, 2013, **33**(13-14), p 2823-2829. https://doi.org/10.1016/j.jeurceramsoc.2013.05.005
23. G. Sivakumar, M. Ramakrishna, R.O. Dusane, and S.V. Joshi, Effect of SPPS Process Parameters on In-Flight Particle Generation and Splat Formation to Achieve Pure α-Al2O3 Coatings, *J. Therm. Spray Technol.*, 2015, **24**(7), p 1221-1234. https://doi.org/10.1007/s11666-015-0284-5
24. T. Tesar, R. Musalek, J. Medricky, J. Kotlan, F. Lukac, Z. Pala, P. Ctibor, T. Chraska, S. Houdkova, V. Rimal, and N. Curry, Development of Suspension Plasma Sprayed Alumina Coatings with High Enthalpy Plasma Torch, *Surf. Coat. Technol.*, 2017, **325**(25), p 277-288. https://doi.org/10.1016/j.surfcoat.2017.06.039
25. M.I.B. Bernardi, S.C.L. Crispim, A.P. Maciel, A.G. Souza, M.M. Conceição, E.R. Leite, and E. Longo, Synthesis and Characterization of Al2O3/Cr2O3-Based Ceramic Pigments, *J. Therm. Anal. Calorim.*, 2004, **75**(2), p 475-480
26. H.-J. Lunk, Discovery, *Properties and Applications of Chromium and Its Compounds, ChemTexts*, 2015, **1**(1), p 6. https://doi.org/10.1007/s40828-015-0007-z
27. B.D. Fahlman and A.R. Barron, CVD of Chromium-Doped Alumina "Ruby" Thin Films, *Chem. Vap. Depos.*, 2001, **7**(2), p 62-66
28. G. Salek, A. Devoti, E. Lataste, A. Demourgues, A. Garcia, V. Jubera, and M. Gaudon, Optical Properties versus Temperature of Cr-Doped γ-and α-Al2O3: Irreversible Thermal Sensors Application, *J. Lumin.*, 2016, **179**(3), p 189-196. https://doi.org/10.1016/j.jlumin.2016.07.004
29. D.K. Nguyen, H. Lee, and I.T. Kim, Synthesis and Thermochromic Properties of Cr-Doped Al2O3 for a Reversible Thermochromic Sensor, *Materials (Basel)*, 2017, **10**(5), p 476-489
30. K. Nassau, The Physics and Chemistry of Color: The 15 Mechanisms, *The Science of Color*, 2nd ed., S.K. Shevell, Ed., Elsevier, Amsterdam, 2003, p 247-280
31. S.W.S. McKeever, *Thermoluminescence of Solids*, Cambridge University Press, Cambridge, 1988
32. D. Liu, Effects of Cr Content and Morphology on the Luminescence Properties of the Cr-Doped Alpha-Al2O3 Powders, *Ceram. Int.*, 2013, **39**(5), p 4765-4769. https://doi.org/10.1016/j.ceramint.2012.11.063
33. M. Hrabovsky, V. Kopecky, V. Sember, T. Kavka, O. Chumak, and M. Konrad, Properties of Hybrid Water/Gas DC Arc Plasma Torch, *IEEE Trans. Plasma Sci.*, 2006, **34**(4), p 1566-1575. https://doi.org/10.1109/TPS.2006.878365
34. R. Musalek, J. Medricky, T. Tesar, J. Kotlan, Z. Pala, F. Lukac, K. Illkova, M. Hlina, T. Chraska, P. Sokolowski, and N. Curry, Controlling Microstructure of Yttria-Stabilized Zirconia Prepared from Suspensions and Solutions by Plasma Spraying with High Feed Rates, *J. Therm. Spray Technol.*, 2017, **26**(8), p 1787-1803
35. O. Panák, M. Držková, N. Kailová, and T. Syrový, Colorimetric Analysis of Thermochromic Samples in Different Forms Employing a Digital Camera, *Meas. J. Int. Meas. Confed.*, 2018, **127**, p 554-564
36. O. Panák, M. Držková, and M. Kaplanová, Insight into the Evaluation of Colour Changes of Leuco Dye Based Thermochromic Systems as a Function of Temperature, *Dye. Pigment.*, 2015, **120**, p 279-287
37. A.V. Belykh, A.M. Efremov, and M.D. Mikhailov, Thermochromic Material, European Patent Office, 2012, p 13.
38. D. Chen, E.H. Jordan, and M. Gell, The Solution Precursor Plasma Spray Coatings: Influence of Solvent Type, *Plasma Chem. Plasma Process.*, 2010, **30**(1), p 111-119
39. A. Joulia, G. Bolelli, E. Gualtieri, L. Lusvarghi, S. Valeri, M. Vardelle, S. Rossignol, and A. Vardelle, Comparing the Deposition Mechanisms in Suspension Plasma Spray (SPS) and Solution Precursor Plasma Spray (SPPS) Deposition of Yttria-Stabilised Zirconia (YSZ), *J. Eur. Ceram. Soc.*, 2014, **34**(15), p 3925-3940. https://doi.org/10.1016/j.jeurceramsoc.2014.05.024
40. D. Triantafyllidis, L. Li, and F.H. Stott, Crack-Free Densification of Ceramics by Laser Surface Treatment, *Surf. Coat. Technol.*, 2006, **201**(6), p 3163-3173
41. P. Ballirano and R. Caminiti, Rietveld Refinements on Laboratory Energy Dispersive X-Ray Diffraction (EDXD) Data, *J. Appl. Crystallogr.*, 2001, **34**(6), p 757-762. https://doi.org/10.1107/S0021889801014728
42. I.F. Myronyuk, V.I. Mandzyuk, V.M. Sachko, and V.M. Gunko, Structural and Morphological Features of Disperse Alumina Synthesized Using Aluminum Nitrate Nonahydrate, *Nanoscale Res. Lett.*, 2016, **11**(1), p 153. https://doi.org/10.1186/s11671-016-1366-0
43. H. Sawada, Residual Electron Density Study of Chromium Sesquioxide by Crystal Structure and Scattering Factor Refinement, *Mater. Res. Bull.*, 1994, **29**(3), p 239-245
44. E. Turunen, T. Varis, T.E. Gustafsson, J. Keskinen, T. Fält, and S.P. Hannula, Parameter Optimization of HVOF Sprayed Nanostructured Alumina and Alumina-Nickel Composite Coatings, *Surf. Coat. Technol.*, 2006, **200**(16-17), p 4987-4994
45. P.P. Psyllaki, M. Jeandin, and D.I. Pantelis, Microstructure and Wear Mechanisms of Thermal-Sprayed Alumina Coatings, *Mater. Lett.*, 2001, **47**(1-2), p 77-82
46. Y. Gao, X. Xu, Z. Yan, and G. Xin, High Hardness Alumina Coatings Prepared by Low Power Plasma Spraying, *Surf. Coat. Technol.*, 2002, **154**(2-3), p 189-193

47. R.G. Burns, *Mineralogical Applications of Crystal Field Theory*, 2nd ed., Cambridge University Press, Cambridge, 1993
48. J. Medricky, R. Musalek, M. Janata, T. Chraska, and F. Lukac, Cost-Effective Plasma Spraying for Large-Scale Applications, *ITSC 2018—Proceedings of the International Thermal Spray Conference*, F. Azarmi, K. Balani, T. Eden, T. Hussain, Y.-C. Lau, H. Li, K. Shinoda, F.-L. Toma, and J. Veilleux, Ed., Orlando, ASM International, 2018, p 683-689
49. C. Lempereur, R. Andral, and J.Y. Prudhomme, Surface Temperature Measurement on Engine Components by Means of Irreversible Thermal Coatings, *Meas. Sci. Technol.*, 2008, **19**(10), p 105501

5.5 Overview of papers not directly related to the thesis

The experiences and knowledge acquired within the scope of studies [I – IV] were successfully applied also to other materials deposited in various studies carried out at IPP, which are, nevertheless, not the core part of the thesis. Similarly to the case of alumina deposition, the microstructures of YSZ coatings presented in studies [V, VI, IX-XI] were primarily controlled by the feedstock type, as can be observed in Fig. 18. Furthermore, the analytical procedures, such as the multiscale porosity evaluation, were established and used for e.g., the TBC-relevant coatings, where porosity distribution and its changes are important for explanation of the microstructural evolution during long-term high-temperature exposure. In Fig. 18 and 19, a selection of pictures illustrating the TBC-related research is shown.

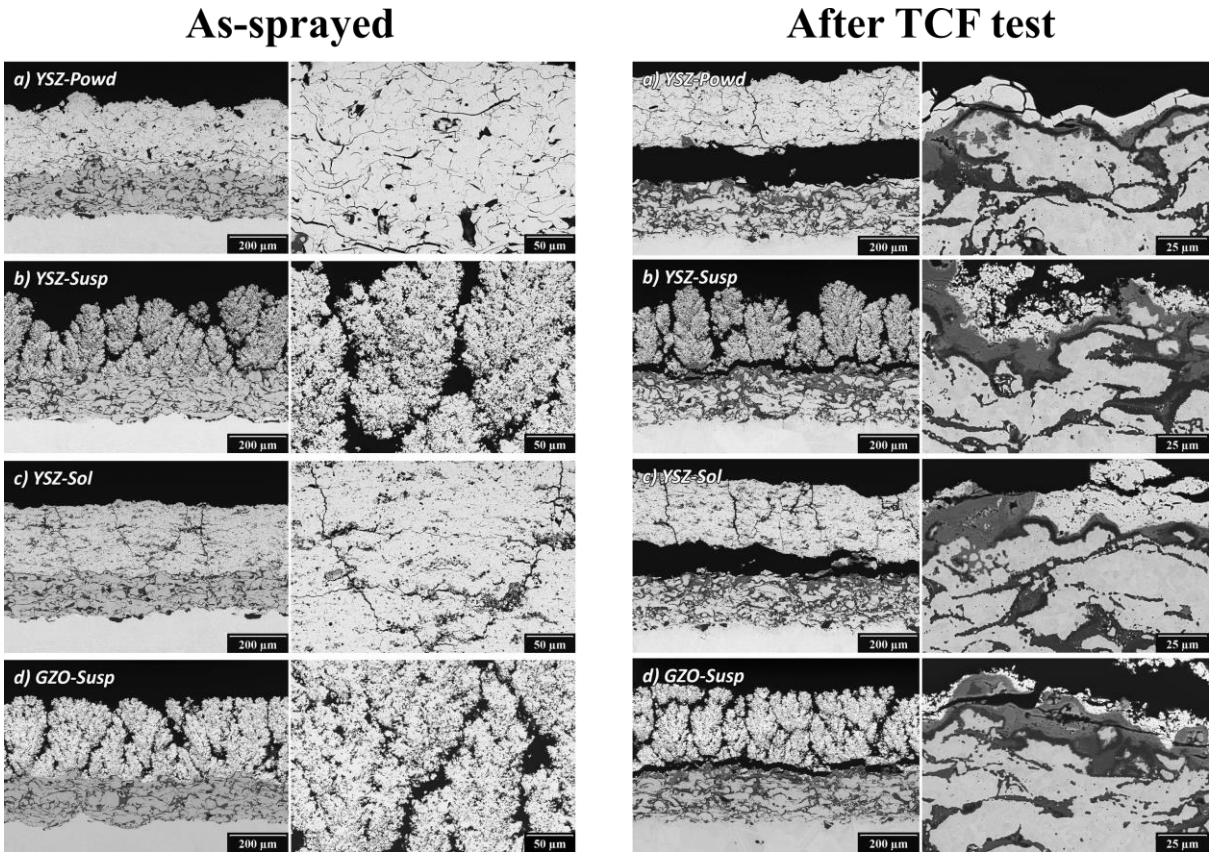

Figure 18. Thermal barrier coatings from article [X] illustrating microstructure control using different feedstocks: a) YSZ powder, b) YSZ suspension, c) YSZ solution, d) $Gd_2Zr_2O_7$ suspension.

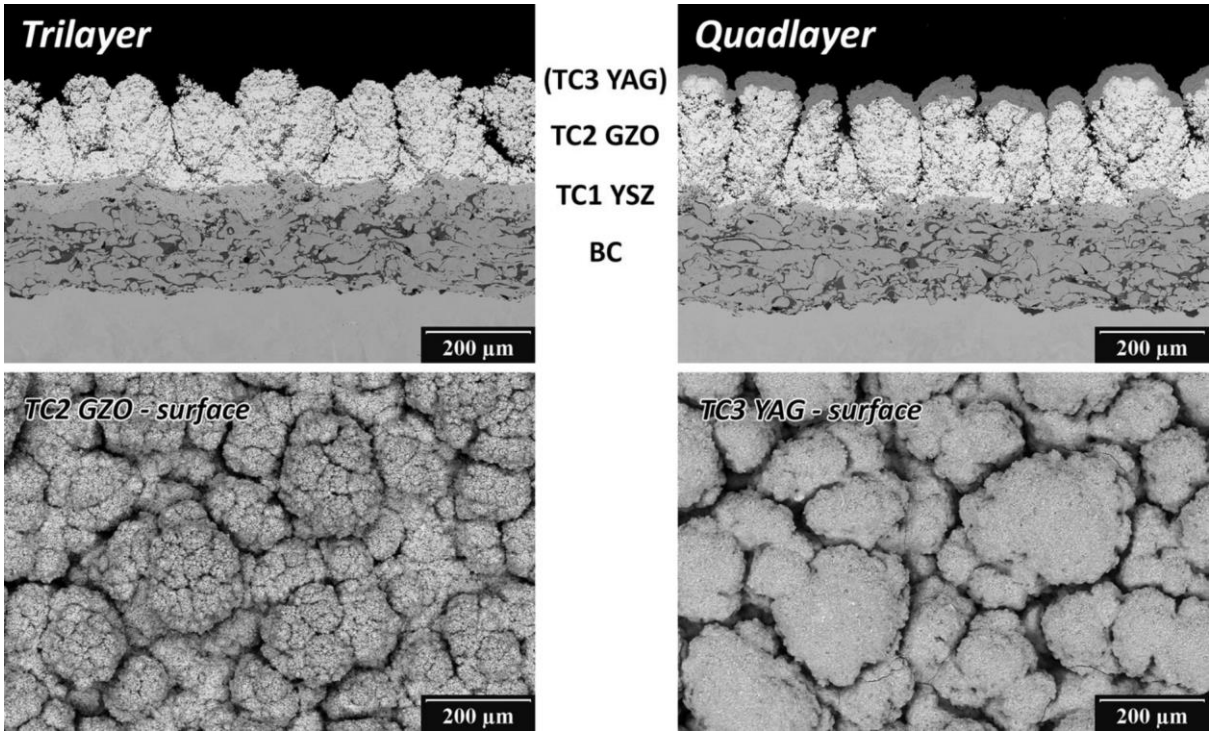

Figure 19. Microstructure cross-sections and free surface of multilayered TBC systems used for ultra-high temperature testing in [XI].

The medicine-relevant HAp coatings in study [VII] were deposited from an in-house made suspension prepared by wet chemical synthesis, providing another level of suspension composition control. The suspension was used in as-prepared condition for deposition of pure HAp coatings and enriched by a dissolved silver nitrate, using the liquid intermixing. The suspensions were successfully sprayed and pure metallic silver nanoparticles were embedded in the coating sprayed from the Ag-precursor-doped suspension, potentially providing a beneficial antibacterial functionality. In Fig. 20, the cross-section micrograph and elemental mapping of the Ag-containing HAp coating are shown.

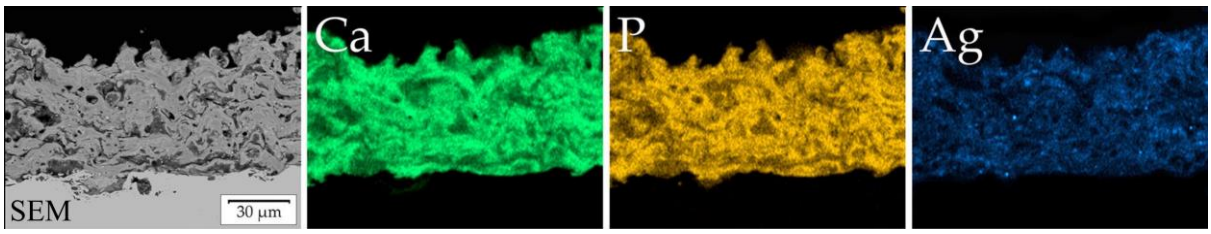

Figure 20. EDX mapping of Ag-doped HAp coating cross-section from article [VII].

6 Synthesis of Results

The presented articles described the path undertaken to develop alumina-based plasma-sprayed coatings deposited from suspensions, solutions, and their combination with conventional coarse powders (the hybrid feedstock concept) using a high-enthalpy plasma torch, to understand their formation under various conditions and from various feedstocks, and to evaluate and compare their functional properties to the conventional coatings.

The first study showed that the feedstock type is the essential input variable which mostly governs the final coating microstructure. Using multitude of suspension compositions and a solution, broad variety of microstructures were deposited, including hard and dense coating, porous columnar coating, and a highly porous soft coating. On top of that, it was shown that it is possible, and may be actually highly efficient, to prepare the liquid-based feedstocks on site using fairly simple laboratory equipment in order to deposit coatings of outstanding functional properties rather than acquiring the considerably more expensive ready-to-spray feedstocks from commercial manufacturers. Also, chemical composition of these feedstocks (and thus coatings) may be readily adjusted in a wide range as opposed to ready-to-spray powders. This may be in particular beneficial for testing of new coatings with new compositions and spraying of coatings with variable/graded composition. In other words, the in-house preparation of feedstocks can lead to highly successful coating deposition, but should not be regarded as the most straightforward approach as specific knowledge to prepare a sprayable feedstock is needed. Also, it is important to bear in mind the intended application of a coating for deposition of which a custom-made feedstock may be suitable while being inappropriate for other applications where a ready-to-spray commercial product may serve better.

In the next step, it was shown that the deposition mechanisms are generally comparable between the widely used gas-stabilized plasma torches and the rather unique hybrid water-stabilized plasma torch employed for the deposition of coatings within the scope of the thesis. Nevertheless, the different plasma compositions and properties may have much stronger impact on the produced coating than in the case of conventional dry coarse powders. This is caused by the much more complex interaction between the liquid feedstock and the plasma jet given by the size of feedstock particles, phases of feedstock involved in the interaction, and the dwell time of the feedstock in the jet. Therefore, a feedstock working well with one torch model and deposition setup may deliver considerably different result when used with a different torch, different plasma-forming gas composition or power setting, or different feeding configuration, i.e., radial or axial. As a result, it is the trends, materials interactions and e.g., coating characterization principles that can be transferred rather than particular results obtained under particular conditions.

The hybrid feedstock spraying concept combining alumina powder and chromia suspensions was tested for the first time to the best of author's knowledge of hybrid spraying literature, bringing new possibilities of phase control of the conventional alumina coatings. It was shown that it is possible to reach very high contents of the corundum phase (almost 90 wt.%) thanks to the combination of alumina intermingling with the α-phase stabilizing chromia and the high deposition temperature, which is inherited from the specific deposition conditions used for hybrid coatings.

Ultimately, full intermixing of alumina and chromia in the coatings was achieved via the deposition from solutions combining precursors for both oxides dissolved and intermixed at

atomic scale. As a result, the range of coatings having different alumina-chromia ratios followed the color scheme of substitutionally Cr-doped alumina – the ruby – and also exhibited reversible thermochromic behavior, all as a result of the modification of the crystal lattice parameters and thus the light absorption properties within the visible spectrum. To the best of author's knowledge, this was one of the first reports of thermochromic coatings prepared by plasma spraying to date. Nevertheless, the mixture of the precursors may be modified arbitrarily using broad variety of materials both prior and during the deposition, opening the potential of precise control of coating chemistry for the in-situ synthesis of e.g., coating materials which are not readily available as powders, or for the manufacturing of fine functionally-graded material coatings.

The recognition of the published papers within the thermal spray community can be documented by the number of citations included in the author's literature list.

7 Conclusions

The presented thesis focused on the development of alumina-based plasma-sprayed coatings deposited from liquid feedstocks, i.e. suspensions and solutions, using a high-enthalpy plasma torch. Overview of suspension and solution plasma spraying technology is given in the introductory section, emphasizing the possibilities of intermixing of different materials given by the character of the employed feedstocks, i.e. fine powders intermixed in a suspension or chemical precursors dissolved in a solution. Moreover, hybrid feedstock plasma spraying utilizing dry coarse powders together with liquids is presented, potentially opening a novel route for coatings with unforeseen properties.

The first goal of development, testing, and deposition of different feedstock suspensions and solutions was achieved. Multiple sprayable suspensions and solutions varying in solid load (or solute concentration), particle size, and solvent type were prepared and successfully deposited in a reproducible manner, thus establishing the liquid feedstock deposition methodology and procedures for the WSP-H torch.

Using the range of feedstocks and deposition conditions, multiple coatings varying in microstructure (porosity, architecture) and phase composition were deposited, fulfilling the goal of new coatings preparation and characterization. The deposited coatings included extremely hard dense coatings, columnar cauliflower-like microstructures, and highly porous deposits. It was shown that the feedstock type largely determines the final coating microstructure which in turn governs the coating properties, such as hardness, wear resistance, adhesion-cohesion strength, etc. The results were published in peer-reviewed papers in Surface & Coatings Technology [I, II].

The last goal of elaboration on alumina-chromia coatings was achieved using the deposition routes of intermixed suspensions of fine powders, hybrid spraying, and intermixed precursor solutions. It was clearly demonstrated that each of the routes offers different degree of intermixing of the starting oxides. Hybrid spraying produced a mixture of coarse splats sprayed from the alumina powder intermingled with fine splats sprayed from the chromia suspension. Intermixing of the fine powders in suspensions produced significantly finer splats of the oxides, which were largely blended together. The addition of chromia promoted the formation of the alumina α-phase in both hybrid and suspension-sprayed coatings with respect to analogous powder and suspension-sprayed coatings deposited from pure alumina under identical deposition conditions. Spraying of intermixed precursor solutions led to the formation of coatings having predominantly the corundum structure with Cr atoms homogeneously incorporated into the Al_2O_3 lattice which was documented by the thermochromic properties of the deposits and by elongation of the lattice parameters of alumina. The results were published in peer-reviewed papers in Surface & Coatings Technology and Journal of Thermal Spray Technology [III, IV].

7.1 Further prospective

Based on the knowledge acquired within the scope of this thesis, the future objectives include, but are not limited to broadening of the experience with hybrid spraying which offers numerous possibilities in coating architectures and material combinations. For example, the liquid in the suspension may serve not only as a carrier of the fine powders, but also as a protection of materials that would otherwise be decomposed in the high-enthalpy plasma jet, i.e., for

deliberate incorporation of unmelted material in the coating for e.g., self-fluxing coatings for sliding applications.

The thesis is finished, but the work carries on.

References

[1] DAVIS, JR. *Handbook of Thermal Spray Technology*. ASM International, 2004. 338 p. ISBN 9780871707956.

[2] PAWŁOWSKI, L. *The science and engineering of thermal spray coatings*. 2nd ed. Chichester: Wiley. 2008. 656 p. ISBN 978-0-471-49049-4.

[3] BOULOS, MI., FAUCHAIS, P., and PFENDER, E. *Thermal Plasmas Fundamentals and Applications*. Springer Science+Business Media, LLC, 1994. ISBN 9781489913395. Available from DOI: 10.1007/978-1-4899-1337-1

[4] HRABOVSKY, M. Generation of thermal plasmas in liquid-stabilized and hybrid dc-arc torches. *Pure and Applied Chemistry*. 2002, **74**(3), 429–433. ISSN 0033-4545. Available from DOI: 10.1351/pac200274030429

[5] JENISTA, J., TAKANA, H., NISHIYAMA, H., *et al*. Integrated parametric study of a hybrid-stabilized argon–water arc under subsonic, transonic and supersonic plasma flow regimes. *Journal of Physics D: Applied Physics*. 2011, **44**(43), 435204. ISSN 0022-3727. Available from DOI: 10.1088/0022-3727/44/43/435204

[6] FAUCHAIS, PL., HEBERLEIN, JVR., and BOULOS, MI. *Thermal Spray Fundamentals*. Springer US, 2014. 452 p. ISBN 978-0-387-28319-7. Available from DOI: 10.1007/978-0-387-68991-3

[7] FAUCHAIS, P., ETCHART-SALAS, R., RAT, V., *et al*. Parameters Controlling Liquid Plasma Spraying: Solutions, Sols, or Suspensions. *Journal of Thermal Spray Technology*. 2008, **17**(1), 31–59. ISSN 10599630. Available from DOI: 10.1007/s11666-007-9152-2

[8] GANVIR, A., CURRY, N., BJORKLUND, S., *et al*. Characterization of Microstructure and Thermal Properties of YSZ Coatings Obtained by Axial Suspension Plasma Spraying (ASPS). *Journal of Thermal Spray Technology*. 2015, **24**(7), 1195–1204. ISSN 10599630. Available from DOI: 10.1007/s11666-015-0263-x

[9] BISSON, JF., GAUTHIER, B., and MOREAU, C. Effect of Plasma Fluctuations on In-Flight Particle Parameters. *Journal of Thermal Spray Technology*. 2003, **12**(1), 38–43. Available from DOI: 10.1361/105996303770348483

[10] MARQUES, JL., FORSTER, G., and SCHEIN, J. Multi-Electrode Plasma Torches: Motivation for Development and Current State-of-the-Art. *The Open Plasma Physics Journal*. 2009, **2**(2), 89–98. ISSN 18765343. Available from DOI: 10.2174/1876534300902020089

[11] HRABOVSKY, M. Water-stabilized plasma generators. *Pure and Applied Chemistry*. 1998, **70**(6), 1157–1162. ISSN 0033-4545. Available from DOI: 10.1351/pac199870061157

[12] MEDRICKY, J., MUSALEK, R., JANATA, M., *et al*. Cost-effective plasma spraying for large-scale applications. In: F. AZARMI, K. BALANI, T. EDEN, T. HUSSAIN, Y.-C. LAU, H. LI, K. SHINODA, F.-L. TOMA a J. VEILLEUX, ed. *ITSC 2018—Proceedings of the International Thermal Spray Conference*. Orlando: ASM International, 2018, s. 683–689.

[13] MILLER, RA. Thermal barrier coatings for aircraft engines: History and directions.

Journal of Thermal Spray Technology. 1997, **6**(1), 35–42. ISSN 10599630. Available from DOI: 10.1007/BF02646310

[14] TOMASZEK, R., PAWLOWSKI, L., ZDANOWSKI, J., *et al*. Microstructural transformations of TiO_2, Al_2O_3+13TiO_2 and Al_2O_3+40TiO_2 at plasma spraying and laser engraving. *Surface and Coatings Technology*. 2004, **185**(2–3), 137–149. ISSN 02578972. Available from DOI: 10.1016/j.surfcoat.2004.01.010

[15] BERNARD, B., QUET, A., BIANCHI, L., *et al*. Thermal insulation properties of YSZ coatings: Suspension Plasma Spraying (SPS) versus Electron Beam Physical Vapor Deposition (EB-PVD) and Atmospheric Plasma Spraying (APS). *Surface and Coatings Technology*. 2017, **318**, 122–128. ISSN 02578972. Available from DOI: 10.1016/j.surfcoat.2016.06.010

[16] CLARKE, DR., OECHSNER, M., and PADTURE, NP. Thermal-barrier coatings for more efficient gas-turbine engines. *MRS Bulletin*. 2012, **37**(10), 891–898. ISSN 0883-7694. Available from DOI: 10.1557/mrs.2012.232

[17] *Is the new GE9X engine on Boeing's 777X as big as a 737 fuselage? No. It's even bigger.* [online][visited on 15-05-2021]. 2019. Available from: http://www.avialogy.com/is-the-new-ge9x-engine-on-boeings-777x-as-big-as-a-737-fuselage-no-its-even-bigger/

[18] PAWŁOWSKI, L. Suspension and solution thermal spray coatings. *Surface and Coatings Technology*. 2009, **203**(19), 2807–2829. ISSN 02578972. Available from DOI: 10.1016/j.surfcoat.2009.03.005

[19] FAUCHAIS, P., MONTAVON, G., and BERTRAND, G. From powders to thermally sprayed coatings. *Journal of Thermal Spray Technology*. 2010, **19**(1–2), 56–80. ISSN 10599630. Available from DOI: 10.1007/s11666-009-9435-x

[20] STAHR, CC., SAARO, S., BERGER, LM., *et al*. Dependence of the stabilization of α-Alumina on the spray process. *Journal of Thermal Spray Technology*. 2007, **16**(5–6), 822–830. ISSN 10599630. Available from DOI: 10.1007/s11666-007-9107-7

[21] LI, D., FENG, J., ZHAO, H., *et al*. Microstructure formed by suspension plasma spraying: From YSZ splat to coating. *Ceramics International*. 2017, **43**(10), 7488–7496. ISSN 02728842. Available from DOI: 10.1016/j.ceramint.2017.03.027

[22] KURODA, S. and CLYNE, TW. The quenching stress in thermally sprayed coatings. *Thin Solid Films*. 1991, **200**(1), 49–66. ISSN 00406090. Available from DOI: 10.1016/0040-6090(91)90029-W

[23] FAUCHAIS, P., MONTAVON, G., LIMA, RS., *et al*. Engineering a new class of thermal spray nano-based microstructures from agglomerated nanostructured particles, suspensions and solutions: an invited review. *Journal of Physics D: Applied Physics*. 2011, **44**(9), 093001. ISSN 0022-3727. Available from DOI: 10.1088/0022-3727/44/9/093001

[24] GANVIR, A., KUMARA, C., GUPTA, M., *et al*. Thermal conductivity in suspension sprayed thermal barrier coatings: Modelling and experiments. *Proceedings of the International Thermal Spray Conference*. 2016, **1**(1), 368–374. ISSN 1544-1016. Available from DOI: 10.1007/s11666-016-0503-8

[25] OBERSTE BERGHAUS, J., LEGOUX, JG., MOREAU, C., *et al*. Mechanical and Thermal Transport Properties of Suspension Thermal-Sprayed Alumina-Zirconia

Composite Coatings. *Journal of Thermal Spray Technology*. 2008, **17**(1), 91–104. ISSN 1059-9630. Available from DOI: 10.1007/s11666-007-9146-0

[26] FAUCHAIS, P., JOULIA, A., GOUTIER, S., *et al*. Suspension and solution plasma spraying. *Journal of Physics D: Applied Physics*. 2013, **46**, 224015. ISSN 0022-3727. Available from DOI: 10.1088/0022-3727/46/22/224015

[27] MARCHAND, O., GIRARDOT, L., PLANCHE, MP., *et al*. An insight into suspension plasma spray: Injection of the suspension and its interaction with the plasma flow. *Journal of Thermal Spray Technology*. 2011, **20**(6), 1310–1320. ISSN 10599630. Available from DOI: 10.1007/s11666-011-9682-5

[28] COTLER, EM., CHEN, D., and MOLZ, RJ. Pressure-based liquid feed system for suspension plasma spray coatings. *Journal of Thermal Spray Technology*. 2011, **20**(4), 967–973. ISSN 10599630. Available from DOI: 10.1007/s11666-011-9624-2

[29] FAUCHAIS, P., VARDELLE, M., VARDELLE, A., *et al*. What Do We Know, What are the Current Limitations of Suspension Plasma Spraying? *Journal of Thermal Spray Technology*. 2015, **24**(7), 1120–1129. ISSN 1059-9630. Available from DOI: 10.1007/s11666-015-0286-3

[30] AUBIGNAT, E., PLANCHE MP., ALLIMANT, A., *et al*. Effect of suspension characteristics on in-flight particle properties and coating microstructures achieved by suspension plasma spray. *Journal of Physics: Conference Series*. 2014, **550**, 012019. ISSN 1742-6588. Available from DOI: 10.1088/1742-6596/550/1/012019

[31] WANG, G., SARKAR, P., and NICHOLSON, PS. Influence of Acidity on the Electrostatic Stability of Alumina Suspensions in Ethanol. *Journal of the American Ceramic Society*. 1997, **80**(4), 965–972. ISSN 1551-2916. Available from DOI: 10.1111/j.1151-2916.1997.tb02928.x

[32] MENON, M., DECOURCELLE, S., RAMOUSSE, S., *et al*. Stabilization of ethanol-based alumina suspensions. *Journal of the American Ceramic Society*. 2006, **89**(2), 457–464. ISSN 00027820. Available from DOI: 10.1111/j.1551-2916.2005.00744.x

[33] JORDAN, EH., JIANG, C., and GELL, M. The solution precursor plasma spray (SPPS) process: A review with energy considerations. *Journal of Thermal Spray Technology*. 2015, **24**(7), 1153–1165. ISSN 1059-9630. Available from DOI: 10.1007/s11666-015-0272-9

[34] SCOTT, HG. Phase relationships in the zirconia-yttria system. *Journal of Materials Science*. 1975, **10**(9), 1527–1535. ISSN 00222461. Available from DOI: 10.1007/BF01031853

[35] CHRASKA, P., DUBSKY, J., NEUFUSS, K., *et al*. Alumina-Base Plasma-Sprayed Materials Part I: Phase Stability of Alumina and Alumina-Chromia. *Journal of Thermal Spray Technology*. 1997, **6**(September), 320–326.

[36] MATEJICEK, J., NEVRLA, B., VILEMOVA, M., *et al*. Overview of processing technologies for tungsten-steel composites and FGMs for fusion applications. *Nukleonika*. 2015, **60**(2), 267–273. ISSN 15085791. Available from DOI: 10.1515/nuka-2015-0049

[37] KOTLAN, J., PALA, Z., MUSALEK, R., *et al*. On reactive suspension plasma spraying of calcium titanate. *Ceramics International*. 2016, **42**(3), 4607–4615. ISSN 02728842.

Available from DOI: 10.1016/j.ceramint.2015.11.159

[38] POTTHOFF, A., KRATZSCH, R., BARBOSA, M., *et al*. Development and Application of Binary Suspensions in the Ternary System Cr_2O_3-TiO_2-Al_2O_3 for S-HVOF Spraying. *Journal of Thermal Spray Technology*. 2018, **27**(4), 710–717. ISSN 1544-1016. Available from DOI: 10.1007/s11666-018-0709-z

[39] MUSALEK, R., MEDRICKY, J., TESAR, T., *et al*. Controlling Microstructure of Yttria-Stabilized Zirconia Prepared from Suspensions and Solutions by Plasma Spraying with High Feed Rates. *Journal of Thermal Spray Technology*. 2017, **26**(8), 1787–1803. ISSN 10599630. Available from DOI: 10.1007/s11666-017-0622-x

[40] SIVAKUMAR, G. and JOSHI, SV. Hybrid metodology for producing composite, multi-layered and graded coatings by plasma spraying utilizing powder and solution feedstock. US 20130095340 A1. 2013. USA. Available from: www.google.com/patents/US20130095340

[41] BJORKLUND, S., GOEL, S., and JOSHI, S. Function-dependent coating architectures by hybrid powder-suspension plasma spraying: Injector design, processing and concept validation. *Materials and Design*. 2018, **142**(1), 56–65. ISSN 07338619. Available from DOI: 10.1016/j.matdes.2018.01.002

[42] CARNICER, V., ALCAZAR, C., SANCHEZ, E., *et al*. Aqueous suspension processing of multicomponent submicronic Y-TZP/Al_2O_3/SiC particles for suspension plasma spraying. *Journal of the European Ceramic Society*. 2018, **38**(5), 2430–2439. ISSN 1873619X. Available from DOI: 10.1016/j.jeurceramsoc.2018.01.006

[43] KIM, SH., JEONG, SH., KIM, TH., *et al*. Effects of solid lubricant and laser surface texturing on tribological behaviors of atmospheric plasma sprayed Al_2O_3-ZrO_2 composite coatings. *Ceramics International*. 2017, **43**(12), 9200–9206. ISSN 0272-8842. Available from DOI: 10.1016/j.ceramint.2017.04.073

[44] DU, L., ZHANG, W., LIU, W., *et al*. Preparation and characterization of plasma sprayed Ni3Al-hBN composite coating. *Surface and Coatings Technology*. 2010, **205**(7), 2419–2424. ISSN 02578972. Available from DOI: 10.1016/j.surfcoat.2010.09.036

[45] CHYOU, YP. and PFENDER, E. Behavior of particulates in thermal plasma flows. *Plasma Chemistry and Plasma Processing*. 1989, **9**(1), 45–71. ISSN 02724324. Available from DOI: 10.1007/BF01015826

[46] GUIGNARD, A., MAUER, G., VASSEN, R., *et al*. Deposition and characteristics of submicrometer-structured thermal barrier coatings by suspension plasma spraying. *Journal of Thermal Spray Technology*. 2012, **21**(3–4), 416–424. ISSN 10599630. Available from DOI: 10.1007/s11666-012-9762-1

[47] DELBOS, C., FAZILLEAU, J., RAT, V., *et al*. Phenomena involved in suspension plasma spraying part 2: Zirconia particle treatment and coating formation. *Plasma Chemistry and Plasma Processing*. 2006, **26**(4), 393–414. ISSN 02724324. Available from DOI: 10.1007/s11090-006-9020-8

[48] KASSNER, H., VASSEN, R., and STOVER, D. Study on instant droplet and particle stages during suspension plasma spraying (SPS). *Surface and Coatings Technology*. 2008, **202**(18), 4355–4361. ISSN 02578972. Available from DOI: 10.1016/j.surfcoat.2008.04.009

[49] VANEVERY, K., KRANE, MJM., and TRICE, RW. Parametric study of suspension plasma spray processing parameters on coating microstructures manufactured from nanoscale yttria-stabilized zirconia. *Surface and Coatings Technology*. 2012, **206**(8–9), 2464–2473. ISSN 02578972. Available from DOI: 10.1016/j.surfcoat.2011.10.051

[50] CHEN, D., JORDAN, EH., and GELL, M. The solution precursor plasma spray coatings: Influence of solvent type. *Plasma Chemistry and Plasma Processing*. 2010, **30**(1), 111–119. ISSN 02724324. Available from DOI: 10.1007/s11090-009-9200-4

[51] GELL, M., JORDAN, EH., TEICHOLZ, M., *et al*. Thermal barrier coatings made by the solution precursor plasma spray process. *Journal of Thermal Spray Technology*. 2008, **17**(1), 124–135. ISSN 10599630. Available from DOI: 10.1007/s11666-007-9141-5

[52] CEDELLE, J., VARDELLE, M., and FAUCHAIS, P. Influence of stainless steel substrate preheating on surface topography and on millimeter- and micrometer-sized splat formation. *Surface and Coatings Technology*. 2006, **201**(3–4), 1373–1382. ISSN 02578972. Available from DOI: 10.1016/j.surfcoat.2006.02.003

[53] CHANDRA, S. and FAUCHAIS, P. Formation of solid splats during thermal spray deposition. *Journal of Thermal Spray Technology*. 2009, **18**(2), 148–180. ISSN 10599630. Available from DOI: 10.1007/s11666-009-9294-5

[54] MCPHERSON, R. On the formation of thermally sprayed alumina coatings. *Journal of Materials Science*. 1980, **15**(12), 3141–3149. ISSN 00222461. Available from DOI: 10.1007/BF00550387

[55] OBERSTE-BERGHAUS, J., BOUARICHA, S., LEGOUX, JG., *et al*. Injection conditions and in-flight particles states in suspension plasma spraying of alumina and zirconia nano-ceramics. In: E. LUGSCHEIDER, ed. *Thermal Spray 2005: Proceedings of the International Thermal Spray Conference*. Basel: DVS, 2005, s. 512–518.

[56] VANEVERY, K., KRANE, MJM., and TRICE, RW., *et al*. Column formation in suspension plasma-sprayed coatings and resultant thermal properties. *Journal of Thermal Spray Technology*. 2011, 20(4), 817–828. ISSN 1059-9630. Available from DOI: 10.1007/s11666-011-9632-2

[57] FAUCHAIS, P., VARDELLE, M., GOUTIER, S., *et al*. Key Challenges and Opportunities in Suspension and Solution Plasma Spraying. *Plasma Chemistry and Plasma Processing*. 2014, **35**(3), 511–525. ISSN 0272-4324. Available from DOI: 10.1007/s11090-014-9594-5

[58] CURRY, N., VANEVERY, K., SNYDER, T., *et al*. Thermal Conductivity Analysis and Lifetime Testing of Suspension Plasma-Sprayed Thermal Barrier Coatings. *Coatings*. 2014, **4**(3), 630–650. ISSN 2079-6412. Available from DOI: 10.3390/coatings4030630

[59] GOSWAMI, AP., ROY, S., MITRA, MK., *et al*. Influence of powder, chemistry and intergranular phases on the wear resistance of liquid-phase-sintered Al_2O_3. *Wear*. 2000, **244**(1–2), 1–14. ISSN 00431648. Available from DOI: 10.1016/S0043-1648(00)00407-5

[60] GITZEN, WH., ed. *Alumina as a Ceramic Material*. Columbus: American Ceramic Society, 1970. 264 p. ISBN 0916094464.

[61] HAWLEY, GG. and LEWIS, RJ. *Hawley's condensed chemical dictionary*. Wiley,

2007. ISBN 9780470114735.

[62] LEIVO, EM., VIPPOLA, MS., SORSA, PPA., *et al*. Wear and corrosion properties of plasma sprayed Al_2O_3 and Cr_2O_3 coatings sealed by aluminum phosphates. *Journal of Thermal Spray Technology*. 1997, **6**(2), 205–210. ISSN 10599630. Available from DOI: 10.1007/s11666-997-0014-8

[63] DI GIROLAMO, G., BRENTARI, A., BLASI, C., *et al*. Microstructure and mechanical properties of plasma sprayed alumina-based coatings. *Ceramics International*. 2014, **40**(8 PART B), 12861–12867. ISSN 02728842. Available from DOI: 10.1016/j.ceramint.2014.04.143

[64] LAMARRE, JM., MARCOUX, P., PERRAULT, M., *et al*. Performance analysis and modeling of thermally sprayed resistive heaters. *Journal of Thermal Spray Technology*. 2013, **22**(6), 947–953. ISSN 10599630. Available from DOI: 10.1007/s11666-013-9946-3

[65] LEVI, CG., JAYARAM, V., VALENCIA, JJ., *et al*. Phase selection in electrohydrodynamic atomization of alumina. *Journal of Materials Research*. 1988, **3**(5), 969–983. ISSN 20445326. Available from DOI: 10.1557/JMR.1988.0969

[66] LEVIN, I. and BRANDON, D. Metastable Alumina Polymorphs: Crystal Structures and Transition Sequences. *Journal of the American Ceramic Society*. 1998, **81**(8), 1995–2012. ISSN 0002-7820. Available from DOI: 10.1111/j.1151-2916.1998.tb02581.x

[67] HEINTZE, GN. and UEMATSU, S. Preparation and structures of plasma-sprayed γ- and α-Al_2O_3 coatings. *Surface and Coatings Technology*. 1992, **50**(3), 213–222. ISSN 02578972. Available from DOI: 10.1016/0257-8972(92)90004-T

[68] AULT, NN. Characteristics of Refractory Oxide Coatings Produced by Flame-Spraying. *Journal of the American Ceramic Society*. 1957, **40**(3), 69–74. ISSN 15512916. Available from DOI: 10.1111/j.1151-2916.1957.tb12578.x

[69] BONDIOLI, F., FERRARI, AM., LEONELLI, C., *et al*. Reaction Mechanism in Alumina/Chromia (Al_2O_3-Cr_2O_3) Solid Solutions Obtained by Coprecipitation. *Journal of the American Ceramic Society*. 2004, **83**(8), 2036–2040. ISSN 00027820. Available from DOI: 10.1111/j.1151-2916.2000.tb01508.x

[70] FUJITA, M., INUKAI, K., SAKIDA, S., *et al*. Sintering of Al_2O_3-Cr_2O_3 powder prepared by sol-gel process. *Zairyo/Journal of the Society of Materials Science, Japan*. 2007, **56**(6), 526–530. ISSN 05145163. Available from DOI: 10.2472/jsms.56.526

[71] NORMAND, B., FERVEL, V., CODDET, C., *et al*. Tribological properties of plasma sprayed alumina-titania coatings: Role and control of the microstructure. *Surface and Coatings Technology*. 2000, **123**(2–3), 278–287. ISSN 02578972. Available from DOI: 10.1016/S0257-8972(99)00532-0

[72] TOMA, FL., BERGER, LM., SCHEITZ, S., *et al*. Comparison of the microstructural characteristics and electrical properties of thermally sprayed Al_2O_3 coatings from aqueous suspensions and feedstock powders. *Journal of Thermal Spray Technology*. 2012, **21**(3–4), 480–488. ISSN 10599630. Available from DOI: 10.1007/s11666-012-9761-2

[73] GADOW, R., FRIEDRICH, C., KILLINGER, A., *et al*. Development of Atmospheric Plasma Sprayed Dielectric Ceramic Coatings for High Efficiency Tubular Ozone

Generators. *Journal of Water Resource and Protection*. 2010, **02**(09), 799–808. ISSN 1945-3094. Available from DOI: 10.4236/jwarp.2010.29094

[74] MEDRICKY, J. *Nanocrystalline Al_2O_3-based materials prepared by plasma spraying*. 2019. Doctoral Thesis. Faculty of Nuclear Sciences and Physical Engineering, Czech Technical University in Prague.

[75] RIETVELD, HM. A profile refinement method for nuclear and magnetic structures. *Journal of Applied Crystallography*. 1969, **2**(2), 65–71. ISSN 00218898. Available from DOI: 10.1107/s0021889869006558

[76] HILL, MR., BASTOW, TJ., CELOTTO, S., *et al*. Integrated study of the calcination cycle from gibbsite to corundum. *Chemistry of Materials*. 2007, **19**(11), 2877–2883. ISSN 08974756. Available from DOI: 10.1021/cm070078f

[77] *Accepted Practice to Test Bond Strength of Thermal Spray Coatings* [online] [visited on 04-06-2016]. Available from: http://www.asminternational.org/documents/17679604/17683439/AcceptedPracticeBondStrengthApprovedformatted_Intro.pdf/4bcf5903-414d-413f-ab69-7cf0cc9123bd

[78] TESAR, T. *Plazmové stříkání Al_2O_3 suspenze*. 2015. Research Project. Faculty of Nuclear Sciences and Physical Engineering, Czech Technical University in Prague.

Appendix A

List of author's publications related to the doctoral thesis (impacted journals)

[I] TESAR, T., MUSALEK, R., MEDRICKY, J., KOTLAN, J., LUKAC, F., PALA, Z., CTIBOR, P., CHRASKA, T., HOUDKOVA, S., RIMAL, V., CURRY, N. Development of suspension plasma sprayed alumina coatings with high enthalpy plasma torch. *Surface and Coatings Technology*, 2017, **325**, 277–288. ISSN 02578972. Available from DOI: 10.1016/j.surfcoat.2017.06.039

Cited 22 times.

[II] TESAR, T., MUSALEK, R., MEDRICKY, J., CIZEK, J. On growth of suspension plasma-sprayed coatings deposited by high-enthalpy plasma torch. *Surface and Coatings Technology*. 2019, **371**, s. 333–343. ISSN 02578972. Available from DOI: 10.1016/j.surfcoat.2019.01.084

Cited 5 times.

[III] TESAR, T., MUSALEK, R., LUKAC, F., MEDRICKY, J., CIZEK, J., RIMAL, V., JOSHI, S., CHRASKA, T. Increasing α-phase content of alumina-chromia coatings deposited by suspension plasma spraying using hybrid and intermixed concepts. *Surface and Coatings Technology*. 2019, **371**, s. 298–311. ISSN 02578972. Available from DOI: 10.1016/j.surfcoat.2019.04.091

Cited 4 times.

[IV] TESAR, T., MUSALEK, R., LUKAC, F., MEDRICKY, J., CIZEK, J., CSAKI, S., PANAK, O., DRZKOVA, M. Solution Precursor Plasma Spraying of Cr-Doped Al_2O_3 Thermochromic Coatings, *Journal of Thermal Spray Technology*, 2020, **29**, s. 199-211. ISSN 1059-9630. Available from DOI: 10.1007/s11666-019-00945-2.

Cited 1 time.

List of other author's publications (impacted journals)

[V] MUSALEK, R., MEDRICKY, J., TESAR, T., KOTLAN, J., PALA, Z., LUKAC, F., ILLKOVA, K., HLINA, M., CHRASKA, T., SOKOLOWSKI, P., CURRY, N. Controlling Microstructure of Yttria-Stabilized Zirconia Prepared from Suspensions and Solutions by Plasma Spraying with High Feed Rates. *Journal of Thermal Spray Technology*, 2017, 26(8), 1787–1803. ISSN 10599630. Available from DOI: 10.1007/s11666-017-0622-x

Cited 13 times.

[VI] MUSALEK, R., MEDRICKY, J., TESAR, T., KOTLAN, J., PALA, Z., LUKAC, F., CHRASKA, T., CURRY, N. Suspensions Plasma Spraying of Ceramics with Hybrid Water-Stabilized Plasma Technology. *Journal of Thermal Spray Technology*, 2017, 26(1–2), 37–46. ISSN 10599630. Available from DOI: 10.1007/s11666-016-0493-6

Cited 15 times.

[VII] CIZEK, J., BROZEK, V., CHRASKA, T., LUKAC, F., MEDRICKY, J., MUSALEK, R., TESAR, T., SISKA, F., ANTOS, Z., CUPERA, J., MATEJKOVA, M., SPOTZ, Z., HOUDKOVA, S., KVERKA, M. Silver-Doped Hydroxyapatite Coatings Deposited by Suspension Plasma Spraying. *Journal of Thermal Spray Technology*. 2018, 27(8), s. 1333–1343. ISSN 1059-9630. Available from DOI: 10.1007/s11666-018-0767-2

Cited 9 times.

[VIII] MEDRICKY, J., LUKAC, F., CSAKI, S., HOUDKOVA, S., BARBOSA, M., TESAR, T., CIZEK, J., MUSALEK, R., KOVARIK, O., CHRASKA, T. Improvement of mechanical properties of plasma sprayed Al_2O_3-ZrO_2-SiO_2 amorphous coatings by surface crystallization. *Materials*. 2019, 12(19), 3232. ISSN 19961944. Available from DOI: 10.3390/ma12193232

Cited 2 times.

[IX] GUPTA, M., MUSALEK, R., TESAR, T. Microstructure and Failure Analysis of Suspension Plasma Sprayed Thermal Barrier Coatings, *Surface and Coatings Technology*, 2020, 382, 125218, 9 pages, Available from DOI: 10.1016/j.surfcoat.2019.125218.

Cited 5 times.

[X] MUSALEK, R., TESAR, T., MEDRICKY, J., LUKAC, F., CHRASKA, T., GUPTA, M. Microstructures and Thermal Cycling Properties of Thermal Barrier Coatings Deposited by Hybrid Water-Stabilized Plasma Torch, *Journal of Thermal Spray Technology*, 2020, 29, s. 444-461, ISSN 15441016. Available from DOI: 10.1007/s11666-020-00990-2

Cited 2 times.

[XI] MUSALEK, R., TESAR, T., MEDRICKY, J., LUKAC, F., LIMA, R.S. High-Temperature Cycling of Plasma Sprayed Multilayered NiCrAlY/YSZ/GZO/YAG Thermal Barrier Coatings Prepared from Liquid Feedstocks. *Journal of Thermal Spray Technology*. 2020. ISSN 15441016. Available from DOI: 10.1007/s11666-020-01107-5

[XII] TKACHIVSKYI, D., JUHANI, K., SURZENKOV, A., KULU, P., TESAR, T., MUSALEK, R., LUKAC, F., ANTOS, J., VOSTRAK, M., ANTONOV, M., GOLJANDIN, D. HVOF sprayed Fe-based wear-resistant coatings with carbide reinforcement, synthesized

in situ and by mechanically activated synthesis. *Coatings*. 2020, 10(11), 1–15. ISSN 20796412. Available from DOI: 10.3390/coatings10111092

[XIII] MUSALEK, R., NARDOZZA, E., TESAR, T., MEDRICKY, J. Evaluation of Internal Cohesion of Multiphase Plasma-Sprayed Coatings by Cavitation Test: Feasibility Study. *Acta Polytechnica CTU Proceedings*. 2020, 27(0), 73–78. ISSN 2336-5382. Available from DOI: 10.14311/app.2020.27.0073

[XIV] CIZEK, J., DUKOVSKY, D., MUSALEK, R., MEDRICKY, J., TESAR, T., LUKAC, F., CHRASKA, T. Suspension Spraying Tip: High Molecular Weight Solvent. *Journal of Thermal Spray Technology*, 2021, 30(5), s.1148-1158. ISSN 1059-9630. Available from DOI: 10.1007/s11666-021-01192-0

List of author's conference proceedings

[i] MUSALEK, R., TESAR, T., STRASKY, J., CECH, J. Combined indentation testing of spark plasma sintered steels. *Key Engineering Materials*. 2015, 662, 43-46. ISSN 10139826. Available from DOI: 10.4028/www.scientific.net/KEM.662.43

[ii] MUSALEK, R., MEDRICKY, J., TESAR, T., KOTLAN, J., LUKAC, F. Deposition of titania from solution by hybrid water-stabilized plasma torch. In: *METAL 2016 - 25th Anniversary International Conference on Metallurgy and Materials, Conference Proceedings*. 2016. ISBN 978-808729467-3.

[iii] MUSALEK, R., MEDRICKY, J., KOTLAN, J., TESAR, T., PALA, Z., LUKAC, F., CHRASKA, T. Plasma Spraying of Suspensions with Hybrid Water-Stabilized Plasma Technology. In: *ITSC 2016: International Thermal Spray Conference and Exposition*. 2016, 1, 267–272. ISSN 1059-9630.

[iv] MUSALEK, R., MEDRICKY, J., KOTLAN, J., TESAR, T., LUKAC, F., CTIBOR, P., ILLKOVA, K., CHRASKA, T. High feed rate plasma spraying of YSZ from various suspensions. In: *Proceedings of the International Thermal Spray Conference*. 2017, s. 36–41. ISBN 9781510858220.

[v] MUSALEK, R., CTIBOR, P., MEDRICKY, J., TESAR, T., KOTLAN, J., LUKAC, F. Suspension plasma spraying of sub-stoichiometric titania by hybrid water/argon stabilized plasma torch. In: *METAL 2017 - 26th International Conference on Metallurgy and Materials, Conference Proceedings*. 2017. ISBN 9788087294796.

[vi] TESAR, T., MUSALEK, R., MEDRICKY, J., CIZEK, J., LUKAC, F., CHRASKA, T. Deposition of multiphase coatings from liquid feedstock using hybrid water-stabilized (WSP-H) plasma torch. In: *Proceedings of the International Thermal Spray Conference*. 2018, s. 456–462. ISBN 9781510880405.

[vii] MUSALEK, R., T. TESAR, J. MEDRICKY, F. LUKAC, T. CHRASKA a M. GUPTA. Microstructures and properties of thermal barrier coatings deposited by hybrid water-stabilized plasma torch. In: *Proceedings of the International Thermal Spray Conference*. ASM International, 2019, s. 738–745. ISBN 9781510888005.

[viii] TESAR, T., MUSALEK, R., MEDRICKY, J., CIZEK, J., LUKAC, F., CSAKI, S. CHRASKA, T. Cr-doped Al_2O_3 deposited by solution precursor plasma spraying by hybrid water-stabilized plasma torch. In: *Proceedings of the International Thermal Spray Conference*. ASM International, 2019, s. 714–719. ISBN 9781510888005.